Regulation of N-WASP-dependent actin polymerisation

Ashley Ceinwen Humphries

University College London

and

Cancer Research UK London Research Institute

PhD Supervisor: Michael Way

A thesis submitted for the degree of

Doctor of Philosophy

University College London

September 2013

Declaration

I, Ashley Ceinwen Humphries, confirm that the work presented in this thesis is my own. Where information has been derived from other sources, I confirm that this has been indicated in the thesis.

Abstract

N-WASP activates the Arp2/3 complex to stimulate actin polymerisation during a number of cellular processes. These include, phagocytosis, endocytosis, and invadopodia and podosome formation. In addition, it is also frequently recruited by pathogens to assist in their actin-dependent spread. During its egress from the cell, vaccinia virus fuses with the plasma membrane and promotes the activation of Src and Abl family kinases. This event leads to phosphorylation of tyrosine 112 and tyrosine 132 of the viral transmembrane protein, A36, triggering a signalling cascade that stimulates actin polymerisation. The phospho-tyrosine residues provide docking sites for the cellular adaptors Nck and Grb2, with Nck recruiting WIP-N-WASP and in turn the Arp2/3 complex. I found that clathrin is transiently recruited to vaccinia in the moments before actin polymerisation. Clathrin performs an organisational role, clustering A36 beneath the virus to enhance robust actin tail formation. Loss of clathrin recruitment resulted in a more disperse localisation of A36 and N-WASP, which led to an altered actin tail morphology, indicating that the spatial organisation of N-WASP is a parameter affecting actin polymerisation. During actin tail formation, I additionally found that Cdc42 could regulate N-WASP activity. Cdc42 supported the main signalling nexus of Nck-WIP-N-WASP, with its major role attributed to stabilising N-WASP beneath the viral particle. I further found that Cdc42 acts in a feed-forward loop with N-WASP and the RhoGEF intersectin-1. This pathway is conserved in FcγR-mediated phagocytosis, validating the use of pathogens to understand the molecular detail of Arp2/3-dependent actin-signalling pathways.

Acknowledgement

Firstly, I would like to say that I have thoroughly enjoyed my time in the Way lab, and have been incredibly fortunate to work with so many talented people over the past four years. My thanks for this should go to Michael, who has also been incredibly supportive throughout my entire Ph.D.

I must thank Mark, who taught me much of what I learnt in the lab. Your enthusiasm for your work is infectious and I am truly grateful to have been able to work with you. I owe much to my elder students; Charlotte, Sara and Judy, your example, help and support has made my time in the lab so much easier and also incredibly enjoyable. If I have passed on even a fraction of what you taught me to our newer recruits, I will have done well. On that note, Xenia, it has been a genuine pleasure and I am sure you will go on to great things.

The Way lab as far as I am concerned would not be what it was, if it were not for our amazing scientific officers. Theresa, your genuine lab spirit and unending patience, and Antonio your sharp mind and remarkable knowledge. I must also pay note to my one time neighbours Amy and Jasmine, I truly admire your approach to science and I hope some of it has rubbed off on me. I also cannot forget the boys, Dave and Joe. Thank you for bringing a fresh perspective to the lab and for making admirable pub companions.

Finally, I would like to thank my family and Mike. I am very fortunate to be surrounded by people that understand me, as well as the job that I do. I hope I have, and will continue to make you proud.

Table of Contents

Table of figures

List of tables

Abbreviations

Φ	Bulky hydrophobic amino acid
ADP	Adenosine diphosphate
Ai	Attachment index
AP-2	Adaptor protein 2
ANTH	AP180 N-terminal homology domain
Arp2/3	Actin related proteins 2 and 3
ATP	Adenosine triphosphate
BAR	Bin-amphiphysin-rvs domain
BDT	Big dye terminator
BH	Bcl homology domain
BSA	Bovine serum albumin
CB	Cytoskeletal buffer
Cc	Critical concentration
CCV	Clathrin-coated vesicle
Cdc42	Cell division cycle 42
CEV	Cell-associated enveloped virion
CHC	Clathrin heavy chain
CLC	Clathrin light chain
CME	Clathrin-mediated endocytosis
CR3	Complement receptor 3
CRIB	Cdc42/Rac interactive binding domain
CSTN	Calsyntenin
DAPI	4’,6-diamidino-2-phenylindole
DH	Dbl-homologous domain
DMSO	Dimethyl sulfoxide
DNA	Deoxyribonucleic acid
dNTP	Deoxyribonucleotide triphosphate
ECM	Extracellular matrix
EDTA	Ethylenediaminetetraacetic acid
EEV	Extracellular enveloped virion
EGFR	Epidermal growth factor receptor
EGTA	Ethylene glycol tetraacetic acid
EM	Electron microscopy

EPEC	Enteropathogenic *Escherichia Coli*
Eps15	Epidermal growth factor substrate 15
ExB5	Extracellular B5 stain
F-actin	Filamentous actin
FcγR	Fc gamma receptor
FCHo	F-BAR-containing Fer/Cip4 homology domain-only protein
FCS	Fetal calf serum
FH	Formin homology domain
FRAP	Fluorescence recovery after photo-bleaching
FSB	Final sample buffer
GEF	Guanine nucleotide exchange factor
GFP	Green fluorescent protein
Grb2	Growth factor receptor-bound protein 2
GST	Glutathione-S-transferase
GTP	Guanosine-5'-triphosphate
GTPase	Guanosine-5'-triphosphatase
GVB	Gelatin veronal buffer
HEPES	4-(2-hydroxyethyl)-1-piperazineethanesulfonic acid
Hip1R	Huntingtin interacting protein 1-related
Hr	Hour
HRP	Horseradish peroxidase
IEV	Intracellular enveloped virion
IMV	Intracellular mature virion
ITSN	Intersectin
IV	Immature virion
Kb	Kilobases
KLC	Kinesin light chain
L	Litre
LB	Luria-Bertani
LCa	Clathrin light chain, isoform a
LDL	Low-density lipoprotein
LRR	Leucine rich repeat region
MEF	Mouse embryonic fibroblast
MEM	Minimum essential media
MES	2-(N-morpholino)-ethanesulphonic acid

Min	Minute
MOI	Multiplicity of infection
MT	Microtubule
MTOC	Microtubule organising centre
Nck	Non-catalytic region of tyrosine kinase adaptor protein
NPF	Nucleation promoting factor / Asparagine-Proline-Phenylalanine
n.s.	Not significant
N-WASP	Neural Wiskott-Aldrich syndrome protein
OD	Optical density
Oligo	Oligonucleotide
ORF	Open reading frame
PBSA	Phosphate buffered saline A
PBST	Phosphate buffered saline tween
PCR	Polymerase chain reaction
PFA	Paraformaldehyde
PFU	Plaque forming units
Pi	Inorganic phosphate / Phagocytic index
$PI(4,5)P_2$	Phosphatidylinositol 4,5-bisphosphate
PM	Plasma membrane
PNS	Post-nuclear stock
PRD	Polyproline-rich domain
PTB	Phospho-tyrosine binding domain
RBC	Red blood cell
RFP	Red fluorescent protein
Ri	Relative index
RNAi	Ribonucleic acid interference
rpm	Rotations per minute
SDS	Sodium dodecyl sulphate
PAGE	Polyacrylamide gel electrophoresis
SEM	Standard error of the mean
siRNA	Small interfering ribonucleic acid
Src	Sarcoma
SI	Structured illumination
TBE	Tris-borate-EDTA buffer
TD	Terminal domain

TGN	Trans-Golgi network
THATCH	Talin-Hip1/R/Sla2p-actin-tethering C-terminal homology domain
TEM	Transmission electron microscopy
TM	Transmembrane
TMB	Tetramethylbenzidine
TS	Tris saline
V	Volts
WCA	WASP homology 2, central and acidic region
WH	WASP homology domain
WIP	WASP interacting Protein
WR	Western Reserve
WT	Wild-type
w/v	Weight / Volume
Y	Tyrosine
YFP	Yellow fluorescent protein

Chapter 1. Introduction

1.1 Vaccinia virus

1.1.1 General

Vaccinia virus is the prototypic member of the *Poxviridae* family from the *Orthopoxvirus* genus. It is widely recognised for its role in the global eradication of smallpox, but its origin and natural host remain unknown. Vaccinia is widely studied as a potential tool for gene and oncolytic therapy (Gomez et al., 2011; Kirn and Thorne, 2009). Due to concerns of the related variola virus being used in bioterrorism, there is also heightened interest in its replication cycle and dissemination. In addition, vaccinia virus has been used successfully over a number of years to study the host immune response, as well as host cell biology, as it takes advantage of many cellular processes during its infectious cycle (Roberts and Smith, 2008).

1.1.2 Genome and gene expression

Vaccinia virus has a large double stranded DNA genome of approximately 200 kb and performs its entire replication cycle in the cytoplasm of the host cell (Goebel et al., 1990; Minnigan and Moyer, 1985; Roberts and Smith, 2008). The nomenclature of vaccinia genes is derived from the HindIII restriction map, leading to 16 fragments (assigned A-P according to decreasing size). ORFs are assigned the fragment letter and a number that increases stepwise 5' to 3' along the fragment. They are additionally allocated an L or R to signify the direction of transcription, as genes are encoded on both strands (Figure 1.1) (Goebel et al., 1990).

Upon entry, the naked viral core is released into the cytoplasm, before it is transported on microtubules further into the cell (Carter et al., 2003). The subsequent transcription of early mRNAs, which are synthesised by pre-packaged virus-encoded enzymes, leads to core uncoating and DNA replication (Moss, 1990). Vaccinia gene expression is tightly controlled and consists of three waves of transcription, with each reliant on the

expression of the former. In general the earliest wave consists of proteins involved in DNA replication, nucleotide biosynthesis, evasion of host defences and intermediate gene transcription (Assarsson et al., 2008; Broyles, 2003). While, intermediate and late genes are largely required for viral morphogenesis, assembly and the next round of infection (Rosel and Moss, 1985).

1.1.3 Viral assembly

Vaccinia virus has a complex morphogenic pathway, which produces distinct infectious forms (Roberts and Smith, 2008). Morphogenesis begins in a specialised compartment termed the viral factory. The factory is located at a perinuclear location and is largely devoid of cellular organelles (Ichihashi and Dales, 1971). The first observed structures within the factory are crescents composed of virus proteins and host-derived lipid, which grow to form the non-infectious immature virus (IV) (Rodriguez et al., 1998; Zhang and Moss, 1992). The DNA genome is packaged into the IV, then proteolytic cleavage of several capsid proteins and condensation of the virus core leads to the formation of a brick-shaped intracellular mature virion (IMV) (Figure 1.2) (Moss and Rosenblum, 1973). IMV, which are surrounded by a single lipid membrane represent the majority of infectious progeny and are released upon cell lysis (Heuser, 2005; Hollinshead et al., 1999). IMV, however, are not sufficient for efficient viral spread and IMV-derived enveloped forms of the virion are required (Smith et al., 2002).

During infection a small percentage of IMV leave the viral factory via microtubule-dependent transport and are directed to a site near the microtubule organising centre (MTOC) (Sanderson et al., 2000; Ward, 2005). At this site the IMV are wrapped in a double membrane that is derived from the trans-Golgi network (TGN) and/or endosomes (Figure 1.2) (Schmelz et al., 1994; Tooze et al., 1993). These membranes are modified by the incorporation or association of the following viral proteins; F12, F13, A33, A34, A36, A56, B5, E2 and K2 (Domi et al., 2008; Duncan and Smith, 1992; Parkinson and Smith, 1994; Roper et al., 1996; Smith et al., 2002; Wagenaar and Moss, 2007; Wolffe et al., 1993; Zhang et al., 2000). F13 and B5 are required for membrane wrapping, and in their absence only IMV particles are produced leading to a small plaque phenotype (Blasco and Moss, 1992; Engelstad and Smith, 1993; Wolffe et al., 1993). Interestingly, both F13 and B5 are among several IEV proteins that undergo endocytic recycling during the vaccinia replication cycle (Husain and Moss,

2003, 2005; Ward and Moss, 2000), perhaps explaining why the wrapping membrane derives from the endosomal membrane, in addition to the TGN. F13 is inserted post-translationally into the membrane through palmitoylation at cysteine 185 and 186 and exhibits similarity to phospholipase D (Grosenbach et al., 1997; Husain and Moss, 2003). Its phospholipase activity is required to induce the formation of post-Golgi vesicles that are precursors of the vaccinia IEV membrane (Husain and Moss, 2002; Ponting and Kerr, 1996). The other IEV proteins are then recruited to these vesicles, with A34 required for B5 and A33 incorporation, and A33 chaperoning A36 (Earley et al., 2008; Husain and Moss, 2002; Perdiguero et al., 2008; Wolffe et al., 1998). In recent years, it has additionally been shown that F12 and E2 form a complex that is required for efficient wrapping (Dodding et al., 2009; Domi et al., 2008).

1.1.4 Egress

After their assembly is complete, IEV are transported to the cell periphery on microtubules by kinesin-1 (Figure 1.2) (Geada et al., 2001; Hollinshead et al., 2001; Moss and Ward, 2001; Rietdorf et al., 2001). A36 is responsible for microtubule-based transport of the virus as it interacts directly with the kinesin-1 light chain through a bipartite tryptophan-based motif (Dodding et al., 2011; Ward and Moss, 2004). Interestingly, F12-E2 is maintained on the IEV during their microtubule-based transport and F12 has been implicated in the transport process (Dodding et al., 2011; Morgan et al., 2010; van Eijl et al., 2002). It is possible, however, that F12-E2 functions to restrict A36-mediated kinesin-1 recruitment, as the binding sites of F12 and KLC on A36 overlap (Dodding et al., 2011; Johnston and Ward, 2009; Ward and Moss, 2004). It may be that F12 prevents premature IEV transport before wrapping is complete, though why the complex would be maintained at the virus during microtubule-dependent transport is unclear.

Once the virion reaches the cell surface the outer IEV membrane fuses directly with the plasma membrane, however, the precise mechanism of how this process occurs remains to be established. Nonetheless, it exposes the virus on the cell surface, which when attached to the plasma membrane is referred to as a cell-associated enveloped virion (CEV). In contrast, if it is released it becomes an extracellular enveloped virion (EEV) (Figure 1.2) (Roberts and Smith, 2008). CEV are important for cell-cell transmission and induce the formation of actin tails, which is described in 1.3.3 (Blasco

and Moss, 1992; Cudmore et al., 1995; Stokes, 1976; van Eijl et al., 2000). Actin tails propel CEV into surrounding uninfected cells, whilst EEV are thought to mediate the long range spread of the virus in cell culture and *in vivo* (Boulter and Appleyard, 1973; Payne, 1980).

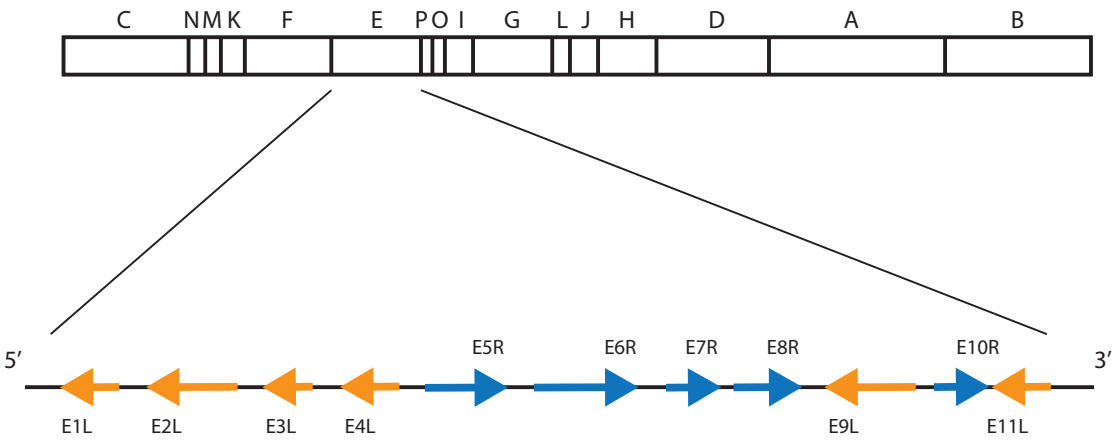

Figure 1.1 The vaccinia genome

Vaccinia virus has a linear, double-stranded DNA genome with covalently closed ends. The genome is divided into 16 fragments (A-P) according to the HindIII restriction map. The ORFs within each fragment are then assigned a number as indicated, as well as an L or R, depending on the direction of transcription. The ORFs of the E fragment are shown as an example.

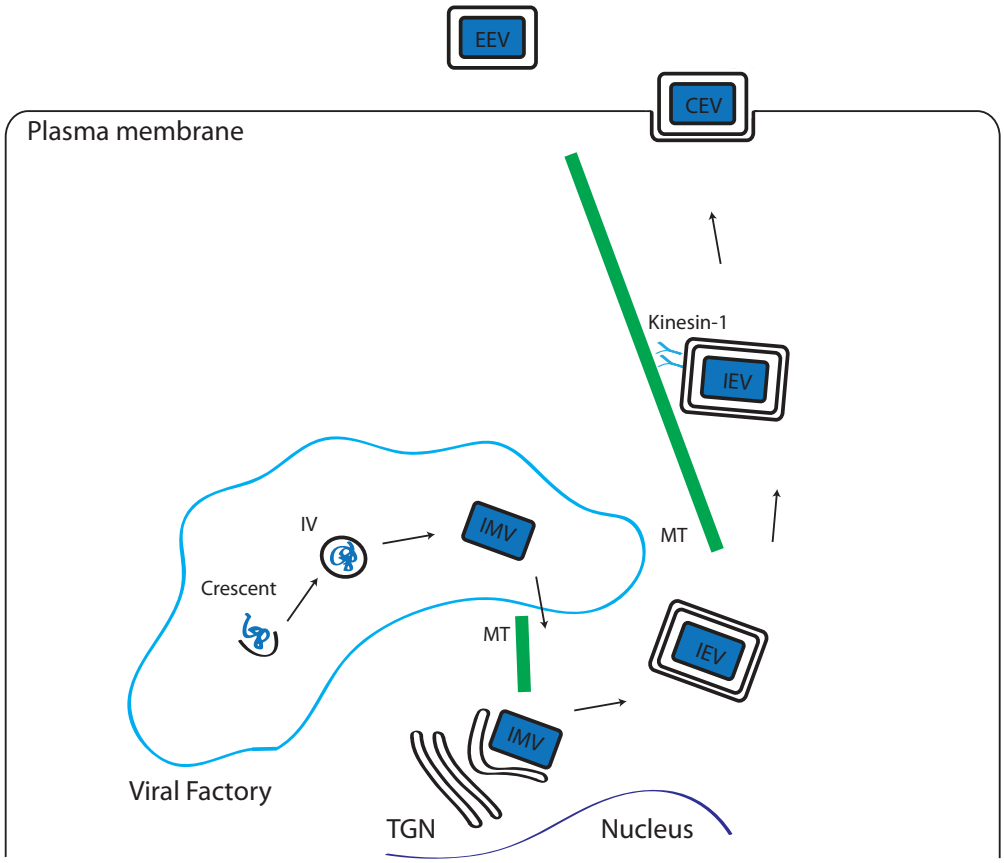

Figure 1.2 The vaccinia replication cycle

Vaccinia virus undergoes its entire replication cycle in the cytoplasm of the cell. After DNA replication, DNA and lipids form crescents within the viral factory. These develop into immature virions (IV), which progress into the brick-shaped intracellular mature virion (IMV). A small number of IMV are then transported from the viral factory on microtubules, where they become encased in a double membrane modified by the inclusion of several viral proteins. The resulting virion is referred to as an intracellular enveloped virion (IEV), and is subsequently transported in a microtubule-dependent manner to the periphery of the cell by kinesin-1. The outer viral membrane then fuses directly with the plasma membrane, if the virus remains at the surface of the cell it is referred to as a cell-associated enveloped virion (CEV), however, if released it is termed an extracellular enveloped virion (EEV).

1.2 The actin cytoskeleton

Actin is a highly abundant, and conserved protein, which forms from monomers (G-actin) into characteristic filaments (F-actin) through self-polymerisation (Dominguez and Holmes, 2011; Erickson, 2007; Firat-Karalar and Welch, 2011). The capacity to undergo reversible polymerisation is essential for a wide-array of cellular processes from cell migration and actin-based motility of pathogens, to trafficking and cytokinesis. Consequently, actin polymerisation requires tight regulation in both a spatial and temporal manner (Anitei and Hoflack, 2012; Pollard and Cooper, 2009; Ridley, 2011).

1.2.1 Actin

G-actin is a 42 kDa protein that assembles into filaments comprising two chains of monomers wrapped in a helical fashion (Hanson and Lowy, 1964). To form the many actin-based structures within cells, the filament must be organised in different ways (Figure 1.3) (Chhabra and Higgs, 2007; Pellegrin and Mellor, 2007). In lamellipodia, where actin filaments are thought to provide the force to drive motile cells forward, the filaments form a dense meshwork that is highly crosslinked (Abercrombie et al., 1971; Small et al., 2002; Svitkina and Borisy, 1999). A similar structure is formed in lamellae, but consistent with their location behind the protruding lamellipodia, the actin meshwork is thicker and less dynamic (Abercrombie et al., 1970b, 1971; Chhabra and Higgs, 2007). Other protrusive structures are actin-rich ruffles, of which two types exist, peripheral and dorsal. Peripheral ruffles form at the leading edge to regulate cell migration and may reflect lamellipodia that have lost attachment to the substrate (Abercrombie et al., 1970c). In contrast, dorsal ruffles form a circular morphology on the dorsal surface that is associated with receptor internalisation (Abella et al., 2010; Abercrombie et al., 1970a). The force provided by actin polymerisation is also used to sculpt the plasma membrane to envelope extracellular particles during phagocytic uptake, and in a similar fashion during endocytosis (Jaumouille and Grinstein, 2011; Mooren et al., 2012). Actin can additionally form a highly bundled arrangement, which is required for the thin protrusive filopodia spikes, or microspikes if they emanate from lamellipodia (Chhabra and Higgs, 2007; Lewis and Bridgman, 1992; Rottner et al., 1999), as well as stress fibres, where bundled filaments of actin interact with myosin II to form contractile arrays (Pellegrin and Mellor, 2007). Finally, actin is required for the

specialised adhesive structures, podosomes, which degrade extracellular matrix to allow migration through tissues, and for invadopodia, which promote invasion and migration of cancer cells (Figure 1.3) (Murphy and Courtneidge, 2011).

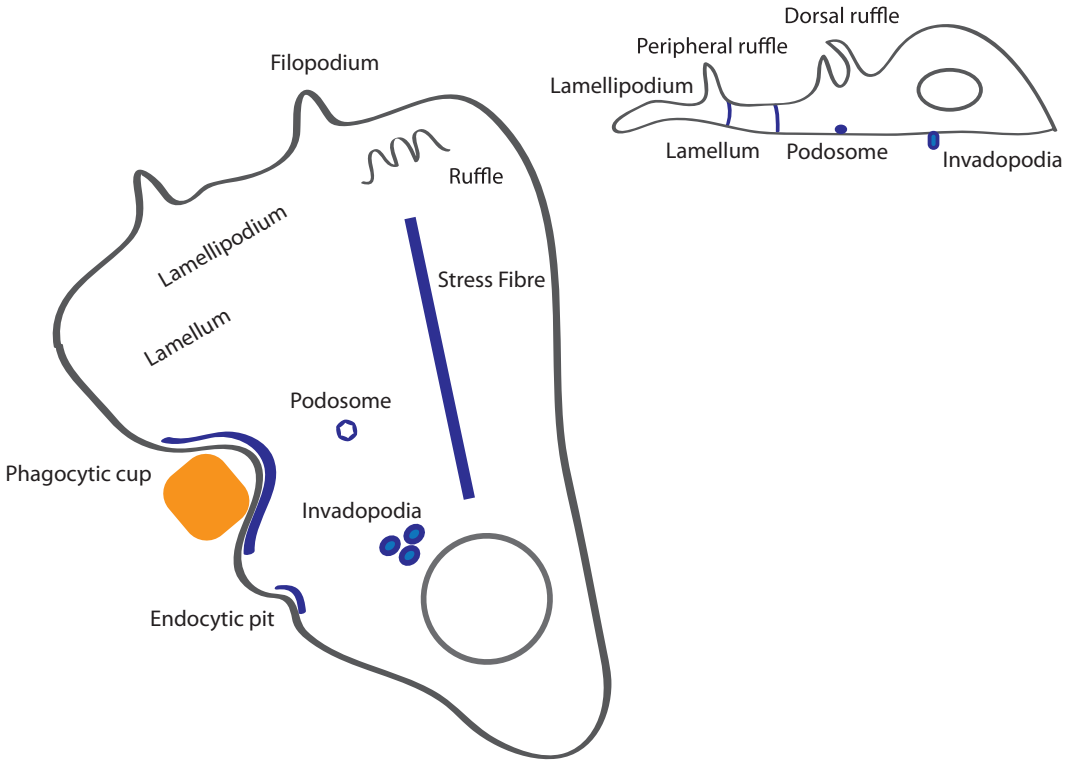

Figure 1.3 Actin-based structures within the cell

Schematic depicting the actin-based structures found within the cell and their location. The left hand image is a bird's eye view of the cell and the right hand image is a side view of the same cell. The schematic is adapted from Chhabra and Higgs, 2007.

1.2.2 Actin polymerisation

In vitro, G-actin monomers can spontaneously self-assemble into polarised filaments (Panner and Honig, 1967; Woodrum et al., 1975). The polarised filament consists of a fast growing plus end and a slower growing minus end, which are distinguished by their different structural characteristics and thus kinetic properties (Goley and Welch, 2006; Pollard and Borisy, 2003). The plus end of the filament is referred to as the barbed end and the minus, the pointed end, due to the appearance of the filament in transmission electron microscopy following decoration with myosin (Woodrum et al., 1975).

The rate-limiting step in actin polymerisation is the establishment of nuclei, which are three actin monomers that act as a 'seed' from which a filament can rapidly assemble (Nishida and Sakai, 1983). In line with this, biochemical analysis showed that crosslinking actin monomers to form trimers, was more effective than dimers or higher-order oligomers at promoting actin polymerisation (Gilbert and Frieden, 1983). After the seed has formed, which is referred to as the nucleation phase, actin polymerisation enters an elongation phase. At this stage, monomers are added to either end of the filament, but with a strong bias towards the barbed end (Woodrum et al., 1975). The rate of growth is dependent on the concentration of free G-actin monomers in the solution and thus, as their concentration is reduced, a steady state is reached where there is no net change in filament length (Pollard, 1983). The concentration of G-actin monomers at this state is known at the critical concentration (C_C) and G-actin will only assemble into filaments when above this value (Figure 1.4). The C_C required at the pointed end is 7 times higher than that at the barbed end explaining the bias for unidirectional filament growth (Pollard and Borisy, 2003; Wegner and Isenberg, 1983).

The dynamics of actin assembly and disassembly are regulated by the inherent structural asymmetry of actin, as well as by the hydrolysis of the nucleotide bound to the actin monomer (Rafelski and Theriot, 2004). The nucleotide bound to actin can exist in three states, ATP, ADP and ADP-Pi (Korn et al., 1987). G-actin preferentially binds ATP, whilst F-actin promotes the hydrolysis of ATP and its conversion to ADP-Pi (Blanchoin and Pollard, 2002; Carlier and Pantaloni, 1986). This event is irreversible and in the context of the filament leads to a 'cap' of ADP-Pi intermediates at the barbed end of newly assembled filaments (Carlier, 1988). The phosphate is removed slowly

over time resulting in ADP-F-actin, which can induce a conformational change that increases the flexibility of the actin filament resulting in disassembly (Janmey et al., 1990; Orlova and Egelman, 1992). Collectively, this leads to the net incorporation of ATP-actin monomers at the barbed end and dissociation of ADP-actin monomers from the pointed end, in a process termed actin treadmilling (Figure 1.4) (Fujiwara et al., 2002; Wegner, 1976). As well as studies *in vitro*, there is considerable evidence that actin treadmilling occurs *in vivo* (Symons and Mitchison, 1991; Theriot and Mitchison, 1991; Wang, 1985; Watanabe and Mitchison, 2002). Arguably, the most compelling data has come from advanced microscopy techniques including photo-bleaching, which revealed the incorporation of fluorescent actin in regions adjacent to the plasma membrane and its rearward flow within the cell (Lai et al., 2008; Millius et al., 2012; Watanabe and Mitchison, 2002; Waterman-Storer et al., 1998).

1.2.3 Regulation of actin polymerisation

Despite evidence for treadmilling *in vivo*, the slow rate measured *in vitro* cannot solely account for the rapid rate of cell migration. Thus, additional regulatory proteins are necessary to enhance the rate of actin polymerisation in cells (Bonder et al., 1983; Pollard and Borisy, 2003; Wang, 1985). Seminal studies detailing the minimum requirements of Arp2/3-dependent actin-based motility have been established through the reconstitution of *Listeria* propulsion *in vitro*, using purified proteins (Cameron et al., 1999; Loisel et al., 1999; Welch et al., 1997b; Welch et al., 1998). These studies found that the key proteins required are profilin, ADF/Cofilin, capping protein, as well as a nucleator i.e. Arp2/3 and a nucleation promoting factor (Figure 1.5).

1.2.3.1 Profilin

Profilin is conserved in all eukaryotic cells, and forms a 1:1 complex with G-actin (Carlsson et al., 1976). It prevents spontaneous actin polymerisation *in vitro* and is a key regulator of actin polymerisation *in vivo* (Carlsson et al., 1977). Profilin facilitates the nucleotide exchange of actin monomers, decreasing the affinity of actin for ADP and promoting an open conformation that permits exchange with ATP from the surrounding environment (Blanchoin and Pollard, 1998; Lu and Pollard, 2001; Porta and Borgstahl, 2012; Selden et al., 1999). Profilin acts to sequester ADP-actin, and inhibits its binding to the ends of an actin filament. Thus, in a cell, profilin provides a

large pool of ATP-bound G-actin ready for rapid filament assembly. Profilin-actin-ATP complexes can only be added to the barbed end and thus filament growth occurs in a manner consistent with actin treadmilling (Figure 1.5) (Pollard and Cooper, 1984; Tilney et al., 1983).

1.2.3.2 ADF/Cofilin

ADF/Cofilin, which is also highly conserved, can interact with both G- and F-actin and promotes filament disassembly through severing as well as by increasing the dissociation of subunits from the pointed end (Andrianantoandro and Pollard, 2006; Blanchoin and Pollard, 1998; Carlier et al., 1997). ADF/Cofilin preferentially binds to the actin filament and more specifically ADP-Pi-F-actin, causing a localised twist that weakens the longitudinal interactions between the monomers (Galkin et al., 2011; McGough et al., 1997; Okreglak and Drubin, 2007). ADF/Cofilin also promotes the release of Pi, leading to the dissociation of the resultant ADP-actin from the filament (Blanchoin and Pollard, 1999). In this manner, it is thought that ADF/Cofilin acts as a molecular timer to sever older actin filaments. ADF/Cofilin supports actin polymerisation in two ways, firstly by increasing the number of uncapped barbed ends, and secondly by increasing the pool of free G-actin monomers available for assembly (Figure 1.5) (Bravo-Cordero et al., 2013).

1.2.3.3 Capping protein

Capping protein, which was first identified in muscle but was later shown to be universal in eukaryotes, is a heterodimer of alpha and beta subunits (Isenberg et al., 1980). Capping protein binds to the end of actin filaments to prevent both the addition and loss of monomers (Cooper and Sept, 2008; Wear et al., 2003). Capping regulates the length of the actin filament, which is important for force generation, as shorter filaments push on the membrane more efficiently (Mogilner and Oster, 1996; Pollard and Borisy, 2003). Capping protein can also regulate the rate of actin polymerisation by a mechanism termed the funnelled treadmilling model (Figure 1.5) (Carlier and Pantaloni, 1997; Pantaloni et al., 2000; Pantaloni et al., 2001). In this model, capping at the barbed end promotes disassembly from the pointed end. This enhances the pool of free actin, the concentration of which is proportional to the rate of assembly (Pantaloni et al., 2000).

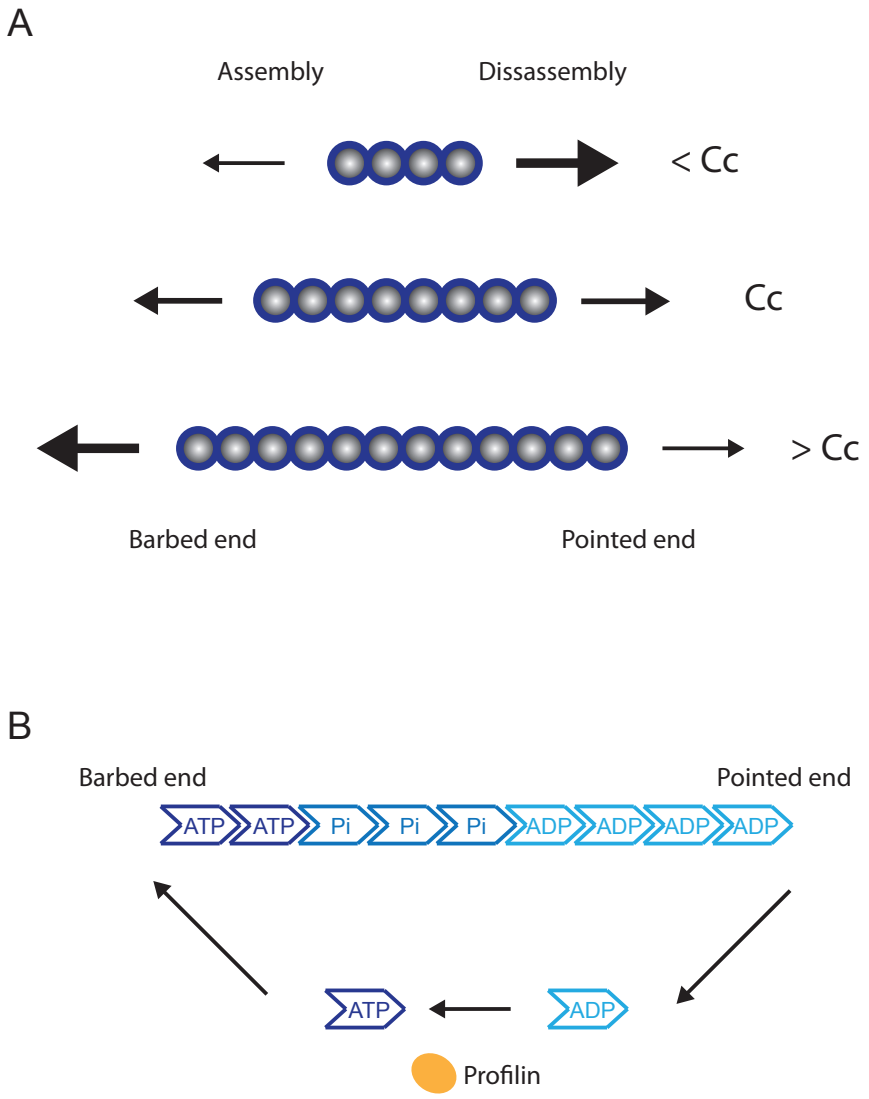

Figure 1.4 Actin treadmilling

A Schematic depicting filament growth in different conditions. When the amount of G-actin is below the critical concentration (Cc) the filament shrinks, whereas if it is above the Cc the filament grows. If the amount is equivalent to the Cc, the filament length remains constant and a steady state is achieved, with the filament treadmilling. **B** Schematic showing actin treadmilling, ATP-actin is added at the barbed end and undergoes hydrolysis to ADP-Pi, the phosphate is slowly released promoting the dissociation of ADP from the pointed end. Schematic is adapted from Pantaloni et al., 2001.

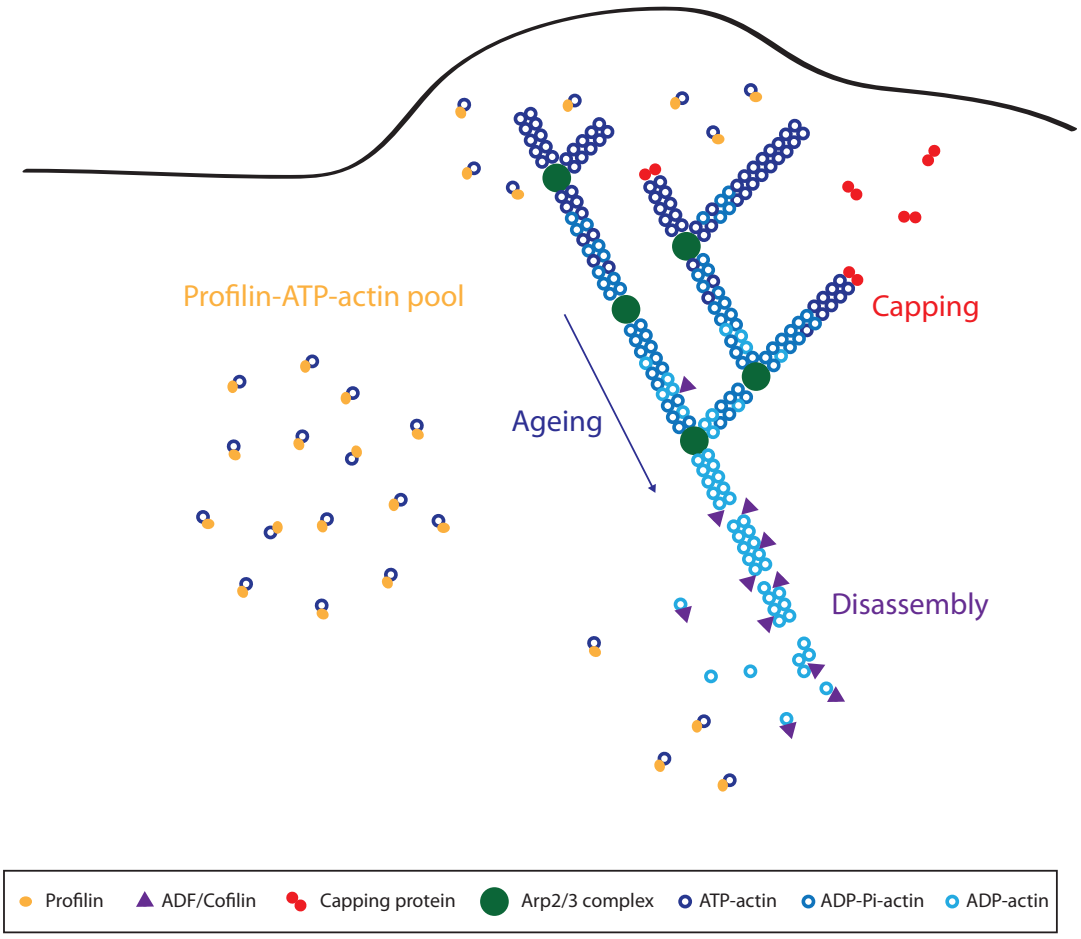

Figure 1.5 Actin-binding proteins

The actin-binding proteins essential for Arp2/3-dependent actin-based motility include profilin, ADF/cofilin and capping protein. Profilin binds to G-actin and promotes the exchange of ADP for ATP. This creates a pool of ATP-actin monomers for incorporation into filaments. ADF/cofilin promotes severing of the filament and also promotes release of Pi from ADP-Pi, leading to dissociation of ADP-actin from the pointed end. Capping protein additionally binds to the barbed ends of filaments controlling filament length and the dissociation of filaments from the pointed end. Schematic is adapted from Pollard and Borisy, 2003.

1.2.4 Actin filament nucleators

As previously discussed the formation of the nucleating seed is the rate-limiting step in actin polymerisation, thus, a number of proteins have evolved to overcome this kinetically unfavourable event. These proteins are called nucleators and consist of three major classes, formins, WH2-domain containing nucleators and the Arp2/3 complex (Campellone and Welch, 2010).

1.2.4.1 Formins

Formins elicit both an actin nucleation and an actin elongation activity. However, their mechanism of action *in vivo* is not fully elucidated (Paul and Pollard, 2008; Sagot et al., 2002). Formins are characterised by the presence of two conserved domains, known as formin homology 1 and 2 (FH1 and FH2) (Li and Higgs, 2003; Pruyne et al., 2002; Romero et al., 2004). The FH2 domain is thought to compete with capping protein for binding at the barbed end and can facilitate the addition of an actin monomer to elongate an unbranched actin filament (Otomo et al., 2005; Pruyne et al., 2002). The FH2 domain forms a homodimer with a ring organisation that can bind in a closed conformation to cap the filament, or an open conformation that promotes actin monomer addition (Otomo et al., 2005). The FH1 domain, which is adjacent to the FH2 domain, binds profilin to supply the FH2 domain with G-actin for rapid elongation (Courtemanche and Pollard, 2012; Paul and Pollard, 2008).

1.2.4.2 WH2-domain containing nucleators

As the name suggests, the WH2-domain nucleators are so defined as they contain at least one WH2 (WASP homology 2) domain, which is one of the most abundant actin-binding motifs (Symons et al., 1996). The WH2-domain containing nucleators are less well characterised in comparison to the formins and the Arp2/3 complex but are known to include, Spire, leiomoden proteins, Cordon-Blue (COBL) and JMY (Ahuja et al., 2007; Conley et al., 2001; Firat-Karalar et al., 2011; Quinlan et al., 2005). Spire contains 4 tandem WH2 domains and creates a nucleus through tethering three actin monomers in a side-by-side or longitudinal arrangement (Ducka et al., 2010; Quinlan et al., 2005). Spire is also able to cap the pointed end to inhibit disassembly of the actin

filament (Quinlan et al., 2005). The leiomoden family, which are specifically expressed in muscle, have three distinct domains that can each interact with an actin monomer, an N-terminal actin-binding domain followed by a leucine rich repeat (LRR) region and finally the WH2 domain (Conley et al., 2001). They are also thought to bind and promote the formation of an actin trimer, from which actin can polymerise (Chereau et al., 2008). COBL contains 3 WH2 domains and again promotes a trimeric arrangement of actin (Ahuja et al., 2007; Husson et al., 2011; Qualmann and Kessels, 2009), while JMY has 3 WH2 domains and a linker region that function in a manner reminiscent of spire (Firat-Karalar et al., 2011).

1.2.5 The Arp2/3 complex

The Arp2/3 complex was first purified from *Acanthamoeba castellanii*, on a profilin affinity column (Machesky et al., 1994). The complex is 220 kDa in size and consists of 7 subunits, Arp2, Arp3 and as they are now defined ARPC1-5 (Figure 1.6) (Goley and Welch, 2006). Arp2 and Arp3 bear structural similarity to actin and were thus proposed to mimic an actin dimer, serving as the seed for nucleation (Kelleher et al., 1995). In addition to its role as a nucleator, the Arp2/3 complex also regulates the organisation of actin as it generates a branched network (Mullins et al., 1998; Svitkina and Borisy, 1999). This is achieved through binding to the side of an existing filament, and promoting the formation of a nascent filament at an approximate 70-degree Y branch angle (Goley and Welch, 2006). The complex caps the nascent filament at the pointed end, allowing elongation from the barbed end. However, the molecular basis of the Y branch is not fully understood, as structural studies have failed to capture an active form of the complex (Robinson et al., 2001). Instead homology modelling and electron tomography, have suggested that ARPC2 and ARPC3 form contacts with the existing actin filament, whilst Arp2 and Arp3 associate with the pointed end of the nascent filament (Figure 1.6) (Beltzner and Pollard, 2004; Rouiller et al., 2008).

To date the only known direct inhibitor of the Arp2/3 complex is coronin (Cai et al., 2007; Humphries et al., 2002). Coronin can displace the Arp2/3 complex from Y branches *in vitro* and indirectly activates cofilin to promote recycling of both actin and the Arp2/3 complex through severing and disassembly of older actin filaments (Brieher et al., 2006; Cai et al., 2008; Cai et al., 2007; Gandhi et al., 2009; Kueh et al., 2008).

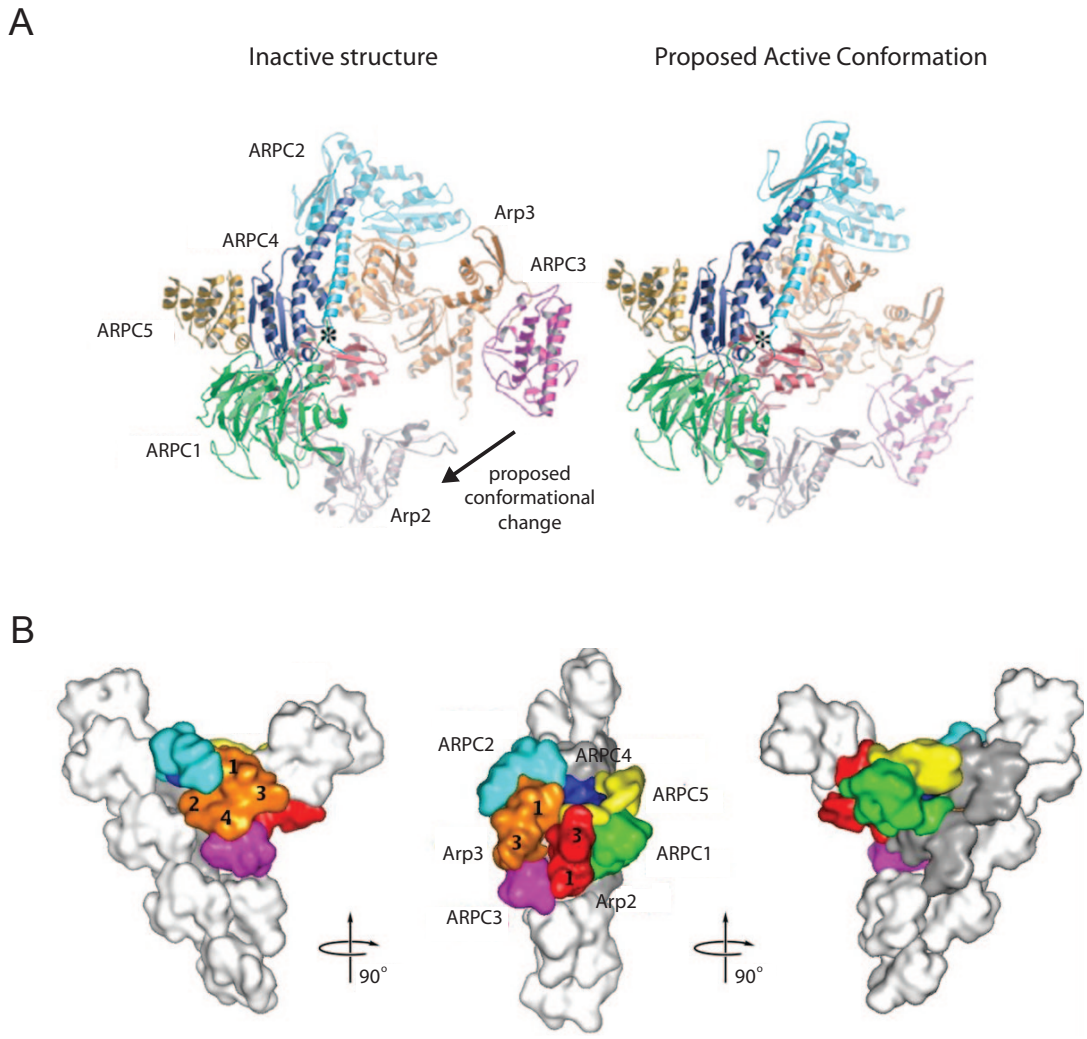

Figure 1.6 Structure of the Arp2/3 complex

A A model of the crystal structure of the inactive Arp2/3 complex, along with the proposed active conformation. In the inactive structure, the Arp2 and Arp3 subunits are not close enough to eachother to act as the seed for filament nucleation. © Robinson et al., 2001. Originally published in *Science* 294:1679-84. **B** Representation of the best-fit molecular envelope of the Arp2/3 complex at a branchpoint derived from electron tomograms. Actin filaments are shown in white or grey. The three views are related by 90-degree clockwise rotations. © Rouiller et al., 2008. Originally published in *Journal of Cell Biology* 180:887-95.

1.2.6 Arp2/3 complex nucleation promoting factors

In isolation, the Arp2/3 complex is an extremely inefficient nucleator of actin filaments, but can be activated by binding so called nucleation promoting factors (NPFs) (Figure 1.7) (Ma et al., 1998b; Mullins et al., 1998; Rohatgi et al., 1999; Welch et al., 1998). The NPFs are regulated by signal-transduction pathways and coordinate actin polymerisation in both a spatial and temporal manner.

The largest group of mammalian NPFs (class I) have a conserved C-terminal WCA domain that binds actin and also promotes Arp2/3 complex activation (Figure 1.7). In contrast, the N-terminus of class I NPFs are divergent in their sequence, regulation and function (Figure 1.7) (Stradal and Scita, 2006). The WCA domain consists of a WH2 domain that binds to G-actin and a central and acidic region that bind the Arp2/3 complex (Chereau et al., 2005; Marchand et al., 2001; Panchal et al., 2003). The simplest model of WCA domain function is that it assembles a trimer of Arp2, Arp3 and actin that creates the seed for filament nucleation. However, it is likely that the mechanism is more complex. Firstly, NPFs have different activation potentials, but this does not correlate with their affinity for either the Arp2/3 complex or G-actin (Panchal et al., 2003; Zalevsky et al., 2001). Secondly, kinetic modelling has indicated that there is a distinct activation step that follows the formation of the NPF-Arp2/3-actin complex (Zalevsky et al., 2001). Finally, tethering the WH2 domain to the Arp2/3 complex is not sufficient for its activation, suggesting that the CA region plays an additional function (Goley et al., 2004). In fact, it appears that it promotes structural rearrangement of the Arp2/3 complex, to bring Arp2 and Arp3 in closer proximity (Goley et al., 2004; Rodal et al., 2005). Thus, a model exists whereby the acidic region binds to the Arp2/3 complex, while the central region promotes conformational change in the complex. The WH2 and central region subsequently present G-actin, creating the seed of filament nucleation.

As seen with actin, the Arp2/3 complex is also regulated by nucleotide hydrolysis, with its conformation altered upon nucleotide binding (Goley et al., 2004). Both Arp2 and Arp3 bind ATP, and hydrolysis of ATP by Arp2, but not Arp3 is required for actin polymerisation (Dayel et al., 2001; Le Clainche et al., 2001). The interaction of Arp2 with ATP requires the presence of a WCA domain, suggesting there is cooperation between NPFs, Arp2/3 and ATP (Le Clainche et al., 2001). Hydrolysis has also been

shown to promote debranching and consequent recycling of the Arp2/3 complex, to regulate the temporal events of branching (Goley et al., 2004; Martin et al., 2006; Martin et al., 2005; Nolen et al., 2004; Zencheck et al., 2009). Another level of regulation is provided by threonine and tyrosine phosphorylation, which is required for the nucleating activity of the Arp2/3 complex *in vitro* (LeClaire et al., 2008). In the absence of phosphorylation, the NPF is still able to engage with the complex, however, WCA-mediated activation does not occur (Narayanan et al., 2011). Molecular dynamic simulations suggest that phosphorylation induces a conformation change in the Arp2/3 complex that facilitates its activation by the WCA (Narayanan et al., 2011). Due to the importance of the NPFs in Arp2/3 complex activation, their regulation and function will be described briefly in the following sections. N-WASP will be described in more detail, as it has the most relevance to my work.

1.2.6.1 WAVE

There are three mammalian isoforms of WAVE (1-3), which exist in complex with HSPC300, Abi1, Nap1 and Sra1 (Eden et al., 2002; Gautreau et al., 2004; Ismail et al., 2009). The WAVE protein is active, but the complex controls its ability to regulate Arp2/3 complex activation. Removal of any subunit results in protein degradation, or loss of the localisation of the other subunits, demonstrating that the WAVE complex functions as a combined unit (Innocenti et al., 2004; Steffen et al., 2004). The main prescribed function of WAVE is in plasma membrane protrusion and in cell motility.

1.2.6.2 WASH

WASH contains multiple domains that likely mediate the formation of a multiprotein complex. These include the WCA domain, a WASH homology domain (WAHD1) and tubulin-binding region (Figure 1.7). WASH interacts with capping protein and FAM21, which confers its localisation at endosomes (Derivery et al., 2009; Gomez and Billadeau, 2009). Consequently, WASH has been shown to function at both early and recycling endosomes (Derivery et al., 2009; Duleh and Welch, 2010; Gomez and Billadeau, 2009).

1.2.6.3 WHAMM and JMY

WHAMM and JMY both have a WCA domain with adjacent polyproline motifs and a central region predicted to form coiled-coils, but vary in their N-termini (Figure 1.7). The WCA domain of WHAMM contains two WH2 domains whereas JMY has three. It is the three WH2 domains and an additional actin monomer binding linker that allow JMY to nucleate actin assembly even in the absence of the Arp2/3 complex (Zuchero et al., 2009). JMY appears to function in the nucleus and at lamellipodia, whereas WHAMM localises to the cis-Golgi and tubulovesicular membranes and is implicated in Golgi morphology and anterograde trafficking (Campellone et al., 2008b; Zuchero et al., 2009).

1.2.6.4 Cortactin

Cortactin is a class II NPF, which lacks a WH2 domain but contains a repetitive sequence that mediates its interaction with F-actin. It has been suggested that in addition to binding and activating Arp2/3 via an acidic region, the interaction with F-actin additionally enables weak activation of the Arp2/3 complex (Uruno et al., 2001; Weaver et al., 2001). The protein contains a polyproline-rich region with regulatory phosphorylation sites and SH3 domains that promote its interaction with many proteins including WIP and N-WASP (Figure 1.7) (Kinley et al., 2003; Weaver et al., 2002). Cortactin and N-WASP can bind simultaneously to the Arp2/3 complex, and whilst N-WASP is released, cortactin remains associated at the branchpoint preventing Arp2/3 complex dissociation (Egile et al., 2005; Weaver et al., 2002; Weaver et al., 2001). Cortactin can also enhance N-WASP-mediated activation of the Arp2/3 complex, which is described in the following section (Martinez-Quiles et al., 2004; Tehrani et al., 2007). The available evidence suggests that the primary role of cortactin is not in Arp2/3 complex activation but in supporting N-WASP, as well as promoting branchpoint stability.

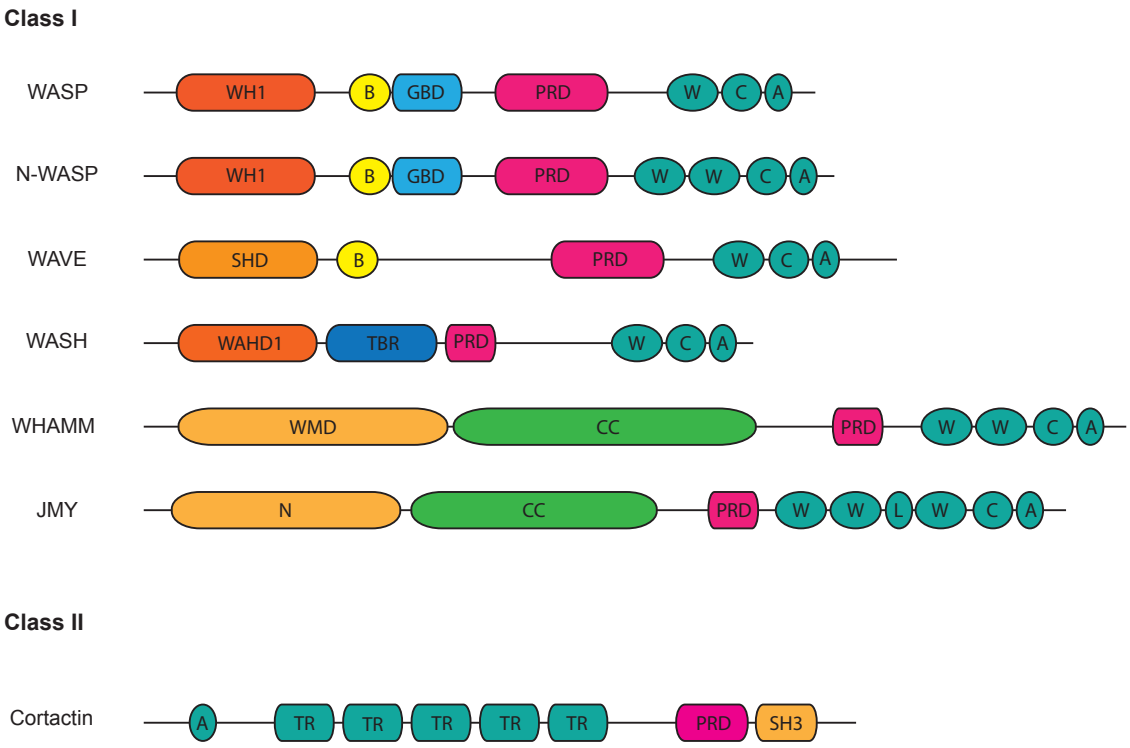

Figure 1.7 Nucleation promoting factors

The nucleation promoting factors are split into 2 classes, with the presence of a WH2 domain being the distinguishing factor. The NPFs are multidomain proteins and thus can interact with several binding partners that modify their activity, function and localisation. The domains are as follows WH1 (WASP homology 1), B (Basic region), GBD (GTPase binding domain), PRD (Polyproline-rich domain), WCA (WASP homology 2, central and acidic region), SHD (Src homology domain), WADH1 (WASH homology domain), TBR (Tubulin binding region), WMD (WHAMM membrane-interaction domain), CC (Coiled-coil), N (N-terminal region), L (Linker), A (Acidic region), TR (Tandem repeats) and SH3 (Src homology 3). Schematic is adapted from Campellone, 2010.

1.2.7 N-WASP regulation

N-WASP is conserved in eukaryotes and expressed in most cell types (Miki et al., 1996; Snapper et al., 2001). This is in contrast to the closely related WASP, which was identified first but is restricted to haematopoietic cell types (Derry et al., 1994; Symons et al., 1996). WASP/N-WASP exhibit similar mechanisms of regulation and thus this section will focus predominantly on N-WASP.

1.2.7.1 Autoinhibition

N-WASP is a multidomain protein that contains an N-terminal WASP homology 1 domain (WH1), a basic region (B), a Cdc42/Rac-interactive binding (CRIB) motif and autoinhibitory motif (AI) that is collectively termed the GTPase binding domain (GBD), and finally a polyproline-rich domain (PRD) adjacent to the WCA (Figure 1.7). N-WASP exists in an autoinhibited conformation that is maintained by intramolecular interactions between the WCA domain and the AI motif of the GBD (Figure 1.8) (Kim et al., 2000; Miki et al., 1996; Prehoda et al., 2000; Rohatgi et al., 2000). This inactive conformation is also stabilised by interaction with WIP (Anton et al., 2007; Ho et al., 2004). N-WASP thus requires activation, to promote conformational change and allow binding of the Arp2/3 complex and G-actin to the WCA.

Multiple signals contribute to the activation of N-WASP. One of the first characterised activators was Cdc42, which belongs to the Rho family of GTPases. These proteins act as molecular switches and interconvert between an active GTP-bound and inactive GDP-bound conformational state (Hall, 2012). The conversion between theses two states is regulated by guanine-nucleotide exchange factors (GEFs), GTPase activation proteins (GAPs) and guanine-nucleotide-dissociation inhibitors (GDIs). Identification of GEF function was first discovered though characterisation of Dbl, which activates Cdc42 (Hart et al., 1991), whereas, the first GAP identified was the product of the *bcr* gene, which stimulates intrinsic hydrolysis of Rac (Diekmann et al., 1991). To date, 67 BH (bcr homology domain) GAPs and 71 DH (Dbl homology domain) GEFs have been identified in the human genome (Hall, 2012). A second family of GEFs have also been characterised based on DOCK, of which 11 currently exist (Meller et al., 2005). Finally,

3 human GDIs have been identified, which prevent the dissociation of GDP from the Rho protein (Matsui et al., 1990).

Active GTP-bound Cdc42 can bind to the GBD of N-WASP, inducing a conformational change to free the WCA domain (Figure 1.8) (Kim et al., 2000). The GBD cannot bind to both Cdc42 and the WCA domain simultaneously, suggesting that Cdc42 activates N-WASP by competing at this binding site (Kim et al., 2000; Miki et al., 1998). Therefore, the favoured model is that when Cdc42 engages with the GBD, the WCA domain is free to interact with and activate the Arp2/3 complex (Kim et al., 2000). PI(4,5)P_2 can synergise with Cdc42 to potently activate N-WASP, as it binds the basic domain, which contributes to the stability of the autoinhibited conformation (Figure 1.8) (Papayannopoulos et al., 2005; Prehoda et al., 2000; Rohatgi et al., 2000; Rohatgi et al., 1999). In line with this, addition of a peptide comprising the GBD alone is not sufficient to maximally inhibit N-WASP, with a peptide including the GBD and basic region required (Prehoda et al., 2000).

The polyproline rich region that links the GBD to the WCA is the site of interaction for many SH3 containing proteins including Nck, Grb2, Toca-1, FBP-17, Abi1, syndapin, SNX9 and Abp1 (Figure 1.8) (Carlier et al., 2000; Ho et al., 2004; Innocenti et al., 2005; Kessels and Qualmann, 2004; Pinyol et al., 2007; Rohatgi et al., 2001; Shin et al., 2007; Takano et al., 2008). Although the polyproline-rich domain does not directly participate in the intramolecular interaction, binding at this site can promote destabilisation to release the WCA (Rohatgi et al., 2001).

Each of the factors mentioned in this section can activate the Arp2/3 complex, but multiple inputs can be integrated to promote more efficient or enhanced activation, as well as providing greater control. For example, Nck and PI(4,5)P_2 synergise to activate N-WASP in a Cdc42-independent manner, whilst Grb2 functions with Cdc42 to enhance activation (Carlier et al., 2000; Rohatgi et al., 2001). As discussed WIP stabilises the autoinhibited conformation of N-WASP, and it has also been shown to inhibit the ability of N-WASP to activate the Arp2/3 complex *in vitro* (Ho et al., 2004; Martinez-Quiles et al., 2001). Both PI(4,5)P_2 and Toca-1 can individually and synergistically promote activation of N-WASP by Cdc42 in the presence of WIP (Bu et al., 2010; Ho et al., 2006; Ho et al., 2004; Martinez-Quiles et al., 2001; Takano et al.,

2008). Altogether, this suggests that WIP spatially restricts the activation of N-WASP within cells, providing a further degree of regulation to these signalling networks.

Phosphorylation has also been shown to regulate the activation of WASP/N-WASP. Phosphorylation at tyrosine 291 in the GBD decreases its affinity for the WCA domain of WASP (Cory et al., 2003; Cory et al., 2002; Torres and Rosen, 2003), with a similar effect observed for the equivalent tyrosine 256 in N-WASP (Torres and Rosen, 2006). It is thought that after release of WASP/N-WASP autoinhibition by active Cdc42, phosphorylation by Src family kinases results in prolonged activation. Therefore, phosphorylation could act to temporally regulate the signalling network (Torres and Rosen, 2003).

1.2.7.2 Oligomerisation of N-WASP enhances its ability to active Arp2/3

It has been proposed that N-WASP functions more efficiently in an oligomeric complex, achieved by multivalent binding sites or multimerisation of N-WASP binding proteins (Campellone et al., 2008a; Padrick et al., 2008; Torres and Rosen, 2006). Additionally, dimerisation of the WCA domain increases the affinity of the NPF for the Arp2/3 complex and the efficiency of actin nucleation (Figure 1.8) (Higgs and Pollard, 2000; Padrick et al., 2008). The molecular basis of this increased efficiency is due to the discovery of two binding sites for the WCA in the Arp2/3 complex (Padrick et al., 2011; Ti and Pollard, 2011). The high affinity canonical binding site comprises Arp3 and ARPC3 (Xu et al., 2012), whilst the other is the cortactin-binding site in the Arp2/3 complex, comprising Arp2 and ARPC1 (Padrick et al., 2008; Padrick et al., 2011). It appears that maximal activation of the Arp2/3 complex requires the delivery of actin monomers to Arp2/3 by both WCA domains, although delivery to Arp3 is more critical for actin polymerisation (Padrick et al., 2011). In line with these findings, that indicate two WCA domains interact with each Arp2/3 complex, antibody-mediated clustering of Nck SH3 domains at the plasma membrane showed the ratio of N-WASP to Arp2/3 was 2:1 in cells (Figure 1.8) (Ditlev et al., 2012).

The WH2 domain of the WCA can also mediate attachment of the actin filament network to the membrane (Co et al., 2007). Abrogating the binding of WH2 to actin destabilises N-WASP within the signalling network, suggesting that the actin filament network regulates N-WASP in a positive feedback by stabilising and increasing the

local density of N-WASP (Co et al., 2007; Delatour et al., 2008; Weisswange et al., 2009). Binding at this site may also suggest that N-WASP competes with capping protein to further promote actin polymerisation through filament elongation (Carlier et al., 2013; Weisswange et al., 2009).

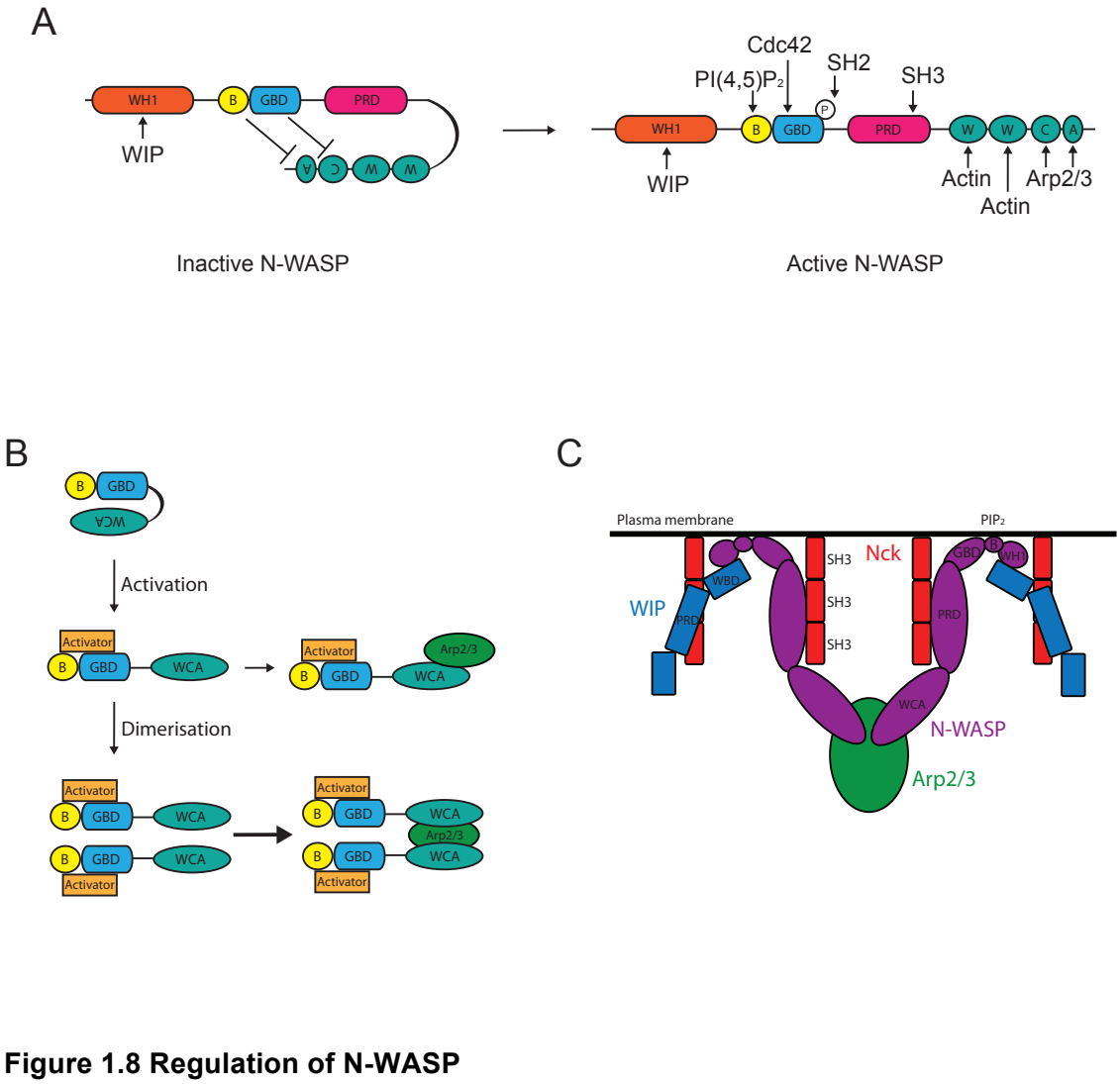

Figure 1.8 Regulation of N-WASP

A Schematic depicting the intramolecular interactions of N-WASP in its autoinhibited conformation (left). Also shown is the active conformation and binding sites of interacting proteins (right). Schematic is adapted from Campellone, 2010. **B** Schematic adapted from Padrick et al., 2008, depicting the activation of N-WASP. An activator binds to free the WCA domain, to allow binding of the Arp2/3 complex. However, if dimerisation occurs the WCA domain can bind Arp2/3 with higher affinity. **C** Schematic adapted from Ditlev et al., 2012, of the proposed ratio of signalling components in cells induced by antibody-mediated clustering of the SH3 domains of Nck. Two N-WASP molecules bind to one Arp2/3 complex, consistent with two binding sites for the WCA.

1.3 N-WASP in cellular processes

N-WASP is implicated in Arp2/3 complex activation during a number of cellular processes, including phagocytosis, invadopodia formation and endocytosis. It is also frequently used in the actin-based motility of pathogens. The signalling pathways that regulate these different processes will be described in the following sections with the exception of endocytosis, which will be discussed in more detail in 1.4.4.

1.3.1 Fc gamma receptor-mediated phagocytosis

Phagocytosis, which is the receptor-driven engulfment of particles over 0.5 μm diameter into the cell, involves local remodelling of the actin cytoskeleton at the plasma membrane (Kwiatkowska and Sobota, 1999). The two best-characterised phagocytosis receptors are Fcγ and complement receptor 3 (CR3), which use distinct signalling pathways to promote particle uptake (Caron and Hall, 1998; Groves et al., 2008). FcγR-mediated phagocytosis is associated with actin-rich ruffles, whilst CR3 promotes uptake with minimal membrane extensions (Aderem and Underhill, 1999; Allen and Aderem, 1996). The Arp2/3 complex is involved in both cases, as well as Rho family GTPases (May et al., 2000). FcγR drives phagocytosis using Rac and Cdc42, whereas CR3 favours Rho (Caron and Hall, 1998; Chimini and Chavrier, 2000; Cox et al., 1997; Hoppe and Swanson, 2004; Massol et al., 1998; Park and Cox, 2009; Yamauchi et al., 2004). WASP/N-WASP is activated downstream of FcγR, furthermore macrophages derived from Wiskott-Aldrich syndrome patients, lacking functional WASP, are defective in phagocytic uptake and cup formation (Lorenzi et al., 2000; Park and Cox, 2009). Phosphorylation of tyrosine 282 and 298 on the cytoplasmic tail of FcγR by Src leads to the recruitment of Nck (Figure 1.9) (Dart et al., 2012; Greenberg et al., 1993, 1994). In the absence of phosphorylation neither N-WASP nor Cdc42 is recruited to the phagocytic cup, consistent with Nck being upstream in the signalling network (Dart et al., 2012). For efficient phagocytosis Cdc42 is required and specifically its interaction with the CRIB domain of N-WASP (Figure 1.9) (Dart et al., 2012). A parallel pathway also regulates Fcγ phagocytosis, with the RhoGEF Vav activating Rac, which is recruited in its inactive form (Patel et al., 2002). Consistent with these parallel pathways, localised recruitment of active Rac or artificial clustering of active Cdc42 or

N-WASP beneath membrane-bound beads is sufficient to promote actin polymerisation and membrane protrusion (Castellano et al., 2000).

1.3.2 Invadopodium formation

Invadopodia are dynamic actin-rich structures frequently observed in migrating cancer cells that mediate degradation of the extracellular matrix (ECM) (Buccione et al., 2009; Chen, 1989; Linder, 2007; Tarone et al., 1985; Yamaguchi and Condeelis, 2007). The invadopodium contains an actin-rich core surrounded by adhesion and scaffolding proteins (Desai et al., 2008; Mueller et al., 1992). Src is integral to invadopodia formation and indeed the structure was first observed in Src-transformed fibroblasts (Chen, 1989; Tarone et al., 1985). A number of Src substrates have also been identified at the invadopodia, including the adaptor Tks5, which is a distinguishing marker for the structure (Abram et al., 2003; Oikawa et al., 2008; Stylli et al., 2009). Additional Src substrates are cortactin and N-WASP, with cortactin phosphorylation enhancing actin assembly as well as binding to Nck and WIP (Dovas et al., 2009; Tehrani et al., 2007). In fact Nck1, Cdc42, WIP, N-WASP and the Arp2/3 complex are all required for invadopodia formation (Figure 1.9) (Buccione et al., 2009; Yamaguchi and Condeelis, 2007). It appears that Tks5 is recruited by $PI(3,4)P_2$ via its PX domain and it may act as a scaffold to promote cortactin recruitment and aggregation at the forming invadopodia (Figure 1.9) (Abram et al., 2003; Oikawa et al., 2008; Oser et al., 2009). Tks5 then directly or indirectly recruits Nck1/2, N-WASP and Grb2, with cortactin also associated with WIP, dynamin and N-WASP, which is activated by Cdc42 (Figure 1.9) (Gimona et al., 2008; Oikawa et al., 2008; Stylli et al., 2009; Yamaguchi and Condeelis, 2007). Generation of membrane curvature is also important and CIP4 appears to act as a membrane-curving scaffold protein that may also promote Cdc42 and N-WASP recruitment (Pichot et al., 2010). Another key protein in invadopodia formation is the metalloprotease MT1-MMP, which is important for degradation of the ECM (Figure 1.9). The adaptor Tks4 regulates the localisation of MT1-MMP, while cortactin promotes its secretion (Artym et al., 2006; Clark and Weaver, 2008; Clark et al., 2007). MT1-MMP is actively transported to the invadopodia tip by vesicle trafficking and microtubule transport (Schoumacher et al., 2010). The vesicle-tethering exocyst then captures vesicles at the plasma membrane with Abl tyrosine kinase also implicated in targeting or retaining the MMP (Poincloux et al., 2009; Smith-Pearson et al., 2010).

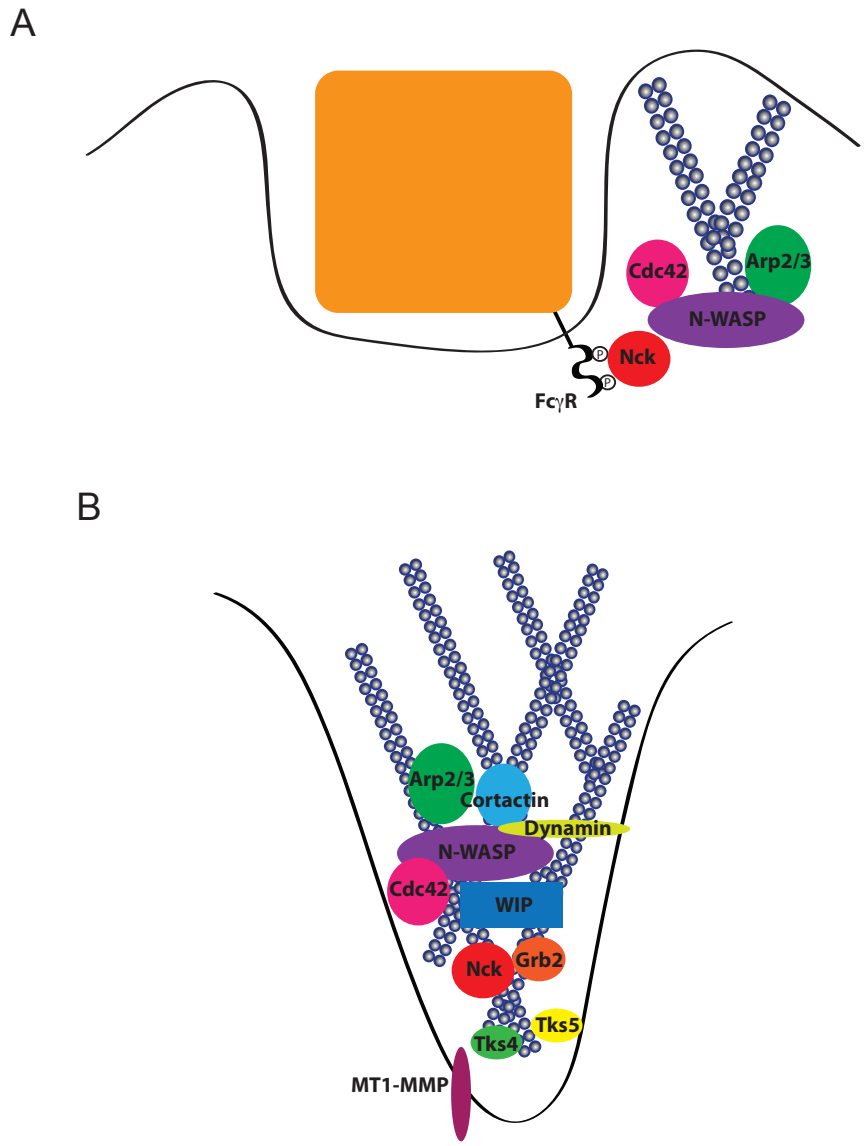

Figure 1.9 Cellular N-WASP signalling networks

Schematic depicting the signalling network required for actin polymerisation downstream of the Fcγ receptor during phagocytosis (**A**) and during invadopodia formation (**B**). The two structures use an overlapping set of proteins to promote and regulate Arp2/3-dependent actin polymerisation.

1.3.3 Vaccinia actin tail formation

In addition to recruiting kinesin-1 during microtubule-dependent transport, A36 also mediates the actin-based motility of vaccinia virus (Rottger et al., 1999; Wolffe et al., 1998). Fusion of the outer IEV membrane leads to incorporation of A36 with the plasma membrane. A36, which has a large cytoplasmic domain, then accumulates beneath the CEV (Rottger et al., 1999; Smith et al., 2002; van Eijl et al., 2000). Additionally, after viral fusion, Src and Abl family kinases are locally activated through outside-in signalling, which triggers a cascade that mimics receptor tyrosine kinase-signalling (Frischknecht et al., 1999b; Newsome et al., 2004; Newsome et al., 2006; Reeves et al., 2005). Kinase activation leads to phosphorylation of tyrosine 112 and 132 of A36, which promotes kinesin-1 release and provides binding sites for Nck and Grb2 (Figure 1.10) (Frischknecht et al., 1999b; Newsome et al., 2004; Scaplehorn et al., 2002). Binding of Nck promotes the recruitment of N-WASP via WIP (Figure 1.10). Grb2 recruitment is then dependent on the polyproline-rich domain of N-WASP (Donnelly et al., 2013; Frischknecht et al., 1999b; Moreau et al., 2000; Snapper et al., 2001; Zettl and Way, 2002). N-WASP in turn recruits and activates the Arp2/3 complex to polymerise actin beneath the CEV (Figure 1.10) (Frischknecht et al., 1999a; Snapper et al., 2001; Weisswange et al., 2009). The core components of the actin-signalling complex rapidly exchange and therefore do not form a stable complex beneath the virion (Weisswange et al., 2009). Furthermore, the exchange rate of N-WASP was shown to control the rate of Arp2/3-complex-dependent actin-based motility. Leading to the suggestion, it regulates the extent of actin polymerisation by antagonising capping (Weisswange et al., 2009).

It has also recently been demonstrated that actin polymerisation promotes the release of vaccinia virus (Horsington et al., 2013). It is thought that actin polymerisation disrupts the luminal interactions of the IEV proteins that bridge the CEV and plasma membrane (Horsington et al., 2013). In addition, actin tails have been shown to enhance the spread of infection through super-repulsion (Doceul et al., 2010). Whereby, actin tails form on the surface of newly infected cells bypassing the replication cycle, in a process that requires early expression of A33 and A36 (Doceul et al., 2010). Altogether highlighting the importance of actin-based motility for the efficient dissemination of the virus.

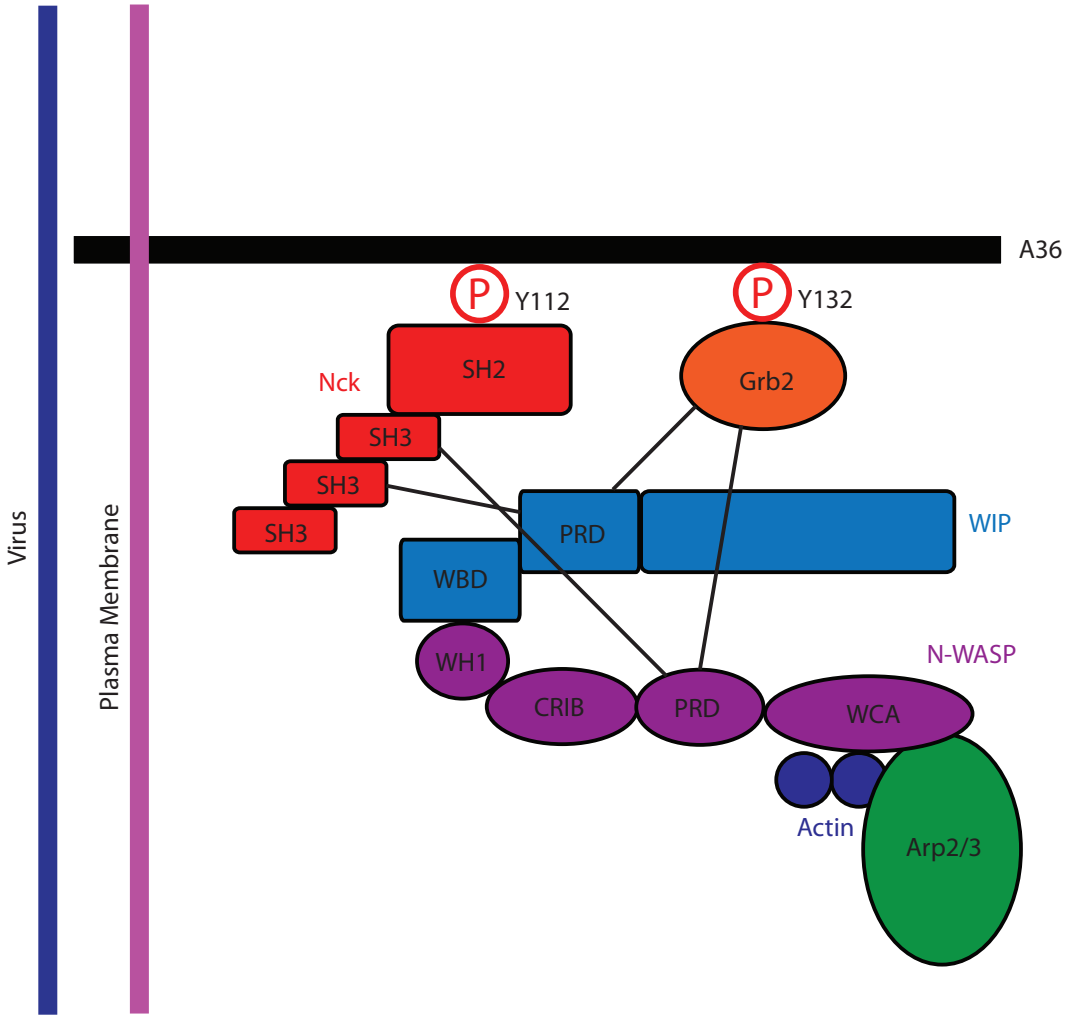

Figure 1.10 The vaccinia actin-signalling network

Schematic showing the vaccinia actin-signalling network, which induces the formation of an actin tail beneath the virion. The proteins are recruited in a Nck-dependent manner, with N-WASP required for Arp2/3 complex activation. The domains are as follows SH2 (Src homology 2), SH3 (Src homology 3), WBD (WASP binding domain), PRD (Polyproline-rich domain), WH1 (WASP homology 1), CRIB (Cdc42/Rac-interacting domain) and WCA (WASP homology 2, central and acidic region).

1.3.4 Actin-based motility of pathogens

In addition to vaccinia, a number of pathogens use actin-based motility to promote their efficient spread. Although several studies had previously observed the movement of bacteria inside the cell, it was not until the late 1980's that an association with the host actin cytoskeleton was identified (Bernardini et al., 1989; Heinzen et al., 1993; Mounier et al., 1990; Tilney and Portnoy, 1989). These studies found that *Listeria*, *Shigella* and *Rickettsia*, all use actin-based motility to promote intracellular movement, protrusion formation and penetration into neighbouring uninfected cells (Bernardini et al., 1989; Heinzen et al., 1993; Tilney and Portnoy, 1989). Later studies then identified the bacterial proteins required for actin polymerisation, including the *Shigella* IcsA protein and the *Listeria* ActA protein (Bernardini et al., 1989; Cameron et al., 1999; Goldberg and Theriot, 1995; Jeng et al., 2004; Kocks et al., 1992; Smith et al., 1995). IcsA was shown to recruit and activate N-WASP, whilst ActA mimics N-WASP to directly activate the Arp2/3 complex (Egile et al., 1999; Tilney and Portnoy, 1989; Welch et al., 1997a; Welch et al., 1998). *Rickettsia* was also shown to express an NPF termed RickA, which activates the Arp2/3 complex (Gouin et al., 2004; Jeng et al., 2004). It also bypasses all host nucleators and encodes a formin-like protein, Sca2 that interacts directly with actin (Haglund et al., 2010; Kleba et al., 2010; Serio et al., 2010).

In general, it appears that the bacteria that hijack actin within the cytoplasm target further downstream signalling components. Whereas, the surfing pathogens such as vaccinia virus and enteropathic *Escherichia coli* (EPEC), so called as they induce actin polymerisation at the surface of the cell, use more upstream signalling factors (Frischknecht and Way, 2001). Both vaccinia virus and EPEC encode receptor tyrosine kinase mimics that contain host phospho-tyrosine motifs to recruit Nck (Frischknecht et al., 1999b; Gruenheid et al., 2001). Therefore, the signalling pathway used by vaccinia and EPEC are similar. The combined study of actin-based motility by pathogens has greatly enhanced our knowledge of cytoskeletal proteins, their regulation and mechanisms of function (Haglund and Welch, 2011). Pathogens also provide a quantifiable readout, and have locally focused or exaggerated signals that make them more amenable for study (Haglund and Welch, 2011).

1.4 Clathrin-mediated endocytosis

1.4.1 Clathrin

Clathrin is synonymous with endocytosis, a process of internalisation that removes or recycles lipid and protein cargo from the plasma membrane into the cell (Brodsky et al., 2001; McMahon and Boucrot, 2011). Clathrin-mediated endocytosis (CME) is important for many processes, including, but not limited to, neurotransmission, signal transduction, regulating the surface expression of proteins, and the uptake of nutrients (Brodsky et al., 2001; McMahon and Boucrot, 2011). It is also frequently hijacked by pathogens to facilitate their entry into the host cell (Gruenberg, 2009; Marsh and Helenius, 2006; Mercer et al., 2010; Pizarro-Cerda et al., 2010). Along with its role at the plasma membrane, clathrin also regulates trafficking at other cellular locations including the TGN and endosomes (Bonifacino and Traub, 2003; Brodsky, 1988; Brodsky et al., 2001; McNiven and Thompson, 2006; Traub, 2005). However, as this thesis is concerned with events at the plasma membrane, I will focus only on the process of mammalian CME.

In 1964, Roth and Porter described a dense protein coat, exhibiting a bristle-like morphology, on vesicles containing yolk proteins (Roth and Porter, 1964). The protein responsible for the coat was later identified and termed clathrin (Pearse, 1976). Clathrin has a triskelion shape composed of three identical clathrin heavy chains (CHC), with its central portion, known as the hub, involved in CHC trimerisation (Figure 1.11) (Kirchhausen et al., 1987; Liu et al., 1995). The hub also provides binding sites for one clathrin light chain (CLC) to each CHC (Liu et al., 1995). The triskelion can self-assemble into a polyhedral lattice formed of hexagons and pentagons, the relative ratio of which accommodates different membrane curvatures (Brodsky, 1988; McMahon and Boucrot, 2011). The CLC regulates clathrin assembly by modulating the tendency of the CHC to self-assemble (Greene et al., 2000; Liu et al., 1995). This is achieved through conformational changes at the N-terminus of the CLC, which modifies the CHC knee, preventing self-assembly (Wilbur et al., 2010). The N terminus of the CHC comprises a globular terminal domain (TD), which contains binding sites for many clathrin-interacting proteins (ter Haar et al., 1998). Adaptors have been shown to bind the TD to promote clathrin oligomerisation *in vivo* (Gallusser and Kirchhausen, 1993;

Shih et al., 1995), thereby restricting assembly to specific membrane localisations. Drugs targeting the TD completely arrest the formation of the CCV, suggesting it is also important for regulating vesicle progression (von Kleist et al., 2011).

1.4.2 Clathrin adaptors

The term endocytic adaptor was coined in 1981, to describe an as yet unidentified group of proteins that could mediate the link between clathrin and its cargo (Pearse and Bretscher, 1981). The canonical and best-described adaptor is adaptor protein 2 (AP-2), which, in the vesicle, is second in abundance only to clathrin itself (Brodsky et al., 2001; Pearse and Robinson, 1984). AP-2 provides a link between the clathrin lattice and the plasma membrane through specific interactions with the headgroups of $PI(4,5)P_2$, and through interaction with sorting signals in the cytoplasmic tail of membrane proteins (Ohno et al., 1995; Owen and Evans, 1998; Rohde et al., 2002; Roth and Porter, 1964; Shih et al., 1995; ter Haar et al., 1998; von Kleist et al., 2011; Wilbur et al., 2010). AP-2 engages with clathrin by binding a consensus signature known as the clathrin box motif, (LΦ[D/E]Φ[D/E]), where Φ signifies a bulky hydrophobic residue (Dell'Angelica et al., 1998; Krupnick et al., 1997; Ramjaun and McPherson, 1998; Shih et al., 1995; ter Haar et al., 1998). The sorting signals that distinguish the cargo destined for incorporation are also well defined and consist of tyrosine (YxxΦ) and dileucine-based motifs ([D/E]xxxL[L/I/M] (Doray et al., 2007; Kelly et al., 2008; Owen et al., 2004).

AP-2 is composed of a heterotetrameric complex of α, β2, μ2 and σ2-adaptin subunits (Figure 1.11). The large subunits α and β2 function in plasma membrane targeting, clathrin binding and also recruit additional accessory proteins to the growing vesicle (Owen et al., 1999; Traub et al., 1999). The μ2 subunit interacts with tyrosine-based internalisation motifs and also contains lipid-binding motifs (Kirchhausen, 1999; Owen et al., 2004), whilst the σ2 subunit binds dileucine-based motifs and stabilises the complex (Collins et al., 2002; Doray et al., 2007; Kelly et al., 2008). It was found that two conformations of AP-2 exist in solution, an open and a locked form, with the latter suggested to be predominate (Jackson et al., 2010). To allow simultaneous engagement of both lipids and cargo, the complex undergoes a large conformational change. In the locked conformation, the two endocytic binding motifs are hidden by the β2 subunit. However, upon rearrangement, the four lipid binding sites and two

endocytic motif binding sites become co-planar, allowing for simultaneous engagement (Jackson et al., 2010). It has also been shown that phosphorylation of AP-2 can regulate its recruitment to the plasma membrane, its interaction with cargo and assembly with clathrin, adding a further level of regulation to this complex (Fingerhut et al., 2001; Ricotta et al., 2002; Wilde and Brodsky, 1996).

There is some controversy as to whether AP-2 constitutes an essential component of the CCV. One study found that upon AP-2 depletion, very few clathrin coats were formed but those that did were suggested to contain a residual amount of AP-2 (Boucrot et al., 2010). However, several studies have shown that a number of proteins that are internalised in a clathrin-dependent manner are still internalised upon AP-2 depletion (Hinrichsen et al., 2003; Keyel et al., 2006; Lakadamyali et al., 2006; Maurer and Cooper, 2006; Motley et al., 2003). This suggests that additional adaptors could function in place of AP-2 and in fact there is more likely a cargo-specificity in the choice of adaptor. Due to their ability to bind lipid, clathrin, cargo and other accessory proteins, epsin1/2, ARH/NUMB/Dab2 and β-arrestin have all been proposed as cargo-specific adaptor proteins that may function in an AP-2-independent manner (Gallagher et al., 2004; Goodman et al., 1996; Keyel et al., 2006; Mishra et al., 2002b; Overstreet et al., 2003). Epsin contains ubiquitin interacting motifs and can therefore bind ubiquitinylated cargo such as EGFR (Chen et al., 1998; Overstreet et al., 2003), NUMB promotes Notch internalisation (Kandachar and Roegiers, 2012) and ARH/Dab2 contain a phospho-tyrosine-binding domain (PTB) that engages the NPXY motif in the LDL receptor family (Gallagher et al., 2004; Mishra et al., 2002a; Mishra et al., 2002b; Uhlik et al., 2005). Other potential adaptors include AP180/CALM that can bind lipid, clathrin and other accessory proteins but has not, as yet, been shown to bind cargo (Ford et al., 2001), Eps15 that can bind cargo and accessory proteins but not lipid and clathrin (Benmerah et al., 1996), and finally, FCHo1/2 that binds lipids and accessory proteins (Henne et al., 2010).

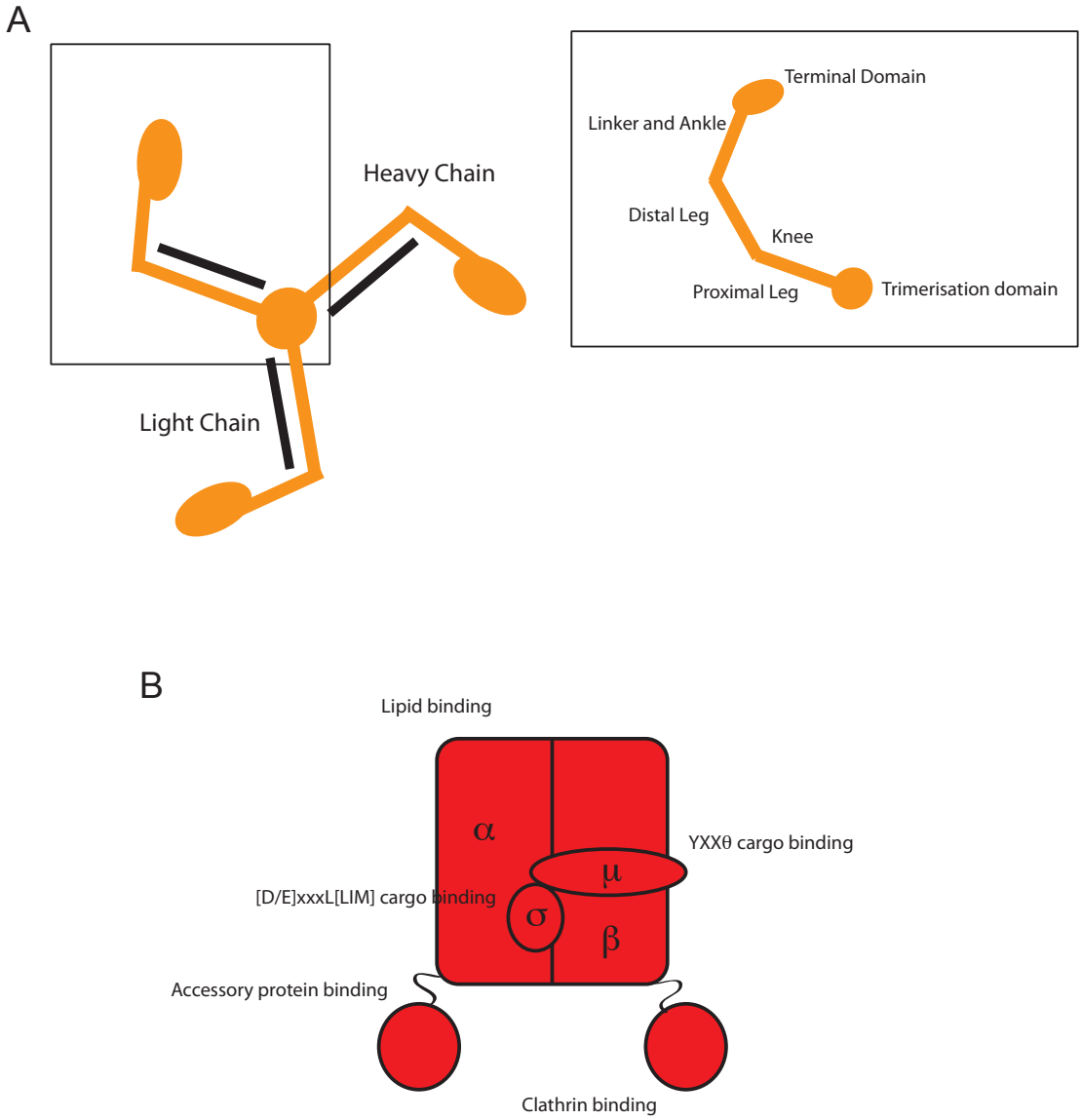

Figure 1.11 Structure of clathrin and AP-2

A Schematic depicting the structure of the clathrin triskelion composed of three heavy chains and three light chains. The magnified box highlights the different regions of the clathrin heavy chain. **B** The subunits of the AP-2 complex, along with their prescribed functions.

1.4.3 Temporal stages of endocytosis

The stages of CME are well defined and include nucleation, cargo selection, coat assembly, scission and uncoating (Figure 1.12) (McMahon and Boucrot, 2011). The site of CCV formation is initiated by the coordinated arrival of one clathrin triskelion and two adaptor proteins to $PI(4,5)P_2$ rich sites in the plasma membrane (Cocucci et al., 2012). $PI(4,5)P_2$ is essential for clathrin-coated pit initiation, and also regulates its stabilisation and size (Antonescu et al., 2011). Many proteins are recruited to CCVs in part by low affinity interactions with $PI(4,5)P_2$ (Haucke, 2005). This includes AP-2, which has brought forward the model of coincidence detection for their recruitment (Carlton and Cullen, 2005; Schmid and McMahon, 2007). While it has also been proposed that FCHo1/2 proteins define the initiation site, recent work has shown they are not essential for initiation but for the continued growth of the invagination (Cocucci et al., 2012; Henne et al., 2010). In fact, FCHo1/2 is just one constituent of a wider group of proteins called the rim complex, which includes epsin, Eps15 and intersectin (Figure 1.12) (Henne et al., 2010). These proteins engage in multiple interactions with eachother, as well as additional endocytic accessory proteins. Depletion of any component of the rim complex significantly increases the lifetime of the CCV (Loerke et al., 2009; Mettlen et al., 2009). Eps15 can form homodimers and tetramers, and has also been shown to heterodimerise with intersectin, a scaffold protein that links to several signalling pathways (Cupers et al., 1997; Hunter et al., 2013). Eps15 can also interact with AP-2 and epsin, with the latter additionally binding AP-2 and clathrin (Salcini et al., 1999; Slepnev and De Camilli, 2000). As well as building up the cooperative interactions required to promote vesicle formation, the rim complex, as the name would suggest, localises to the edge of the developing pit, with Eps15 and epsin promoting membrane curvature to support the invagination process, while AP-2 selectively sequesters cargo (Saffarian et al., 2009).

The final stages of endocytosis constitute the scission of the vesicle from the plasma membrane, before uncoating and recycling of clathrin (Figure 1.12). Membrane scission is dependent on the GTPase dynamin, which oligomerises into tetramers that stack into open rings and form tubules around the membrane neck (Hinshaw, 2000). The role of dynamin in scission was first identified in *Drosophila*, where a temperature-sensitive mutant shibire (ts1) accumulated CCVs attached to the plasma membrane

(Kosaka and Ikeda, 1983). Further evidence of its importance came from additional mutants, including dynamin K44A that has defects in GTP binding and hydrolysis and is deficient in scission (McNiven et al., 2000). It appears that dynamin is recruited by BAR-domain containing proteins, which have a preference for the curvature of the vesicle neck, however, its precise mechanism of action remains unclear (Ferguson et al., 2009; Sundborger et al., 2011; Wigge et al., 1997). Once detached from the plasma membrane, the clathrin coat is disassembled by HSC70 and its co-factor auxillin (Schlossman et al., 1984; Ungewickell et al., 1995). Auxillin is recruited after budding and binds the TD and ankles of the clathrin triskelia, localising under the hub of the neighbouring triskelion (Massol et al., 2006; Scheele et al., 2001). Auxillin then recruits HSC70 and the uncoating step is initiated.

1.4.4 Actin during endocytosis

An essential role for actin during yeast endocytosis has been well defined, but until recently, the involvement of actin within mammalian endocytosis was significantly less clear (Ayscough, 2000; Ayscough et al., 1997; Kaksonen et al., 2006). Inhibiting actin polymerisation in mammalian systems in many cases led to only a partial block in endocytic uptake, suggesting that actin does not play an essential role (Gottlieb et al., 1993; Lamaze et al., 1997). However, strong evidence for its role during mammalian endocytosis came from live-cell imaging, showing several cytoskeletal regulators localise to sites of CME (Merrifield, 2004; Taunton et al., 2000). Furthermore, the inward movement of vesicles occurred immediately after a transient accumulation of actin at the plasma membrane (Merrifield et al., 2002).

In recent years, the confusion over the importance of actin in mammalian endocytosis has, to some extent, been resolved. A number of studies found that the level of tension at the membrane defines whether actin is required for internalisation (Batchelder and Yarar, 2010; Boulant et al., 2011; Liu et al., 2009). It was shown that cortical tension can affect the lifetime of CME, and direct manipulation of the ECM to enhance adhesion had a negative impact on internalisation (Batchelder and Yarar, 2010; Liu et al., 2009). Further to this, there was a stronger requirement for actin in areas of cell adhesion (Batchelder and Yarar, 2010). It appears that if membrane tension is too high and clathrin-coat assembly stalls then actin polymerisation can take over to drive membrane internalisation (Boulant et al., 2011). Consistent with this, alleviating the

high turgor pressure in yeast cells reduces the absolute requirement for actin, and also revealed a greater requirement for actin at the later stages of internalisation (Aghamohammadzadeh and Ayscough, 2009). Recent work has shown the organisation of actin filaments at the endocytic site, through electron microscopy (Collins et al., 2011). The actin filament barbed ends are orientated towards the CCV, and manifest as a small lateral patch at the periphery of shallow CCVs or a collar-like arrangement around partly invaginated vesicles (Collins et al., 2011). Furthermore and consistent with the observation of rocketing endosomes, actin also formed a polarised comet tail (Collins et al., 2011; Merrifield et al., 1999; Taunton et al., 2000). These data are consistent with a role for actin in constricting and elongating the budding neck, before driving the vesicle inwards from the plasma membrane (Figure 1.12).

A number of proteins have been associated with the regulation of actin polymerisation during CME. Many of these proteins, which include N-WASP, cortactin, Hip1R and dynamin are initially recruited at low levels, followed by a sharp increase in recruitment immediately prior to scission (Figure 1.12) (Taylor et al., 2011). The polyproline-rich domain of dynamin is capable of binding to intersectin and other accessory proteins, and was suggested to recruit N-WASP (Da Costa et al., 2003; Hussain et al., 2001; Kessels et al., 2006; Kessels and Qualmann, 2002; Otsuki et al., 2003). N-WASP could then in turn activate the Arp2/3 complex to initiate actin assembly (Benesch et al., 2005; Innocenti et al., 2005; Merrifield, 2004). Dynamin also binds to cortactin, suggesting it regulates actin polymerisation at the endocytic site (Cao et al., 2003; McNiven et al., 2000). However, the final burst of dynamin lags the onset of actin polymerisation by ~20s, but this may represent the GTPase activity of dynamin in scission and not its role in the regulation of actin polymerisation (Merrifield et al., 2005).

One protein that has been suggested to link clathrin and the actin cytoskeleton is Hip1R, which contains an ANTH domain that binds lipid and a THATCH domain that can mediate a direct interaction with F-actin (Brett et al., 2006; Hyun et al., 2004; Legendre-Guillemin et al., 2005; McCann and Craig, 1997; Wilbur et al., 2008). Hip1R can also interact with the N-terminus of the clathrin light chain (CLC) and was suggested to act as a bridge maintaining an interaction between clathrin and the actin cytoskeleton (Brett et al., 2006; Chen and Brodsky, 2005; Engqvist-Goldstein et al., 1999; Engqvist-Goldstein et al., 2001; Legendre-Guillemin et al., 2005; Newpher et al., 2006). Depletion of Hip1R or disruption of the interaction been Hip1R and CLC leads to

the formation of aberrant actin assemblies at CCV, supporting the concept that Hip1R negatively regulates actin assembly during CME (Chen and Brodsky, 2005; Le Clainche et al., 2007; Newpher et al., 2005; Poupon et al., 2008; Saffarian et al., 2009; Wilbur et al., 2008). In fact, the role of Hip1R during endocytosis appears more complex, as binding of Hip1R to CLC negatively regulates the interaction between Hip1R and F-actin (Boettner et al., 2011). These observations suggest that the role of Hip1R is likely to be both temporally and spatially restricted. There is some evidence to suggest that Hip1R-CLC promotes clathrin assembly, by releasing the CLC N-terminal regulation on the CHC (Chen and Brodsky, 2005; Legendre-Guillemin et al., 2005). However, it is also clear that Hip1R can bind to cortactin through its SH3 domain and competes with other proteins that bind at this site including dynamin, to limit actin polymerisation (Le Clainche et al., 2007). It has been proposed that the Hip1R-cortactin complex blocks actin filament barbed end elongation and promotes actin polymerisation at distinct sites such as the vesicle neck (Le Clainche et al., 2007). In this manner, the negative regulation of CLC upon Hip1R-F-actin could also restrict the number and/or site of actin polymerisation (Boettner et al., 2011). One final level of regulation appears with the accessory protein, epsin, which has been shown to promote the membrane recruitment and phosphorylation of Hip1R in *Dictyostelium*, highlighting further the complexity of CCV organisation.

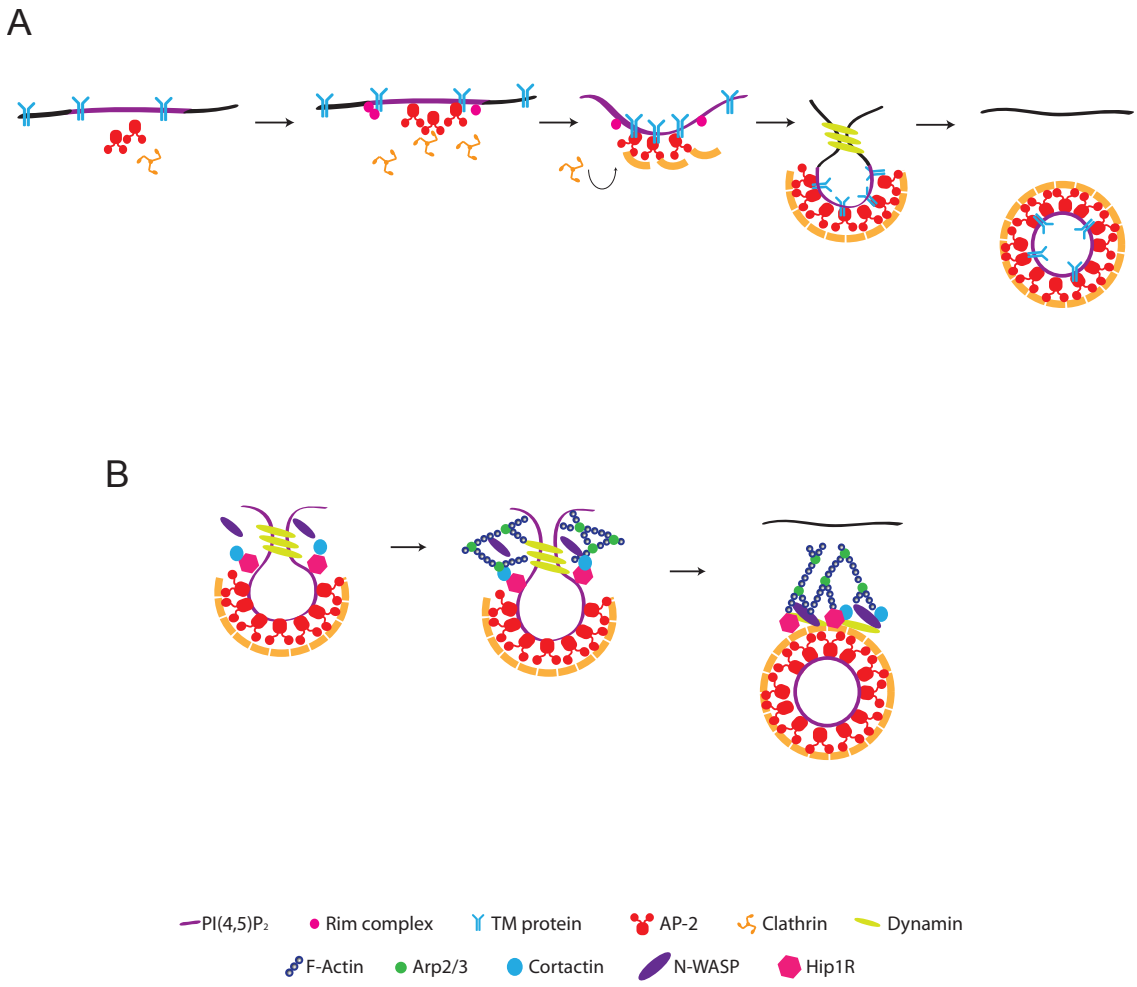

Figure 1.12 Stages of mammalian CME

A Schematic detailing the steps of TM protein internalisation during clathrin-mediated endocytosis. The site of nucleation is defined by the coordinated arrival of two AP-2 molecules and one clathrin triskelion. Vesicle progression and cargo incorporation is then reliant on the recruitment of additional accessory proteins, before scission from the plasma membrane by dynamin. **B** Schematic depicting the proteins that coordinate actin polymerisation during clathrin-mediated endocytosis.

1.4.5 Clathrin plaques

An interesting observation regarding clathrin was the identification of clathrin plaques, which are longer-lived structures with larger and less sharply curved coats (Signoret et al., 2005; Saffarian et al., 2009). The clathrin lattice appears to favour a hexagonal array, unlike the polyhedral lattice observed at clathrin-coated pits, and their formation and function have an absolute requirement for actin (Saffarian et al., 2009). It has been suggested that the plaque is more predominant at the adherent surface of cells, and may represent stalling of clathrin internalisation by steric interference from cargo, thereby engaging the actin cytoskeleton (Boulant et al., 2011). In line with this, blocking the interaction between Hip1R and CLC led to late stage arrest in endocytosis, specifically in polarised cells (Boulant et al., 2011). Interestingly, Hip1R does play an important role at the clathrin plaque and its organisation appears to span the plaque along with epsin, which would usually target to the edge of the vesicle (Saffarian et al., 2009). This suggests that endocytic proteins are arranged differently in the clathrin plaque and contribute to its unique morphology. However, there remain many questions surrounding this structure. There is some debate as to whether the structures actually internalise, or whether clathrin-coated pits could bud off from the stable structure (Signoret et al., 2005; Traub, 2009). In addition, plaque structures have also been observed at the basal surface of the cell (Signoret et al., 2005), therefore, it is unclear what the function of the structure is. Thus further studies are required to understand how these structures form and their contribution to endocytic trafficking on a whole.

1.4.6 Clathrin and pathogens

Many different pathogens hijack the classic function of clathrin to facilitate their entry into cells (Cossart and Sansonetti, 2004; Gruenberg, 2009; Marsh and Helenius, 2006; Mercer et al., 2010; Pelkmans and Helenius, 2003; Schelhaas, 2010). Studies with pathogens have also expanded our understanding of the versatility of clathrin within the internalisation process. This is aptly demonstrated by vesicular stomatis virus (VSV), which is internalised in an actin-dependent manner through partial CCVs (Cureton et al., 2009). Further studies have shown that a mutant virus, 75 nm in length compared to the wild-type 200 nm virion, internalises in a complete clathrin coat without the need

for actin (Cureton et al., 2010). Therefore, it appears that the recruitment and stimulation of actin polymerisation can help to overcome the physical constraints and force required to internalise large particles such as pathogens (Humphries and Way, 2013). Studies with pathogens have thus highlighted the ability of clathrin to internalise large particles, which can be over 1 μm in diameter, and also have illustrated how this flexibility is achieved (Bonazzi et al., 2008; Cossart and Veiga, 2008; Cureton et al., 2010; Moreno-Ruiz et al., 2009; Veiga et al., 2007).

In recent years, further studies have highlighted the interplay of clathrin and the actin cytoskeleton outside the context of internalisation. A study to determine the universality of clathrin in the entry of bacteria showed that clathrin is recruited to EPEC in a fashion that is dependent on phosphorylation of tyrosine 474 in the Tir receptor (Veiga et al., 2007). In this case, clathrin appears to form part of the signalling network upstream of actin polymerisation and is required for pedestal formation. Studies aimed at characterising other endocytic proteins that constitute part of this signalling network found that AP-2 was neither recruited nor required at the pedestal (Lin et al., 2011). In fact, Dab2, along with the rim complex proteins epsin1 and Eps15, could fulfil the adaptor function and promote clathrin recruitment (Lin et al., 2011). CD2AP, a protein that binds to cortactin also localised to the tip of the actin pedestal (Guttman et al., 2010). The manipulation of clathrin by EPEC can be described as the creation of a stable clathrin platform to promote cytoskeletal rearrangements and therefore seems to share many parallels with the clathrin plaque (Humphries and Way, 2013).

1.5 The aims of this thesis

N-WASP is frequently hijacked by pathogens to promote their actin-based motility and understanding how they achieve this has helped elucidate the regulation of this process at a molecular level. My thesis aims to further explore the cooperative nature of these signalling networks using vaccinia virus as a model system, and in addition, to show the relevance of understanding the molecular detail of its motility for other N-WASP-dependent cellular processes. A broad aim of my thesis is also to investigate the interplay between clathrin and the actin cytoskeleton, which unite to perform essential roles in both cellular processes and during the spread of infection.

Chapter 2. Materials & Methods

2.1 General buffers and culture media

Many of the general buffers and culture media used in this thesis were provided by the in-house central service at Cancer Research UK, their details are listed below. Additional general items that were purchased include; Dulbecco's Modified Eagle Medium 1000 mg/dm^3 glucose (D-5546) and Dulbecco's Modified Eagle Medium 4500 mg/dm^3 (D-6546) from Sigma, fetal calf serum from PAA laboratories (A15-041), and Opti-MEM (31985) and penicillin G sodium / streptomycin sulphate 100x stock from Invitrogen (1540-122). Specific buffers will be described in their relevant sections.

2.1.1 General Buffers

Phosphate Buffered Saline A (PBSA)

8.00 g	NaCl (137 mM)
0.20 g	KCl (2.7 mM)
1.43 g	Na_2HPO_4 (10 mM)
0.25 g	KH_2PO_4 (1.8 mM)

The reagents were dissolved in distilled water, with the pH adjusted to 7.2, in a total volume of 1 L. The solution was additionally autoclaved.

2.1.2 Cell Culture Media

Tris Saline (TS)

8.00 g	NaCl (137 mM)
2.00 ml	19% (w/v) KCl solution (5.1 mM)
0.10 g	Na_2HPO_4 (0.7 mM)
1.00 g	D-Glucose (5.6 mM)
3.00 g	Trizma Base (24.8 mM)
0.06 g	Penicillin (0.2 mM)
0.10 g	Streptomycin (0.2 mM)
1.50 ml	1% (w/v) Phenol red solution (0.15%)

Trypsin Solution: 0.25% in Tris Saline

The TS reagents were dissolved in distilled water, with the pH adjusted to 7.7, in a total volume of 200 ml. 0.06 g of penicillin and 0.1 g of streptomycin was then added. To make the trypsin solution, 2.5 g of trypsin (Difco 1:250) was dissolved in 200 ml of distilled water (pH 7.7). The TS and the trypsin solution were mixed and distilled water added, with the pH adjusted to 7.7 in a final volume of 1 L. The solution was sterilised by filtration through a 0.22 µm filter and stored at -20 ºC.

Versene Solution

8.00 g	NaCl (137 mM)
0.20 g	KCl (2.7 mM)
1.15 g	Na_2HPO_4 (8.1 mM)
0.20 g	KH_2PO_4 (0.2 mM)
0.20 g	EDTA (0.7 mM)
1.50 ml	1% (w/v) Phenol red solution

The reagents were dissolved in distilled water, with the pH adjusted to 7.2, in a total volume of 1 L. The solution was additionally autoclaved and stored at room temperature.

Glutamine Solution

A 10x stock solution (0.24 M) was prepared by dissolving 35.05 g of L-Glutamine in 1 L of distilled water. The solution was sterilised by filtration through a 0.22 µm filter and stored at -20 ºC.

2.1.3 Bacteriological Media

Luria-Bertani (LB) Medium

10 g	NaCl (171 mM)
10 g	Bacto-tryptone (1% (w/v))
5 g	Bacto-yeast extract (0.5% (w/v))

The reagents were dissolved in distilled water, with the pH adjusted to 7.2, in a total volume of 1 L. The solution was additionally autoclaved and stored at room temperature.

LB Agar

15 g (1.5% (w/v)) of Bacto-agar was dissolved in 1 L of LB medium and the resulting solution autoclaved.

2.2 Cell Culture

2.2.1 Culturing stocks

Cells were grown at 37 ºC in 5% CO_2 and passaged every 2-3 days at a confluency of 70%. To recover frozen stocks, an aliquot from liquid nitrogen was rapidly thawed and resuspended in complete media (10% FCS) in a 10 cm dish. The media was refreshed after the cells had attached to remove DMSO. The cell lines used in this thesis along with their culture conditions are listed in Table 2.1. Newly created cell lines are described in section 2.3.5.

Table 2.1 List of cell lines

Cell Line	Species	Medium	Source
HeLa	Human	MEM, 10% FCS, Pen/Strep, 2 mM Glutamine	Dr Sally Cudmore (EMBL)
HeLa RFP-KLC2	Human	MEM, 10% FCS, Pen/Strep, 2 mM Glutamine	Mark Dodding (LRI)
HeLa LifeAct-Cherry	Human	MEM, 10% FCS, Pen/Strep, 2 mM Glutamine, 1 µg/ml puromycin	Charlotte Durkin (LRI)
HeLa GFP-N-WASP	Human	MEM, 10% FCS, Pen/Strep, 2 mM Glutamine	Ina Weisswange (LRI)
293 FT	Human	DMEM high glucose, 10% FCS, Pen/Strep, 2 mM Glutamine	Invitrogen
BS-C-1	Monkey	DMEM low glucose, 10% FCS, Pen/Strep, 2 mM Glutamine	ATCC

N-WASP +/+ and -/- MEFs	Mouse	DMEM high glucose, 10% FCS, Pen/Strep, 2 mM Glutamine	Dr Scott Snapper (MGH)
Nck 1/2 +/+ and -/- MEFs	Mouse	DMEM high glucose, 10% FCS, Pen/Strep, 2 mM Glutamine	Dr Tony Pawson (SLRI)
DX3	Human	DMEM high glucose, 10% FCS, Pen/Strep, 2mM Glutamine	Dr John Marshall (Bart's cancer institute)

2.2.2 Freezing stocks

To generate frozen stocks, cells were trypsinised and collected by centrifugation at 1000 rpm for 5 minutes. They were then resuspended in 1 ml FCS with 10% DMSO /10 cm dish, aliquoted in a cryovial and transferred to -80 ºC before final storage in liquid nitrogen.

2.3 Transfection

In this thesis, several transfection reagents were used, their use was dependent on both the assay and cell type.

2.3.1 Effectene

Effectene (Qiagen) was used in all assays, unless otherwise stated. At T=0 hrs, 1.5 x 10^5 cells were plated per well in a 6 well plate. At T=24 hrs, 400 ng of DNA was diluted in 100 µl EC buffer. 3.2 µl of enhancer was then added and the solution incubated for 5 mins at room temperature. Afterwards 5 µl of effectene was added and the mixture incubated for a further 10 mins at room temperature. After incubation the mixture was added directly to cells.

2.3.2 Fugene 6

Fugene 6 (Roche) was used to transfect HeLa cells prior to phagocytosis assays, due to its lower toxicity. At T=0 hrs, for a 6 well plate, 1.5 x 10^5 cells were plated per well. At T=24 hrs, 1 µg of DNA was added to 50 µl Opti-MEM, before the addition of 3 µl Fugene 6, the mixture was then incubated for 15 mins at room temperature, before its addition to cells. Cells were then used at T=48 hrs, allowing for adequate expression.

2.3.3 HiPerFect

HiPerFect (Qiagen) was used for RNAi transfection in HeLa cells, using the fast-forward protocol. For a 6 well dish, 2 µl siRNA (20 µM) was diluted in 100 µl MEM, with the addition of 12 µl HiPerFect. The mixture was then incubated at room temperature for 5 mins, before its addition to 2 ml of freshly seeded HeLa cells at a density of 0.5x10^5 per ml. Cells were then used 56 hrs post-transfection, with the media refreshed after 24 hrs.

2.3.4 Lipofectamine RNAi max

To transfect DX3 cells with siRNA, Lipofectamine RNAi max transfection reagent (Invitrogen) was used following the reverse transfection method. At T=0 hrs, for a 6 well plate, 2.4 µl siRNA duplex (20 µM) was resuspended in 200 µl of Opti-MEM and in a separate tube 4 µl of RNAi max was added to 200 µl of Opti-MEM. The tubes were then combined and incubated at room temperature for 15 mins. Cells were trypsined and 1x10^5 cells plated in 2 ml of complete media. After incubation the transfection mixture was added to cells. At T=24 hrs, the media was refreshed, and cells were assayed at T=56 hrs.

Table 2.2 Target sequences of siRNA

Gene	Target sequence	Source
AP-2	AGAGCAUGUGCACGCUGGC GCGAGAGGGUAUCAAGUAU	Motley et al., 2003 Dharmacon J-008270-005
CHC	GAAAGAAUCUGUAGAGAAA UGACAAAGGUGGAUAAAUU	Dharmacon D-004001-01 and 03

ITSN1	GAUAUCAGAUGUCGAUUGA GGCCAUAACUGUAGAGGAA	Dharmacon D-008365-03 and 04

2.3.5 Generation of stable cell lines

Stable cell lines were generated using the pLVX vector (Clontech), which contained a puromycin resistance cassette to allow for rapid selection. To generate stable cell lines, at T=0 hrs, 293 FT cells were seeded in a 10 cm dish at a density of $4x10^6$ cells. At T=24 hrs, cells were transfected with 10 µg of the construct of interest cloned into the pLVX vector, along with 7 µg of pPAX and 3 µg of pMDG2.3 packaging vectors. At T=40 hrs, the medium was refreshed with 7 ml of complete media. Lentivirus was harvested after T=56 and 72 hrs, with the media taken off the cells and passed through a 0.45 µM Millex HV filter (Millipore SLV033RB). The media was then incubated on the cells of interest for 48 hrs prior to selection with 1 µg/ml puromycin.

Table 2.3 Generated stable cell lines

Cell Line	Protein Introduced	Species of Induced Protein
N-WASP -/-	GFP-N-WASP	Rat
N-WASP -/-	GFP-N-WASP-H208D	Rat
N-WASP -/-	GFP-N-WASP-ΔNck-H208D	Rat

2.4 FcγR-mediated phagocytosis

2.4.1 Reagents

The following reagents were used for phagocytosis assays: HEPES (Invitrogen), Sheep red blood cells (RBC) (TCS Biosciences), Gelatin veronal buffer (GVB) (Sigma), Rabbit anti-RBC IgG (MP Biomedicals) and pRK5-FcγRIIa (Caron and Hall, 1998).

2.4.2 Assay

At T=0 hrs, $1x10^5$ HeLa cells were plated onto coverslips, at T=8 hrs cells were transfected with the FcγRIIa construct to prime them for phagocytic uptake. Where cells were treated with 20 nM siRNA, cells were transferred onto coverslips 24 hrs after siRNA transfection, and for expression of GFP-tagged constructs this was carried out in co-transfection with the FcγRIIa construct. The phagocytic assay was then carried out 24 hrs post-transfection.

Red blood cells were prepared with the addition of 0.2 µl RBC (~$1x10^7$) to 100 µl GVB per coverslip. The cells were then spun at 4000 rpm for 4 mins, the supernatant removed, and the process repeated. Cells were then resuspended in 500 µl GVB and an equal volume of IgG to RBC added, i.e. 0.2 µl per coverslip. This mixture was then incubated at room temperature on a rotating wheel for 30 mins. It was then spun at 4000 rpm for 6 mins, and washed with 100 µl GVB. A final spin at 4000 rpm for 6 mins was then repeated before the RBCs were resuspended in 500 µl of serum free media with 10 mM HEPES per coverslip.

To perform the assay, media was removed from the HeLa cells and was replaced with serum free media containing 10 mM HEPES for 1 hr. After serum starvation the media was replaced by the 500 µl RBC mix. The plate was incubated at 4°C for 15 mins and then 37°C for 30 mins. The cells were then washed with PBSA, and fixed with 4% PFA in PBSA for 10 mins. Cells were washed with PBSA before immunofluorescence staining with anti-rabbit secondary antibodies was carried out. Protocols for fixation and immunofluorescence are described in sections 2.9.2 and 2.9.3.

2.4.3 Quantification

To quantify the relative index (Ri) the total number of RBC per HeLa cell, and the number of internalised RBC per HeLa cell was determined. The attachment index (Ai) represents the total number of RBC divided by the number of HeLa cells, and the phagocytic index (Pi) represents the number of internalised RBC divided by the number of HeLa cells. The percentage phagocytosis was determined by dividing the number of internalised RBC by the total number of RBC per HeLa cell.

2.5 Invadopodia assay

2.5.1 Reagents

The following reagents were used for invadopodia assays: Poly-D-Lysine (Sigma), Gluteraldehyde (TAAB), Clear gelatin (Sigma) and 488-gelatin (Invitrogen).

2.5.2 Preparation of gelatin-coated coverslips

To perform the invadopodia assay, DX3 cells were plated onto gelatin-coated 13 mm coverslips. The protocol detailed below was used for their preparation.

PBSA was heated and clear gelatin added to make a solution of 1% gelatin, the mixture was then autoclaved and maintained at 50 °C in a water bath. Glass coverslips were placed in a 12 well plate, and coated with 0.3 ml of chilled poly-D-lysine (50 µg/ml) for 20 mins at room temperature. The pol-D-lysine was then aspirated and the coverslips washed 3x with PBSA. Coverslips were then coated with 0.3 ml of 0.5% gluteraldehyde and incubated at room temperature for 15 mins. The gluteraldehyde was then aspirated and the coverslips washed 3x with PBSA. To make clear gelatin, coverslips were coated with 0.3 ml 1% gelatin for 30 minutes. Coverslips were then carefully washed 3x with PBSA, and stored wrapped in foil in the fridge. To make fluorescently coated coverslips, 5 mg of 488-gelatin powder was mixed in 5 ml of autoclaved water. This was then added at a 1:30 dilution to the 1% clear gelatin before incubation on coverslips. The same protocol was performed on a 96 well format, with adjusted volumes of 50 µl per well.

2.5.3 Assay

To perform the assay, DX3 cells were plated at T=0 hrs onto gelatin-coated coverslips at $3x10^4$ cells per 12 well. At T=16 hrs, cells were fixed with 4% PFA in PBSA for 10 mins. Cells were washed with PBSA before immunofluorescence staining was carried out. Protocols for fixation and immunofluorescence are described in sections 2.9.2 and 2.9.3. For cells treated with siRNA, cells were plated 48 hrs after transfection, and for

expression of tagged-constructs, cells were plated 24 hrs post transfection. For gel degradation assays, experiments were performed in 96 well plates (PAA image glass plates), using fluorescent gelatin. The assay was performed as described above, however, 2000 cells were plated per well.

2.6 Vaccinia virus

The wild-type vaccinia virus strain used in this thesis is Western Reserve strain (WR). Modified versions of WR used in this study are listed in Table 2.4.

Table 2.4 Virus strains

Virus name	Generated by / Received from
WR / RFP-A3L	Sybille Schleich
WR / YFP-A3L	Sybille Schleich
A36R-YdF	Anna Holmström (Rietdörf et al., 2001)
Δ*A36R*	Geoffrey Smith (Parkinson and Smith, 1994)
A36R Y132F	Niki Scaplehorn
A36R Y132F / RFP-A3L	Ina Weisswange
A36-TM-SKIP-GFP	Mark Dodding
A36-TM-CSTN1-GFP	Mark Dodding

2.6.1 Virus stock preparation

Cells were infected using vaccinia virus prepared from post-nuclear stocks (PNS). Stocks were prepared by infecting 5x 15 cm dishes of 80% confluent HeLa with the relevant virus in serum free media at an MOI of 0.1 (described in 2.6.4). The media was then replaced by complete media 1 hr post-infection, and cells left for 2-3 days. The media was then collected, and dishes scraped in 5 ml PBSA. The collected media and PBSA was then spun at 1700 rpm for 5 mins at 4°C. The supernatant was removed and the pellet resuspended in 1.25 ml (250 µl per dish) of ice-cold viral lysis buffer (10mM Tris.HCl pH 9, 10mM KCl, 3mM Magnesium acetate). This suspension was then put at -20 °C for 16 hrs. The suspension was then thawed, and the cell membranes and nuclei sheared 10x through uptake with a 21G needle. A final spin at

5200 rpm for 5 mins at 4°C was then performed, before the supernatant was divided into 100 µl aliquots. This method resulted in a preparation containing mostly IMV particles, with a small population of EEV. The virus was put at -20 °C as a working aliquot for up to 3 months and at -80 °C for long-term storage.

2.6.2 Infection

To infect cells, an aliquot of the virus preparation was thawed and then sonicated for 30 seconds. The titre of the individual virus preparation was calculated by plaque assay, to allow determination of the units of virus per ml, and thus the multiplicity of infection (MOI), this is described further in section 2.6.4. An MOI of 2 /cell was used to infect cells for both immunofluorescence and live-cell imaging.

At T=0 hrs, HeLa cells were seeded at a density of $1x10^5$. At T=24 hrs, to infect the cells, the media was removed and serum free media containing the appropriate amount of virus was added to the cells. 1 hr post-infection the media was removed and was replaced with complete media. HeLa cells were fixed 9 hrs post-infection; while MEF and DX3 cells were fixed at 15 hrs post-infection due to a delay in the vaccinia replication cycle in these cell lines.

2.6.3 Drug treatments

HeLa cells were treated with the following drugs during the course of infection, their use is detailed in Table 2.5.

Table 2.5 Drug treatments during infection

Compound	Concentration	Use during infection	Source
Cytochalasin D	1 µg/ml	30 mins prior to fixation	Tocris
Nocodazole	20 mM	Added 4hrs post-infection after incubation of cells at -20°C for 5 mins, released 6 hrs post-infection	Sigma
Chlorpromazine	10 mM	Addition from point of	Sigma

		nocodazole release until fixation at 8 hrs post-infection	
PP3	25 mM	2 hrs prior to fixation	Millipore
PP1	25 mM	2 hrs prior to fixation	Millipore

2.6.4 Plaque assay

To assess virus titre, BS-C-1 cells were selected due to their ability to form a confluent monolayer, as well as the regular clearance formed upon viral infection. Importantly, the titre calculated in BS-C-1 cells could be translated effectively to both HeLa and MEF cell lines.

BS-C-1 cells were grown to a confluent monolayer in 6 well dishes. After sonication the virus preparation was serially diluted 1:10 in 1 ml of serum free media. The media was removed from BS-C-1, and replaced with 10^{-5}, 10^{-6} and 10^{-7} dilutions of the virus. 1 hr post-infection, the media was removed and replaced with an overlay containing 1x MEM, 5% FBS and 0.9% agarose. After 48 hrs, the cells were fixed with 4% PFA in PBSA for 1 hr before staining with crystal violet solution (0.1% crystal violet (w/v) and 20% ethanol in distilled water). The plaque forming unit (PFU/ml) was determined by counting the number of plaques formed (clearances in the cell monolayer) taking into account the dilution factor. The multiplicity of infection (MOI) was determined from the PFU of the virus stock and the number of cells used in the particular experiment.

A plaque assay was also performed to show the spread of infection in N-WASP -/- rescued stable cell lines. The same protocol was followed, with the exception that N-WASP -/- cell lines were plated to confluency in place of BS-C-1. The plaques were also labelled using antibody staining, the method is described in section 2.9.4.

2.7 Molecular biology

2.7.1 General buffers

5x TBE

54 g Tris Base (445 mM)

27.5g Boric Acid (445 mM)

20 ml 0.5 M EDTA (10 mM)

All reagents were diluted in a final volume of 1 L with distilled water.

5x DNA loading buffer

0.25% (w/v) Bromophenol blue

30% (v/v) Glycerol

Reagents were diluted in 5x TBE.

2.7.2 Expression vectors

A number of different expression vectors were used in this thesis, however, pLVX and pE/L were used in the majority of cases. pLVX is described in 2.3.5, and was used to make stable cell lines and for expression outside the context of infection. Two further mammalian expression vectors were also used, pCB6 and pRK5. Expression vectors used during the course of infection were pE/L driven. This vector contains a synthetic early/late vaccinia promoter to promote expression during the course of infection in mammalian cells (Chakrabarti et al., 1997). The expression constructs used in this thesis are listed in Table 2.6.

Table 2.6 List of expression vectors

Vector	Figure	Created by
pEL-GFP-LCa	3.4, 3,5	A. Humphries
pEL-Cherry-LCa	3.5	A. Humphries
pEL-GFP-PA-Cherry-β-actin	3.11	A. Humphries
pEL-A36-TM-Cherry	3.17, 3.18	Dodding et al., 2011
pEL-A36-TM-CSTN 879-971-Cherry	3.18	Dodding et al., 2011

pEL-A36-YdF-YFP	3.18	Frischknecht et al., 1999
pEL-GFP-stop	4.8-11, 5.6-8	Rietdörf et al., 2001
pEL-GFP-Cdc42	4.7-8, 4.10-11, 4.19-20, 5.7	Moreau et al., 2000
pEL-GFP-Cdc42-N17	4.8, 4.10, 4.11, 5.7	Moreau et al., 2000
pEL-GFP-N-WASP	4.9, 4.20, 5.8	Frischknecht et al., 1999
pEL-GFP-N-WASP-H208D	4.9, 5.8	Moreau et al., 2000
pEL-GFP-WH1-CRIB	4.18	Moreau et al., 2000
pEL-GFP-WH1-CRIB-H208D	4.18	Moreau et al., 2000
pEL-GFP-ITSN1L	5.1	A. Humphries
pEL-GFP-ITSN1S	5.1	A. Humphries
pEL-GFP-ITSN1L siRNA*	5.6	A. Humphries
pEL-GFP-ITSN1S siRNA*	5.6	A. Humphries
pEL-GST-stop	3.13, 5.8	Rietdörf et al., 2001
pEL-GST-A36 24-221	3.13	I Weisswange
pEL-GST-Cdc42	5.8	J. Cordiero
pRK5-FcγRIIa	5.10	Caron and Hall, 1998
pCB6-GFP-stop	5.10, 6.6	M. Way
pCB6-GFP-Nck	5.10	Scaplehorn et al., 2002
pCB6-GFP-Cdc42	5.10	J. Cordiero
pCB6-GFP-N-WASP	5.10	S. Donnelly
pLVX-GFP-ITSN-1L	5.10, 6.6	A. Humphries

2.7.3 Construction of DNA plasmids

New constructs were generated in one of three ways: PCR, sub-cloning or site-directed mutagenesis.

2.7.3.1 Polymerase Chain Reaction

PCR reactions were used to amplify DNA with the addition of suitable restriction sites for sub-cloning. A standard 100 µl PCR reaction contained 100 ng of DNA template, 1 µM of each primer, 1x Phusion HF buffer, 1 µM dNTP mix (0.25 µM of each nucleotide), and 2 units of Phusion High Fidelity DNA polymerase (NEB). The PCR reaction was performed using an Applied Biosystems GeneAmp PCR machine, using the following standard conditions:

1.	98 °C	1 minute	
2.	98 °C	15 seconds	
	55 °C	30 seconds	
	72 °C	30 seconds / kb of product length	25 cycles
3.	72 °C	10 minutes	

The PCR product was resolved in a 1% (w/v) agarose gel in TBE containing 1:10,000 SYBR safe DNA gel stain (Invitrogen). The product was visualised at 470 nm using a Safe Imager (Invitrogen). The product was then cut out of the gel and purified using the Qiagen QIAquick gel extraction kit. The product was eluted in 35 µl of distilled water and used in sub-cloning.

2.7.3.2 Sub-cloning

Constructs were generated from a PCR amplified product, or using a sequence verified insert from a pre-existing vector. 1 µg of insert and vector were digested in a mixture containing 10U of restriction enzyme (NEB) and the appropriate NEB buffer, the mixture was then put at 37 °C for 2 hrs. The reactions were resolved in a 1% (w/v) agarose gel and the appropriate products purified using the Qiagen QIAquick gel extraction kit. The products were eluted in 35 µl of distilled water. A ligation reaction was then performed with a 3:1 ratio of insert to vector size. The reaction also contained 1x T4 ligase buffer and 200U T4 ligase (NEB), and was left for 1 hr at room temperature. The ligation reaction was then transformed into chemically competent XL-10 cells (2.7.4). Digestion of purified DNA was performed to check for correct insertion, and where PCR had been used the insert was sequenced.

2.7.3.3 Site-directed mutagenesis

Mutations in the gene of interest were introduced into pre-existing vectors using a protocol based on Quick-change site-directed mutagenesis (Stratagene). Complimentary forward and reverse primers were designed to introduce single or multiple point mutations, with the mutation in the centre and complementary sequence to the gene of interest either side. The PCR was carried out with the following

conditions: 100 ng DNA, 125 ng of each primer, 1x Phusion HF buffer, 1 µM dNTP mix (0.25 µM of each nucleotide) and 2 units of Phusion High Fidelity DNA polymerase (NEB) in 100 µl total volume.

1.	98 °C	3 minutes	
2.	98 °C	15 seconds	
	55 °C	30 seconds	
	72 °C	8 minutes	21 cycles
3.	72 °C	10 minutes	

The PCR products were then exposed to 1 µl of Dpn1 restriction enzyme at 37 °C for 1 hr. Dpn1 specifically digests methylated DNA, and therefore targeted the template DNA. An additional PCR reaction was set up containing only the DNA template and buffer to be used as a control. The newly synthesised DNA was then precipitated by the addition of 250 µl ethanol and sodium acetate at a final concentration of 0.3 M, this mixture was stored at -20 °C for 1 hr. It was then spun at 13,000 rpm for 20 mins at 4 °C, the pellet was washed with 70% ethanol and a final spin of 13,000 rpm for 10 mins at 4 °C performed. After it had dried, the pellet was resuspended in 5 µl of distilled water and transformed into chemically competent XL-10 cells (2.7.4).

Table 2.7 Primers used in site-directed mutagenesis

Construct	Primer sequence
pLVX-GFP-N-WASP-H208D	CCAAGTAATTTCCAGGACATTGGACATGTTGG
pEL-GFP-ITSN1L siRNA*	TATCTGGGCGATTACAGTTGAAGAGAGAGCGAAGC
pEL-GFP-ITSN1S siRNA*	TATCTGGGCGATTACAGTTGAAGAGAGAGCGAAGC

2.7.4 Plasmid DNA transformation of bacteria

To transform DNA into bacteria, either the ligation reaction or 50 ng of plasmid DNA was incubated with 25 µl of chemically competent XL-10 cells on ice for 15 mins. The bacteria was then subjected to a 45 second heat shock at 42°C, and then placed on ice for 2 mins. 100 µl of LB was added to the mixture, and it was incubated at 37 °C for 30

mins with shaking. The bacterial culture was spread on LB-agar plates containing the appropriate antibiotics (usually 100 µg/ml ampicillin).

2.7.5 Preparation of chemically competent bacteria

Chemically competent XL-10 cells were prepared by inoculating 500 ml of LB media with 2 ml of a 5 ml culture grown overnight. To ensure the bacteria were in an exponential growth phase, the culture was grown with shaking at 37°C until an OD_{600} of 0.5 was reached. The bacterial culture was then incubated in ice for 30 mins, before centrifugation at 2500 rpm for 12 mins. The pellet was resuspended in RF1 buffer, and incubated on ice for a further 15 mins before centrifugation at 2500 rpm for 9 mins. The pellet was resuspended in 7 ml of RF2 buffer on ice, and the suspension snap frozen in liquid nitrogen in 100 µl aliquots and stored at -80 °C.

RF1 Buffer

12 g	Rubidium chloride (99 mM)
9 g	Manganese chloride (72 mM)
2.94 g	Potassium acetate (30 mM)
15% (w/v)	Glycerol

The reagents were dissolved in 900 ml distilled water, the pH adjusted to 5.8 with acetic acid, before adjusting the final volume to 1 L. The buffer was filtered through a 0.45 µm filter and stored at 4 °C.

RF2 Buffer

2.09 g	MOPS (10 mM)
1.2 g	Rubidium chloride (10 mM)
11 g	Calcium chloride (99 mM)
15% (w/v)	Glycerol

The reagents were dissolved in 900 ml distilled water, the pH adjusted to 6.8 with sodium hydroxide, before adjusting the final volume to 1 L. The buffer was filtered through a 0.45 µm filter and stored at 4 °C.

2.7.6 Plasmid DNA preparation

Plasmid DNA was purified from XL-10 cultures using Miniprep or Midiprep kits (Qiagen) according to manufacturers instructions. XL-10 cultures were grown from a single colony overnight in 5 ml or 50 ml of LB containing antibiotic (usually 100 µg/ml ampicillin) at 37 °C with shaking.

2.7.7 DNA sequencing

To check the sequence of newly constructed vectors, primers were designed to match DNA sequence flanking the region of sense or antisense strand and every 500 bases throughout the region of interest. The sequencing PCR reaction contained 3.2 pmol primer, 8 µl BDTv3.1 reaction mix (Big Dye Terminator Cycle sequencing kit) and 200 ng of plasmid DNA, and the conditions were as follows:

1.	95 °C	1 minute	
2.	95 °C	10 seconds	
	55 °C	5 seconds	
	60 °C	4 minutes	25 cycles

The PCR product was then purified using DyeEx columns (Qiagen) and vacuum dried. The LRI equipment park then performed sequencing.

2.8 Biochemistry

2.8.1 Whole cell lysate

Cells were washed with PBSA before the addition of a suitable volume of final sample buffer (FSB) (usually 50 µl in a 6 well plate). Cells were then scraped in FSB and transferred to an eppendorf. 0.5 µl of benzonase (Novagen) was added to degrade DNA where required. The lysate was then put at 95 °C for 5 mins before resolving by SDS-PAGE.

2x FSB

50% (w/v)	Glycerol
3%	SDS
50 mM	Tris.HCl, pH 6.8
2%	β-mercaptoethanol
Bromophenol blue	

2.8.2 Immunoblot analysis

For immunoblot analysis pre-cast NU-PAGE 4-12% Bis-Tris 1.0 mm gels (Invitrogen) were used. Gels were run using MES running buffer (Invitrogen) at 200V for ~40 mins. After separation, proteins were transferred onto nitrocellulose membranes using the iBlot and iBlot gel transfer kit (Invitrogen). The membrane was blocked in 5% milk in PBSA with 0.1% Tween (PBST) (Sigma) for 1 hr at room temperature. Primary antibody was incubated on the membrane in 5% milk in PBST for 1 hr at room temperature or at 4 °C overnight. The membrane was washed 3x with PBST for 10 mins before incubation with HRP conjugated secondary antibody in 5% milk TBST for 30 mins. The membrane was again washed 3x with PBST for 10 mins before incubation with ECL (Amersham Biosciences). The membrane was exposed to Hyperfilm-ECL (Amersham Biosciences) and developed using an IGP compact automated developer (IPG limited).

Table 2.8 Antibodies used in immunoblot analysis

Antibody	Species	Dilution	Origin
CHC	Rabbit	1:2500	AbCam
AP-2α	Mouse	1:1000	Thermo Scientific
AP-2μ	Mouse	1:1000	BD Transduction
GST	Rabbit	1:5000	Sigma
FLAG	Mouse	1:1000	Sigma
β-actin	Mouse	1:5000	Sigma
ITSN-1	Rabbit	1:1000	Peter McPherson (McGill)
GFP	Mouse	1:2500	CRUK

Nck	Rabbit	1:1000	Millipore
Cdc42	Rabbit	1:1000	Santa Cruz
N-WASP	Rat	1:1000	Way Lab
HRP-Rabbit	Goat	1:5000	Jackson Immunoresearch
HRP-Mouse	Goat	1:5000	Jackson Immunoresearch
HRP-Rat	Goat	1:5000	Jackson Immunoresearch

2.8.3 GST-pull down assay

At T=0 hrs, $3x10^6$ HeLa cells in a 6 cm plate were infected with vaccinia virus at an MOI of 2. 1 hr post-infection the media was changed, and the relevant pE/L-GST-tagged constructs transfected into cells using effectene. At T=16 hrs, the media was removed and the cells were washed 1x with PBSA on ice. The PBSA was subsequently removed and 250 µl of lysis buffer added. The cells were scraped into the lysis buffer and transferred to an eppendorf, which rotated at 4 °C for 10 mins. The lysate was then spun at 13,000 rpm at 4 °C for 5 mins and the supernatant retained. 25 µl of the lysate was retained to run as an input sample.

10 µl of glutathione sepharose beads (Amersham biosciences) were added to an eppendorf and washed 2x with ice-cold PBSA. The lysate was then added to the beads, and the mixture rotated for 2 hrs at 4 °C. The beads were then washed 3x with ice-cold wash buffer, before they were resuspended in 25 µl of PBSA. FSB was added to both the beads and the input samples and they were put at 95 °C for 10 mins before resolving by SDS-PAGE.

Lysis buffer

50 mM Tris.HCl, pH7.5
150 mM NaCl
0.5 mM EDTA
0.5% NP-40
0.5% Triton-X
Protease Inhibitor

Wash buffer

50 mM Tris.HCl, pH7.5

150 mM NaCl
0.5 mM EDTA
Protease Inhibitor

2.8.4 GFP-trap

At T=0 hrs, $3x10^6$ HeLa cells in a 6 cm plate were infected with vaccinia virus at an MOI of 2. 1 hr post-infection the media was changed, and the relevant pE/L-GST-tagged constructs transfected into cells using effectene. At T=16 hrs, the media was removed and the cells were washed 1x with PBSA on ice. The PBSA was subsequently removed and 100 µl of lysis buffer added. The cells were scraped into the lysis buffer and transferred to an eppendorf, which rotated at 4 °C for 10 mins. The lysate was then spun at 13,000 rpm at 4 °C for 5 mins and the supernatant retained, 150 µl of wash buffer was then added. 25 µl of the lysate was retained to run as an input sample. 10 µl of GFP-trap beads (Chromotek) were added to an eppendorf and washed 2x with ice-cold PBSA. The lysate was then added to the beads, and the mixture rotated for 1 hr at 4 °C. The beads were then washed 3x with ice-cold wash buffer, before they were resuspended in 25 µl of PBSA. FSB was added to both the beads and the input samples and they were put at 95 °C for 10 mins before resolving by SDS-PAGE.

Lysis buffer
10 mM Tris.HCl, pH7.5
150 mM NaCl
0.5 mM EDTA
0.5% NP-40
Protease Inhibitor

Wash buffer
10 mM Tris.HCl, pH7.5
150 mM NaCl
0.5 mM EDTA
Protease Inhibitor

2.9 Imaging

2.9.1 General reagents

1x Cytoskeletal buffer (CB)

10 mM	MES, pH 6.1
150 mM	NaCl
5 mM	EGTA
5 mM	$MgCl_2$
5 mM	Glucose

The reagents were dissolved in distilled water.

Blocking buffer

1%	BSA
2%	FCS

The reagents were dissolved in 1x CB, and filtered through a 0.45 µm filter and stored at -20 °C in aliquots.

Mowoil

2.4 g	Mowoil
6 g	Glycerol (33% w/v)
12 ml	200 mM Tris.HCl, pH 8.5 (133 mM)

Mowoil and glycerol were added to 6 ml of distilled water. The mixture was then incubated for 2 hrs at room temperature with stirring, before the addition of Tris.HCl. The resultant solution was then stirred for 10 mins at 60 °C, before centrifugation at 5000 rpm for 5 mins. Mowoil was stored at -20 °C in aliquots.

10% and 4% paraformaldehyde (PFA)

50 g of PFA was added to 500 ml of warm PBSA, and the solution gently stirred. 1 M NaOH tablets were added until the PFA had dissolved. After cooling, the pH was adjusted to 7.5, and the solution passed through a 0.45 µm filter and stored at -20 °C in aliquots. 10% aliquots were thawed and freshly diluted to 4% with PBSA before use.

2.9.2 Fixation

Cells were fixed using paraformaldehyde (PFA) or in some cases a paraformaldehyde-methanol (P-M) fixation was performed. For PFA fixation, cells were incubated with 4% PFA in PBSA for 10 mins before washing 1x with PBSA. For the P-M fixation, 4% PFA in PBSA was added to cells for two mins, before it was replaced with methanol that had been stored at -20 °C, for one minute. The cells were then washed 2x with PBSA.

2.9.3 Immunofluorescence

Blocking buffer was added to cells for 10 mins, before incubation with antibody. For extracellular virus labelling, and for labelling of attached red blood cells, the B5 antibody and rabbit secondary antibody were added prior to permeabilisation. In other cases, cells were permeabilised for 45 seconds with 0.1% Triton-X in PBSA. The coverslips were then washed 3x with PBSA. Cells were incubated with primary antibody in blocking buffer for 1 hr, before washing 3x with PBSA. Secondary antibody in blocking buffer was then added for 30 mins, and DAPI (300 nM in PBS) was added for 2 mins before cells were washed 3x with PBSA. Coverslips were dipped in distilled water before mounting using Mowoil on microscopy slides. F-actin was stained using Phalloidin, which was diluted 1:1000 in blocking buffer, and was added at the same time as secondary antibody.

Table 2.9 Antibodies used in immunofluorescence

Antibody	Species	Dilution	Source
B5	Rat	1:500	Gerhardt Hiller
B5-488	Rat	1:10,000	Way Lab
A27	Mouse	1:500	Mariano Esteban
A36	Rabbit	1:200	Way Lab
CHC	Rabbit	1:200	AbCam
AP-2	Mouse	1:200	AbCam
ITSN1	Rabbit	1:200	Peter McPherson
Nck	Rabbit	1:200	Millipore
WIP	Rabbit	1:200	Way Lab
Grb2	Rabbit	1:200	Santa Cruz

N-WASP	Rat	1:200	Way Lab
Cortactin	Mouse	1:200	Millipore
Phalloidin (TR / 488)	N/A	1:1000	Molecular probes

2.9.4 Antibody staining of viral plaques

In addition to staining with crystal violet, plaques were also visualised using the B5 antibody. After fixation, cells were permeabilised for 2 mins with 0.1% Triton-X in PBSA. The cells were then washed 3x with PBSA. Cells were incubated with B5 antibody in blocking buffer at a dilution of 1:1000 for 1 hr with gentle rocking, before washing 3x with PBSA. An anti-rat HRP conjugated secondary antibody diluted 1:1000 in blocking buffer was then added for 45 mins with gentle rocking, before cells were washed 3x with PBSA. 0.5 ml of TMB peroxidase substrate (Sigma) was then added to each well, and left for 5-15 mins with gentle rocking. The substrate was removed once plaques were visible, and distilled water added for 1 min, before it was removed and the plate was left to dry.

2.9.5 Microscopes

2.9.5.1 Zeiss Axioplan Upright

For imaging of fixed samples, a Zeiss Axioplan2 microscope equipped with a Photometrics Cool Snap HQ cooled CCD camera, external Prior Scientific filter wheels (DAPI; FITC; Texas Red; Cy5) and a 63x / 1.4 Plan Achromat objective was used. The system was purchased from Zeiss and Universal Imaging Corporation Limited and was controlled with MetaMorph 6.3r7 software. Images were analysed using the MetaMorph software and were processed with the Adobe software package.

2.9.5.2 Spinning-disk confocal

Live-cell imaging, FRAP and photoactivation was carried out on a Zeiss Axio Observer microscope equipped with a Plan Achromat 63x / 1.4 Ph3 M27 oil lens, an Evolve 512 camera and a Yokagawa CSUX spinning disk. The system was purchased from 3i

Intelligent Imaging Innovations and was controlled by Slidebook 5.0. Movies were analysed using either the Slidebook or MetaMorph software.

2.9.5.3 OMX

Super-resolution microscopy was performed using an Applied Precision OMX V3 structured illumination system with an Olympus 100x / 1.4 objective and four Photometric Cascade II 512 EMCDD cameras. The microscope has 5 laser lines; 405 nm, 488 nm, 514 nm, 592 nm and 642 nm, and the live emission filter set was used 465-500 nm, 525-575 nm and 602-656 nm.

2.9.6 Live-cell imaging

Live-cell imaging was performed using the spinning-disk confocal (2.9.5.2). $2x10^5$ cells were plate in a 35 mm dish. Imaging was performed at 8 hrs post-infection for HeLa cells with transfection of pE/L constructs at 4 hrs post-infection. For MEFs cells were infected at T=0 hrs, transfected with pE/L constructs at T=1 hrs, and imaging performed at T=15 hrs. The exposure times used varied depending on the experiment, in general, images were acquired at 2 second intervals.

2.9.7 FRAP

Fluorescence recovery after photobleaching (FRAP) experiments were performed on cells infected with either WR RFP-A3L or Y132F RFP-A3L virus, the cells used also stably expressed the protein of interest with a GFP-tag. For HeLa cells, imaging was performed at 8 hrs post-infection, and for MEFs imaging was performed at 15 hrs post-infection. Images were acquired using the spinning-disk confocal (2.9.5.2) at an interval of 350 ms with an exposure time of 100 ms for each channel. The GFP signal at an RFP-A3 positive particle was bleached using 5 iterations of the 488 nm laser at 100% power.

The fluorescence recovery of bleached GFP was subsequently measured using the Slidebook software. A threshold intensity mask was applied to each movie to allow detection of GFP-positive particles, with the frames containing the bleached signal

added to the mask manually. The intensity was then tracked over the course of the movie using the particle-tracking feature within the software. The background intensity was then determined and subtracted from the signal at the particle. The intensity was then normalised to the intensity of the pre-bleach signal, and the values compiled in a graph using the Prism software. Kinetic modelling of the data was then carried out in Prism using the equation $Y_{(t)} = (Ymax-Ymin)(1-e^{-kt}) + Ymin$, where Y = intensity and t = time. The rate constant of recovery (k) and the percentage recovery (compared to the pre-bleach intensity), were calculated from the best-fit curve. The half-time of fluorescence recovery was calculated from the rate constant of recovery ($T_{1/2}=In2/k$).

2.9.8 Photoactivation

Photoactivation experiments were performed on cells infected with WR YFP-A3L virus, the cells were also transiently expressing GFP-PA-Cherry-β-actin driven through pE/L expression. Images were acquired using the spinning-disk confocal (2.9.5.2) at an interval of 350 ms with an exposure time of 100 ms for each channel. A region of the vaccinia actin tail was activated using 5 iterations of the 405 nm laser at 100% power, which converted the fluorescence signal from Cherry to GFP in this region.

The decay in GFP intensity after photoactivation was subsequently measured using the Slidebook software. The region of photoactivation was manually selected and a mask applied to track the region through the course of the movie. The background intensity was also determined and subtracted from the GFP signal. The intensity was then normalised, and the values compiled in a graph using the Prism software. Kinetic modelling of the data was then carried out in Prism using the same parameters as for FRAP experiments.

2.9.9 Structured-Illumination microscopy

To improve resolution, structured illumination (SI) super-resolution microscopy was performed. SI uses a wide-field imaging technique, in which a striped pattern of light illuminates the whole imaging field. The illumination pattern interacts with fluorescent probes in the sample to generate interference patterns termed moiré fringes. Different orientations of illumination are used to produce a series of moiré fringes, and as the illumination pattern is known this can be used to reconstruct a super-resolution image.

Cells were plated on 0.17 mm square coverslips (Zeiss), and immunofluorescence was performed as described in 2.9.3 with the exception that coverslips were mounted using Vectashield (Vector Labs) and secured with nail polish.

2.9.10 Electron Microscopy

Transmission electron microscopy (TEM) was carried out by the electron microscopy department at the London Research Institute. HeLa cells were plated on 13 mm coverslips at 80% confluency, and were infected with vaccinia virus before fixing at 9 hrs post-infection with 1.5% gluteraldehyde / 2% PFA in 0.1 M phosphate buffer, pH 7.4 for 30 mins at room temperature. Cells were then post-fixed in 1.5% potassium ferrocyanide / 1% osmium for 1 hr and stained with 1% tannic acid in 0.05 M sodium cacodylate, pH 7.4 for 45 mins. Coverslips were then dehydrated stepwise through ethanol, infiltrated with 50:50 propylene oxide: epon, followed by two changes of pure resin and embedded overnight ‘en face’ at 60°C. Sections of ~120 nm were collected using an UCT ultramicrotome (Leica Microsystems), post-stained with lead citrate and viewed using a Tecnal G2 Spirit 120 kV transmission electron microscope (FEI company) and imaged with a XC1000 Orlus CCD camera (Gatan).

2.10 Statistical Analysis

Data in all graphs are presented as mean and standard error of the mean, unless otherwise stated. Prism 5.0 (GraphPad) was used to perform standard statistical analysis of data sets. When two data sets were compared a Student’s t test was performed, if multiple data sets were compared a One Way Anova analysis followed by Tukey Multiple Comparison was used to compare all pairs of samples. A p value of <0.05, <0.01 and <0.001 is represented as *, ** and ***, respectively. Data was not considered statistically significant if the p value gave > 0.05, and in this event the data was labelled, n.s., for not significant.

Chapter 3. Clathrin promotes actin polymerisation through modulating the spatial organisation of A36

3.1 Introduction

Many stages of the vaccinia replication cycle have been well characterised, however, we lack detailed understanding of the processes that occur at the plasma membrane during the latter stages of viral egress. To enhance our knowledge of these ill-defined events, we used electron microscopy to examine viral particles at the periphery of cells. Electron micrographs revealed a hazy, spiked structure around the individual membranes of several viral particles, which was reminiscent of a clathrin coat. I therefore sought to determine whether clathrin is indeed recruited to viral particles, and if so, whether this recruitment modulates vaccinia virus egress and/or actin tail formation.

3.2 Results

3.2.1 Clathrin is recruited to extracellular virus particles

During egress, vaccinia undergoes two stages of motility to enhance its spread. In the first stage, vaccinia is efficiently directed to the periphery of cells using kinesin-1-dependent microtubule-based transport (Dodding et al., 2011; Geada et al., 2001; Hollinshead et al., 2001; Newsome et al., 2004; Rietdorf et al., 2001; Ward and Moss, 2004). After fusion with the plasma membrane, the virus then induces actin-based motility with the formation of a tail (Cudmore et al., 1995; Newsome et al., 2004). The factors that mediate this switch in motility and the events that occur between these two phases, however, are not well defined. To further analyse the processes that occur at the plasma membrane, HeLa cells were infected with the Western Reserve (WR) strain of vaccinia and processed for electron microscopy (EM) by Lucy Collinson. A spikey structure was visible around the membrane of several individual viral particles at the cell periphery, which was highly reminiscent of a clathrin coat (Figure 3.1). This was

rather unexpected, as the classic role of clathrin is in internalisation, whereas in this case, the viral particles were in the process of leaving the cell.

To confirm that the structure around the viral particles was indeed clathrin, immunofluorescence staining was carried out on vaccinia infected HeLa cells. Cells were fixed at 9 hrs post-infection to allow sufficient time for the virus to replicate, and to undergo egress. Cells were then stained with an antibody against the viral protein B5, which recognises an epitope that becomes exposed upon viral fusion (Hiller and Weber, 1985). Staining prior to permeabilisation thus allows visualisation of extracellular viral particles on the plasma membrane. After permeabilisation, staining with an antibody against the clathrin heavy chain (CHC) revealed co-localisation between CHC and extracellular B5 (exB5) (Figure 3.2A). These puncta were confirmed as viral particles, as they also co-stained for DAPI, which labels the viral DNA (Figure 3.2A). In addition to clathrin, exB5 also co-localised with the plasma membrane specific adaptor, AP-2 (Figure 3.2A). Furthermore, CHC and AP-2 showed extensive co-localisation on viral particles, suggesting that clathrin is recruited to the virus in an AP-2-dependent manner (Figure 3.2B). In line with this, analysis of their percentage co-localisation with extracellular virions gave similar values of 14.0±2.4% for CHC and 15.3±2.8% for AP-2 (Figure 3.2B). Altogether, this data is consistent with the observations from EM, and confirms that clathrin can be recruited to vaccinia during the latter stages of viral egress.

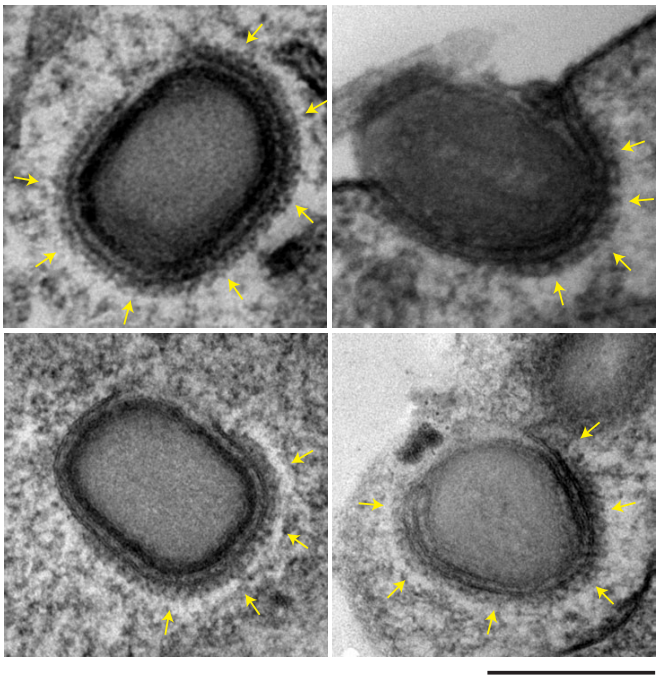

Figure 3.1 Clathrin-like coats around viruses in the cell periphery

Electron micrographs of vaccinia virus particles at the periphery of infected HeLa cells fixed at 9 hrs post-infection. Example images show a hazy spiked structure around the membrane of viral particles that is reminiscent of a clathrin coat (yellow arrows). Scale bar = 250 nm. Electron microscopy was performed by Lucy Collinson.

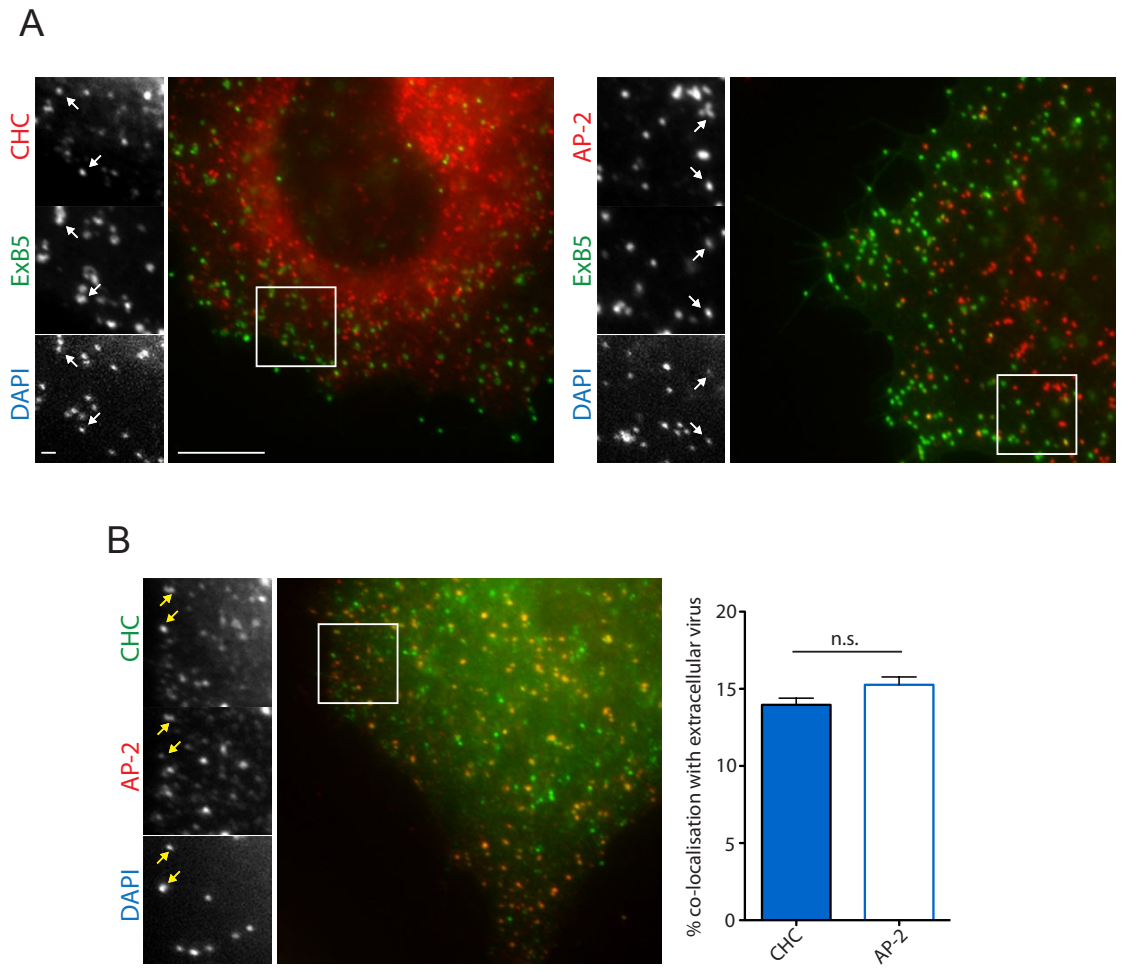

Figure 3.2 Clathrin and AP-2 are recruited to extracellular viral particles

A Representative immunofluorescence images of vaccinia infected HeLa cells fixed at 9 hrs post-infection. Cells were stained prior to permeabilisation with a B5 antibody, which recognises an epitope that is exposed upon viral fusion. The stained puncta represent extracellular viral particles (exB5) that are also positive for DAPI. The left image is stained for clathrin heavy chain (CHC) and the right image, the plasma membrane adaptor AP-2. The zoomed inserts highlight examples of co-localisation (white arrows). **B** Immunofluorescence images showing extensive co-localisation between CHC and AP-2. The zoomed inserts highlight examples of co-localisation at viral particles indicated by the DAPI stain (yellow arrows). The graph shows the percentage co-localisation of extracellular viral particles with CHC and AP-2, error bars represent SEM from a 15 μm^2 box in 30 cells over three independent experiments. The percentage co-localisation in both cases is ~15% consistent with their co-recruitment to viral particles. Scale bars = 1 and 10 μm.

3.2.2 Clathrin recruitment is a transient event

As only a proportion of extracellular viral particles co-localised with AP-2/clathrin, I wondered whether their recruitment could reflect a transient event occurring as the virus fuses with the plasma membrane. As CHC and AP-2 were observed on extracellular viral particles, immunofluorescence staining was carried out to mark the events surrounding viral fusion. Infection of cells that were stably expressing RFP-tagged kinesin light chain 2, showed no co-localisation between kinesin-1 and AP-2/clathrin on viral particles (Figure 3.3A). However, independent examples of kinesin-1-associated and AP-2/clathrin-associated particles could be seen (Figure 3.3A). Therefore, kinesin-1-based transport and clathrin localisation are distinct. Furthermore, staining with phalloidin also revealed that AP-2/clathrin does not localise to the tip of actin tails, suggesting that clathrin recruitment occurs between the two phases of vaccinia virus motility (Figure 3.3B).

To further investigate the transient nature of clathrin localisation, live-cell imaging experiments were performed. HeLa cells were infected with a virus expressing RFP-tagged A3 (a core viral protein), and were transiently transfected with GFP-tagged clathrin light chain (GFP-LCa). The construct contained the pE/L promoter, which is a synthetic early/late vaccinia promoter and therefore drove expression of GFP-LCa during the course of infection (Chakrabarti et al., 1997). In accordance with the data from fixed cells, distinct movements of the viral particle were observed either side of a stationary phase in which clathrin localised at the particle (Figure 3.4). Prior to clathrin recruitment, a directed viral movement was observed, that had speeds indicative of microtubule-based transport (Dodding et al., 2011; Rietdorf et al., 2001) (Figure 3.4). Additionally, following clathrin localisation, the virus moved in a slower fashion that correlated with previously recorded speeds of vaccinia-induced actin-based motility (Rietdorf et al., 2001; Weisswange et al., 2009) (Figure 3.4). This data further supports the notion that clathrin is recruited between the two stages of vaccinia motility, however, it relies on information inferred from the motility pattern and associated speed of the viral particle. To support this assumption, further live-cell imaging experiments were performed, that contained additional markers for different stages of infection.

To monitor viral fusion with the plasma membrane in live cells, the B5 antibody used in fixed cells was conjugated to fluorescent Alexa 488. B5-488 Ab was added directly to the imaging media, and as the virus fused with the plasma membrane the antibody

became enriched at the extracellular viral particle. Addition of the antibody was used in combination with WR infected cells expressing Cherry-tagged clathrin light chain. In all cases the antibody detected viral particles before accumulation of the Cherry signal (Figure 3.5A). Therefore, clathrin recruitment occurs only after viral fusion with the plasma membrane. As kinesin-1 recruitment is lost during fusion, this also supports earlier observations from both fixed and live cells (Figure 3.3A and 3.4) (Newsome et al., 2004).

Next to show the relationship between clathrin recruitment and actin-based motility, cells transiently expressing GFP-LCa and stably expressing LifeAct-Cherry were infected with RFP-A3 expressing virus. LifeAct is a reporter for filamentous actin, therefore, both the viral particle and actin tail could be visualised in the same red fluorescent channel (Figure 3.5B) (Riedl et al., 2008). Vaccinia particles were seen associated with clathrin, before the induction of an actin tail, that appeared to propel the viral particle away from the clathrin (Figure 3.5B). Thus, clathrin is recruited to vaccinia in the moments before actin filament nucleation. As the live-cell imaging experiments suggested formation of an actin tail could be responsible for the dissociation of the virus from clathrin, experiments were carried out to inhibit actin nucleation. This was achieved through infecting MEFs that lacked an essential component of the vaccinia actin-signalling complex (Nck or N-WASP), or though treatment with cytochalasin D, a drug that inhibits actin polymerisation (Figure 3.6) (Brenner and Korn, 1979; Brown and Spudich, 1979; Lin et al., 1980; Mousa et al., 1978). In all cases, blocking actin polymerisation led to a significant increase in the percentage co-localisation of AP-2 with extracellular virions compared to controls (Figure 3.6). Therefore, actin nucleation does contribute to the dissociation of AP-2/clathrin from viral particles.

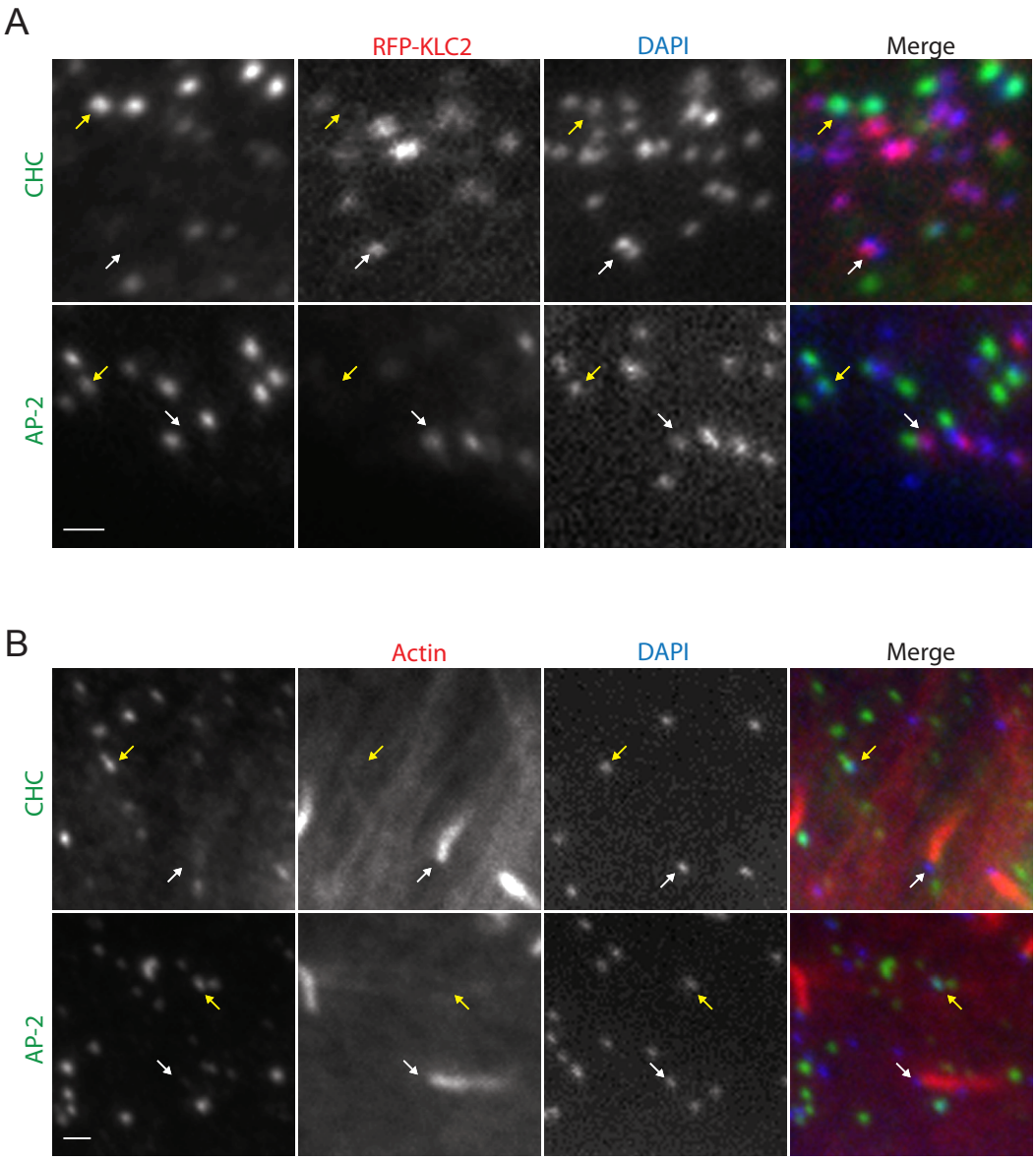

Figure 3.3 Clathrin and AP-2 do not co-localise with either kinesin-1 or actin positive viral particles

A Immunofluorescence images of HeLa cells stably expressing RFP-tagged kinesin-1 light chain 2. Cells were infected with WR for 9 hrs before fixation. White arrows highlight examples of viral particles that co-localise with kinesin-1. CHC and AP-2 were not observed on such particles. CHC and AP-2, however, localised with a different subset of viral particles (yellow arrows). **B** Immunofluorescence images of WR infected HeLa cells. AP-2 and CHC were not observed at virus particles inducing an actin tail (white arrow), however, AP-2 and CHC did localise with a different subset of viral particles (yellow arrows). Scale bars = 1 μm.

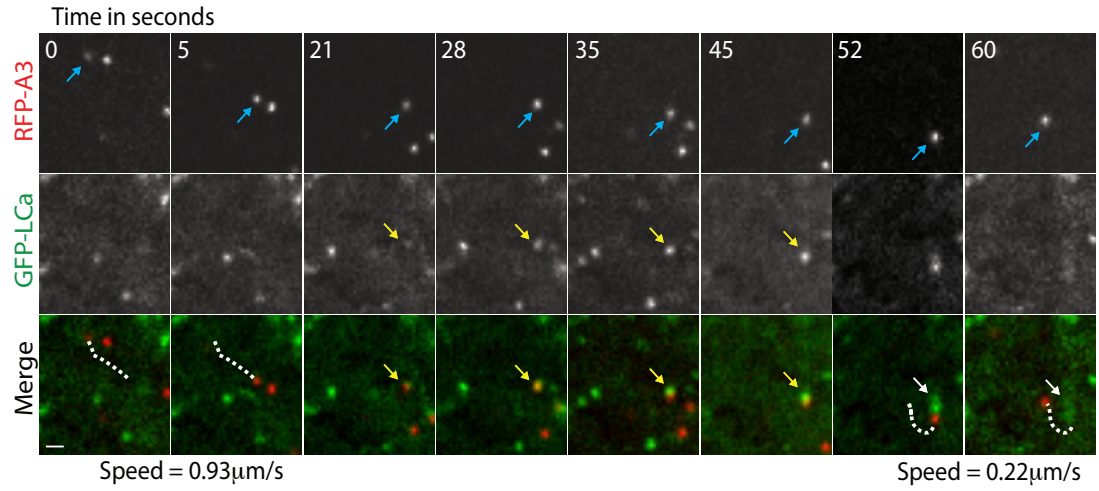

Figure 3.4 Clathrin is transiently recruited to viral particles

Stills from live-cell imaging at 8 hrs post-infection showing the recruitment of clathrin to a viral particle (blue arrows). The stills show a virus particle (RFP-A3) that moves in a directed fashion, before clathrin (GFP-LCa) accumulates on the stationary particle (yellow arrows). The virus then moves away from the clathrin signal, leaving it behind (white arrows). The path of virus motility is drawn with a white dotted line, and the speed of movement indicated below the image. Scale bar = 1 μm.

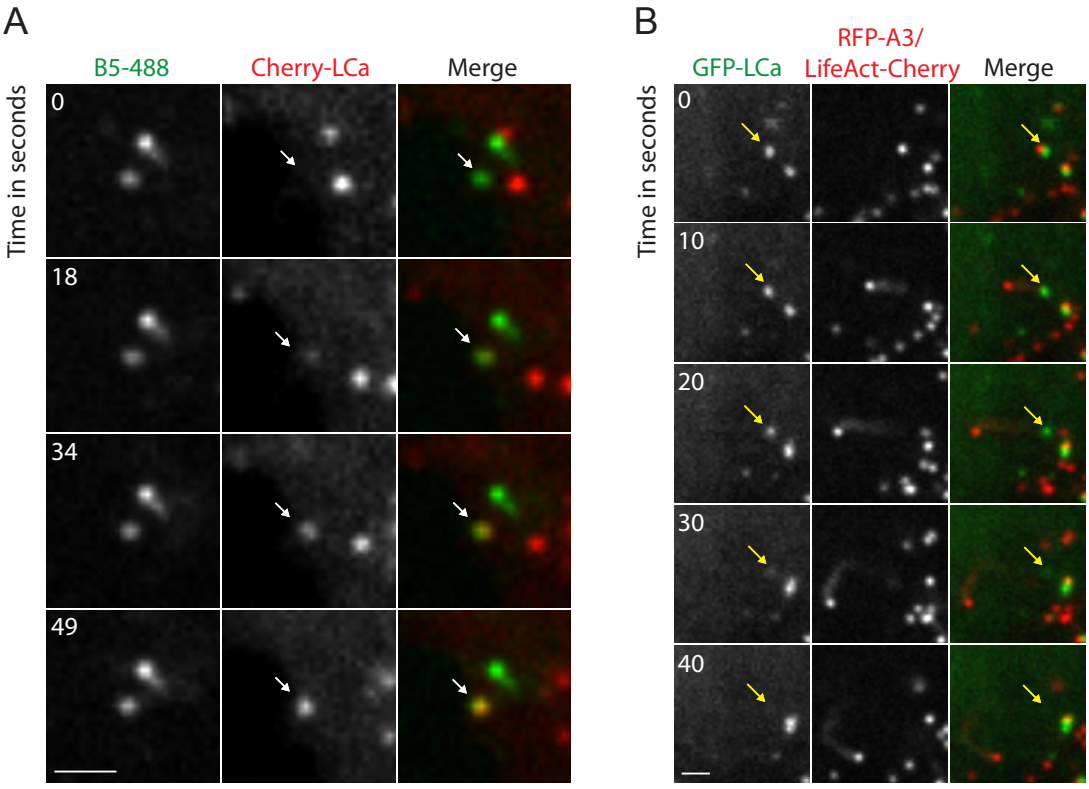

Figure 3.5 Clathrin recruitment precedes actin tail formation

A Stills from live-cell imaging showing an extracellular virion (white arrow) detected with Alexa 488-conjugated B5 antibody (B5-488) that accumulates clathrin over time (Cherry-LCa). **B** Stills from live-cell imaging showing a viral particle (RFP-A3) that is associated with clathrin (GFP-LCa) (yellow arrow). The viral particle induces an actin tail visualised by expression of LifeAct-Cherry. The tail propels the virus away from clathrin, which remains behind (yellow arrows). Scale bars = 1 μm.

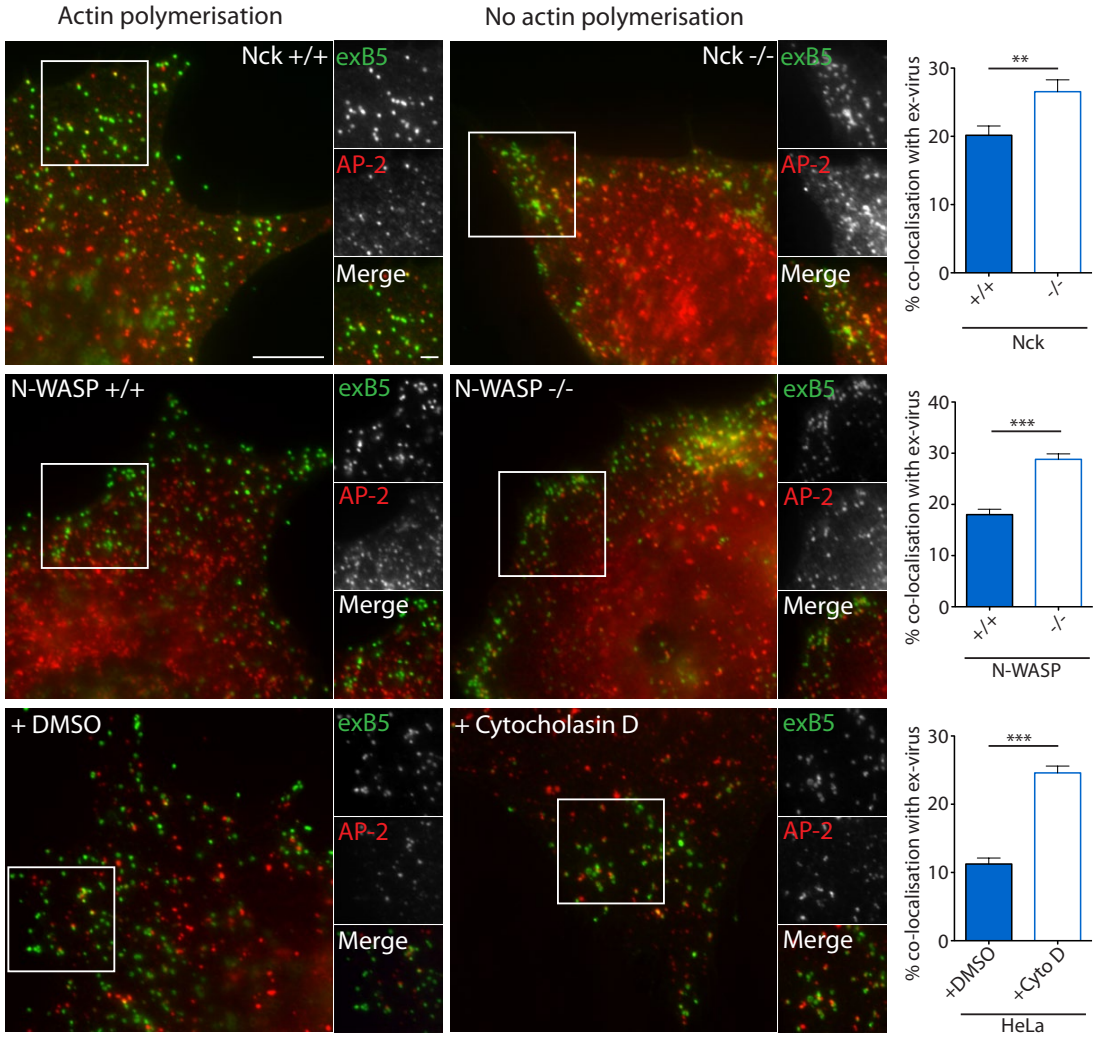

Figure 3.6 Blocking actin nucleation enhances AP-2 localisation at viral particles

Images showing the recruitment of AP-2 to extracellular virions (exB5) in Nck and N-WASP +/+ and -/- MEFs, and HeLa cells treated with DMSO or cytochalasin D. Each example shows co-localisation of AP-2 in a cell that is able to nucleate an actin tail compared to one that is deficient in actin tail formation. In the absence of actin polymerisation, the co-localisation of AP-2 with exB5 is increased. The graphs show the percentage of extracellular virus positive for AP-2. The error bars represent SEM from a 15 μm^2 box in 30 cells over three independent experiments. A p value of < 0.001 and <0.01 is indicated by *** and **, respectively. Scale bars = 1 and 10 μm.

3.2.3 Clathrin recruitment promotes actin tail formation

Immunofluorescence and live-cell imaging experiments revealed that clathrin is recruited to viral particles in the moments before actin nucleation. To determine the functional consequence of this recruitment, knockdown experiments were performed. Firstly, the clathrin heavy chain was targeted by two independent siRNA oligos. Both oligos efficiently depleted CHC protein levels as determined by western blot (Figure 3.7A). Concomitant with this, the percentage co-localisation of extracellular viral particles with CHC was also significantly reduced (Figure 3.7A). Depletion of CHC had no affect on AP-2 localisation, consistent with an upstream role for AP-2 (Figure 3.7A).

CHC depleted cells showed two actin tail phenotypes. The percentage of extracellular viral particles inducing an actin tail was significantly reduced, from 30.7±2.0 to 17.8±1.4.and 19.5±1.5% (Figure 3.7B and C). The morphology of the tails was also affected, with a long actin tail phenotype observed (Figure 3.7B and C). Therefore, clathrin not only regulates actin tail formation but it also somehow modulates the way in which an actin tail forms. In addition to defects in actin tail formation, the total number of extracellular viral particles was also decreased after CHC depletion (Figure 3.7B). As clathrin is involved at multiple locations within the cell and could consequently also regulate other stages of the vaccinia assembly cycle, I additionally performed experiments to target the plasma membrane specific adaptor, AP-2. If AP-2 were responsible for recruiting clathrin to the viral particle, depleting AP-2 levels would lead to the loss of clathrin localisation. To deplete levels of the AP-2 complex, an oligo targeting the alpha (α) subunit and an oligo targeting the mu (μ) subunit were selected. The oligos successfully targeted the associated subunit, as well as leading to a marked reduction of the other subunit, as has been previously observed (Figure 3.8A) (Motley et al., 2003). Consistent with a role for AP-2 in clathrin recruitment, the co-localisation of both AP-2 and CHC with exB5 was markedly reduced upon AP-2 depletion (Figure 3.8A). In line with this, the phenotype observed was comparable to results from CHC knockdown. Both the percentage of extracellular virus producing an actin tail was significantly reduced (20.8±3.2 and 23.3±2.1% compared to 37.7±3.7%), and those tails that were able to form showed an increased length (4.84±0.1 and 4.5±0.1 μm compared to 2.91±0.1 μm) (Figure 3.8B and C). However, in contrast to CHC depletion the number of extracellular virions was equivalent in control and AP-2 depleted cells (Figure 3.8B). As AP-2 and CHC depletion exhibit the same actin tail phenotype,

further experiments targeted AP-2 to maintain specificity towards events at the plasma membrane.

As clathrin is recruited around the time of viral fusion and there was a defect in extracellular virus production upon its depletion, I wanted to exclude the possibility that the AP-2-dependent recruitment of clathrin could modulate viral fusion with the plasma membrane. Infection was synchronised through nocodazole treatment to prevent microtubule polymerisation, thereby inhibiting kinesin-1-dependent transport of viral particles to the cell periphery. Nocodazole was subsequently removed and cells released into control or chlorpromazine containing media, the latter of which interferes with AP-2 function by promoting its relocation away from the plasma membrane (Wang et al., 1993). Prolonged nocodazole treatment successfully prevented progression through the replication cycle as shown by a lack of actin tails (Figure 3.9A). Cells that were released from nocodazole treatment exhibited similar numbers of extracellular viral particles with or without the presence of chlorpromazine (Figure 3.9A and B). In contrast, the number of actin tails was reduced and the length of tails increased, consistent with previously observed phenotypes (Figures 3.9A and B). Therefore, clathrin recruitment via AP-2 regulates actin tail formation but does not modulate viral fusion, consistent with the equivalent number of extracellular virions observed after RNAi-mediated depletion of AP-2 (Figure 3.8B). The reduction in extracellular viral particles resulting from clathrin depletion therefore likely corresponds to an early defect in the replication cycle that is AP-2 independent.

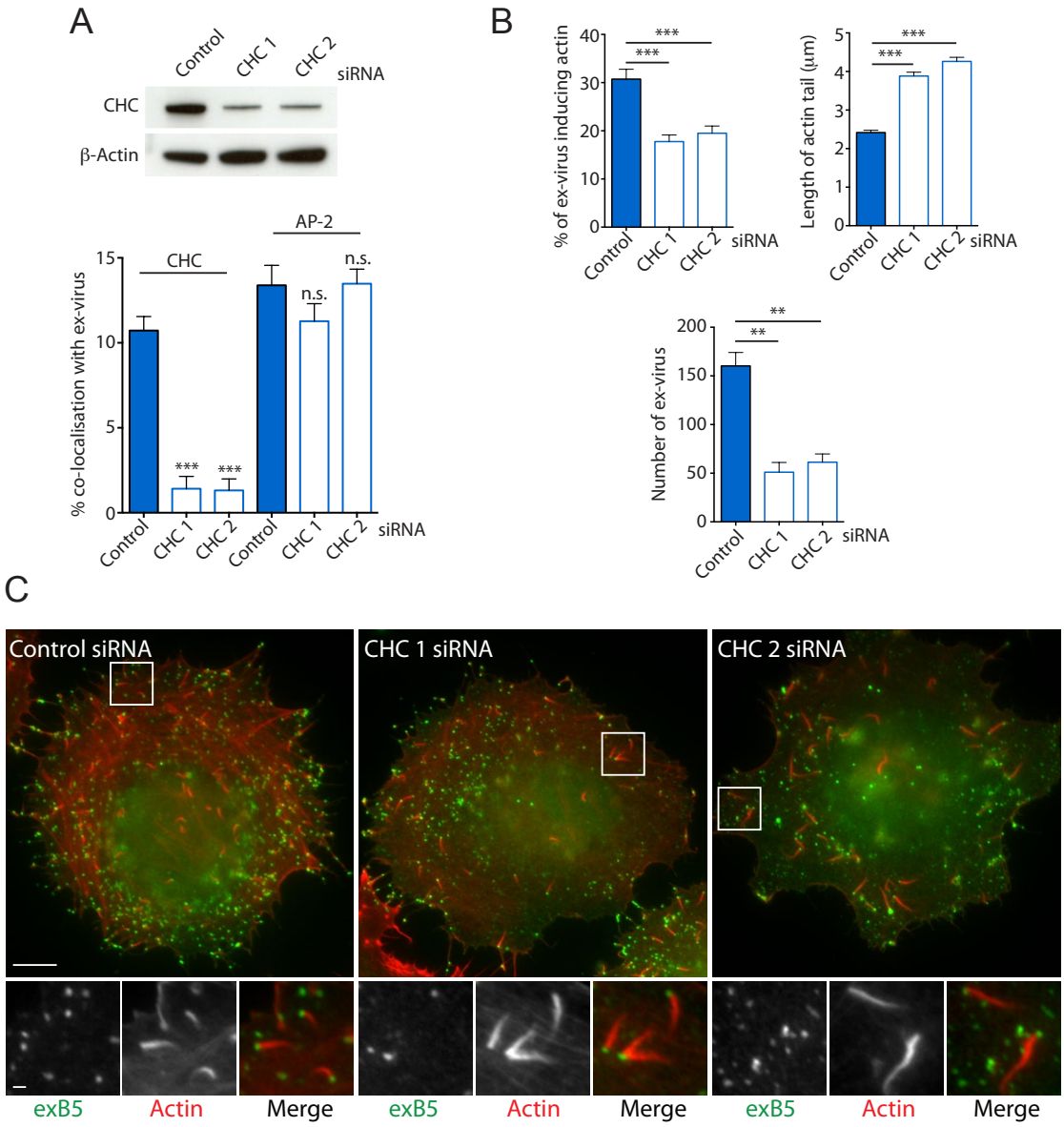

Figure 3.7 Clathrin depletion leads to fewer but longer actin tails

A Western blot showing CHC protein levels after treatment with the indicated siRNA oligos, β-actin is included as a loading control. The graph shows the percentage co-localisation of CHC and AP-2 with exB5 after treatment with the indicated siRNA. Depletion of CHC reduces its recruitment to viral particles but does not affect AP-2 recruitment. Error bars represent SEM from a 15 μm^2 box in 30 cells over three independent experiments. A p value of < 0.001 is indicated by ***. **B** Quantification of the percentage of extracellular virus inducing an actin tail, the length of actin tails and the number of extracellular particles after treatment with the indicated siRNA. Error bars represent SEM from 30 cells over 3 independent experiments, and for the length of tails, 5 tails were measured in each cell. A p value of < 0.001 is indicated by ***. **C** Representative immunofluorescence images of vaccinia infected HeLa cells treated with the indicated siRNA along with magnified inserts to highlight the actin tail length. Scale bars = 1 and 10 μm.

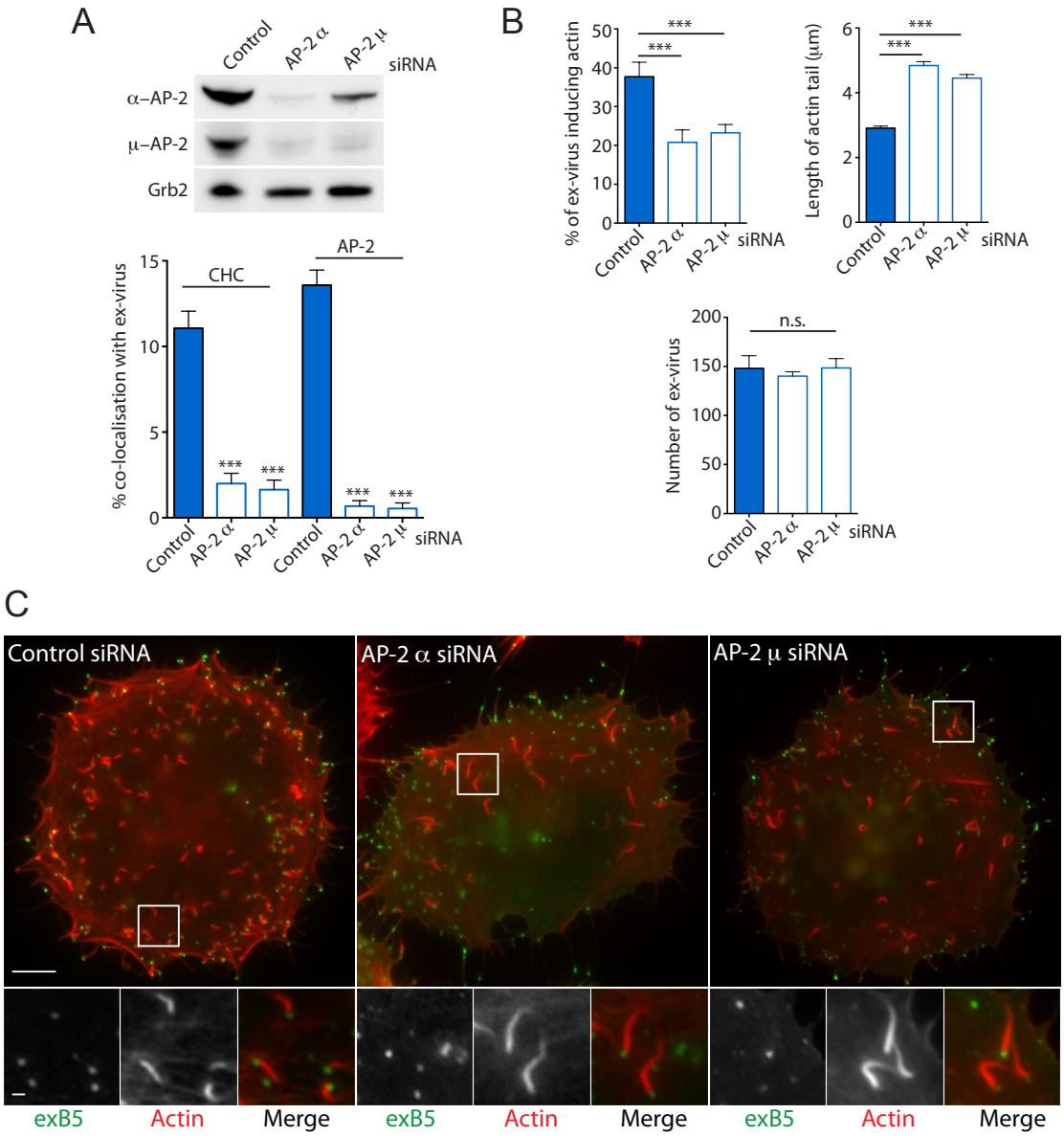

Figure 3.8 AP-2 depletion phenocopies CHC knockdown

A Western blot showing protein levels of the α and μ subunit of the AP-2 complex after treatment with the indicated siRNA oligos, Grb2 is included as a loading control. The graph shows the percentage co-localisation of CHC and AP-2 with exB5 after treatment with the indicated siRNA. Depletion of the AP-2 complex reduces its recruitment to viral particles and also significantly impedes CHC recruitment. Error bars represent SEM from a 15 μm^2 box in 30 cells over three independent experiments. A p value of < 0.001 is indicated by ***. **B** Quantification of the percentage of extracellular virus inducing an actin tail, the length of actin tails and the number of extracellular virions after treatment with the indicated siRNA. Error bars represent SEM from 30 cells over 3 independent experiments, and for the length of tails, 5 tails were measured in each cell. A p value of < 0.001 is indicated by ***. **C** Representative immunofluorescence images of infected HeLa cells treated with the indicated siRNA along with magnified inserts to highlight the actin tail length. Scale bars = 1 and 10 μm.

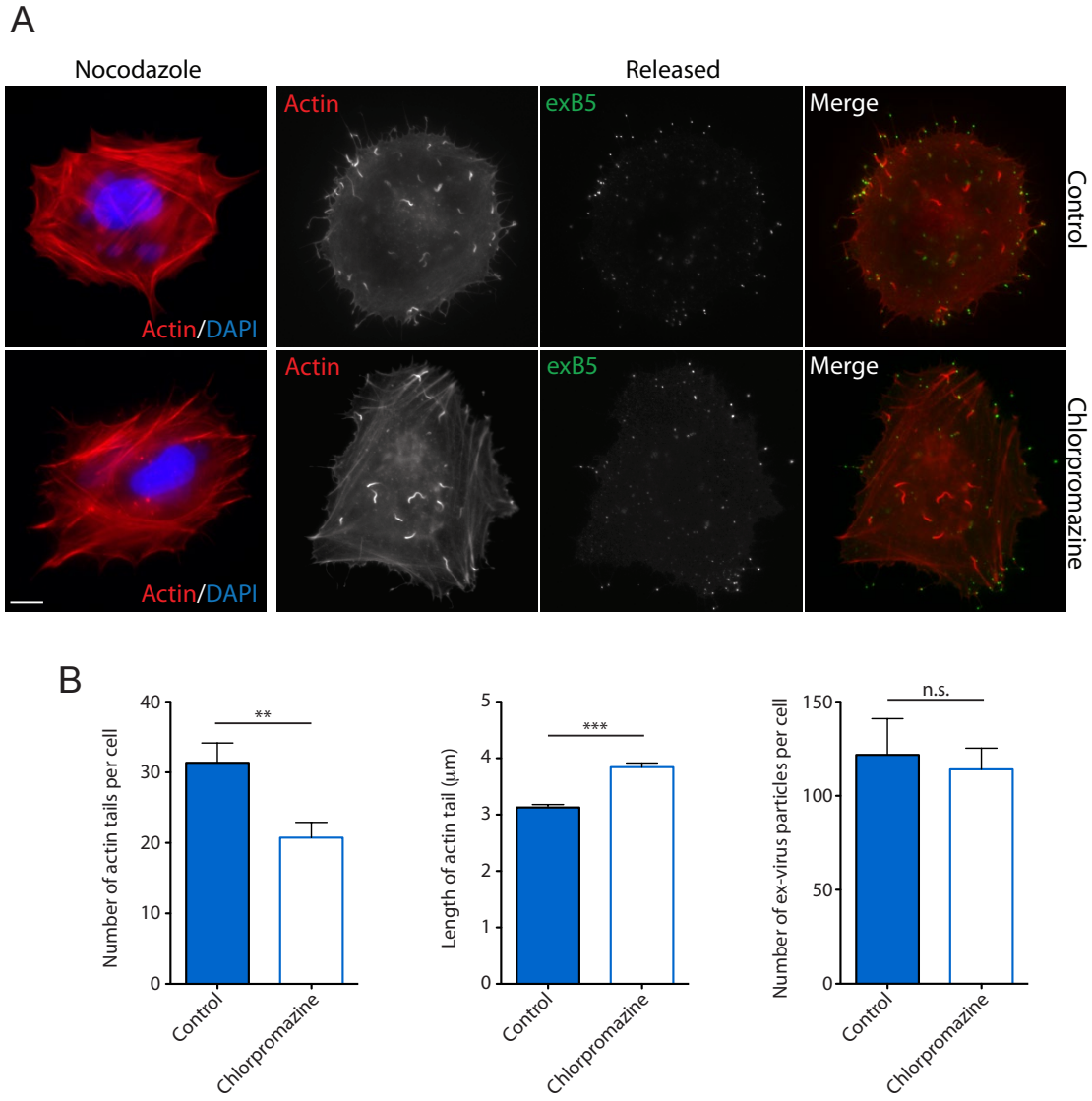

Figure 3.9 Clathrin recruitment does not regulate viral fusion with the plasma membrane

A Representative immunofluorescence images of vaccinia infected HeLa cells treated with the indicated drugs. Prolonged nocodazole treatment prevents progression of the vaccinia replication cycle as shown by a lack of actin tails (left). Those cells that were released from nocodazole treatment (right), however, exhibit extracellular viral particles and actin tails. Cells treated with chlorpromazine have fewer actin tails, that are longer, but have equivalent numbers of extracellular virions compared to control. Scale bar = 10 μm. **B** Quantification of the number of actin tails per cell, the length of actin tails and the number of extracellular viral particles per cell, in cells released from nocodazole in the presence or absence of chlorpromazine. Error bars represent SEM from 30 cells in 3 independent experiments, for length of tails, 5 tails were measured per cell. A p value of <0.001 and < 0.01 is indicated by *** and **, respectively.

3.2.4 AP-2 depletion alters the dynamics of actin polymerisation

Experiments blocking the recruitment of clathrin to viral particles led to a decrease in the number of vaccinia-induced actin tails but also led to an increase in the length of those actin tails that did form. As the tails exhibited an altered morphology, I reasoned that understanding the cause of these changes might also provide insight into their decreased number. To explore this further, experiments were performed to quantify the dynamics of actin polymerisation in control and AP-2 depleted cells. Live-cell imaging in phase contrast was used to allow visualisation of both viral particles and the induced actin tail, these movies were subsequently analysed for a number of parameters (Figure 3.10A and B). Firstly, the time before nucleation, which was recorded from the point a virion became stationary at the periphery of the cell, indicative of viral fusion after microtubule-based transport. AP-2 depleted cells showed a marked increase in the time taken to nucleate an actin tail (Figure 3.10B). The duration of actin-based motility was also reduced, suggesting that actin structures formed in the absence of AP-2 are less stable (Figure 3.10B).

Actin tails in AP-2 depleted cells also had an increased rate of motility, concomitant with their increased length (Figure 3.10A and B). To determine if the disassembly rate of actin filaments was also affected, I used a photo-activatable version of GFP tagged to β-actin (Figure 3.11A) (Welman et al., 2010). Photo-activatable GFP is able to switch from an inactive state to an active fluorescent state upon stimulation that promotes a conformational change (Patterson and Lippincott-Schwartz, 2002). As the photo-activatable GFP is not seen prior to stimulation, a fusion construct containing mCherry was used that allowed simultaneous imaging of both mCherry and activated GFP (Figure 3.11A) (Welman et al., 2010). This construct when expressed in infected cells labelled the actin tail with Cherry, and upon focused activation with a 405nm laser, a small patch of the actin tail became positive for GFP fluorescence (Figure 3.11C). The decay in GFP intensity of this fluorescent patch was then recorded over time and used to determine the disassembly rate of the actin tail. AP-2 depleted cells showed slower disassembly rates compared to control cells (7.34±0.22s compared to 6.45±0.13s), suggesting that the long actin tail phenotype observed in the absence of AP-2 is due to a contribution of decreased disassembly, as well as increased nucleation events (Figure 3.11B and 3.10B).

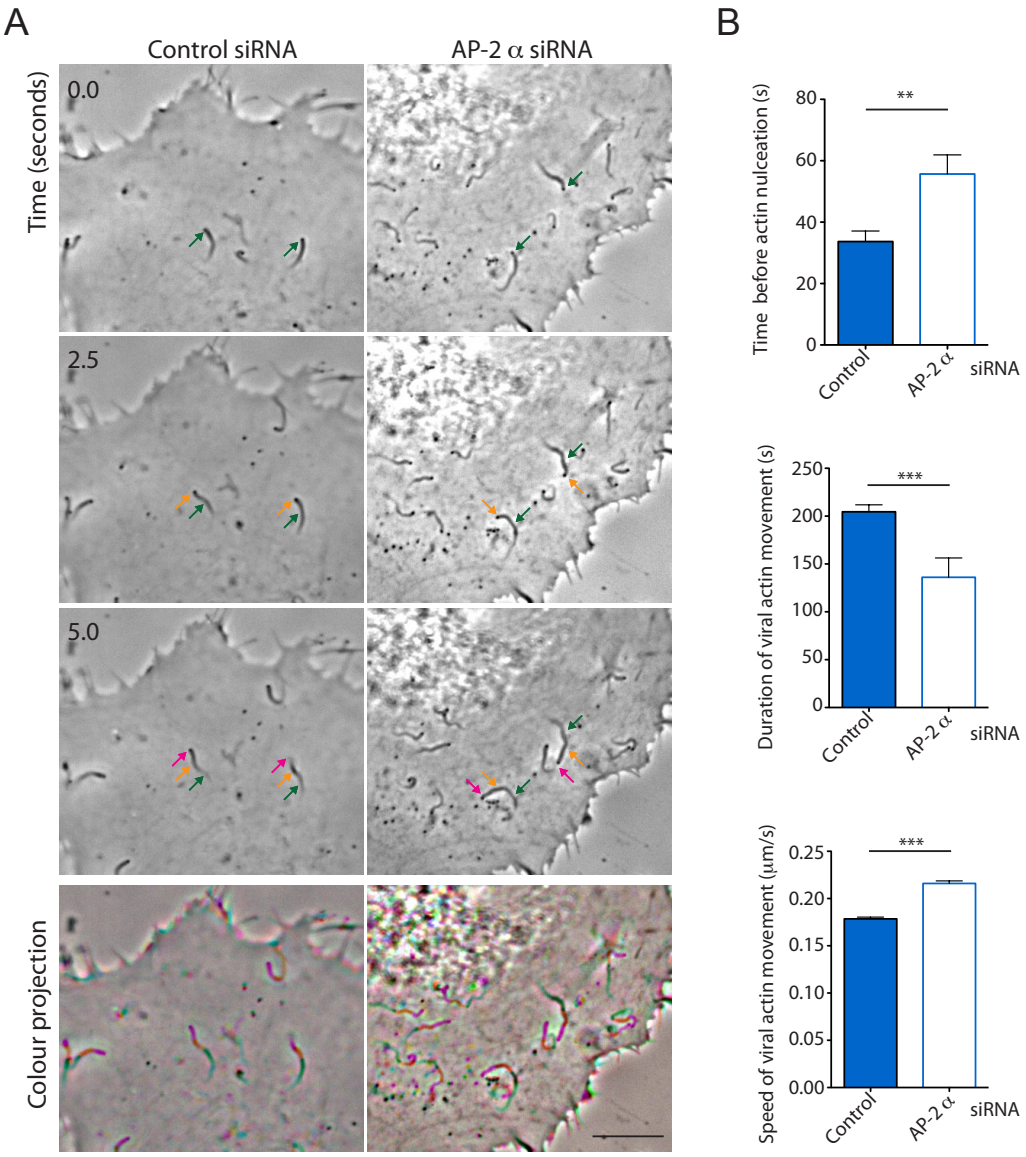

Figure 3.10 AP-2 depletion alters the dynamics of actin tails

A Stills from live-cell imaging at 8 hrs post-infection using phase contrast to visualise viral particles and actin tails. A series of three stills of representative control and AP-2 cells is shown along with a colour projection to highlight actin tail progression during the course of the movie. Progression is also highlighted by the coloured arrows, which show the location of the virus particle in consecutive frames. Scale bar = 5 μm **B** Quantifications from live-cell imaging, including the time before actin nucleation as determined from the time a virus particle became stationary at the periphery of the cell until the induction of an actin tail. Additional graphs show the duration of the actin tail movement and the speed of actin-based motility. Error bars represent SEM from 150 events/tails in 3 independent experiments. A p value of < 0.001 and < 0.01 is indicated by *** and **, respectively.

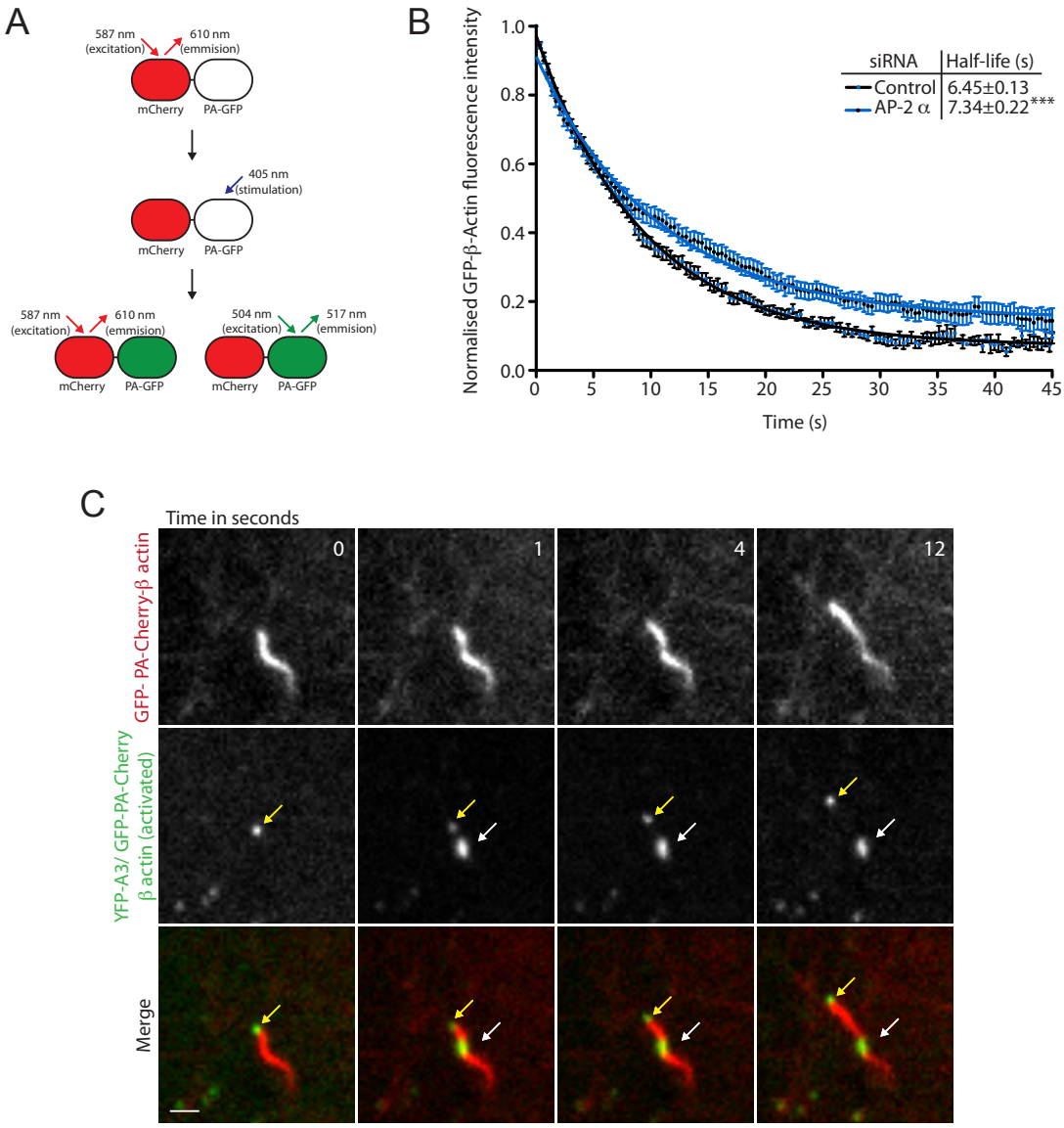

Figure 3.11 Long actin tails exhibit a decreased rate of disassembly

A Schematic of the activation of GFP fluorescence by the GFP-PA-Cherry construct with a 405nm laser. Schematic is adapted from Welman et al., 2010. **B** Quantification of the decay kinetics of photoactivated GFP-PA-Cherry-β-actin in actin tails in control and AP-2 depleted cells. N=41 from three independent experiments, a p value of < 0.001 is indicated by ***. **C** Still images from live-cell imaging showing the actin-based movement of YFP-A3 virus (yellow arrows) in a cell expressing GFP-PA-Cherry-β-actin. The white arrow indicates the position where laser activation promotes GFP fluorescence. Scale bar = 1 μm.

3.2.5 Clathrin recruitment promotes stability of the actin-signalling complex

Our previous work has shown that the actin-signalling network beneath vaccinia is highly dynamic (Weisswange et al., 2009). Furthermore, it was also shown that the rate of N-WASP exchange limits the rate of actin-based motility (Weisswange et al., 2009). Given the observation that AP-2 depleted cells have an increased rate of actin-based motility, I wondered whether this might reflect a change in the dynamic stability of N-WASP. To determine the rate of exchange of N-WASP, fluorescence recovery after photobleaching (FRAP) experiments were performed. HeLa cells stably expressing GFP-N-WASP were treated with control or AP-2 siRNA, before infection with the RFP-A3 expressing virus. Cells were then used in live-cell imaging experiments, where the GFP signal at the virus particle was bleached with a 488 laser. The recovery of the fluorescent signal was recorded and used to determine the percentage recovery and half-life of recovery (Figure 3.12). There was no significant difference in the percentage recovery between control and AP-2 depleted cells, however, the half-life of GFP-N-WASP was significantly increased to 2.04±0.07 s from 2.67±0.11 s (Figure 3.12). This is consistent with the increased rate of actin-based motility induced by the virus, and indicates that in the absence of clathrin, N-WASP is less stable within the signalling complex beneath the virion. Together, this data suggests that clathrin in some way supports the formation of a more stable actin-signalling complex that promotes more efficient actin polymerisation.

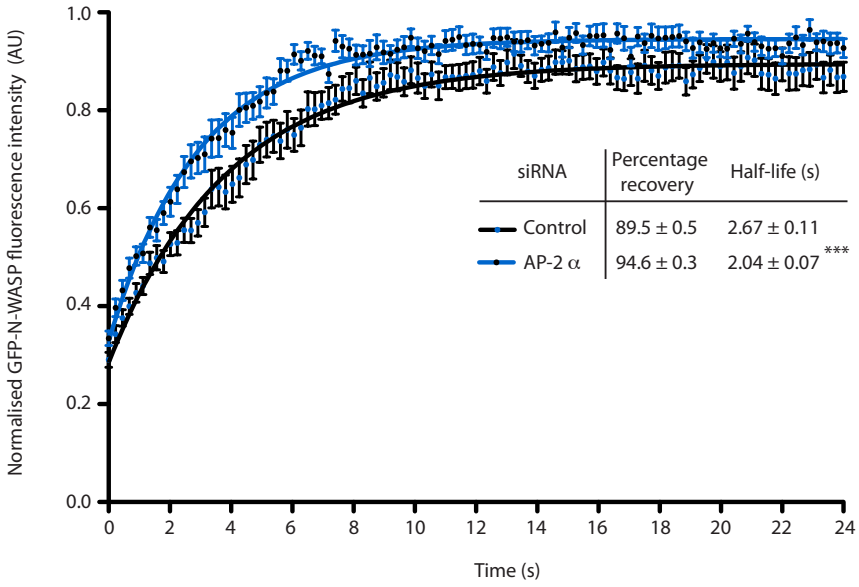

Figure 3.12 AP-2 recruitment enhances N-WASP stability beneath extracellular virions

Graph showing the quantification of GFP-fluorescence after photobleaching. The recovery curve is shown from control and AP-2 depleted cells, along with derived values for percentage recovery and half-life of recovery in each condition. N=30 from three independent experiments, a p value of <0.001 is indicated by ***.

3.2.6 Clathrin clusters A36 and its associated signalling network

As AP-2 and clathrin depletion causes an actin tail phenotype, I next focused my attention on the protein responsible for recruitment of the actin-signalling complex, A36. During CME, AP-2 engages with transmembrane cargo to promote their selective incorporation into the forming vesicle. I therefore wondered whether AP-2 could engage with the cytoplasmic tail of A36, altering both its spatial organisation and consequently that of the actin-signalling complex. Pull-down assays using residues 24-221 of A36 tagged to GST did indeed show an interaction with AP-2 that was not observed with GST alone (Figure 3.13).

I next looked at the localisation of A36 in the presence and absence of AP-2, which due to the small scale of the virus required the use of structured illumination (SI) super-resolution microscopy. Super-resolution imaging is defined by an increase in resolution by at least 2-fold, and in our case structured illumination was preferred over other techniques as it gives a good 3D perspective and is readily amenable to multi-colour acquisition (Langhorst et al., 2009). Staining of the viral particle was carried out using an antibody against the inner viral membrane protein A27, which presented as a ring in cross-section (Figure 3.14). In the absence of an actin tail, A36 also appeared as a ring representative of its localisation around the entire viral membrane (Figure 3.14). Analysis of particles that were inducing an actin tail, however, showed a dramatic refocusing of A36 towards the site of actin nucleation (Figure 3.14). This was quantified by measuring how far the A36 signal extended around the A27 ring, and was represented as a percentage of A27 circumference. Equivalent particles in AP-2 depleted cells exhibited a similar but significantly more disperse polarisation compared to control cells (Figure 3.14). This suggests that AP-2 enhances the sequestration of A36 beneath the viral particle.

As changes to A36 organisation would have a knock-on effect on the actin-signalling complex I also examined the distribution of N-WASP beneath the virus. N-WASP localised to the tip of the actin tail as expected, but its localisation was significantly more disperse in the AP-2 depleted cells, determined using the same quantification method as for A36 (Figure 3.15). As the nucleation of actin would also impact on the spatial organisation of A36 and N-WASP, I also examined the localisation of A36 in the absence of actin tails. Infection of N-WASP -/- MEFs showed that a proportion of viral

particles exhibited A36 polarisation even in the absence of an actin tail (Figure 3.16). This polarisation was also significantly reduced in the absence of AP-2 (Figure 3.16). Altogether, my data suggest that AP-2 promotes the polarisation of A36 beneath the viral particle, which in turn creates a platform for the recruitment of the highly cooperative vaccinia actin-signalling network.

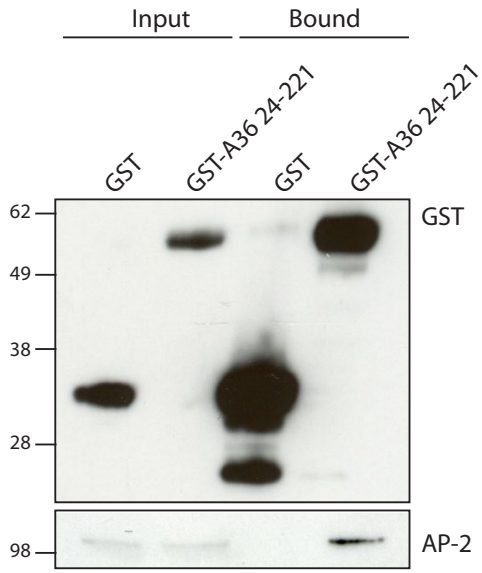

Figure 3.13 AP-2 binds the cytoplasmic tail of A36

Western blot showing AP-2 binding to GST-tagged cytoplasmic tail of A36 (residues 24-221) in vaccinia infected cells, with no binding observed to GST alone.

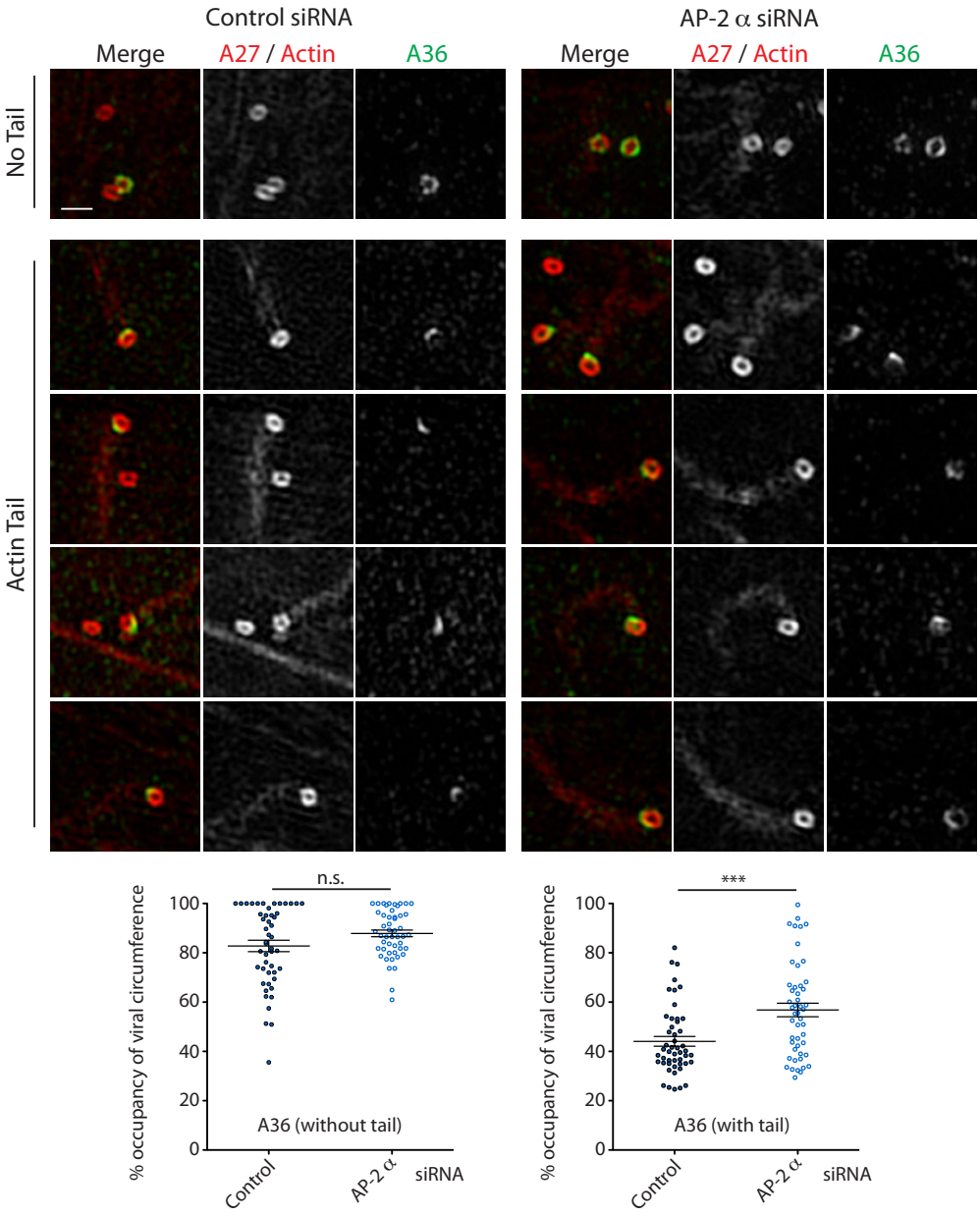

Figure 3.14 A36 clustering is impeded in the absence of AP-2

Images from structured illumination microscopy showing viral particles (A27) with and without the induction of an actin tail. Particles that are not inducing an actin tail show A36 localising around the entire virion signified by a ring. Those particles inducing an actin tail show polarisation of A36 towards the site of actin nucleation. In the AP-2 depleted cells this process was less efficient, resulting in a more disperse localisation. Scale bar = 500 nm. The graphs show the quantification of percentage occupancy of A36 around the viral particle in the absence (left) and presence (right) of an actin tail. Error bars represent SEM from 50 particles, a p value of <0.001 is indicated by ***.

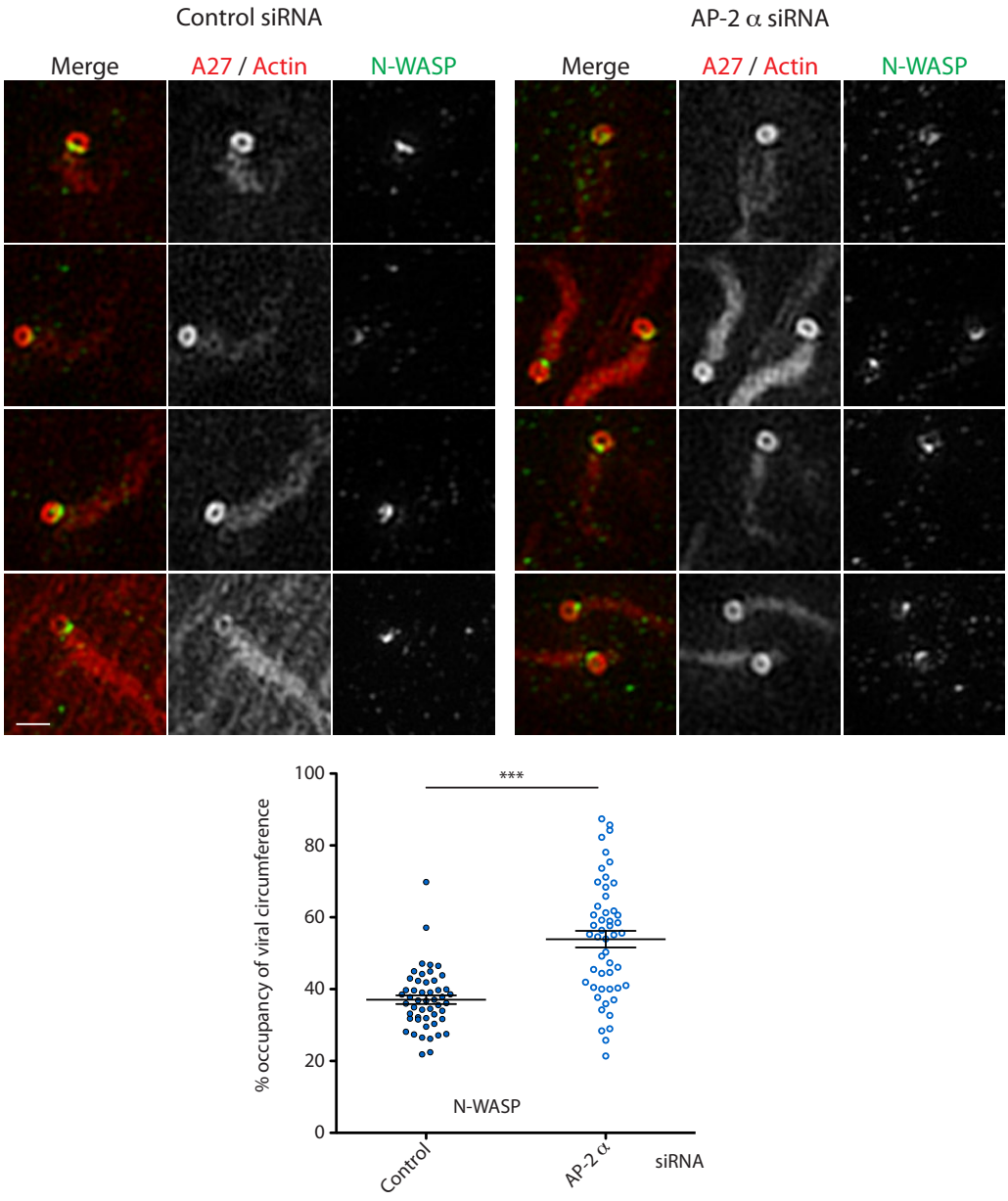

Figure 3.15 The localisation of N-WASP is more disperse in the absence of AP-2

Structured illumination images showing the localisation of N-WASP beneath viral particles inducing an actin tail, in control and AP-2 depleted cells. Scale bar = 500 nm. Graph shows the quantification of percentage occupancy of N-WASP around the viral particle. Error bars represent SEM from 50 particles, a p value of <0.001 is indicated by ***.

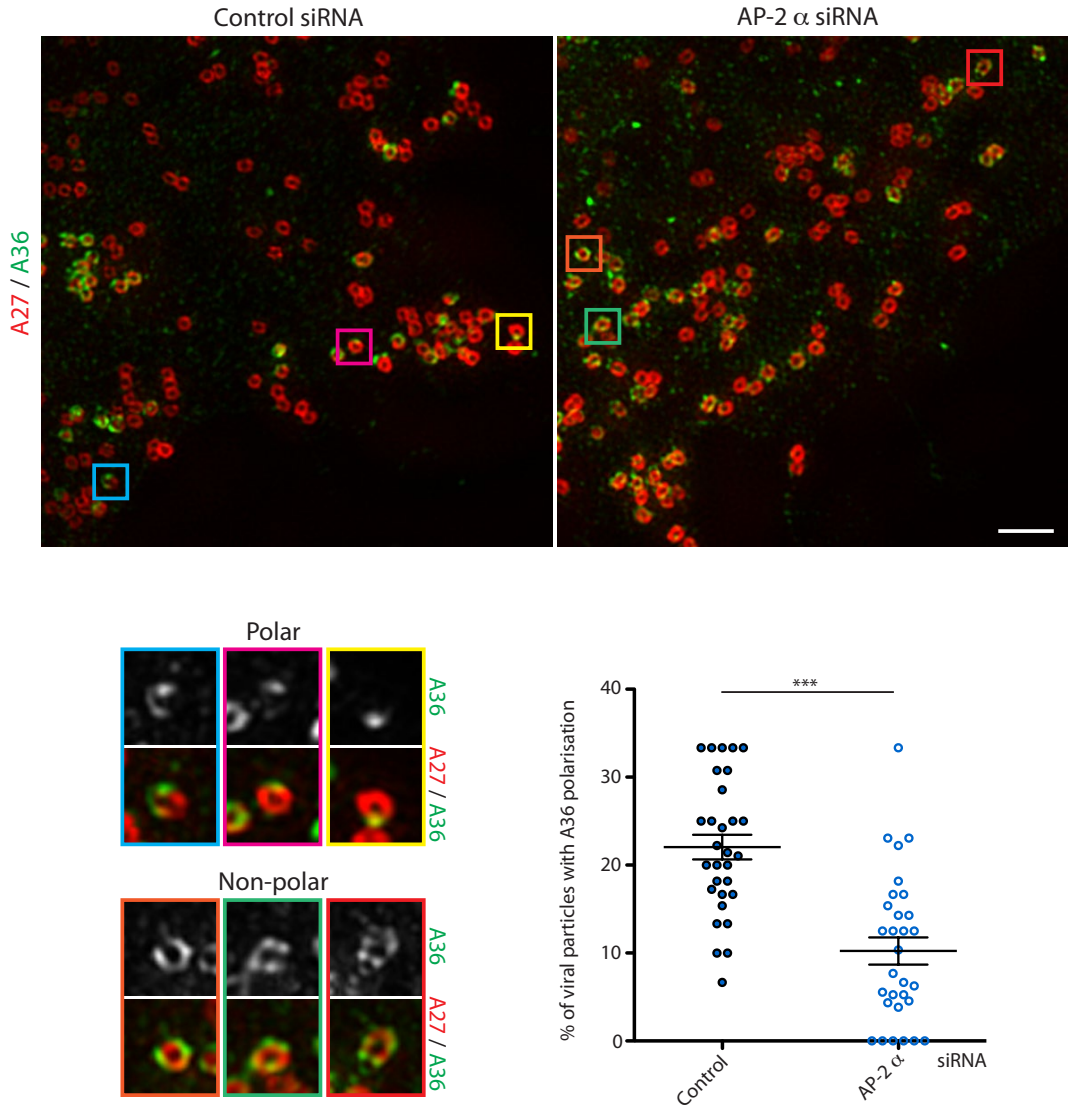

Figure 3.16 A36 can polarise in the absence of actin nucleation

Representative structured illumination images of A36 on viral particles in N-WASP -/- MEFs treated with control or AP-2 siRNA. Magnified inserts highlight examples of polar and non-polar localisation. Scale bar = 1 μm. Graph shows the quantification of percentage of viral particles in the cell periphery that exhibit A36 polarisation. Error bars represent SEM from thirty 15 μm^2 peripheral areas. A p value of <0.001 is indicated by ***.

3.2.7 Artificially modulating A36 clustering phenocopies AP-2 depletion

My data suggests that the phenotype observed upon AP-2 depletion is the result of changes to the spatial organisation of A36. I therefore wondered if I could recapitulate this phenotype by artificially altering the density of functional A36 beneath the viral particle. HeLa cells were infected with a virus lacking the A36 gene (Δ*A36R*), with different ratios of wild-type and an actin nucleation deficient version of A36 expressed into cells. The expressed A36 constructs could then be incorporated into the viral particle, with the deficient A36 acting to spatially restrict wild-type A36 (Figure 3.17A). Three examples of deficient A36 constructs were used, these included the transmembrane domain of A36 fused to Cherry (TM-Cherry), the same construct with the addition of the kinesin-1 binding region of calsyntenin and A36 containing the YdF mutation (Dodding et al., 2011). Expression of decreasing amounts of wild-type A36 (visualised using antibody) and increasing amounts of TM-Cherry could be seen incorporated into viral particles (Figure 3.17B). Analysis of the actin tails produced also showed that with increasing incorporation of actin nucleation deficient A36, there was a corresponding increase in actin tail length (Figure 3.17C). This was true for all three constructs, with an increase in actin-based motility also observed with TM-Cherry expression (Figure 3.18). Therefore, diluting out functional A36 beneath the viral particle recapitulates the phenotypes observed upon AP-2 depletion.

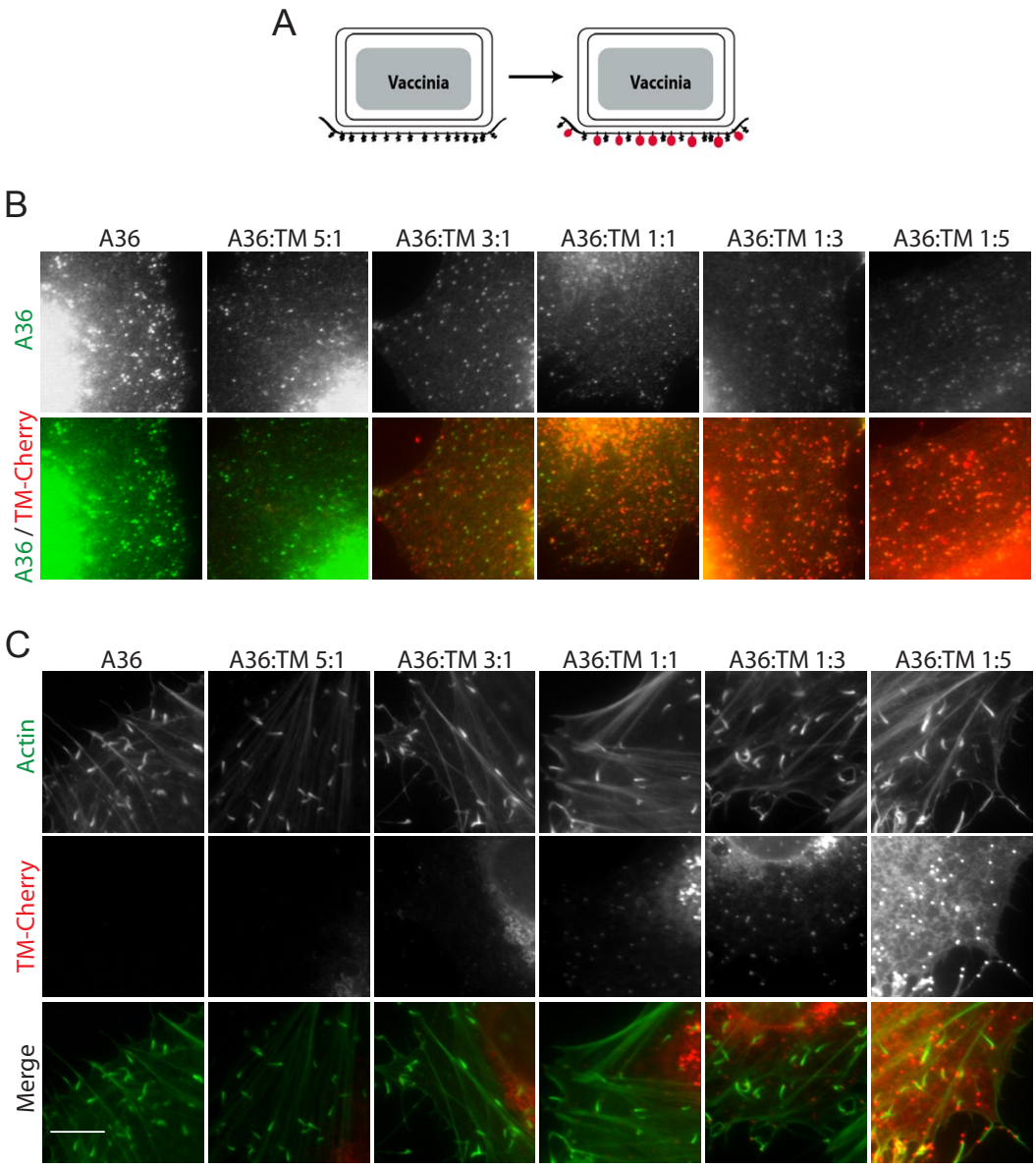

Figure 3.17 Spatially restricting functional A36 leads to longer actin tails

A Schematic depicting the spatial organisation of functional A36 molecules at the plasma membrane (black) with the introduction of the transmembrane domain of A36 fused to cherry (TM-Cherry) (red) **B** Immunofluorescence images showing the increased incorporation TM-Cherry into Δ*A36R* particles. The signal from the wild-type A36, labelled using antibody, diminishes with increasing ratios of TM-Cherry to wild-type A36. **C** Immunofluorescence images showing that increased incorporation of TM-Cherry compared to wild-type A36 results in longer actin tails. The number at the top of images indicates the respective ratio used and scale bar = 10 μm.

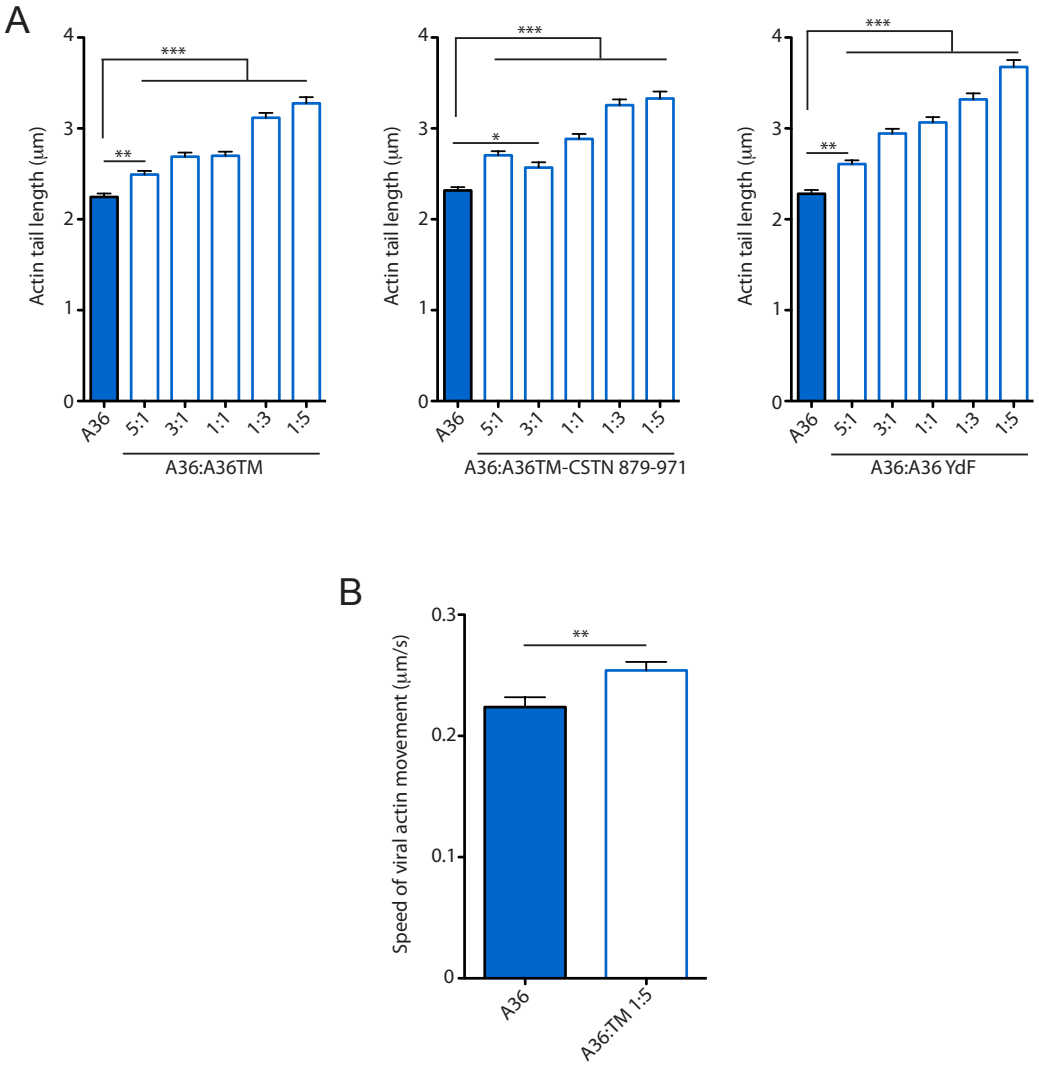

Figure 3.18 Reducing the density of functional A36 induces longer and faster actin tails

A Quantification of actin tail length in Δ*A36R* infected cells expressing different ratios of wild-type and one of three A36 constructs, defective in actin nucleation. These include the transmembrane domain of A36 fused to Cherry (A36TM), the transmembrane domain and kinesin-1 binding region of calsyntenin fused to Cherry (A36TM-CSTN 879-971) and A36 YdF fused to YFP. Error bars represent SEM from 150 tails in three independent experiments. A p value of <0.05, <0.01 and <0.001 is indicated by *, ** and ***, respectively. **B** Quantification of the speed of actin-based motility in Δ*A36R* infected cells expressing either A36 or a 1:5 ratio of A36 to TM-Cherry. Error bars represent SEM of 75 tails from three independent experiments. A p value of <0.01 is indicated by **.

3.2.8 Summary

My work has shown that clathrin is recruited to extracellular vaccinia virus particles in an AP-2-dependent manner during its egress from the cell. Clathrin localisation occurs in the moments before actin tail formation, and was found to enhance the efficiency of actin nucleation. The data presented in this chapter supports the notion that vaccinia hijacks the early stages of endocytosis with the tight clustering of A36 beneath the viral particle. In the absence of clathrin recruitment fewer actin tails were observed suggesting that a threshold density of A36 is required to sustain the cooperative interactions of the vaccinia actin-signalling network. Additionally, in cases where a tail did form the structures were less stable indicating that the organisation beneath the viral particle was sub-optimal. This presented as a long actin tail phenotype, which is explained by the increased dynamics of N-WASP and increased actin-based motility. This is the first demonstration *in vivo* that the spatial organisation of N-WASP dictates a parameter for the regulation of actin polymerisation, supporting earlier *in vitro* findings (Bernheim-Groswasser et al., 2002; Delatour et al., 2008; Wiesner et al., 2003).

Chapter 4. Nck and Cdc42 act cooperatively to stimulate N-WASP-dependent actin tail formation

4.1 Introduction

In chapter 3, I found that the spatial organisation of N-WASP could modulate its ability to promote the actin-based motility of vaccinia virus. In this chapter, I now focus on the interactions of N-WASP with other molecules, and how this further shapes its regulation. Observations from the lab suggested that the YdF virus, which harbours mutations in the Nck and Grb2 binding sites of A36, could still nucleate actin, albeit to a far lesser extent than the wild-type virus. Further experiments found that N-WASP was partially responsible for these vaccinia-induced actin clouds. Recently published data also revealed that the binding between Nck and N-WASP was not required for actin tail formation, and our past studies have shown that N-WASP exhibits a significantly slower turnover compared to the rest of the vaccinia actin-signalling complex (Donnelly et al., 2013; Weisswange et al., 2009). Altogether, this data suggests that additional components are recruited to vaccinia virus that can modulate the activity of N-WASP, thereby promoting actin tail formation. In this chapter I set out to identify components that could help activate N-WASP, and to analyse their molecular role in vaccinia-induced actin tail formation.

4.2 Results

4.2.1 A36-independent actin polymerisation

Observations by Sara Donnelly, an ex-Ph.D. student, suggested that WR virus expressing A36 in which residues Y112 and Y132 of A36 are substituted to phenylalanine (YdF virus) was still able to undergo slow actin-based motility. To confirm these findings I infected HeLa cells with the YdF virus and did live-cell imaging using phase contrast microscopy. At 8 hrs post-infection, several virions were visibly

moving in the periphery of cells, that were in each case associated with a phase dense structure on one side, reminiscent of a short actin tail (Figure 4.1A) (Cudmore et al., 1995). Labelling fixed YdF infected HeLa cells further showed that a subset of extracellular particles, stained with the B5 antibody prior to permeabilisation, co-localised with a small puncta of actin (Figure 4.1B). To characterise further the YdF-induced actin puncta, movies were acquired of HeLa cells stably expressing LifeAct-Cherry infected with WR and YdF viruses. Virions were visualised using the B5-488 antibody added to the media, to focus my analysis on only those viral particles that were extracellular. In agreement with the results from fixed cells, several YdF extracellular virions associated with a small puncta of actin (Figure 4.2A). A number of parameters were then quantified to analyse the differences between WR and YdF-induced actin-based motility. Firstly, the speed was significantly reduced in the YdF-infected cells (0.089±0.019 compared to 0.176±0.020 μm/s) (Figure 4.2B). Furthermore, the actin structures were also less persistent, as less than 50% of YdF virus particles maintained actin polymerisation past one minute compared to 100% of WR-induced actin tails (Figure 4.2B). Concomitant with this, the YdF particles exhibited a start-stop motion, and frequently became stationary before inducing further actin polymerisation (Figure 4.2B). Together, this data confirms that the YdF virus is able to undergo actin-based motility, however, this is significantly less robust compared to WR, perhaps explaining why it had not previously been observed. Due to the weak and transient nature of actin-based transport, the structures induced by the YdF virus from this point on, will be referred to as actin clouds.

As the YdF virus lacks the binding sites for Nck and Grb2 on A36, I next checked for recruitment of the vaccinia actin-signalling complex in fixed cells. Endogenous Nck, WIP and Grb2 were not recruited to YdF-induced actin clouds (Figure 4.3) In contrast, N-WASP was weakly recruited (Figure 4.3). To determine the importance of this recruitment, I next checked the ability of YdF to induce actin clouds in both Nck and N-WASP -/- MEFs. As expected from its lack of recruitment, actin clouds formed equally efficiently in cells with or without Nck (Figure 4.4A and B). In contrast, N-WASP -/- cells showed a significant reduction in the percentage of cells inducing one or more actin clouds compared to control, and additionally showed a significant decrease in the total number of clouds per cell (Figure 4.4A and B).

As N-WASP is recruited to YdF clouds, and positively regulates their formation, I next wanted to determine the factor responsible for its presence. Firstly, Sara Donnelly performed an experiment to determine whether A36 itself was required. HeLa cells were infected with viruses that expressed modified versions of the A36 protein. Two different viruses were used, both expressing the transmembrane domain of A36 but fused to either the kinesin-1 binding region of SKIP or Calsyntenin-1 (Dodding et al., 2011). These hybrid A36 viruses support microtubule-based transport of the virus to the plasma membrane (the site of actin nucleation), in the absence of the cytoplasmic tail of A36. Sara observed no difference in the ability of YdF compared to the two hybrid viruses to induce actin clouds, strongly arguing that actin clouds are A36-independent (Figure 4.5A and C). Further to this, I treated cells with the Src inhibitor PP1, which abrogates 'classic' actin tail formation, and looked at actin cloud formation (Frischknecht et al., 1999a). Cells exhibited equivalent numbers of clouds in cells treated with either PP1 or the structurally similar but inactive compound PP3 (Figure 4.5B and C). Therefore, actin clouds are both Src and A36-independent, and N-WASP is recruited by a distinct mechanism to that of wild-type WR virus.

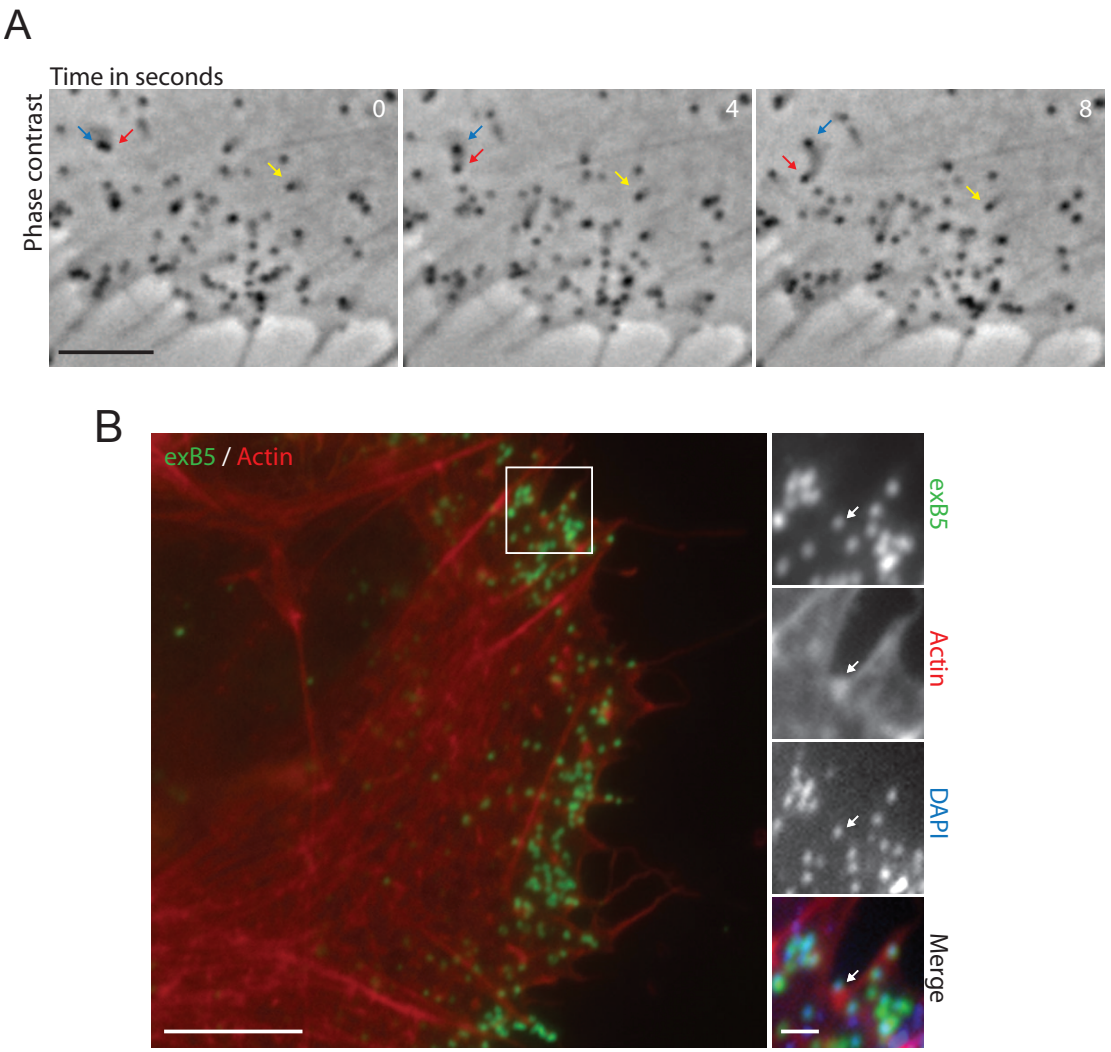

Figure 4.1 The YdF virus induces the formation of actin clouds

A Phase contrast stills from a movie of HeLa cells infected with YdF virus. Blue, red and yellow arrows highlight particles at the periphery of the cell that are undergoing apparent actin-based motility. Scale bar = 5 μm. **B** Immunofluorescence image of a HeLa cell infected with YdF virus, along with magnified insert. The cell is stained with B5 antibody prior to permeabilisation to label extracellular virions (exB5). Actin clouds are seen associated with several extracellular virions, as highlighted by the white arrow in the magnified insert. Scale bars = 10 and 2 μm.

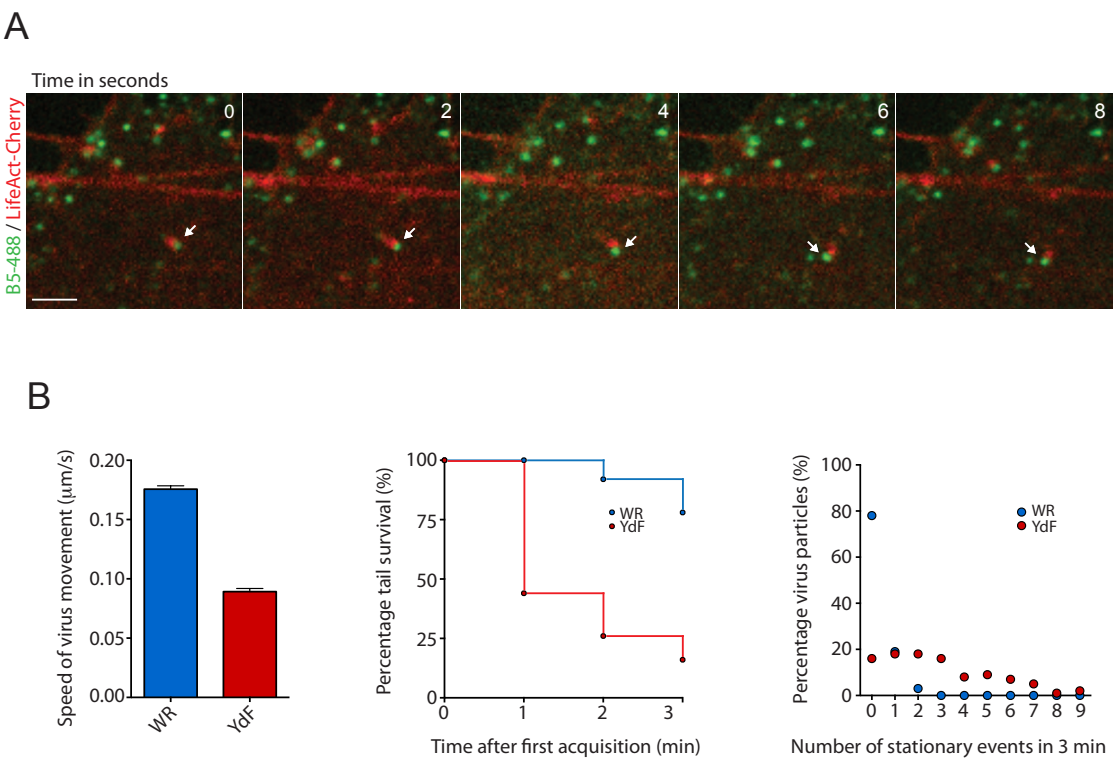

Figure 4.2 The YdF actin cloud is less robust compared to the WR actin tail

A A series of stills from live-cell imaging. LifeAct-Cherry expressing cells were infected with YdF virus, and the B5-Alexa 488 conjugated antibody added to the media just before imaging. White arrows highlight an extracellular virion undergoing actin-based motility. Scale bar = 1 μm **B** Graphs comparing parameters of WR and YdF infected HeLa cells. Graphs show the speed of actin-based motility, the percentage of virions with an actin tail at the indicated time point, and the number of stationary events during the course of a three-minute movie. 50 virions were followed for each condition.

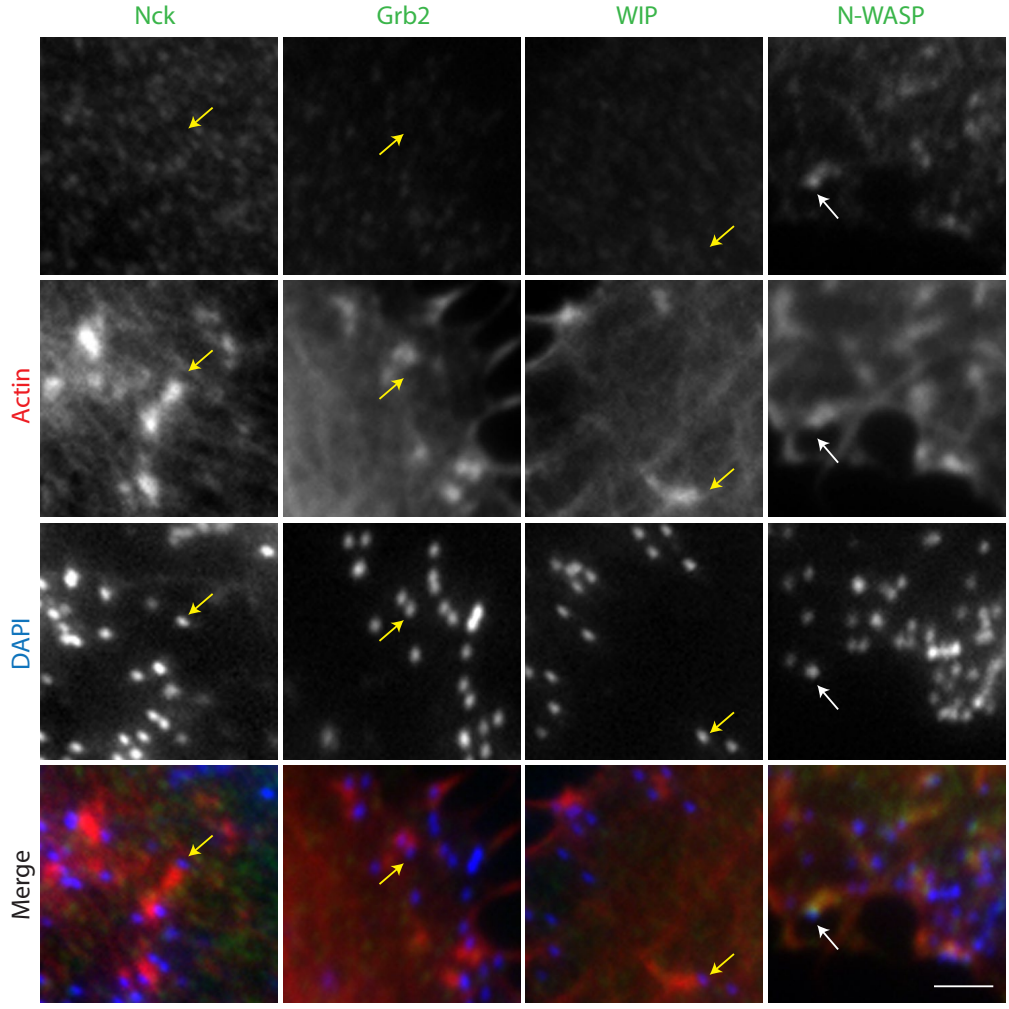

Figure 4.3 N-WASP is recruited to the YdF particle

Representative immunofluorescence images of YdF infected HeLa cells at 8 hrs post-infection. Cells were stained with phalloidin and DAPI to highlight the actin puncta and virus, respectively. Staining showed that endogenous Nck, Grb2 and WIP are not recruited to YdF clouds (yellow arrows). N-WASP, however, was weakly recruited (white arrows). Scale bar = 1 μm

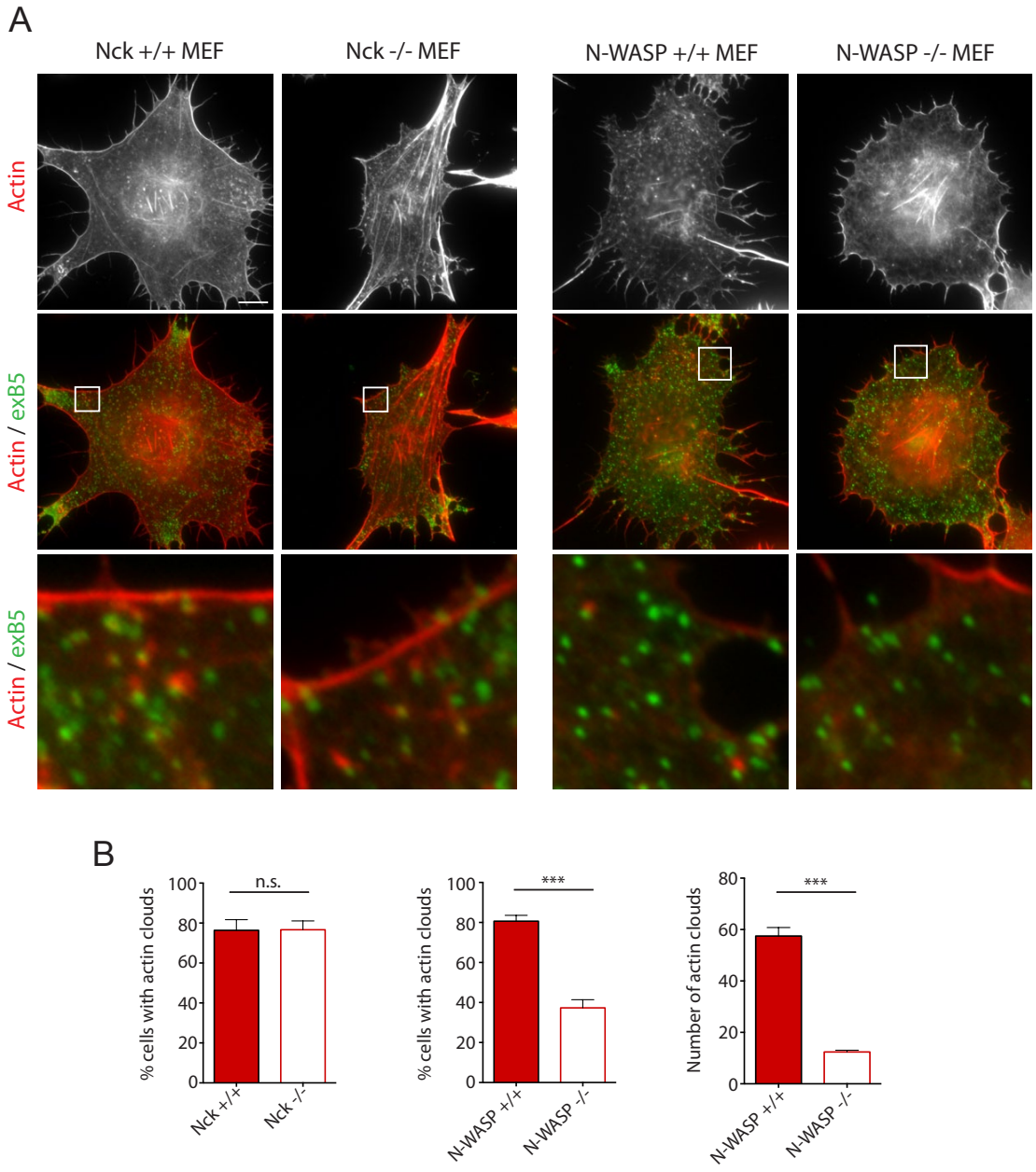

Figure 4.4 Actin clouds are Nck-independent and partially N-WASP-dependent

A Representative immunofluorescence images of Nck and N-WASP +/+ and -/- MEFs infected with the YdF virus at 15 hrs post-infection. Cells are stained for extracellular virions (exB5) and actin, with a magnified insert included to show virus-associated actin clouds. Scale bars = 10 and 1 μm. **B** Quantification of the percentage of cells inducing at least one actin cloud in the indicated cell lines, and the number of actin clouds per cell in N-WASP +/+ and -/- MEFs. Error bars represent SEM from 30 cells in total from 3 independent experiments. A p value of <0.001 is indicated by ***.

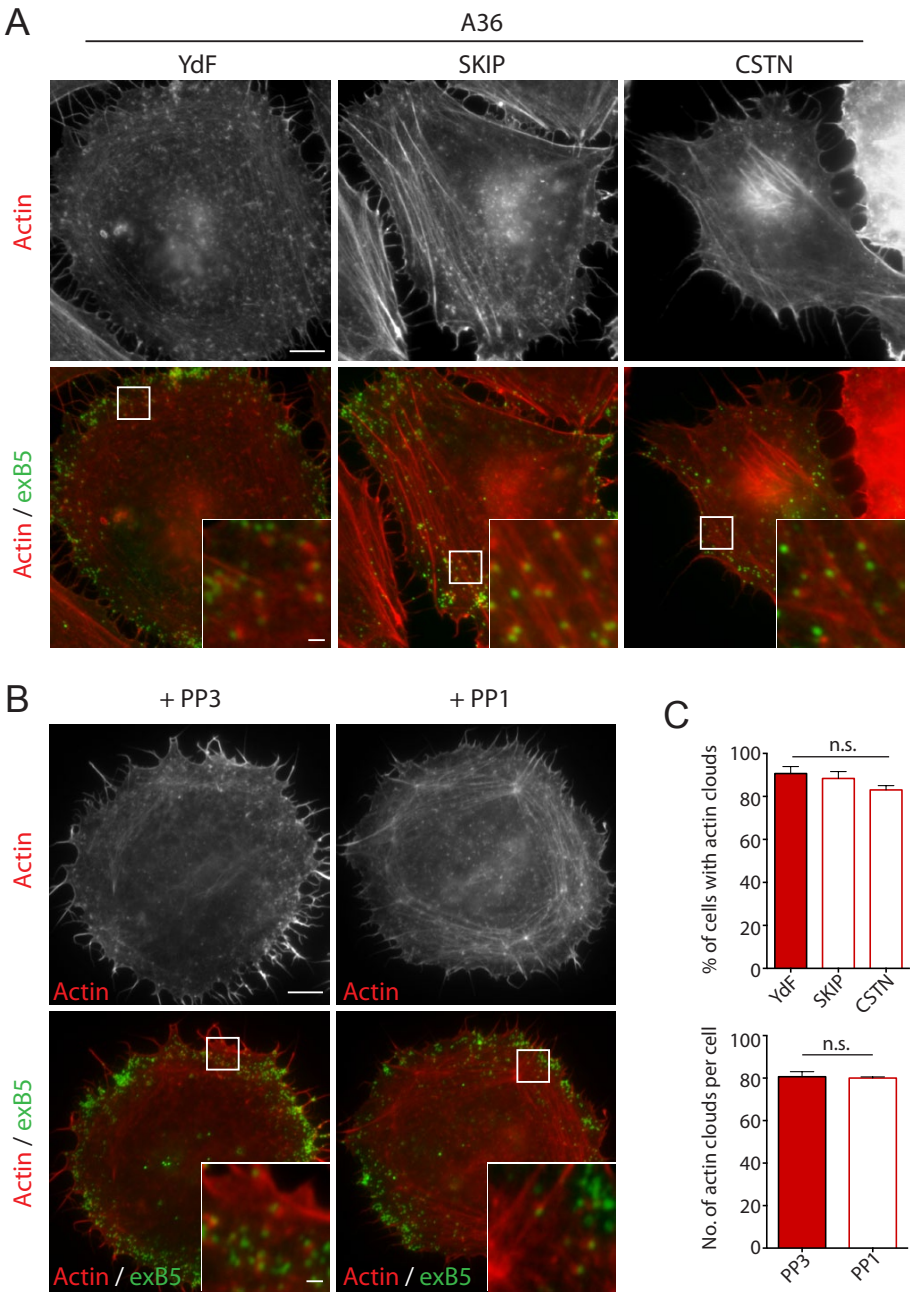

Figure 4.5 Actin clouds are A36 and Src-independent

A Experiment performed by Sara Donnelly. Images of HeLa cells infected with YdF, A36-TM-SKIP or A36-TM-CSTN. Cells are stained for extracellular virions (exB5) and actin. Scale bars = 10 and 1 μm. **B** Representative immunofluorescence images of YdF infected HeLa cells treated with either PP1 a Src inhibitor, or PP3 a structurally similar compound that is not active. Scale bars = 10 and 1 μm. **C** Quantification performed by Sara Donnelly of the percentage of cells inducing at least one actin cloud in YdF, A36-TM-SKIP and A36-TM-CSTN infected cells. Quantification of the number of actin clouds induced by YdF in PP3 and PP1 treated cells is also shown. Error bars represent SEM from 30 cells in total from 3 independent experiments.

4.2.2 Cdc42 and N-WASP promote YdF-induced actin clouds

As my previous work found that AP-2/clathrin are recruited to vaccinia virus, and as N-WASP is highly implicated in actin nucleation at endocytic sites I looked to see if these endocytic proteins were involved in actin cloud formation (Benesch et al., 2005; Taylor et al., 2011). Immunofluorescence staining showed that AP-2 localises to YdF particles inducing actin clouds, suggesting that in contrast to WR, the weak nucleation of actin in this case was not sufficient to drive the virus particle away from clathrin (Figure 4.6A). Treatment with AP-2 siRNA, however, showed no difference in the percentage of cells inducing one or more actin clouds in control and AP-2 depleted cells (Figure 4.6B). Therefore, AP-2 does not appear to play a role in YdF-induced actin-based motility.

Previous work from the lab has shown that the well-known activator of N-WASP, Cdc42, is recruited to the tip of actin tails, but expression of dominant negative Cdc42 did not reduce the percentage of cells inducing one or more actin tails (Moreau et al., 2000). I therefore looked to see if Cdc42 was also recruited to the YdF actin cloud. In agreement with these earlier observations, GFP-tagged Cdc42 localised to actin tails produced during WR infection and additionally to YdF-induced actin clouds, albeit in a less focused manner (Figure 4.7). To test the importance of Cdc42 localisation, I expressed dominant negative (N17) Cdc42 in YdF infected HeLa cells. Expression of wild-type GFP-Cdc42 had no impact on actin cloud formation compared to GFP alone (Figure 4.8A and B). However, expression of the dominant negative Cdc42 (GFP-Cdc42-N17), showed a significant decrease in both the percentage of cells with an actin cloud, as well as the number of actin clouds per cell (Figure 4.8A and B). The recruitment of N-WASP was also lost upon expression of dominant negative Cdc42, suggesting that Cdc42 is responsible for recruiting N-WASP to YdF particles. To further explore this hypothesis, I expressed GFP, GFP-N-WASP and GFP-N-WASP-H208D, which is markedly reduced in Cdc42 binding (Miki et al., 1998), in MEFs lacking the endogenous protein. In N-WASP nulls expressing GFP alone, ~50% of cells had one or more actin clouds (Figure 4.9A and B). Expression of GFP-N-WASP showed an increase in both the percentage of cells inducing actin clouds, as well as the number of actin clouds per cell, compared to GFP alone (Figure 4.9A and B). In contrast, GFP-N-WASP-H208D could not be detected at the viral particle and showed only a modest rescue in actin cloud formation compared to GFP alone (Figure 4.9A and B). Altogether, my data suggests that more that one pathway acts to promote actin-based motility of YdF particles. However, Cdc42 is responsible for the recruitment of N-WASP.

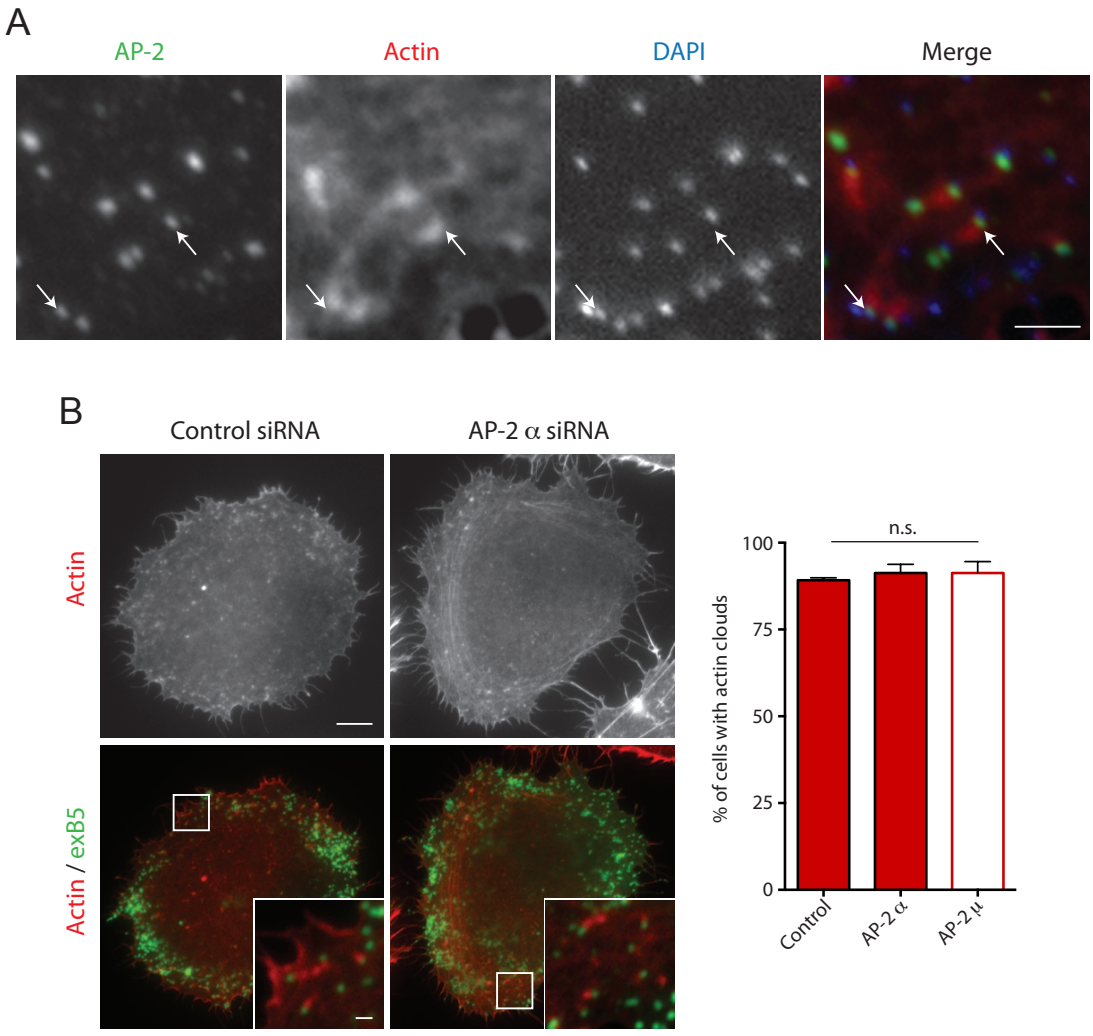

Figure 4.6 AP-2 is not required for actin cloud formation

A Immunofluorescence images of a YdF infected HeLa cell, stained for AP-2, actin and DAPI to label the DNA in the viral particle. AP-2 can be seen associated with virions inducing an actin cloud (white arrows). Scale bar = 2 μm **B** Representative immunofluorescence images of YdF infected HeLa cells treated with control or AP-2 siRNA. Cells are stained for extracellular virions (exB5) and actin, with a magnified insert included to show virus-associated actin clouds. Scale bars = 10 and 1 μm. **C** Quantification of the percentage of cells inducing at least one actin cloud in control or AP-2 depleted cells. Error bars represent SEM from 30 cells in total from 3 independent experiments.

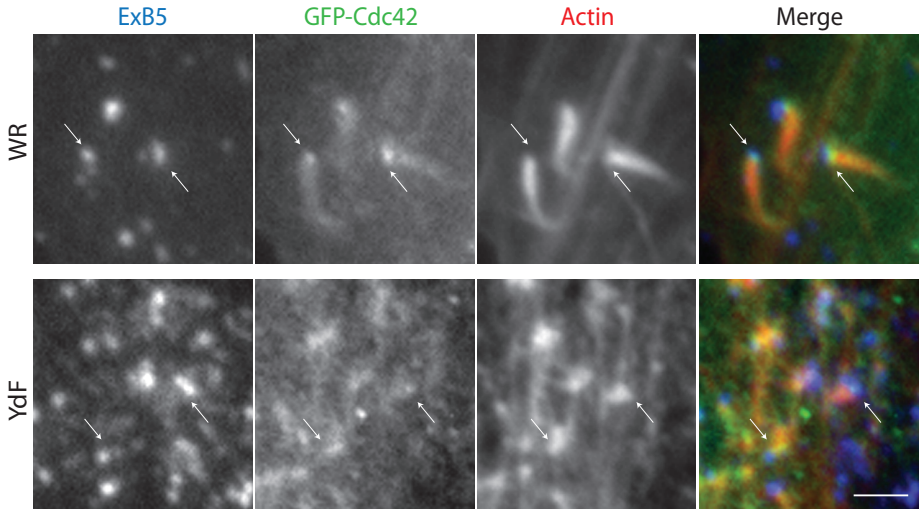

Figure 4.7 Cdc42 localises to both virus-induced actin tails and actin clouds

Immunofluorescence images of HeLa expressing GFP-Cdc42, infected with either WR or YdF virus. Extracellular virions (exB5) inducing actin-based polymerisation are also positive for GFP-Cdc42 (white arrows). Scale bar = 2 μm

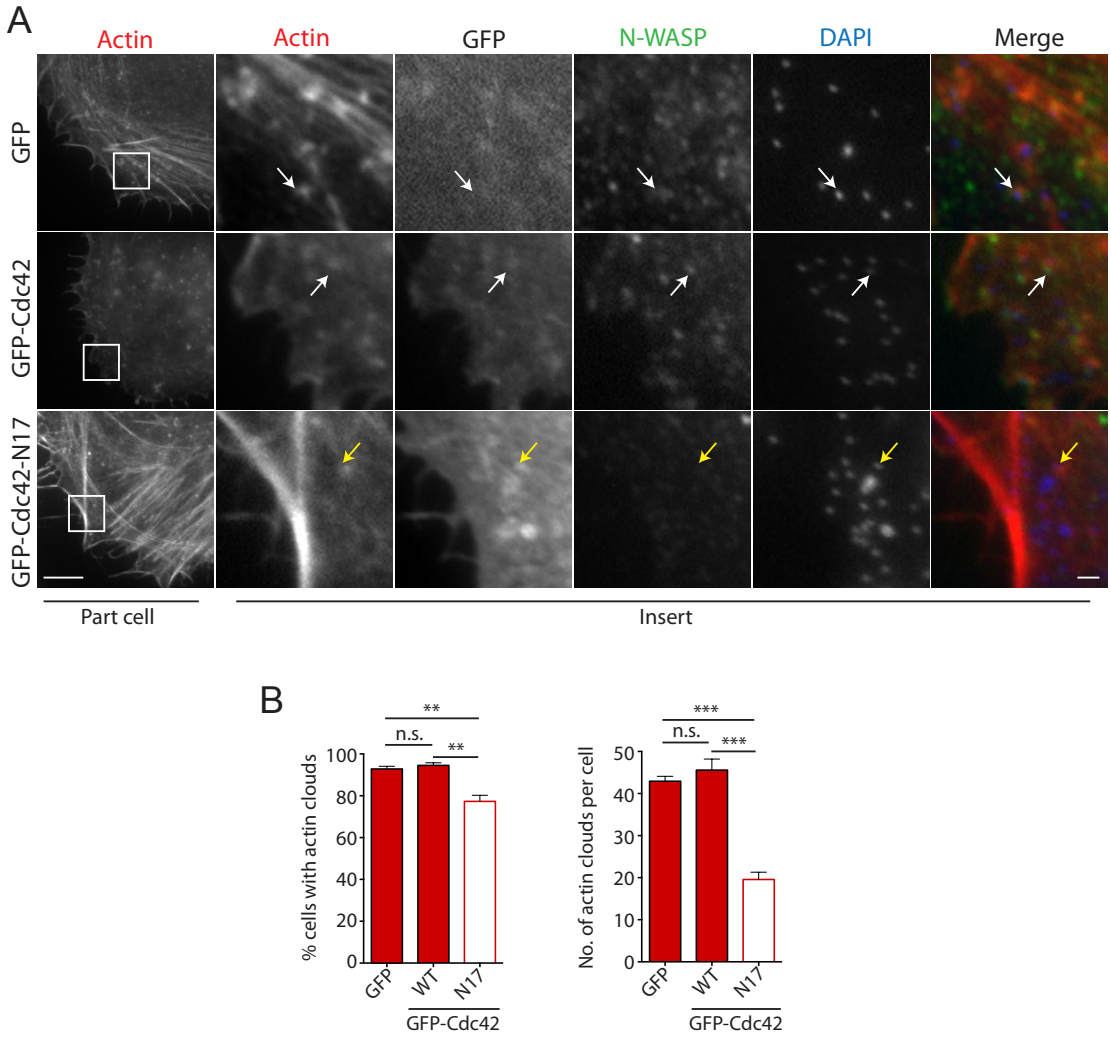

Figure 4.8 Dominant negative Cdc42 reduces actin cloud formation and blocks N-WASP localisation

A Immunofluorescence images of infected HeLa cells, expressing GFP, GFP-Cdc42 or GFP-Cdc42-N17 (dominant negative). N-WASP is recruited to actin clouds induced in GFP or GFP-Cdc42 expressing cells (white arrows). In contrast, it is absent from clouds in GFP-Cdc42-N17 expressing cells (yellow arrows). Scale bars = 10 and 1 μm. **B** Quantification of the percentage of cells with one or more actin clouds, and the number of actin clouds, produced in cells expressing the indicated construct. Error bars represent SEM from 30 cells in total from 3 independent experiments. A p value of <0.01 and <0.001 is indicated by ** and ***, respectively.

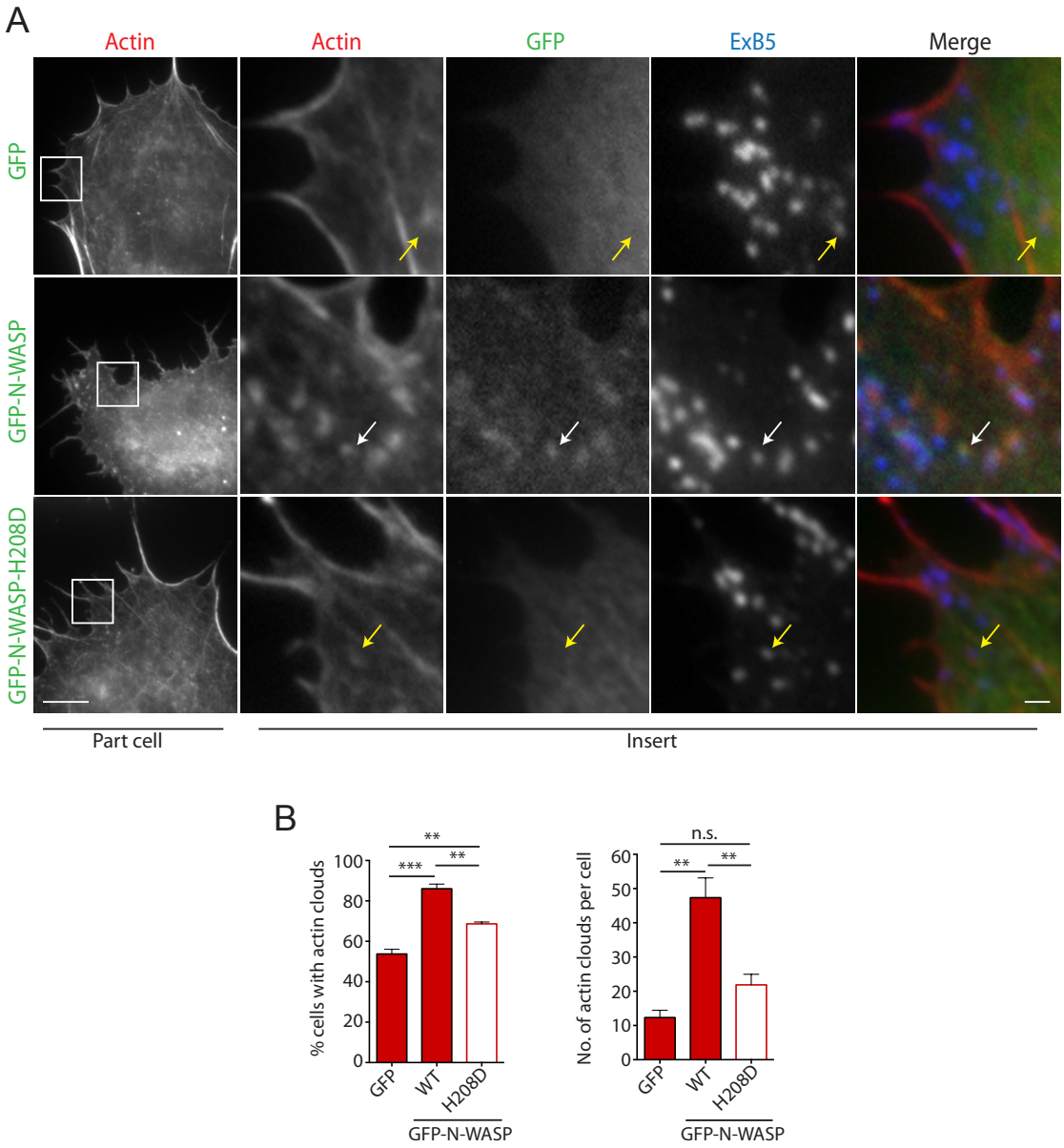

Figure 4.9 Loss of interaction between Cdc42 and N-WASP reduces actin cloud formation

A Immunofluorescence images of YdF infected N-WASP -/- MEFs, expressing GFP, GFP-N-WASP or GFP-N-WASP-H208D, which is deficient in Cdc42 binding. N-WASP is recruited to actin clouds in GFP-N-WASP expressing cells (white arrows). In contrast, it is absent from clouds in GFP and GFP-N-WASP-H208D expressing cells (yellow arrows). Scale bars = 10 and 1 μm. **B** Quantification of the percentage of cells with one or more actin clouds, and the number of actin clouds, produced in cells expressing the indicated construct. Error bars represent SEM from 30 cells in total from 3 independent experiments. A p value of <0.01 and <0.001 is indicated by ** and ***, respectively.

4.2.3 Cdc42 promotes actin tail formation

As Cdc42-N-WASP is able to promote actin-based motility in the absence of Nck, I next wanted to determine if Cdc42 contributes to actin polymerisation during infection with WR (wild-type) virus. Expression of dominant negative GFP-Cdc42-N17 in WR infected HeLa cells had no impact on the percentage of cells making one or more actin tails compared to GFP-Cdc42 or GFP alone (Figure 4.10). The length of actin tails was also not affected, however, the number of actin tails produced in each cell was significantly reduced by ~40% upon expression of dominant negative Cdc42 (Figure 4.10).

To analyse the contribution of Cdc42 further, I infected HeLa cells with the Y132F virus, which expresses a form of A36 that is unable to recruit Grb2 (Scaplehorn et al., 2002). Grb2 is not required for actin tail formation, but acts to enhance the function of the main actin-signalling complex (Scaplehorn et al., 2002; Weisswange et al., 2009). Infecting with the Y132F virus can therefore sensitise actin tail phenotypes as it removes the stabilising capacity of Grb2 on the rest of the signalling network. Expression of GFP-Cdc42-N17 in Y132F infected cells again had no impact on the percentage of cells nucleating one or more actin tails. It did, however, lead to a significant decrease in the number of actin tails per cell (Figure 4.11). Interestingly, expression of GFP-Cdc42 rescued the short actin tail phenotype of the Y132F virus, which was not the case for GFP alone or GFP-Cdc42-N17 (Figure 4.11). This suggests, that Cdc42 helps promote actin tail formation, and its overexpression can partially compensate for defects resulting from decreased stability of the signalling complex, induced by the loss of Grb2.

As with my experiments using the YdF virus, I next took advantage of N-WASP-H208D, to analyse the importance of binding between Cdc42 and N-WASP (Miki et al., 1998). To do this I made stable cell lines, rescuing the N-WASP -/- MEFs with lentivirus expressing either GFP-tagged N-WASP wild-type or H208D mutant. Infection with WR in cells expressing N-WASP-H208D did not impact on the percentage of cells producing one or more actin tail (Figure 4.12). Consistent with the Cdc42-N17 data, the number of tails per cell was significantly reduced and additionally the tails were also significantly shorter (Figure 4.12). Infection with Y132F virus gave a similar phenotype, with an enhanced reduction in both the number of actin tails per cell and a decrease in their length, with no difference observed to the percentage of cells nucleating an actin

tail (Figure 4.13). My data suggests that Cdc42 helps promote actin tail formation. However, as our most stringent assay to test the efficiency of actin tail formation failed to show a difference, Cdc42 most likely plays a supportive role to the rest of the signalling complex.

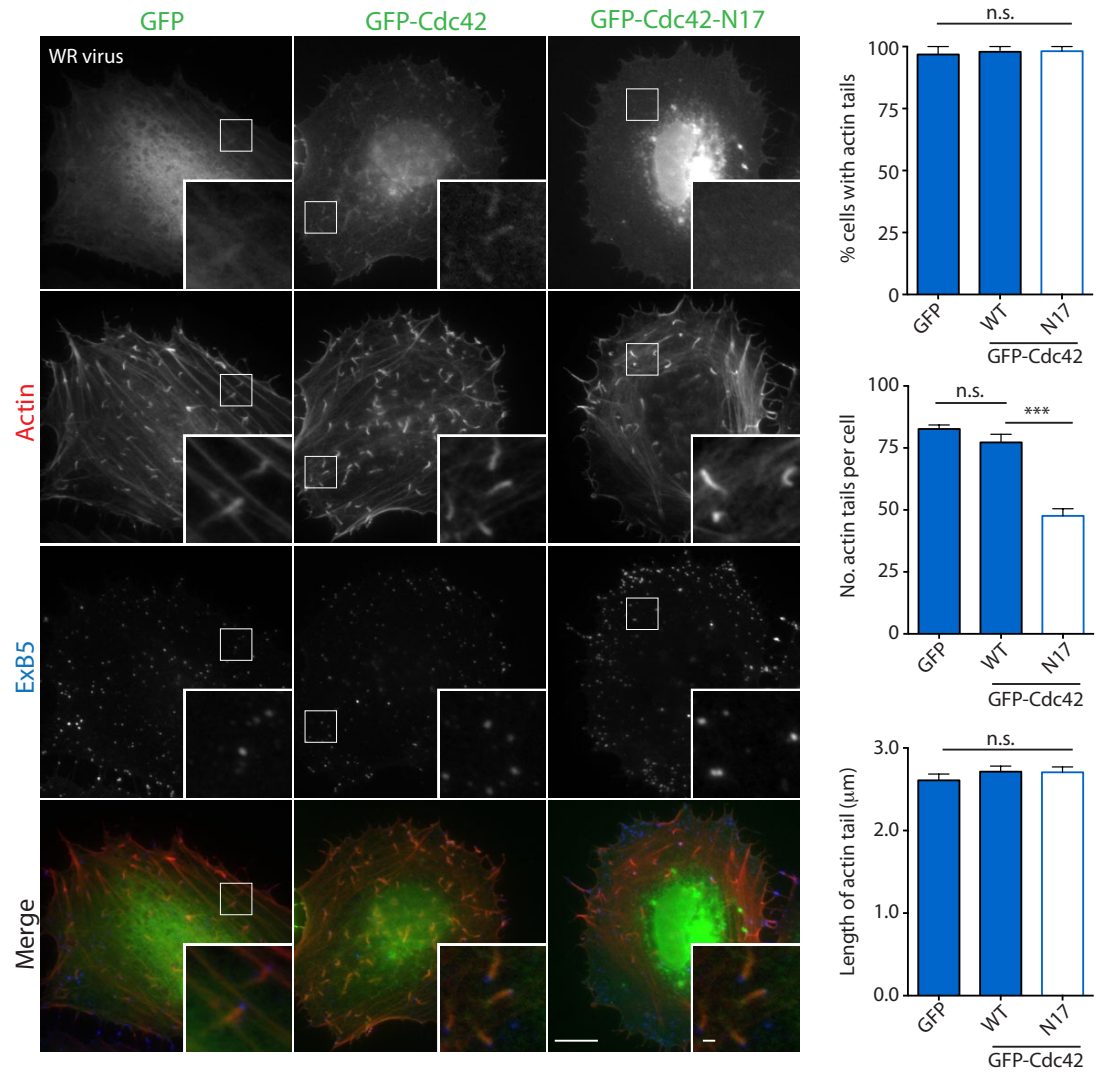

Figure 4.10 Expression of dominant negative Cdc42 reduces the number of actin tails

Immunofluorescence images of WR infected HeLa cells expressing GFP, GFP-Cdc42 or GFP-Cdc42-N17 (dominant negative). Scale bars = 10 and 1 μm. Graphs show quantifications of the percentage of cells with one or more actin tail, the number of actin tails per cell and the length of actin tails produced in cells expressing the indicated constructs. Error bars represent SEM from 30 cells in total from 3 independent experiments. A p value of <0.001 is indicated by ***.

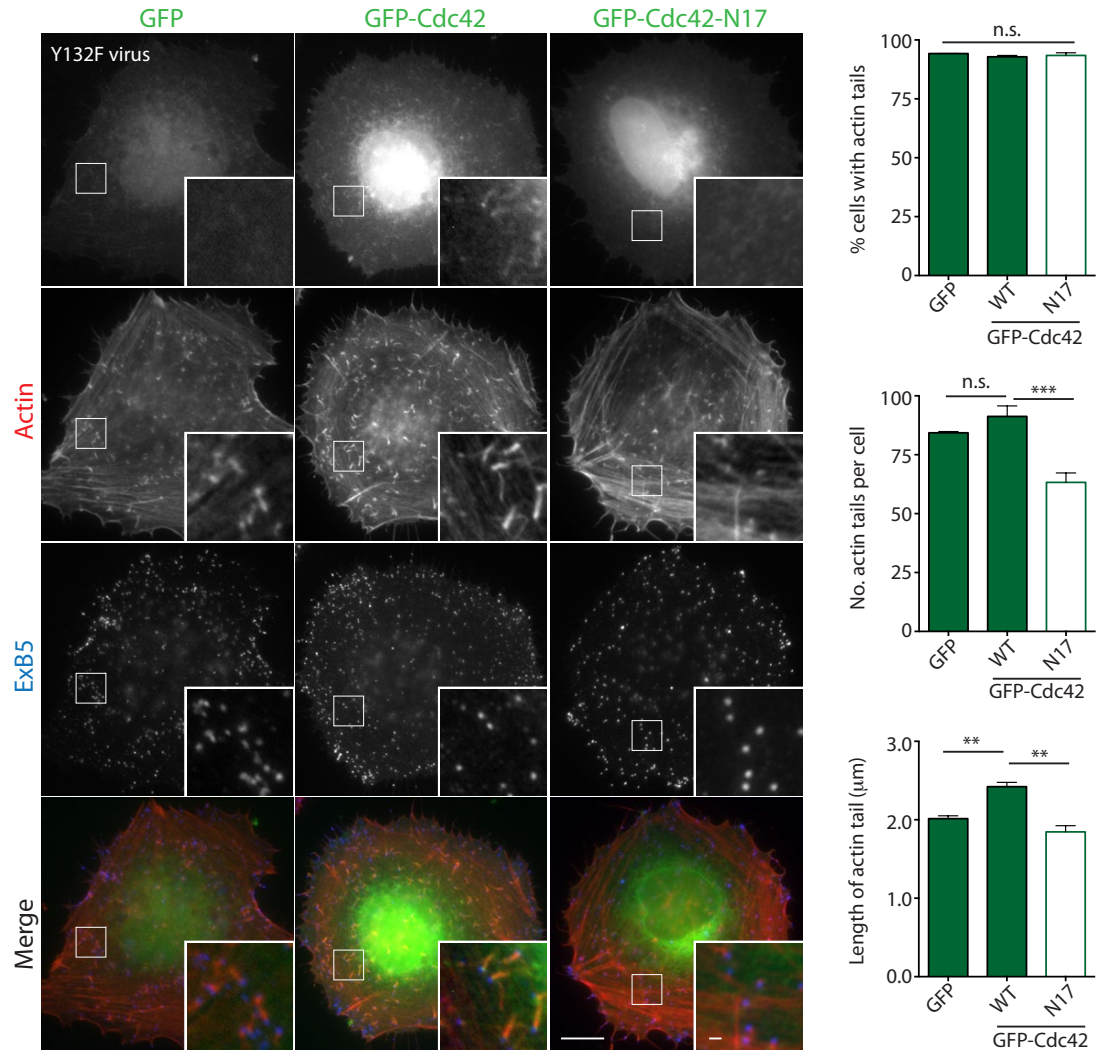

Figure 4.11 GFP-Cdc42 partially rescues the short Y132F virus induced actin tail

Immunofluorescence images of Y132F virus infected HeLa cells expressing GFP, GFP-Cdc42 or GFP-Cdc42-N17 (dominant negative). Scale bars = 10 and 1 μm. Graphs show quantifications of the percentage of cells with one or more actin tail, the number of actin tails per cell and the length of actin tails produced in cells expressing the indicated constructs. Error bars represent SEM from 30 cells in total from 3 independent experiments. A p value of <0.01 and <0.001 is indicated by ** and ***, respectively.

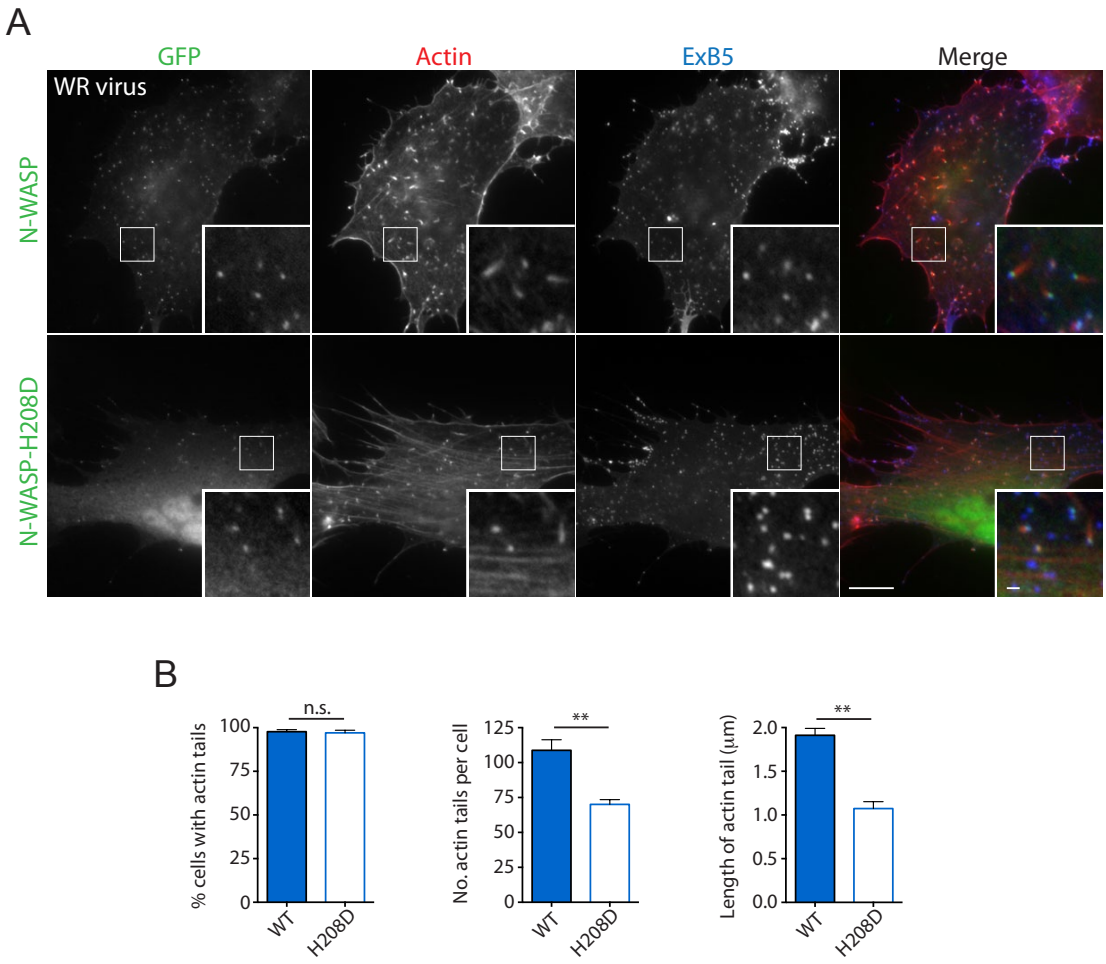

Figure 4.12 An interaction between Cdc42 and N-WASP enhances actin tail formation

A Immunofluorescence images of WR infected N-WASP -/- MEFs stably expressing GFP-N-WASP or GFP-N-WASP-H208D. Scale bars = 10 and 1 μm. **B** Graphs show quantifications of the percentage of cells with one or more actin tail, the number of actin tails per cell and the length of actin tails produced in the indicated cells. Error bars represent SEM from 30 cells in total from 3 independent experiments. A p value of <0.01 is indicated by **.

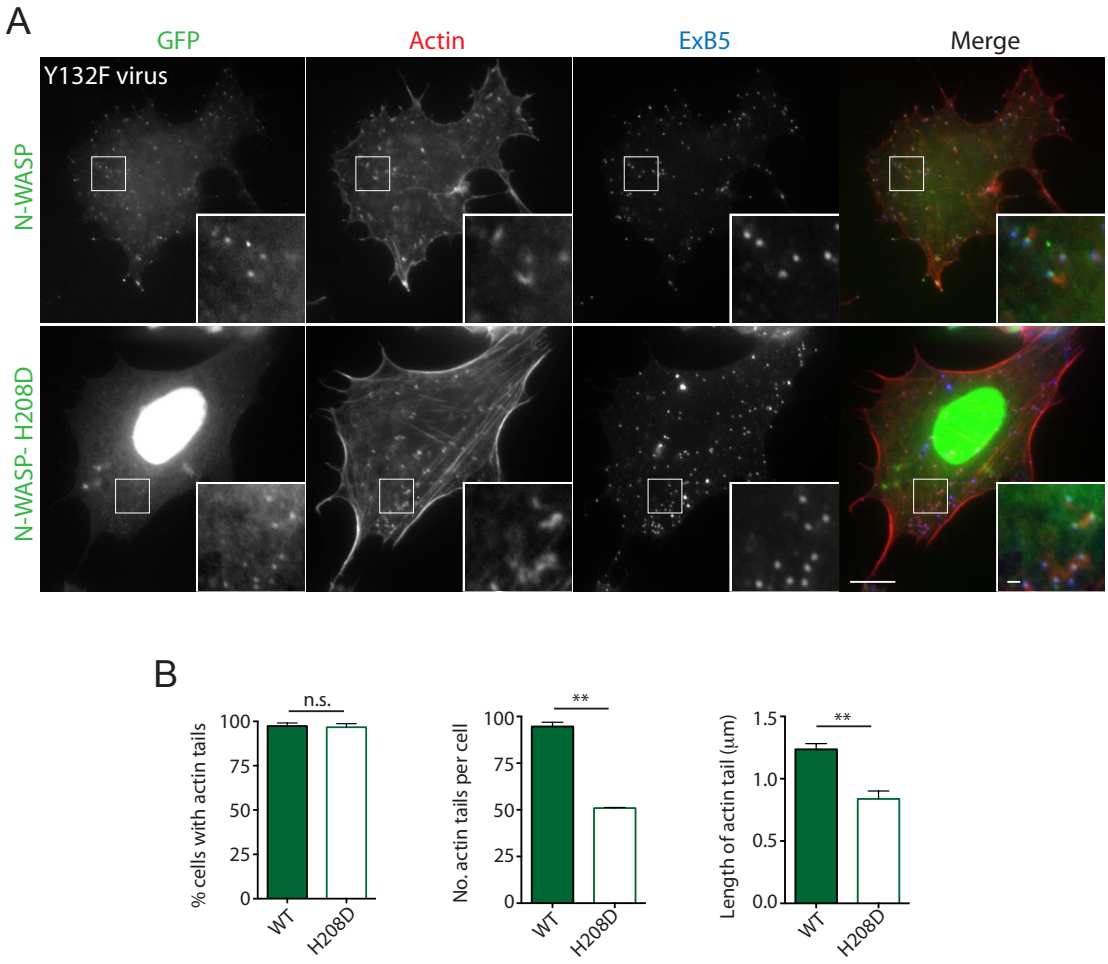

Figure 4.13 Infecting with the Y132F virus exacerbates the N-WASP-H208D phenotype

A Immunofluorescence images of Y132F-infected N-WASP -/- MEFs stably expressing GFP-N-WASP or GFP-N-WASP-H208D. Scale bars = 10 and 1 μm. **B** Graphs show quantifications of the percentage of cells with one or more actin tail, the number of actin tails per cell and the length of actin tails produced in the indicated cells. Error bars represent SEM from 30 cells in total from 3 independent experiments. A p value of <0.01 is indicated by **

4.2.4 Cdc42 acts collaboratively with Nck to promote actin tail formation

To further understand the contribution of Cdc42 to actin tail formation, I next looked at the interplay between Cdc42 and Nck. I introduced the ΔNck mutation, which abrogates Nck binding into N-WASP-H208D (Donnelly et al., 2013), to create a stable cell line expressing N-WASP that is deficient in both Nck and Cdc42 binding. The N-WASP-ΔNck-H208D mutant was further decreased in its ability support actin nucleation, as compared to the H208D mutant (Figure 4.14A and B). It was also markedly deficient in actin-based motility compared to the ΔNck mutant, which had no significant decrease in either the percentage of cells nucleating an actin tail or the number of actin tails per cell (Donnelly et al., 2013). Infection with the Y132F virus also showed that N-WASP-ΔNck-H208D exhibited a significant decrease in the percentage of cells nucleating one or more actin tails, as well as further decreasing the efficiency of actin nucleation compared to WR (Figure 4.15A and B). This data was echoed upon measuring the rate of actin-based motility. Introduction of the H208D mutation led to a decrease in rate of virus motility during both WR and Y132F infections, 0.181 to 0.160 μm/s and 0.191 to 0.135 μm/s, respectively (Figure 4.16A). These rates were further decreased upon incorporation of the ΔNck mutation into N-WASP-H208D (0.151 and 0.118 μm/s) (Figure 4.16A). Altogether, my data shows that Nck and Cdc42 act cooperatively to regulate N-WASP-dependent actin tail formation.

To analyse their contribution to N-WASP regulation, I next performed FRAP experiments to look at the stability of N-WASP beneath the virus in the different mutant cell lines. The half-life of GFP-N-WASP recovery after photo-bleaching in WR infection was 2.72±0.20 s, which is consistent with our previously recorded measurements (Figure 4.16B) (Donnelly et al., 2013; Weisswange et al., 2009). GFP-N-WASP-H208D showed a dramatic increase in its dynamic exchange, with a half-life of 1.18±0.10 s. However, introduction of the ΔNck into H208D N-WASP led to only a modest increase the rate of exchange (0.86±0.06 s) (Figure 4.16B). The same was true during Y132F infections, GFP-N-WASP had a half-life of 1.92±0.015s, which was significantly altered to 0.91±0.08 s by the H208D mutation, and to 0.88±0.08 in the case of N-WASP-ΔNck-H208D (Figure 4.16B). Therefore, the interaction between Cdc42 and N-WASP impacts greatly on the stability of N-WASP within the vaccinia-signalling network during actin-based motility, while Nck contributes only modestly.

To show the impact of these mutations on viral spread, I next looked at the ability of WR virus to spread through confluent monolayers of the stable cell lines. The experiment was performed under a semi-solid overlay of agarose to restrict my analysis to cell-cell transmission. As expected the virus was unable to spread efficiently in the absence of N-WASP (Figure 4.17). The re-introduction of GFP-N-WASP, however, significantly enhanced the spread of infection (Figure 4.17). Whereas expression of N-WASP-H208D in N-WASP -/- MEFs was less efficient at promoting the spread of infection compared to N-WASP, while N-WASP-ΔNck-H208D was further impeded compared to N-WASP-H208D (Figure 4.17). This data further supports the cooperative behaviour between Nck and Cdc42 in N-WASP recruitment and activation.

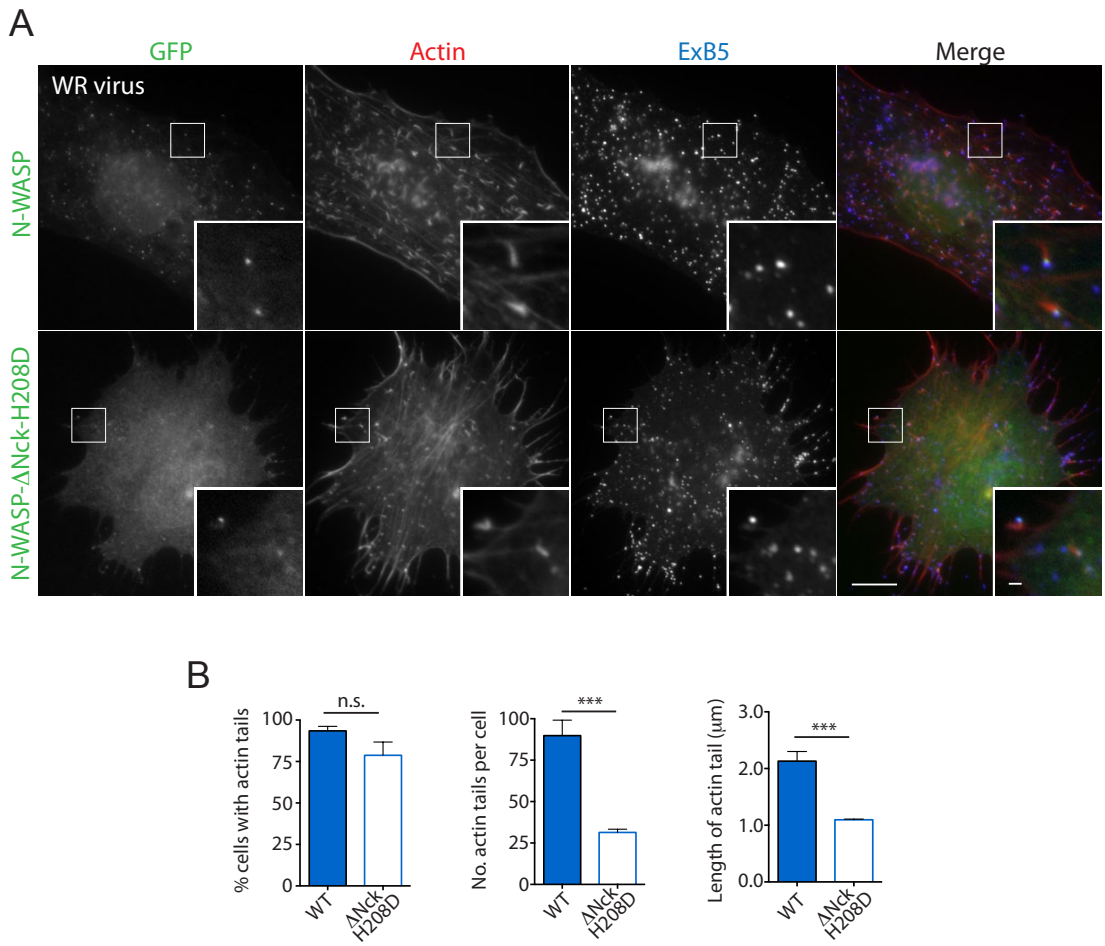

Figure 4.14 Nck and Cdc42 act cooperatively to promote WR virus actin tail formation

A Immunofluorescence images of WR infected N-WASP -/- MEFs expressing GFP-N-WASP or GFP-N-WASP-ΔNck-H208D. Scale bars = 10 and 1 μm. **B** Graphs show quantifications of the percentage of cells with one or more actin tail, the number of actin tails per cell and the length of actin tails produced in the indicated cells. Error bars represent SEM from 30 cells in total from 3 independent experiments. A p value of <0.001 is indicated by ***.

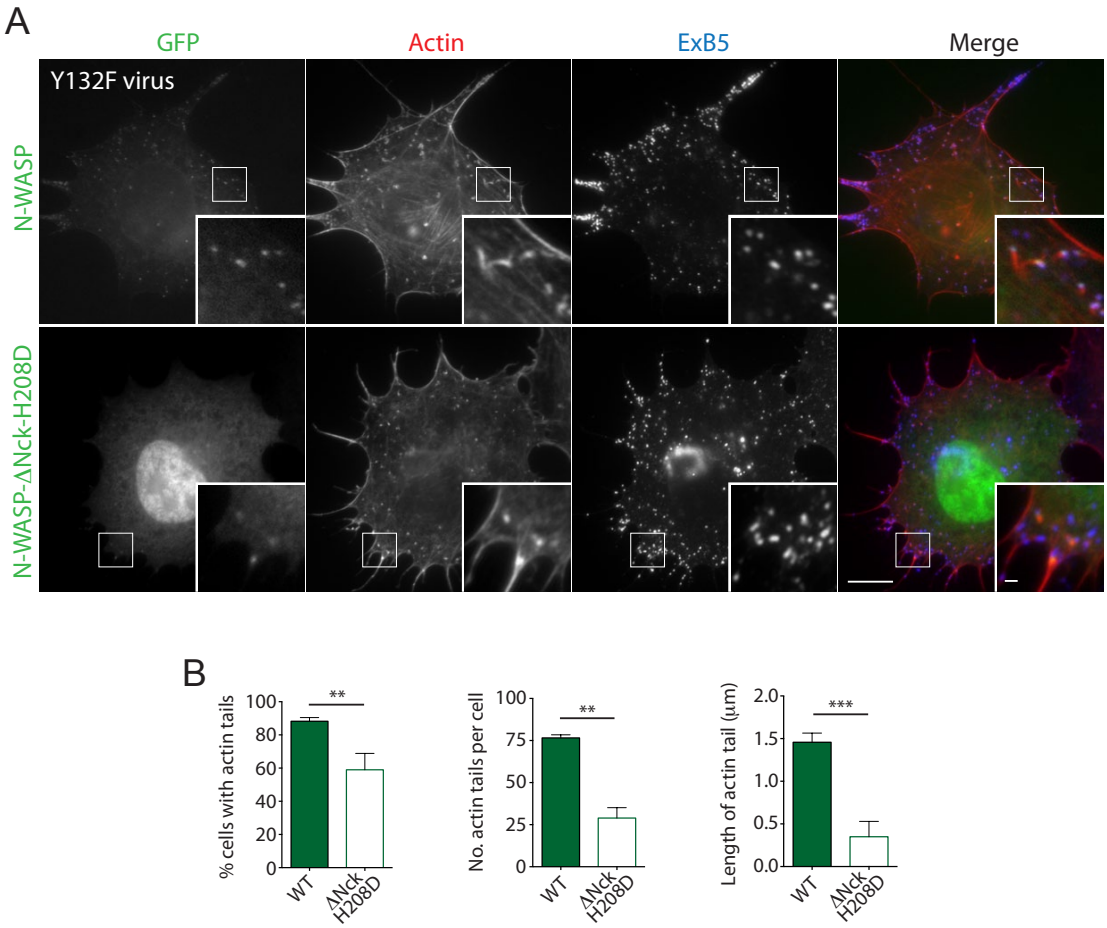

Figure 4.15 N-WASP-ΔNck-H208D causes a significant decrease in actin tail formation during Y132F infection

A Immunofluorescence images of Y132F infected N-WASP -/- MEFs expressing GFP-N-WASP or GFP-N-WASP-ΔNck-H208D. Scale bars = 10 and 1 μm. **B** Graphs show quantifications of the percentage of cells with one or more actin tail, the number of actin tails per cell and the length of actin tails produced in the indicated cells. Error bars represent SEM from 30 cells in total from 3 independent experiments. A p value of <0.01 and <0.001 is indicated by ** and ***, respectively.

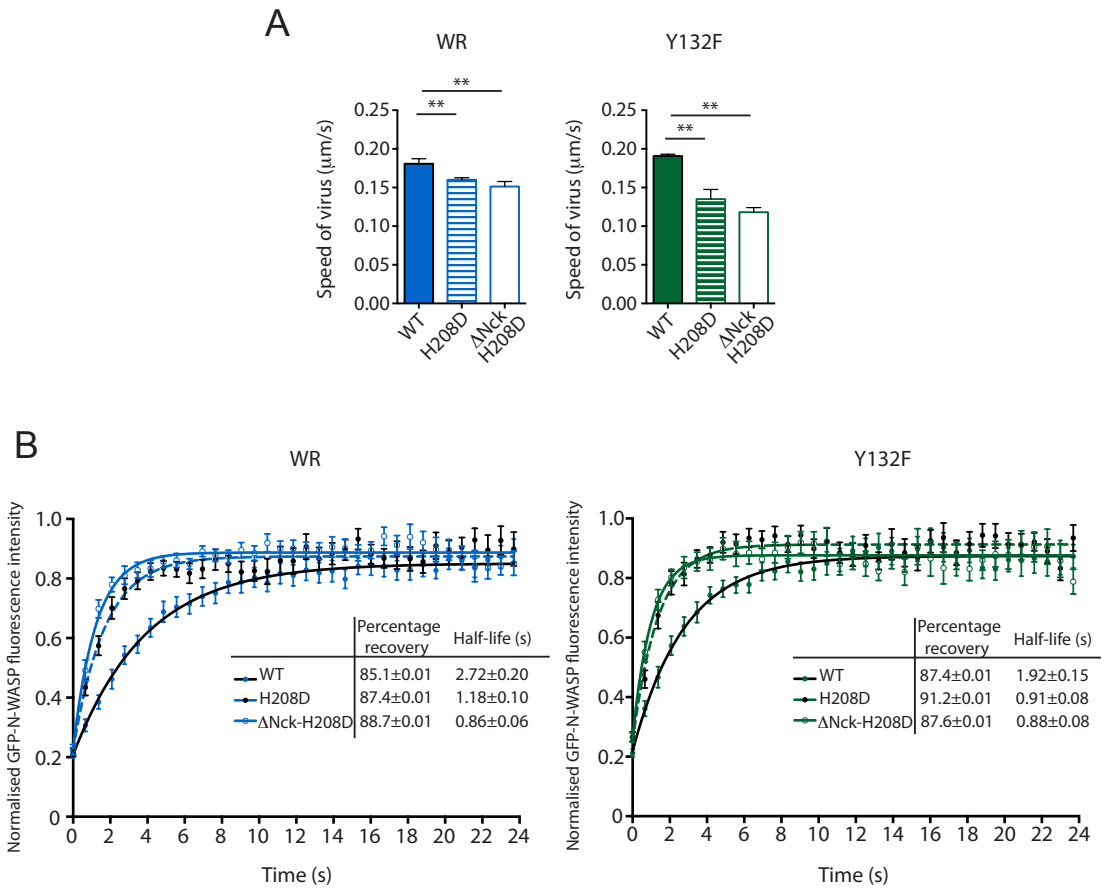

Figure 4.16 N-WASP mutants have decreased actin-based motility and stability

A Quantification of the speed of actin-based motility in the indicated cell lines during both WR (blue) and Y132F infection (green). Error bars represent SEM from 150 events quantified over 3 independent experiments. A p value of <0.01 is indicated by **. **B** Quantification of the recovery of GFP-fluorescence after photobleaching of the different N-WASP mutants in the indicated cell lines, during WR (blue) or Y132F (green) infection. The derived values for percentage recovery and half-life are shown. N= 30.

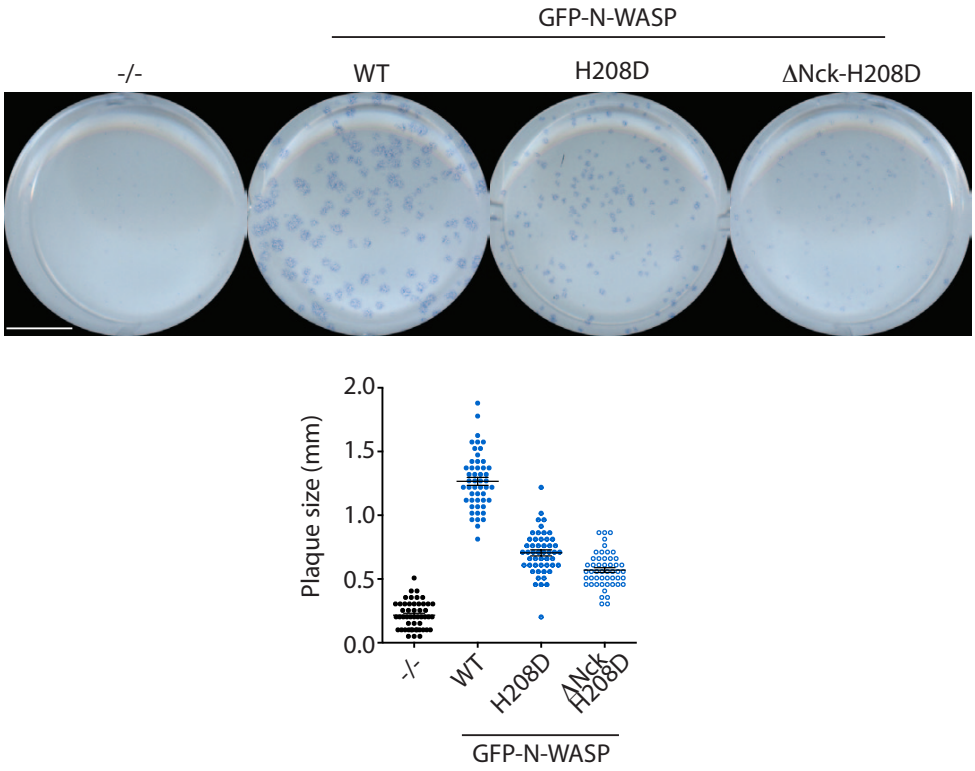

Figure 4.17 N-WASP mutants are deficient in viral spread

Representative images of viral plaques produced in the indicated cell lines, and the associated quantification of plaque size. N=50. Scale bar = 1 cm.

4.2.5 The cooperative nature of Cdc42 and N-WASP recruitment

I next wondered whether Cdc42 could also promote the recruitment of N-WASP to viral particles. I took advantage of the WH1CRIB domains of N-WASP, which act as a dominant negative for actin tail formation (Moreau et al., 2000). WH1CRIB competes with endogenous N-WASP for recruitment to the viral particle, but is unable to nucleate actin as it lacks the WCA domain. As expected, expression of GFP-tagged WH1CRIB in WR infected HeLa cells significantly decreased the percentage of cells with an actin tail (Figure 4.18). Introduction of the H208D mutation into WH1CRIB, however, reduced the dominant negative effect as judged by an increase in the percentage of cells with an actin tail (Figure 4.18). Therefore, suggesting that the interaction between Cdc42 and N-WASP provides a selective advantage to the recruitment of N-WASP at viral particles, as the H208D mutation is less efficient at competing out endogenous N-WASP. Concomitant with this, the intensity of WH1CRIB H208D at viral particles appeared diminished (Figure 4.18).

The WH1CRIB data suggests that Cdc42 contributes to N-WASP recruitment. However, it may also reflect the inability of N-WASP to be maintained at the viral particle due to its decreased stability. To address if this is the case, I expressed either GFP-Cdc42 or GFP-Cdc42-N17 in Nck +/+ and -/- MEFs. N-WASP is robustly recruited to viral particles in Nck +/+ cells in the presence of wild-type or dominant negative Cdc42 (Figure 4.19A). N-WASP was weakly recruited to viral particles in Nck -/- cells expressing GFP-Cdc42. Furthermore, this weak recruitment was lost in Nck -/- MEFs expressing GFP-Cdc42-N17 (Figure 4.19A). This data is consistent with the data from YdF infection, and suggests that Cdc42 can provide a minor contribution to N-WASP recruitment.

The previous data suggest that Cdc42 is upstream of N-WASP during actin tail formation, however, unexpectedly GFP-Cdc42 is only weakly localised to viral particles in N-WASP -/- MEFs (Figure 4.19B). Concomitant with this, live-cell imaging revealed that the intensity of GFP-Cdc42 increases during the initiation and course of actin tail formation (Figure 4.20). The intensity of GFP-N-WASP also increased during actin tail formation, but N-WASP intensity also steadily built prior to actin nucleation (Figure 4.20). Therefore, suggesting that N-WASP acts upstream of Cdc42, with

interdependency occurring between the two proteins during actin tail formation and continued actin polymerisation.

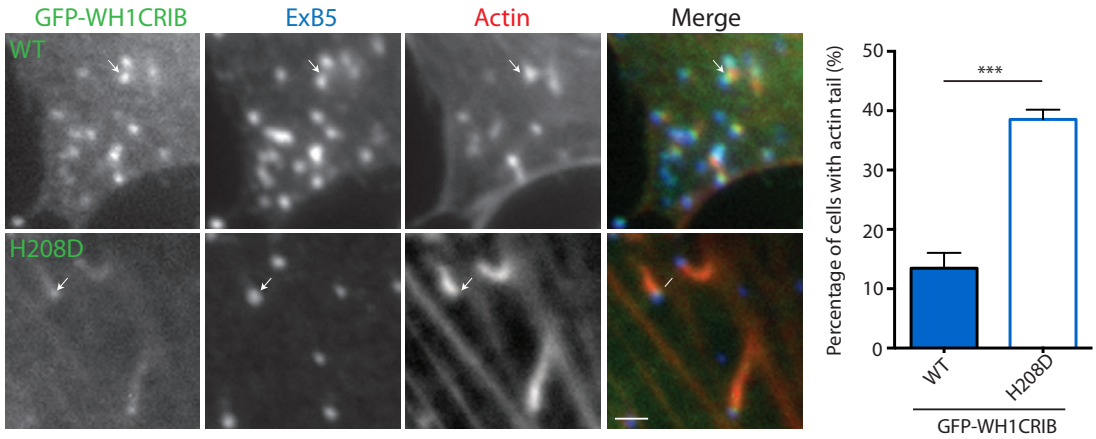

Figure 4.18 WH1CRIB-H208D is a less effective dominant negative against actin tail formation

Representative immunofluorescence images of WR infected HeLa cells expressing either GFP-tagged WH1CRIB or WH1CRIB-H208D. White arrows highlight the recruitment of WH1CRIB to viral particles. Scale bar = 1 μm. Quantification shows the percentage of cells expressing WT or H208D mutant WH1CRIB with an actin tail. Error bars represent SEM from 50 cells analysed in total from 3 independent experiments. A p value of <0.001 is indicated by ***.

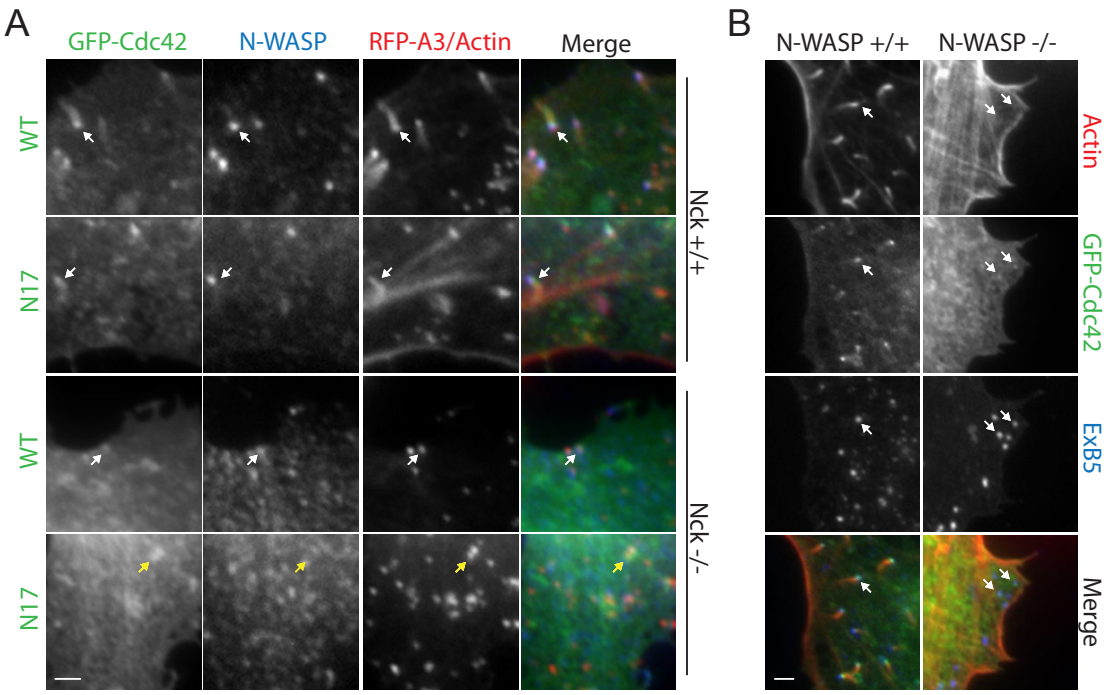

Figure 4.19 Cdc42 and N-WASP recruitment is interdependent

A Representative immunofluorescence images of Nck +/+ and -/- MEFs expressing either GFP-Cdc42 WT or N17. White arrows highlight N-WASP recruitment to viral particles, whereas yellow arrows highlight a lack of recruitment. Scale bar = 1 μm. **B** Representative immunofluorescence images of N-WASP +/+ and -/- MEFs expressing GFP-Cdc42. White arrows highlight GFP-Cdc42 recruitment to viral particles. Scale bar = 1 μm.

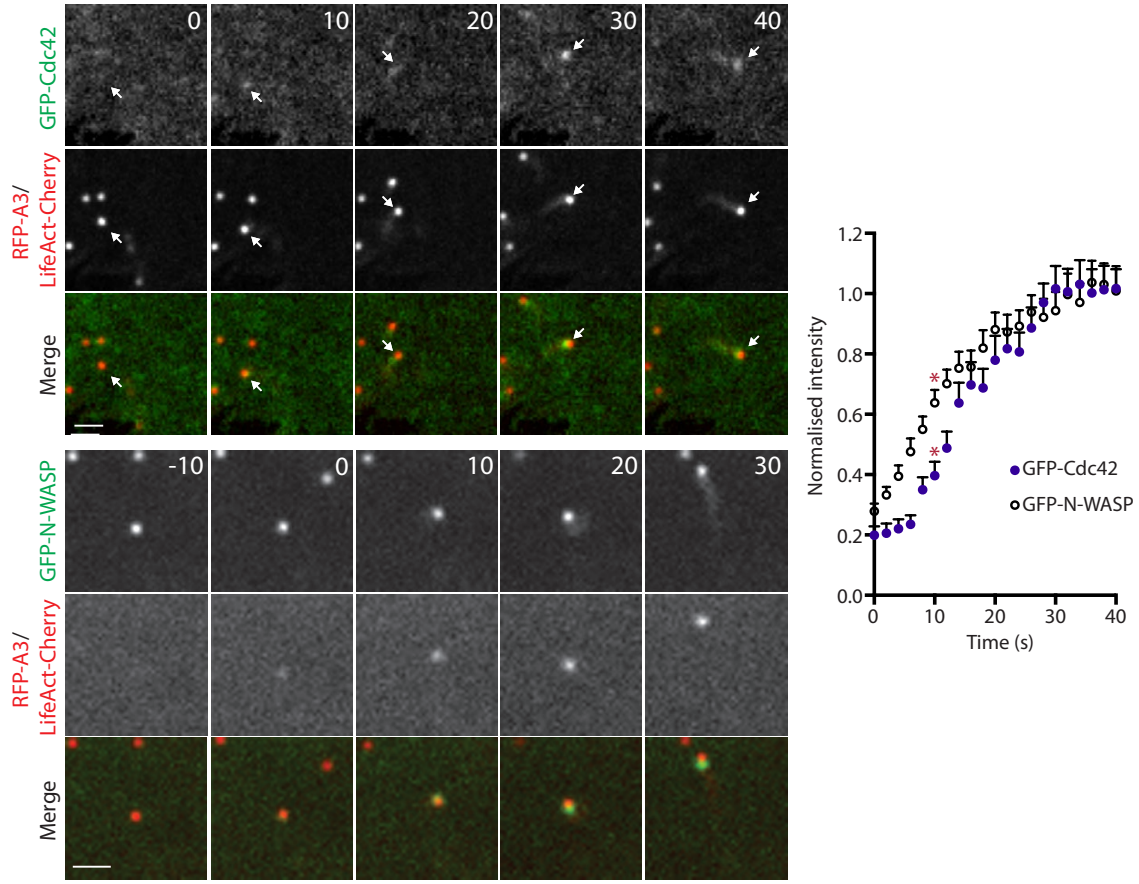

Figure 4.20 GFP-Cdc42 intensity increases during actin tail formation

Stills from live-cell imaging of infected HeLa cells expressing LifeAct-Cherry and either GFP-Cdc42 or GFP-N-WASP. White arrows highlight a viral particle that induces an actin tail, with the intensity of GFP-Cdc42 increasing over time (seconds indicated), stills start from the point of actin tail formation. GFP-N-WASP intensity also builds over time as shown in the lower panels, stills start 10 s prior to actin tail formation. Scale bar = 1 μm. Graph shows the normalised intensity of GFP-Cdc42 and GFP-N-WASP during actin tail formation from 30 nucleation events, red asterisks highlight the point at which an actin tail is induced and the virus begins to move (10 s).

4.2.6 Summary

The data presented in this chapter shows that Cdc42 can be recruited to vaccinia to promote A36-independent actin polymerisation. In the context of the wild-type WR virus, Cdc42 was found to play a supporting role to the main signalling nexus of Nck-WIP-N-WASP, to enhance the efficiency of actin tail formation. A major role of Cd42 was to stabilise N-WASP beneath the viral particle, with a minor contribution to N-WASP recruitment. This is in contrast to Nck, which has been shown to contribute only modestly to N-WASP stability with its major function attributed to the recruitment of N-WASP via WIP (Donnelly et al., 2013). My data shows interdependency between Cdc42 and N-WASP in their recruitment, suggesting that Cdc42 functions in a feed-forward pathway. I therefore, next wanted to determine how Cdc42 is activated at vaccinia virus, to understand further the molecular regulation of this pathway.

Chapter 5. ITSN1 promotes N-WASP-dependent actin polymerisation

5.1 Introduction

In the previous chapter, by investigating the role of Cdc42 in vaccinia actin tail formation, I observed interdependency between Cdc42 and N-WASP. As they appear to function in a feed-forward pathway, in this chapter I set out to determine the factor responsible for Cdc42 activation. I found that the endocytic protein, intersectin1 (ITSN1) activates Cdc42 at vaccinia virus. As the proteins that constitute the vaccinia-signalling network are used widely in other actin-dependent cellular processes, I then went on to examine whether the role of ITSN1 was also conserved during FcγR-mediated phagocytosis.

5.2 Results

5.2.1 ITSN1 is recruited to vaccinia virus

In the third chapter, I identified a role for clathrin in vaccinia induced actin-based motility, thus a strong candidate to activate Cdc42 was the RhoGEF intersectin1 (ITSN1). ITSN1 is an endocytic protein that is recruited during the early stages of clathrin pit formation through its interaction with several endocytic accessory proteins (Henne et al., 2010; Yamabhai et al., 1998). ITSN1 can exist as a long variant (ITSN1L) that harbours a DH GEF domain for Cdc42 activation, or a short variant (ITSN1S) that lacks this C terminal domain (Hussain et al., 2001; Hussain et al., 1999). Immunofluorescence staining revealed that ITSN1 is recruited to extracellular viral particles inducing actin tails (Figure 5.1). The antibody used detected both ITSN1 variants, therefore to test if the localisation was variant specific, GFP-tagged ITSN1L and IS were expressed in cells. However, both GFP-ITSN1L and GFP-ITSNIS were recruited to the tip of actin tails (Figure 5.1). ITSN1 was also detected on extracellular

virions associated with AP-2, suggesting that ITSN1 is recruited prior to vaccinia-induced actin polymerisation, and unlike AP-2/clathrin, is maintained during actin tail formation (Figure 5.1). Consistent with this, immunofluorescence analysis of N-WASP +/+ and -/- MEFs revealed that ITSN1 is recruited to virions in both the presence and absence of actin-based motility (Figure 5.2).

As it appeared that ITSN1 is recruited to virions at the time of clathrin recruitment, I next determined whether AP-2 was responsible for its localisation at viral particles. Depletion of AP-2, however, did not abrogate ITSN1 recruitment (Figure 5.3). This suggests that ITSN1 does not require AP-2 for its localisation at vaccinia virus, and that ITSN1 does not contribute to the phenotype observed upon AP-2 depletion.

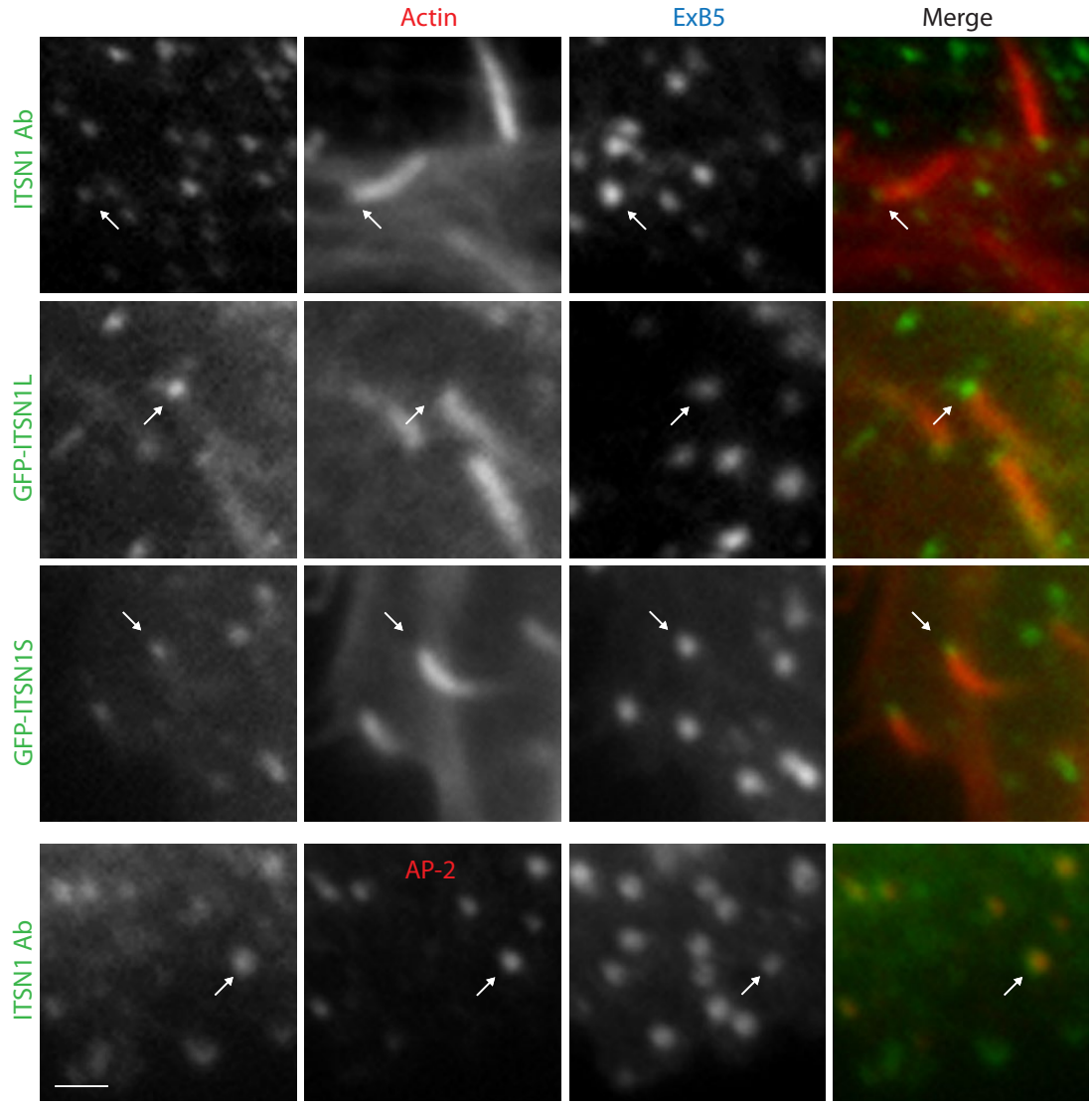

Figure 5.1 ITSN1 localises to vaccinia virus

Immunofluorescence images of vaccinia infected HeLa cells, showing localisation of ITSN1. Endogenous ITSN1, GFP-ITSN1L and GFP-ITSN1S are recruited to the tips of vaccinia-induced actin tails (white arrows). ITSN1 also co-localises with AP-2 on extracellular virions (exB5) prior to actin tail formation (white arrows). The merge image shows only the green and red channels to highlight ITSN1 localisation. Scale bar = 2 μm.

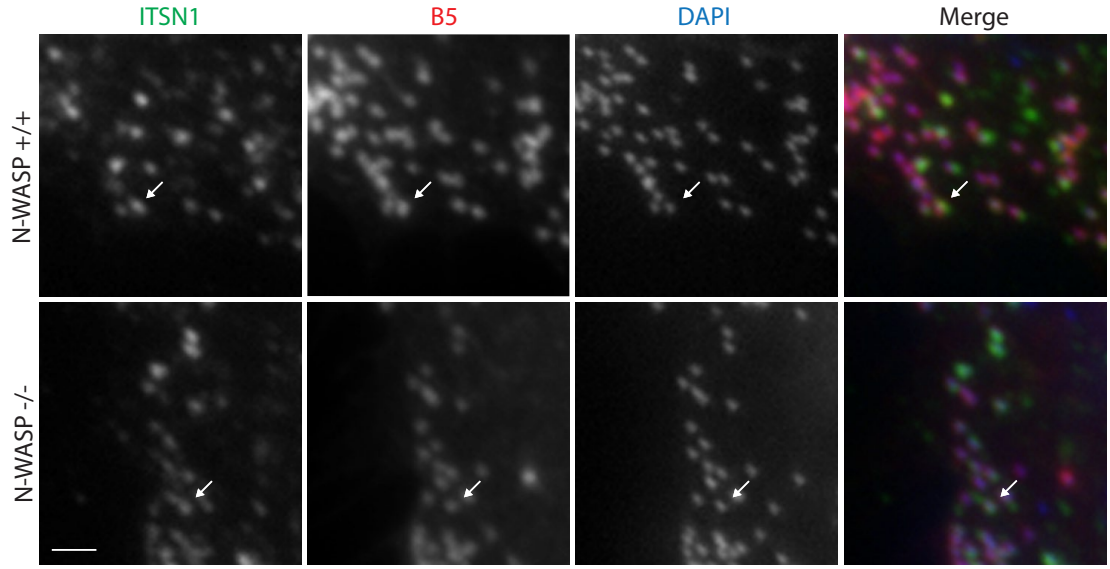

Figure 5.2 ITSN1 localises to vaccinia upstream of actin tail formation

Representative immunofluorescence images of vaccinia infected N-WASP +/+ and -/- MEFs, showing ITSN1 recruitment to viral particles labelled with B5 and DAPI (white arrows). Scale bar = 1 μm.

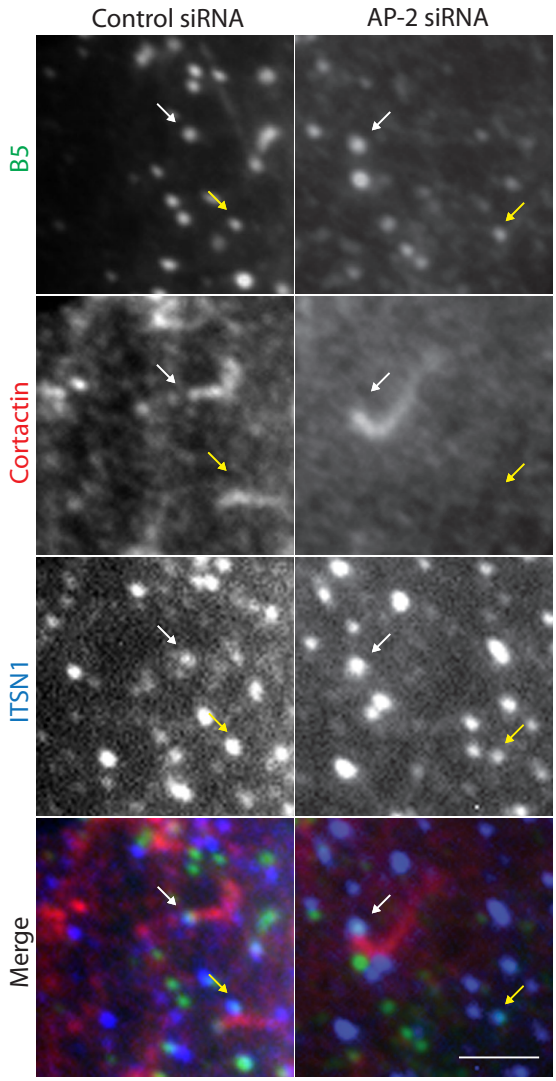

Figure 5.3 AP-2 depletion does not affect ITSN1 recruitment to vaccinia

Representative immunofluorescence images of HeLa cells treated with control or AP-2 siRNA before infection with vaccinia virus. ITSN1 is recruited to viral particles (yellow arrows), and particles inducing actin-based motility (white arrows) in both control and AP-2 depleted cells (white arrows). Scale bar = 2 μm.

5.2.2 ITSN1 acts in a feed-forward loop with Cdc42 and N-WASP

To ascertain whether ITSN1 contributes to actin tail formation, I depleted both ITSN1L and ITSN1S variants using two independent siRNA oligos. Both oligos successfully depleted ITSN1 levels as determined by western blot (Figure 5.4A). Depletion of ITSN1 led to a significant decrease in the percentage of extracellular virions inducing an actin tail (15.8±1.6 and 16.6±1.1% compared to 27.1±1.0%) (Figure 5.4B and C). Importantly, immunofluorescence analysis of control and ITSN1 depleted cells revealed that similar levels of AP-2 co-localised with extracellular virions (Figure 5.5). Therefore, the actin tail phenotype observed upon ITSN1 depletion is not due to loss of AP-2 recruitment, and the roles of ITSN1 and AP-2/CHC in actin tail formation appear distinct.

As both the long variant and short variant were depleted upon RNAi treatment, I next performed a rescue experiment to determine if the GEF domain was required to promote actin tail formation. Expression of siRNA resistant GFP-tagged ITSN1 constructs in ITSN1 depleted cells showed that ITSN1L but not ITSNIS was able to fully rescue the actin tail phenotype (Figure 5.6). This suggests that the GEF activity of ITSN1 promotes actin tail formation. To test whether the GEF domain regulates Cdc42 activation, I combined ITSN1 depletion with expression of dominant negative Cdc42. Depletion of ITSN1 or expression of GFP-Cdc42-N17 led to a significant decrease in the percentage of extracellular virions inducing an actin tail, which was not enhanced by combining both inhibitions (Figure 5.7). This suggests that ITSN1 and Cdc42 function within the same pathway, consistent with ITSN1 functioning as the GEF for Cdc42 at vaccinia virus.

My data suggests that ITSN1 activates Cdc42 at vaccinia virus, and that Cdc42 and N-WASP function within a feed-forward loop. To confirm this is the case, I used a biochemical approach to look at the interactions of the Cdc42-ITSN1-N-WASP signalling nexus. I performed GFP-trap pull-down experiments on HeLa cells depleted of endogenous N-WASP and co-expressing GST-tagged Cdc42 with GFP, GFP-N-WASP or GFP-N-WASP-H208D. GFP-N-WASP, but not the H208D mutant, bound GST-Cdc42 (Figure 5.8). In contrast, ITSN1 bound both WT and H208D N-WASP. In addition, depleting ITSN1 levels reduced the binding of Cdc42 to N-WASP, suggesting that ITSN1 interacts with N-WASP upstream of Cdc42, and that ITSN1 regulates the

binding between Cdc42 and N-WASP (Figure 5.8). Altogether, my data from this and the previous chapter is consistent with Nck recruiting N-WASP via WIP, allowing ITSN1, which is already present at the viral particle, to engage with N-WASP. ITSN1L is then able to locally activate Cdc42, which predominantly stabilises N-WASP beneath the viral particle (Figure 5.9).

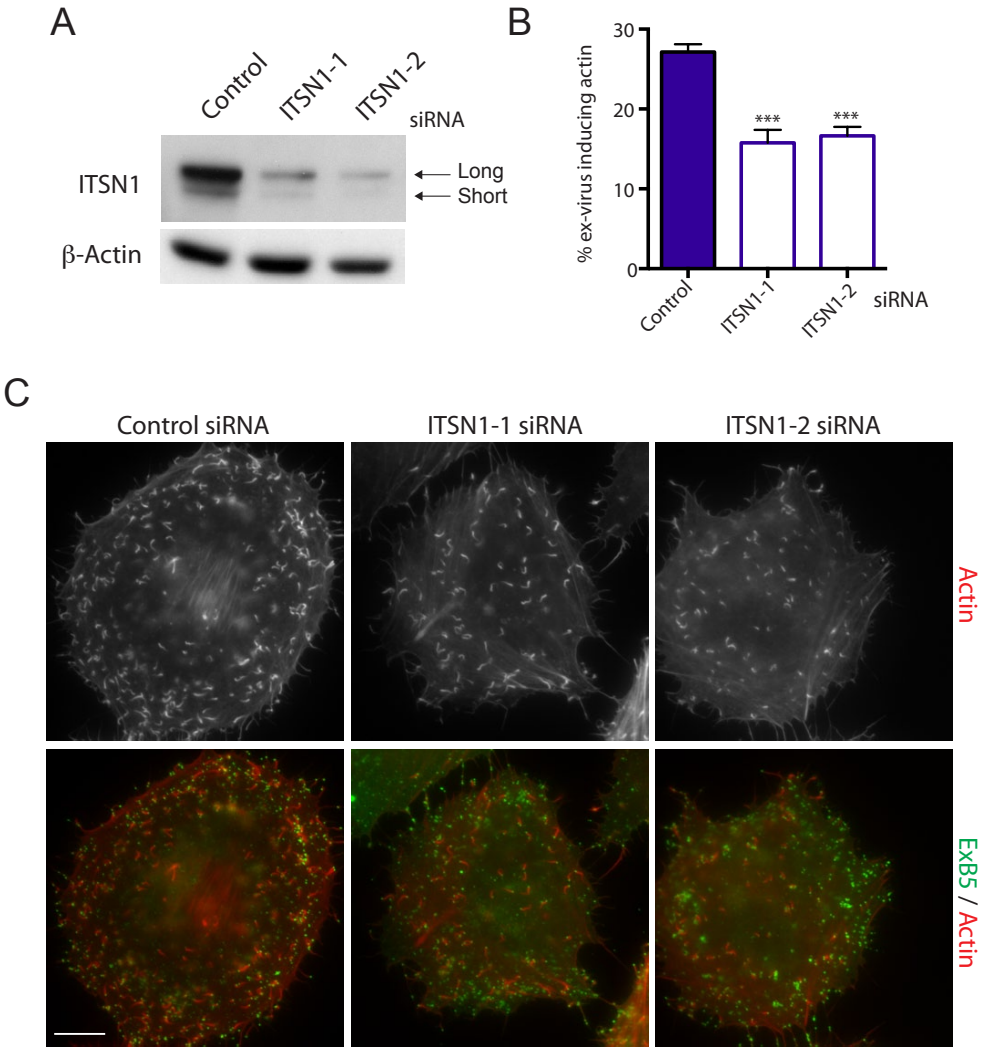

Figure 5.4 ITSN1 promotes actin tail formation

A Western blot showing ITSN1 levels after treatment with control or ITSN1 siRNA. The long and short variants are highlighted with arrows. β-actin is included as a loading control. **B** Quantification of the percentage of extracellular virus inducing an actin tail in control and ITSN1 depleted cells. Error bars represent SEM from 30 cells in total from 3 independent experiments. A p value of <0.001 is represented by ***. **C** Representative immunofluorescence images showing actin tails produced in control and ITSN1 depleted cells. Scale bar = 10 μm.

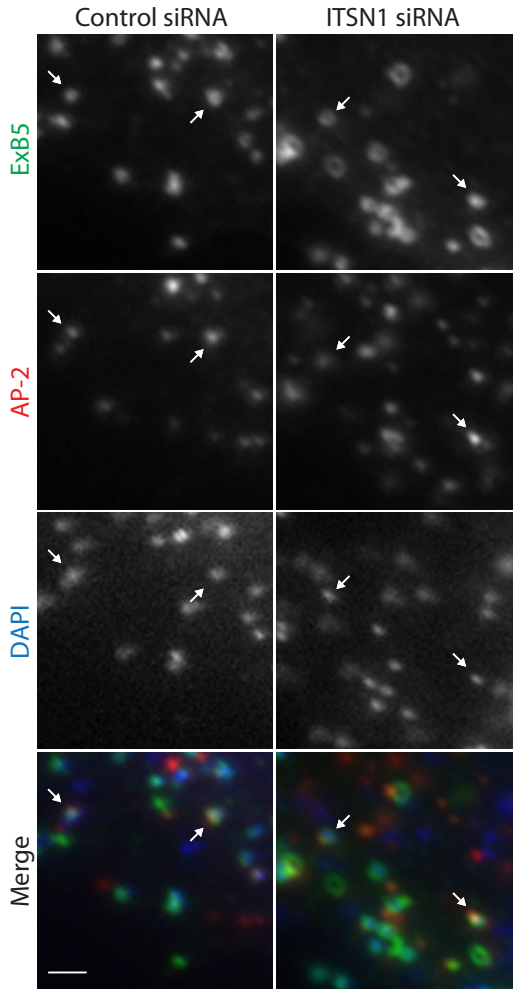

Figure 5.5 The roles of AP-2 and ITSN1 in actin tail formation are distinct

Representative immunofluorescence images of vaccinia infected control and ITSN1 depleted cells. Cells are stained for extracellular virus (exB5) and AP-2, with DAPI highlighting the viral DNA. White arrows highlight examples of co-localisation between extracellular virions and AP-2, which is not altered upon ITSN1 depletion. Scale bar = 1 μm.

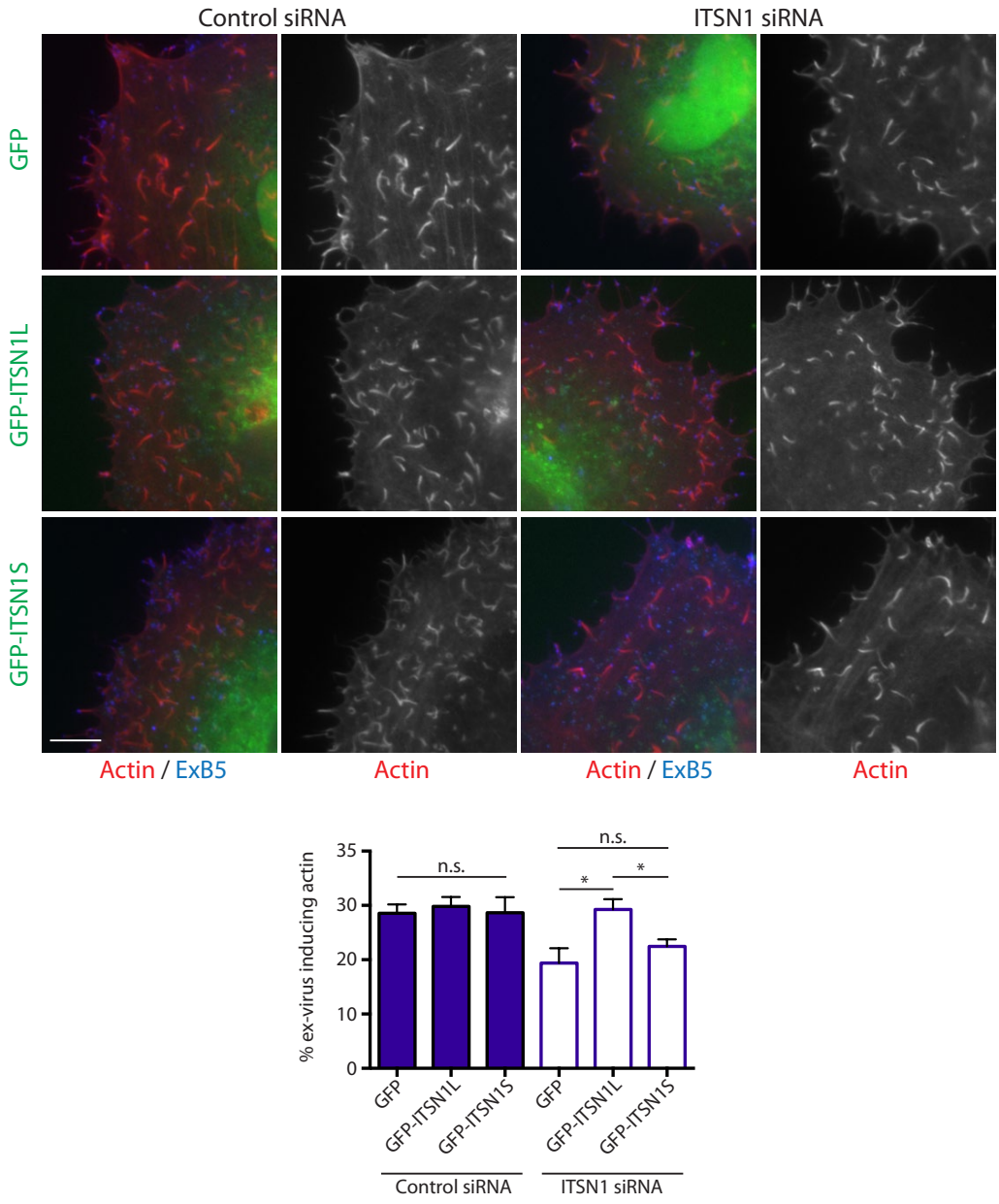

Figure 5.6 The GEF domain of ITSN1 promotes actin tail formation

Representative immunofluorescence images and associated quantification showing the percentage of extracellular virions inducing an actin tail in control or ITSN1 depleted cells, expressing the indicated siRNA resistant constructs. Scale bar = 5 μm. Error bars represent SEM from 30 cells in total from 3 independent experiments. A p value of <0.05 is represented by *.

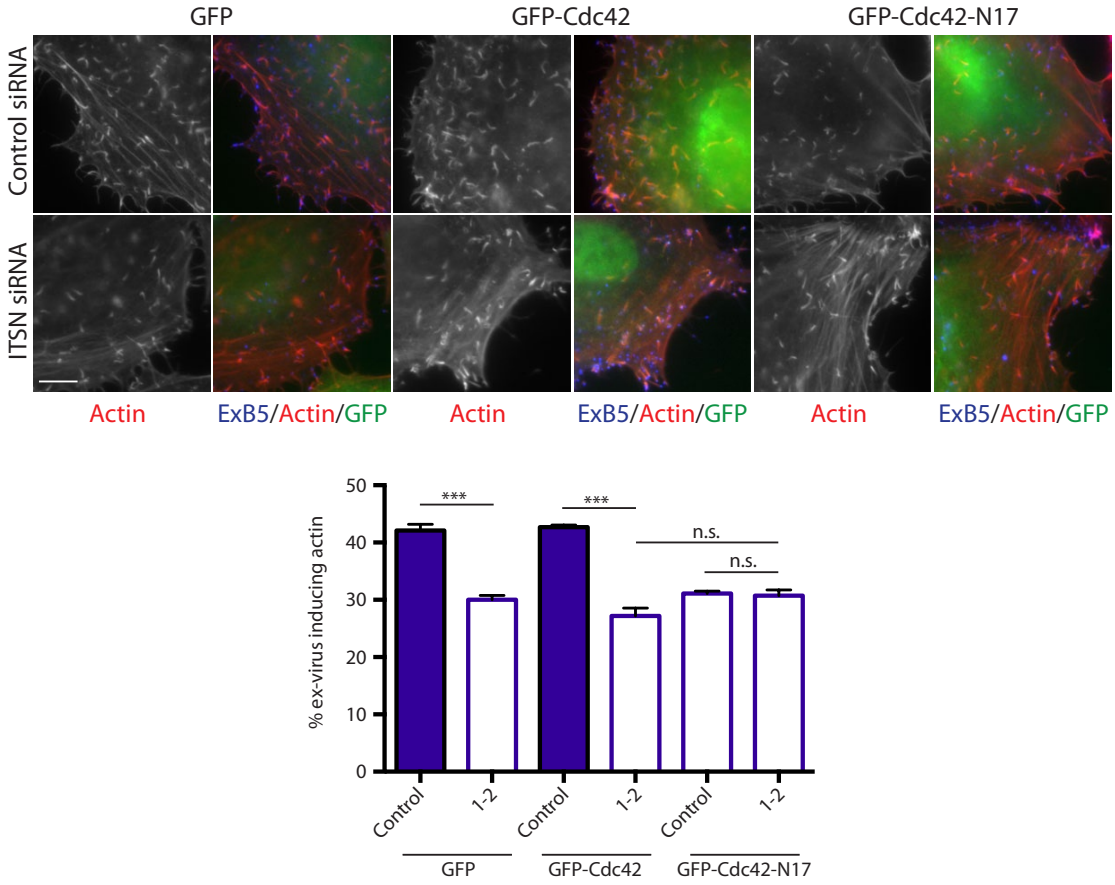

Figure 5.7 Cdc42 and ITSN1 function in the same pathway

Representative immunofluorescence images and associated quantification showing the percentage of extracellular virions inducing an actin tail in control or ITSN1 depleted cells expressing the indicated constructs. Scale bar = 5 μm. Error bars represent SEM from 30 cells in total from 3 independent experiments. A p value of <0.001 is represented by ***.

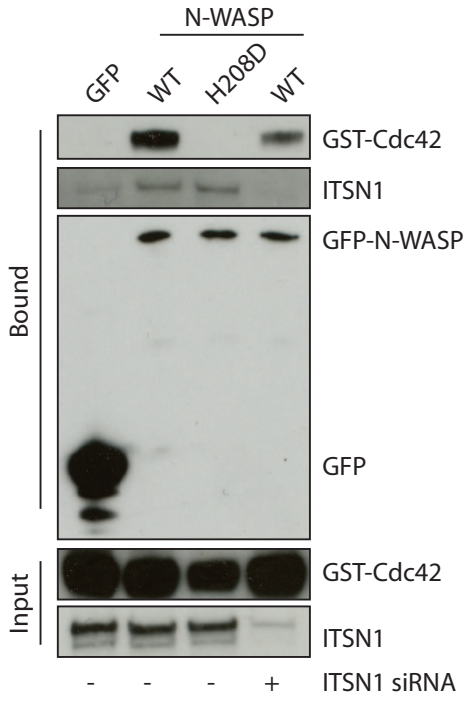

Figure 5.8 Cdc42-ITSN1-N-WASP form a feed-forward loop

Western blot analysis of GFP-trap binding performed on HeLa cells depleted of N-WASP expressing the indicated GFP-N-WASP constructs and GST-Cdc42. ITSN1 was additionally depleted (final lane), to determine its contribution to the interaction between Cdc42 and N-WASP.

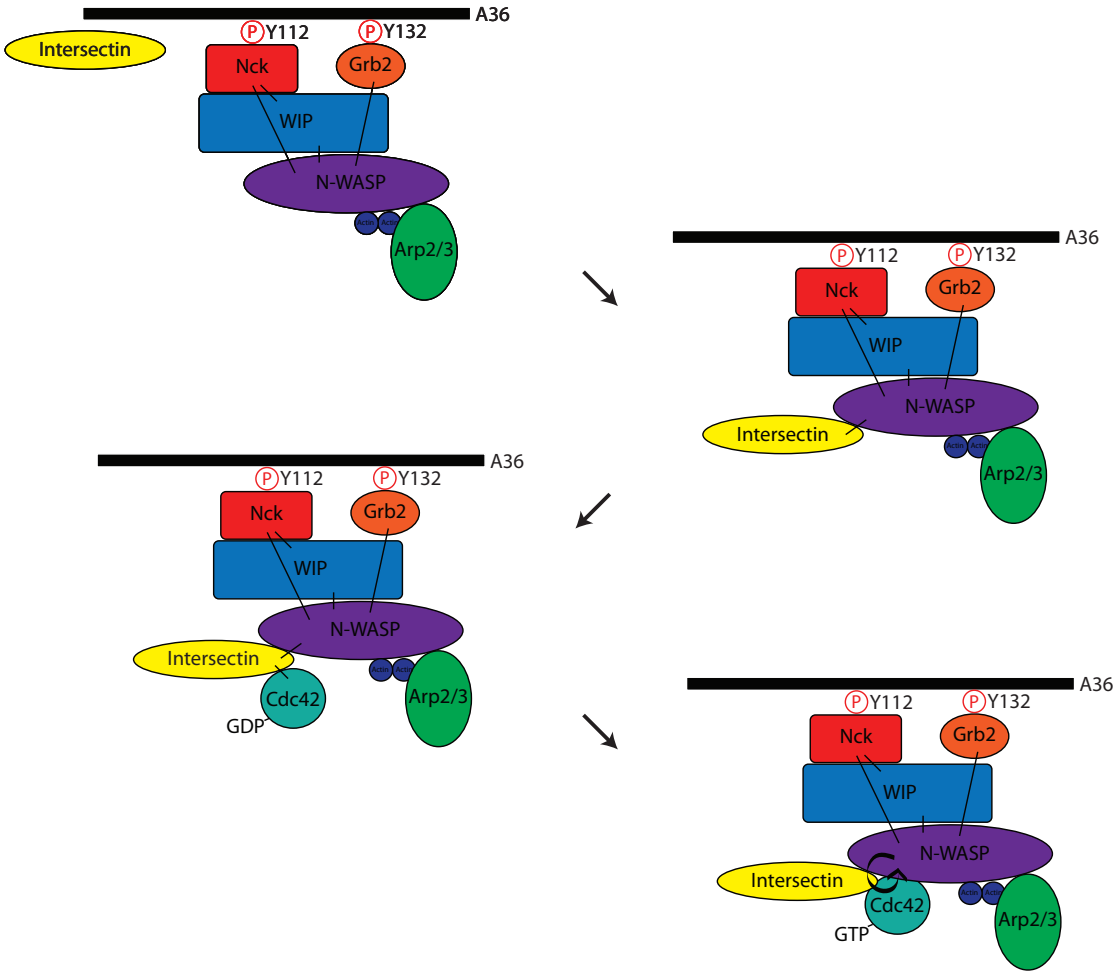

Figure 5.9 The vaccinia actin-signalling complex

Schematic showing the proposed signalling events of vaccinia-induced actin-based motility. Nck recruits WIP-N-WASP, ITSN1 then binds to N-WASP and activates Cdc42, which stabilises N-WASP beneath the viral particle.

5.2.3 ITSN1 regulates FcγR-mediated phagocytosis in a conserved pathway

Given my observations with vaccinia, I wanted to investigate whether ITSN1 is utilised in other N-WASP-dependent cellular processes. To examine this, I investigated whether ITSN1 regulates FcγR-mediated phagocytosis, a process that involves cooperativity between Nck and Cdc42 (Dart et al., 2012). HeLa cells were primed to undergo phagocytosis by expression of Fcγ receptor IIa, before incubation with IgG-coated sheep red blood cells (RBCs). Expression of GFP-ITSN1L in these treated cells revealed that it was recruited to the phagocytic cup, along with GFP-Nck, GFP-Cdc42 and GFP-N-WASP (Figure 5.10).

To assess the contribution of ITSN1 to Fcγ phagocytosis, I quantified the uptake of sheep RBCs in control and ITSN1 depleted cells. Analysis revealed that control and ITSN1 siRNA treated cells were associated with a similar number of total sheep RBCs (Ai), showing there was no defect in binding of sheep RBCs to the receptor (Figure 5.11). The ITSN1 depleted cells, however, showed a significant decrease in their phagocytic index (Pi), meaning fewer RBCs were internalised (Figure 5.11). Consequently, the normalised percentage phagocytosis was diminished by ~50% upon ITSN1 depletion (Figure 5.11).

To further explore the role of ITSN1 during Fcγ phagocytosis, I performed combined knockdown of the actin-signalling complex. A pool of siRNA was used to target Nck1, Cdc42 and N-WASP, with each showing efficient knockdown as assessed by western blot (Figure 5.12A). Depletion of ITSN1, Nck1, Cdc42 and N-WASP all resulted in a significant reduction in normalised percentage phagocytosis (Figure 5.12B and C). Furthermore, combined depletion of ITSN1 with each signalling component showed no enhanced phenotype, suggesting that these proteins function within the same signalling network (Figure 5.12B and C). Therefore, it appears that ITSN1 functions in a similar manner during both FcγR-mediated phagocytosis and vaccinia actin tail formation.

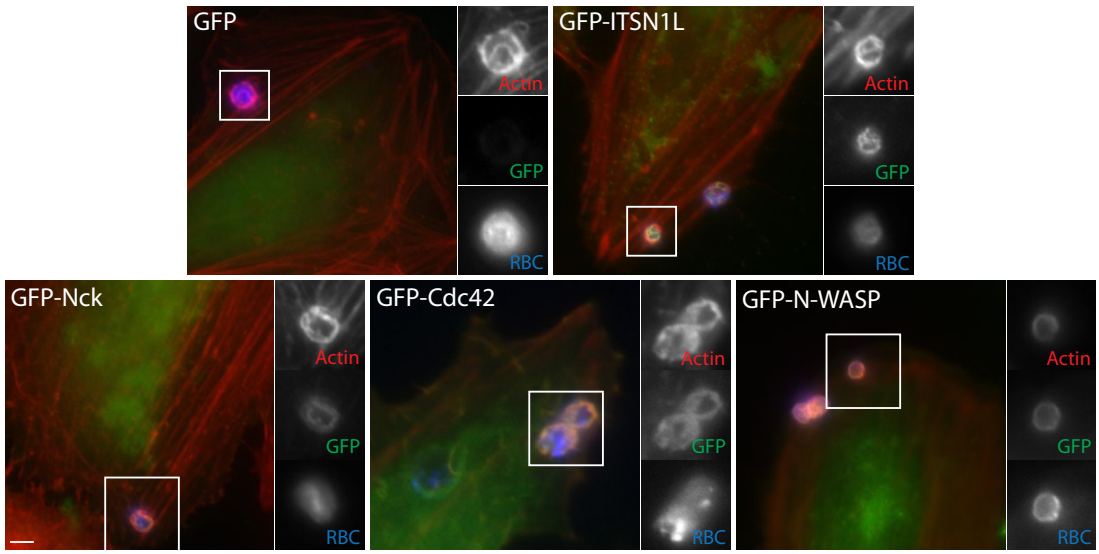

Figure 5.10 GFP-ITSN1L is recruited to the phagocytic cup

Immunofluorescence images of HeLa cells expressing Fcγ receptor IIa and incubated with sheep red blood cells. Cells are also expressing the indicated GFP-tagged constructs. White boxes highlight red blood cells with associated phagocytic cup and localisation of the GFP-tagged proteins. Scale bar = 5 μm.

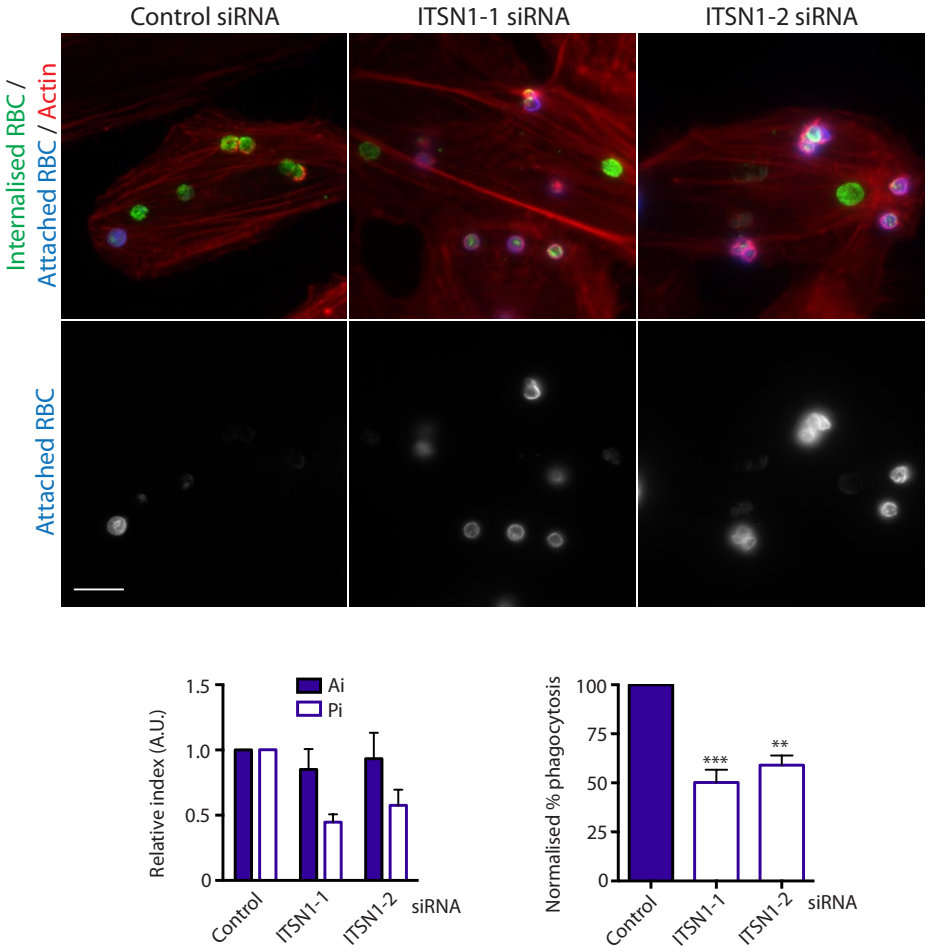

Figure 5.11 ITSN1 enhances phagocytic uptake

Immunofluorescence images of HeLa cells treated with control or ITSN1 siRNA, and incubated with sheep red blood cells. Sheep red blood cells were stained with secondary antibodies pre- and post-permeabilisation to distinguish between those that are attached to the cell surface (blue and green) and those that have been internalised (green). Scale bar = 5 μm. Quantification shows the relative index, including attachment index (total number of sheep red blood cells per HeLa cell) and the phagocytic index (number of internalised red blood cells per HeLa cell). Also shown is the normalised percentage phagocytosis. Error bars represent SEM from a total of 30 cells in 3 independent experiments. A p value of <0.01 and <0.001 is indicated by ** and ***, respectively.

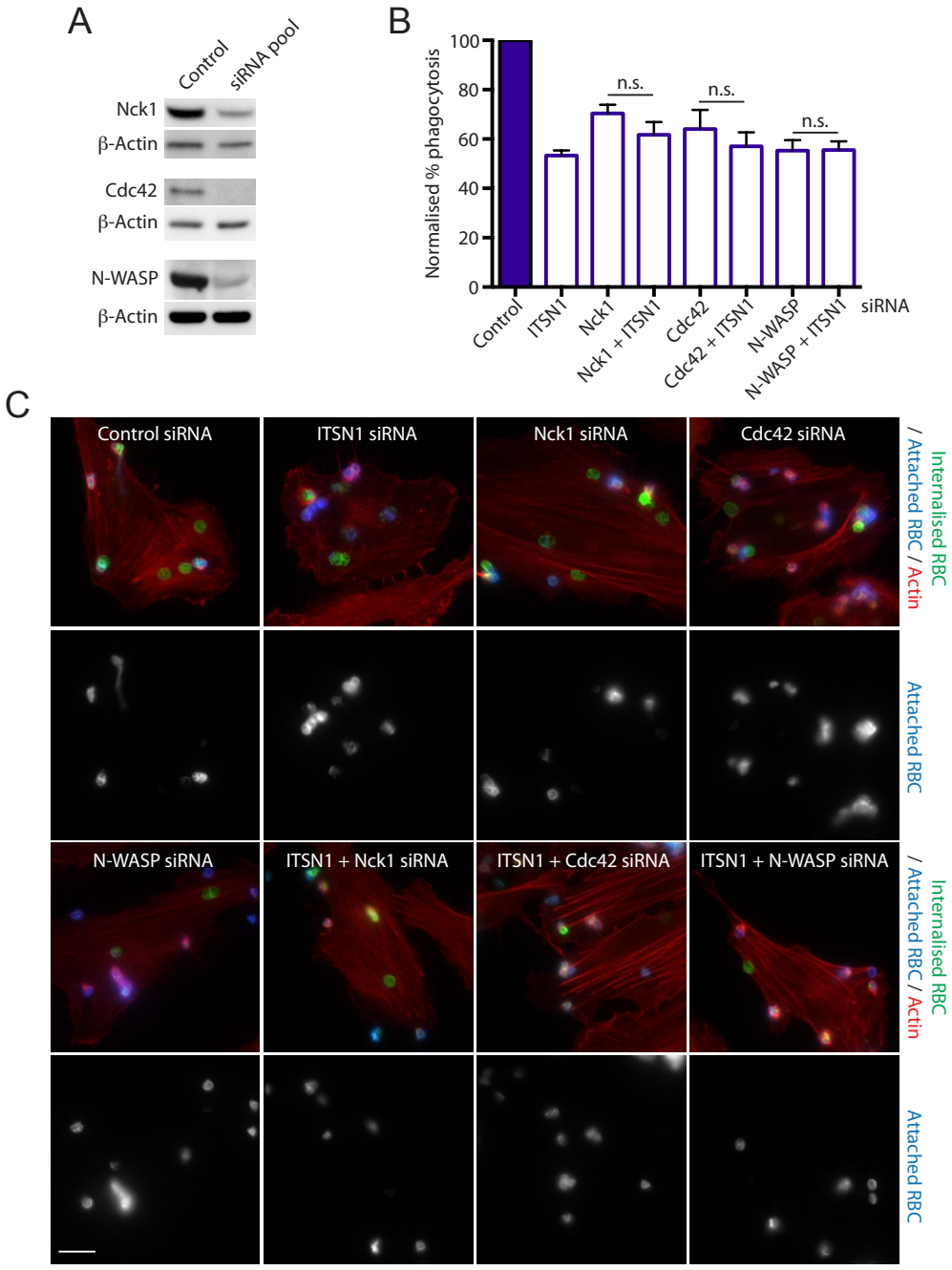

Figure 5.12 ITSN1 functions in a conserved signalling pathway

A Western blot showing levels of the indicated protein after treatment with an siRNA pool directed at Nck1, Cdc42 or N-WASP. β-actin is used in each case as a loading control. **B** Quantification of the normalised percentage phagocytosis in cells treated with the indicated siRNA pools. Error bars represent SEM from a total of 30 cells in 3 independent experiments. **C** Representative immunofluorescence images showing attached and internalised sheep red blood cells in the indicated siRNA treated HeLa cells. Scale bar = 10 μm.

5.3 Summary

My data from this chapter suggest that ITSN1 promotes Cdc42 activation, with Cdc42-ITSN1-N-WASP functioning in a feed-forward loop during vaccinia actin tail formation. I also found that ITSN1 functions independently from AP-2/CHC to promote actin-based motility of vaccinia, indicating that ITSN1 is recruited at the time of clathrin localisation but is retained at the tip of the actin tail due to its ability to bind N-WASP. Importantly, the role of ITSN1 was conserved during FcγR-mediated phagocytosis, validating the use of pathogens to study the molecular detail of actin-signalling networks.

Chapter 6. Discussion

N-WASP-dependent actin polymerisation is critical for a number of cellular processes, and thus requires tight regulation in both a temporal and spatial manner. In this thesis, I have used vaccinia virus as a model system to study the events that lead to and maintain N-WASP-dependent actin polymerisation. I have identified an organisational role for clathrin upstream of actin polymerisation, and have additionally described a supporting signalling pathway that enhances actin-based motility of the virus. Furthermore, I observed conservation of this signalling network during FcγR-mediated phagocytosis, validating the use of pathogens to study the molecular regulation of N-WASP-dependent actin polymerisation.

6.1 Interplay between clathrin and actin

In the third chapter, I found that clathrin localises to vaccinia at an unexpected stage of its replication cycle. Using a combination of immunofluorescence and live-cell imaging, I showed that clathrin is recruited in an AP-2-dependent manner following fusion of the virus with the plasma membrane (Figure 3.2-3.5). My work and previous studies observed pausing of the virus at the plasma membrane for variable amounts of time in between microtubule-based transport and actin tail formation (Dodding et al., 2009) and Figure 3.10). As Src phosphorylation triggers both kinesin-1 release and phosphorylation of A36 (Newsome et al., 2004), it is intriguing that such a pause exists. My data, taken on a whole, now suggests that this pause may represent a time of organisation or priming for actin nucleation. Thus, the recruitment of clathrin has defined a novel stage in the egress of vaccinia virus from the host cell.

6.1.1 Recruitment of clathrin to vaccinia virus

Clathrin is recruited to vaccinia following fusion, and is lost upon induction of actin-based motility (Figure 3.5). These events bookend clathrin localisation, however, I have not defined the signalling events and interactions that lead to clathrin recruitment in the first instance.

I was able to show that AP-2 forms a complex with the cytoplasmic tail of A36 (Figure 3.13), suggesting that A36 can act as a cargo in the canonical sense of clathrin function. It has also previously been reported that the proteins A36, B5, F13 and A33 are all recycled from the plasma membrane back into the cell after release of the viral particle (Husain and Moss, 2005). Additionally, three residues in the cytoplasmic tail of B5 are linked to its internalisation (Ward and Moss, 2000), and an interaction between F13 and AP-2 has been demonstrated (Husain and Moss, 2003). However, the residues responsible for the F13-AP-2 interaction could not be identified, with the authors suggesting multiple motifs in F13 regulate AP-2 binding (Husain and Moss, 2003). The residues required for B5 recycling are tyrosine and dileucine residues, but the surrounding sequence does not conform to a consensus adaptor binding motif (Ward and Moss, 2000). This makes the identification of possible interaction sites within the viral proteins more challenging, with interactions between the individual viral proteins adding a further complication (Chan and Ward, 2012; Johnston and Ward, 2009; Perdiguero and Blasco, 2006; Perdiguero et al., 2008). Analysis of their cytoplasmic domains reveals a number of canonical and potential interaction motifs for AP-2, with the exception of A33 that contains a single tyrosine residue, suggesting that multiple proteins as well as motifs can interact with AP-2 (Figure 6.1).

Clathrin induces A36 clustering beneath the virus, however, it is unclear whether this is a specific process or if other viral proteins are involved actively or passively in clustering. A36 has a large cytoplasmic tail and F13 is palmitoylated, exposing the entire protein to the cytoplasm, whereas B5, A33 and A34 all have a short cytoplasmic tail (Duncan and Smith, 1992; Engelstad et al., 1992; Isaacs et al., 1992; Roper et al., 1996). Hence, A36 and F13 appear more accessible, perhaps explaining why binding of AP-2 has been observed with only these two viral proteins so far (Figure 3.13) (Husain and Moss, 2003). A36 also exhibits a number of unique properties, that could promote its clustering over that of the other IEV proteins. A36 is distinct in its phosphorylation, which coordinates binding of different effectors in a temporal manner (Newsome et al., 2004; Newsome et al., 2006). It is possible that phosphorylation could influence the interaction of A36 with AP-2 directly or indirectly, through conformational change and/or accessibility of the cytoplasmic tail. In addition, A36 is found uniquely in the outer IEV membrane, whilst the other proteins are found in both membranes (Smith and Law, 2004). This makes analysis of their organisation after fusion rather complex, as structured-illumination microscopy would not be able to distinguish between the two

membranes. Interestingly, a recent paper has demonstrated that actin polymerisation can also promote clustering of A36 (Horsington et al., 2013). The authors propose that the force provided by actin polymerisation can enhance the presentation of the virus particle on the cell surface, thereby reducing the interface between the virus particle and the membrane (Horsington et al., 2013). As A36 is incorporated into the plasma membrane upon fusion, the authors data, could also suggest that the highly interconnected nature of the actin filament network is responsible for the clustering activity at the membrane. As A36 directly coordinates actin polymerisation, this adds weight to its AP-2-mediated clustering being unique, with both clustering processes potentially assisting each other during the initial stages of actin tail nucleation.

In support of this hypothesis, analysis of its amino acid sequence reveals the presence of three NPF motifs in A36 that are absent from the other recycling proteins (Figure 6.2). NPF motifs coordinate binding to epsin homology (EH) domains, which are found in several early endocytic proteins including ITSN, epsin and Eps15 (Chen et al., 1998; Wong et al., 1995; Yamabhai et al., 1998). These proteins can interact with AP-2, hence, A36 could recruit the adaptor via a distinct mechanism to the other viral proteins (Benmerah et al., 1995; Chen et al., 1998). This is supported by my data showing that AP-2 depletion does not alter ITSN1 recruitment (Figure 5.3). However, likewise ITSN1 depletion does not lead to a loss of AP-2 localisation (Figure 5.5). Many proteins contain EH domains, so it is possible they act in a redundant manner to recruit AP-2 to the virus. This mechanism could thereby distinguish between its recruitment during A36-mediated clustering, and for the general recycling of IEV proteins at a later stage of infection.

Consistent with different temporal requirements for clathrin during infection, depletion of the heavy chain reduced the number of extracellular virions, whereas AP-2 depletion did not (Figure 3.7 and 3.8). As recycling of viral proteins likely involves AP-2-mediated internalisation and is described to occur after viral release (Husain and Moss, 2005), there must be an additional undescribed earlier requirement for clathrin during the infectious cycle. Clathrin performs a well-characterised role at the Golgi, which is also the site of IEV assembly (Roberts and Smith, 2008). Thus, it is likely that clathrin is used in a higher capacity for vaccinia virus morphogenesis and spread than is thus far appreciated. The coordination, regulation and role of these different and temporally distinct events would therefore constitute a noteworthy avenue of future research.

Figure 6.1 Potential motifs in the recycling viral proteins

A The amino acid sequences of A36, B5, F13 and A33. The predicted transmembrane domain is highlighted in blue. Residues previously identified in B5 recycling are in green. Consensus adaptor binding motifs are in orange, and all tyrosine and dileucine motifs are in red. The arrows highlight which part of the transmembrane proteins is exposed to the cytoplasm. **B** The amino acid sequence of A36 with the predicted transmembrane domain in blue and NPF motifs in pink.

6.1.2 Use of clathrin in pathogen actin-based motility

Despite the mechanistic differences of individual pathogens, it is clear that a role for clathrin not only in pathogen entry but also during egress and spread is emerging (Humphries and Way, 2013). Vaccinia virus hijacks the intrinsic nature of AP-2 to selectively sequester cargo, and thus appears to mimic the early stages of CCV formation. This is in contrast to EPEC, which uses clathrin as a recruitment platform for the actin-signalling complex, mimicking the later stages of CME (Cossart and Veiga, 2008; Veiga et al., 2007). Another pathogen that uses clathrin to promote its spread is *Shigella*, which induces actin-based motility in the cytoplasm of the host cell. This promotes its movement to the plasma membrane, where the bacterium creates a pseudopodium protrusion into the neighbouring uninfected cell (Cossart and Sansonetti, 2004). A recent study revealed that clathrin engulfs the bacteria within this protrusion in a process that requires epsin1 (Fukumatsu et al., 2012). It will be important to determine if the exploitation of clathrin contributes to the egress of further pathogens that use actin-based motility for spread. In line with this, a screen for regulators of *Rickettsia* actin tail number and length identified Hip1R, a protein that directly links clathrin and actin (Serio et al., 2010). The phenotype observed was equivalent to AP-2 depletion during vaccinia infection, in that there were fewer but longer actin tails produced (Serio et al., 2010). Thus, it is possible that Hip1R functions within the vaccinia system, and would be worth investigating. However, as directly altering the density of A36 led to an increase in actin tail length, it suggests that modulating the spatial organisation of N-WASP is sufficient (Figure 3.17 and 3.18). Therefore, it may be that the phenotypes, although similar, are not mechanistically related.

6.1.3 Clathrin as a signalling scaffold

Consistent with their different uses of clathrin, EPEC and vaccinia coerce distinct adaptor proteins. Vaccinia virus hijacks AP-2, while EPEC uses Dab2, Eps15 and epsin1 (Bonazzi et al., 2011; Humphries et al., 2012; Lin et al., 2011). Interestingly, both Dab2 and epsin have also been implicated in the formation of clathrin plaques, which like EPEC pedestals are a long-lived structure (Chetrit et al., 2009; Saffarian et al., 2009). Stabilisation of the clathrin coat appears to be regulated by Src-dependent phosphorylation of the clathrin heavy chain, which is required for actin accumulation

beneath EPEC (Bonazzi et al., 2011; Brodsky, 2012), so why is it that different adaptor proteins are favoured?

Further analysis showed that, epsin, which promotes membrane curvature, is arranged throughout the clathrin lattice at plaques instead of at the edge as in classic endocytosis (Ford et al., 2002; Itoh et al., 2001; Saffarian et al., 2009). Suggesting, that the choice of adaptor along with the stabilising factor of phosphorylation may determine how the conformation of the lattice is regulated at pathogens and in cells. Epsin additionally regulates the recruitment of Hip1R to clathrin-coated pits in *Dictyostelium*, and can modulate both the location and timing of actin nucleation (Brady et al., 2010; Repass et al., 2007). Furthermore, disrupting the interaction between clathrin and Hip1R blocks the formation of large clathrin plaques, reinforcing the potential role of these adaptors in creating a clathrin scaffold for cytoskeletal rearrangement (Saffarian et al., 2009).

In contrast to EPEC, clathrin is transiently recruited to vaccinia virus. As its function at this stage of the replication cycle is to enhance actin-based motility, it is intriguing that vaccinia has evolved to use clathrin in a different manner. Autophosphorylation of tyrosine kinases promotes their clustering at the plasma membrane, creating a docking platform for the subsequent recruitment of downstream signalling molecules (Pawson, 2004). The close proximity of signalling molecules in the plasma membrane is sufficient for actin nucleation, as clustering Nck alone stimulates N-WASP-dependent actin polymerisation in cells (Ditlev et al., 2012; Rivera et al., 2004). In other phospho-tyrosine signalling networks, phosphorylation of the receptor protein is enough to trigger clustering and transmit the signal onwards (Pawson, 2004). In the case of vaccinia, clathrin recruitment adds a selective advantage, which I believe is due to complications imposed by the process of viral egress. During viral fusion the outer viral membrane is incorporated into the plasma membrane. Assuming this transition occurs via a fusion pore intermediate, as illustrated in Figure 6.2, one would expect that the surface area of plasma membrane occupied by viral proteins to be much greater than the area in contact with the virus. Thus, A36 must become tightly concentrated beneath the virus to facilitate the formation of a polarised actin tail (Figure 6.2). I propose that clathrin assists protein clustering due to this complex membrane environment that could make the process more challenging compared to normal situations at the plasma membrane.

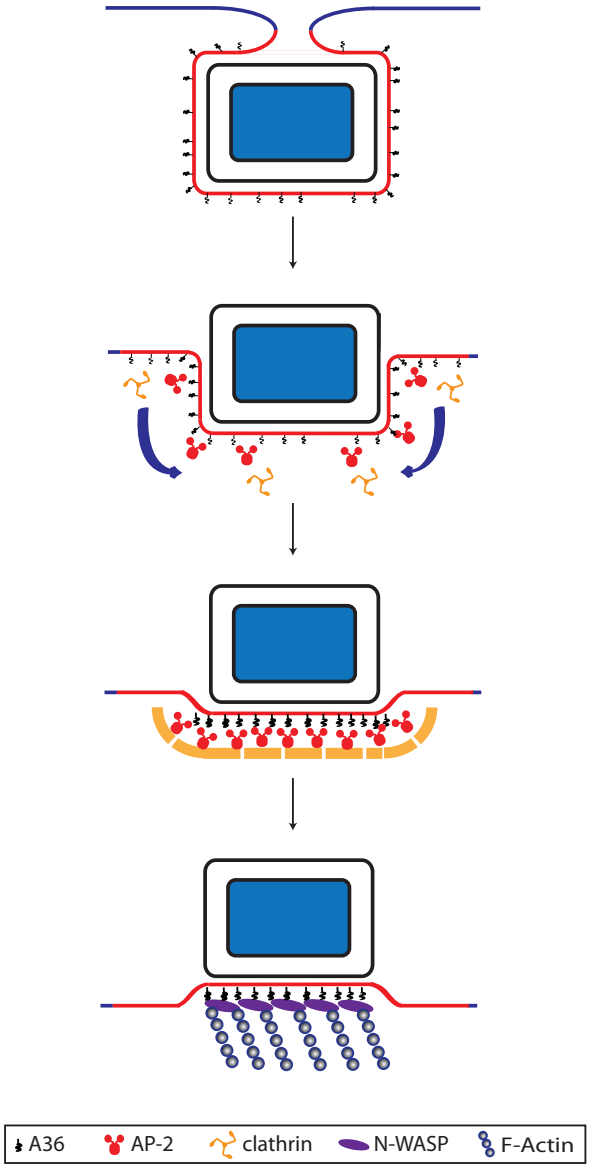

Figure 6.2 Proposed model of clathrin function in actin tail formation

During viral fusion the outer viral membrane is thought to fuse directly with the plasma membrane and the viral proteins, including A36, become incorporated. The phenotypes observed upon AP-2 depletion, are consistent with a role for AP-2/clathrin in clustering A36 beneath the virus particle. Although clustering of TM proteins can occur in other situations through phosphorylation, in this case the curved nature of the membrane surrounding the viral particle may require clathrin to improve the efficiency of this process. This would create a stable protein platform to build up the modular interactions of the actin-signalling network.

6.1.4 The phenotype observed upon AP-2 depletion

Loss of clathrin recruitment to vaccinia led to two phenotypes; fewer actin tails, and actin tails with an altered morphology (Figure 3.7 and 3.8). This can be explained by a requirement of a threshold density of A36 for efficient actin polymerisation (Figure 6.3). If A36 is not clustered sufficiently within the membrane, a multimeric-signalling complex is unable to form, as there is an insufficient density of interaction sites (Figure 6.3). If clustering of A36, however, reaches the threshold requirement, the more disperse organisation results in an actin tail with altered kinetics (Figure 6.3).

Depletion of CHC and AP-2 failed to completely block clathrin recruitment to the viral particle (Figure 3.7 and 3.8). However, I was not able to correlate this recruitment with the subsequent formation of an actin tail, as their localisation is lost upon actin polymerisation (Figure 3.3). I can therefore not definitively say whether clathrin recruitment is absolutely required for actin tail formation. The actin tails that form after RNAi treatment are able to do so either due to residual recruitment of AP-2/CHC, which clusters A36 to some degree, or clustering occurs in a clathrin-independent fashion albeit less efficiently. Perhaps the latter is more consistent with the literature, as actin polymerisation enhances clustering, therefore a small change in distribution may be sufficient to promote actin polymerisation in a feed-forward pathway (Horsington et al., 2013). Consistent with this idea, it is likely that the defect in organisation after AP-2 depletion is more severe than was observed by structured-illumination microscopy, as only those particles that had an actin tail were analysed (Figure 3.15). It would therefore be interesting to analyse extracellular particles in both HeLa and N-WASP -/- MEFs to see the true extent of this phenotype without the complication of actin nucleation.

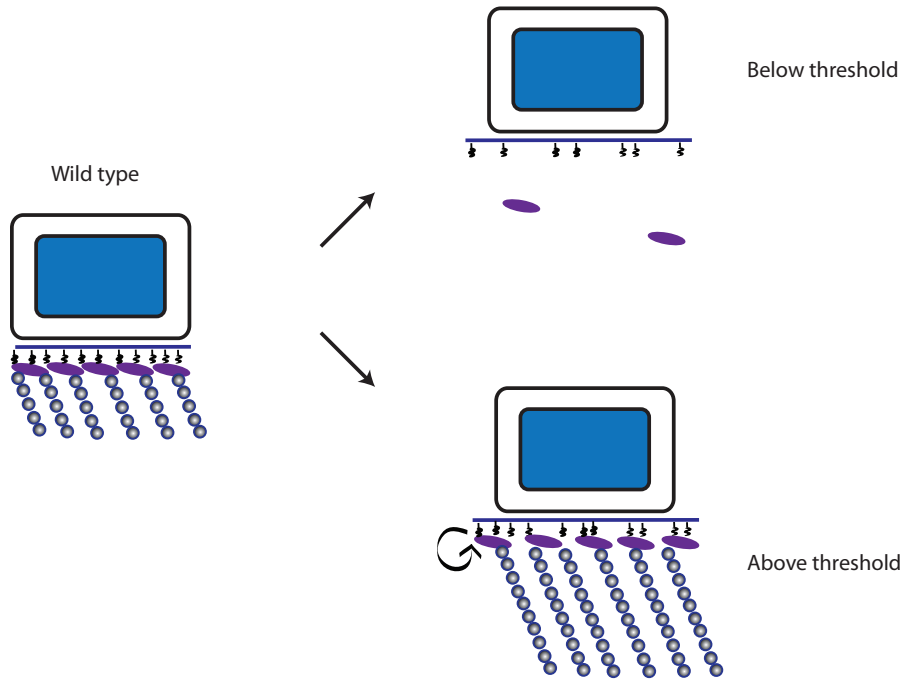

Figure 6.3 Threshold density for actin-based motility

Schematic depicting the two phenotypes observed upon clathrin and AP-2 depletion, explained by the requirement of a threshold density of A36. If the density of A36 is below the threshold, the actin-signalling complex is not recruited and an actin tail will not form. If the threshold is reached an actin tail is induced but the more disperse organisation of the sub-optimal signalling network leads to decreased N-WASP stability and altered tail morphology.

6.2 Regulation of vaccinia-actin based motility

6.2.1 Spatial organisation of N-WASP

A more disperse localisation of A36 and N-WASP led to actin-based motility with a faster velocity, a slower disassembly rate and a decreased persistence (Figure 3.10 and 3.11). Several *in vitro* assays have shown that altering the surface density of N-WASP or indeed its WCA domain on microspheres or vesicles can have a direct effect on the velocity of actin propulsion (Bernheim-Groswasser et al., 2002; Delatour et al., 2008; Wiesner et al., 2003). Segregation of N-WASP at the rear of the vesicle was required to promote continuous propulsion, however, a uniform distribution of N-WASP correlated with decreased speed and saltatory movement (Bernheim-Groswasser et al., 2002; Boukellal et al., 2004; Delatour et al., 2008). Hence, there is a correlation between the ability to maintain a stringent localisation and continuous actin-based movement. Consistent with this idea, in our system the tails produced when N-WASP was more disperse exhibited a shorter duration of actin-based motility (Figure 3.10).

The activity of Arp2/3 is regulated through the stoichiometric relationship of WASP proteins, and it is likely that full activation requires two WASP proteins (Padrick et al., 2011). The stoichiometry of the components of the complex beneath vaccinia virus is not clear and would need to be determined to understand fully the direct contribution of a more disperse organisation on the resulting activity of Arp2/3. However, there is an indication that A36 may form homodimers (Ina Weisswange, unpublished). This could allow for the normal recruitment of components to each dimer, however, the overall stability of the signalling network would be affected by the more disperse overall localisation of A36. There is also a level of complexity due to the dynamic nature of the actin-signalling complex used by vaccinia (Weisswange et al., 2009). It has previously been characterised that an increased turnover of N-WASP correlates with an increased velocity of viral-based actin movement (Weisswange et al., 2009). Therefore, it is likely that in our system the decreased stability of N-WASP caused by the more disperse signalling network, is the main factor driving faster nucleation as opposed to the degree of N-WASP dimer formation and activation.

Upon loss of clathrin recruitment I also observed a slower disassembly of actin filaments (Figure 3.11). The simplest explanation for this is that the filaments themselves are longer and therefore take longer to disassemble. It has been proposed that the WH2 domain of N-WASP binds transiently to the barbed-end of filaments and protects the growing filament from capping protein (Co et al., 2007; Weisswange et al., 2009). I therefore, propose that in our system N-WASP provides protection, and the faster nucleation rate allows the virus to build longer filaments before capping. However, I cannot rule out the possibility that changes in the organisation of actin filaments in the tail also contribute to slower disassembly.

Further studies aimed at analysing how the density of A36 directly correlates with signalling output, would offer an excellent opportunity to further our understanding of the initiation and regulation of phospho-tyrosine based signalling networks, as well as the parameters defining continuous actin propulsion in a freely-exchanging system.

6.2.2 Defining the speed of actin-based motility and the length of an actin tail

Clathrin depletion led to an increase in actin-based motility and a concomitant increase in actin tail length (Figure 3.6, 3.8 and 3.10). This data can be explained by an increase in N-WASP turnover, which regulates the rate of actin-based motility (Weisswange et al., 2009). In contrast, the N-WASP-H208D mutant described in chapter 4, exhibited a decrease in actin tail length, a decrease in actin-based motility and an increase in N-WASP turnover (Figure 4.12 and 4.16). Hence, what are the factors that govern the functional output of actin-based motility, i.e. the vaccinia actin tail?

An important factor is the amount of N-WASP and its degree of activation at the viral particle. With this in mind, the observed phenotypes I hypothesise could be explained as follows (Figure 6.4). Clathrin depletion does not markedly affect N-WASP recruitment or activation, however, it does modulate its stability, leading to faster actin-based motility and a long actin tail. The N-WASP-H208D mutant leads to reduced N-WASP activity and potentially also exhibits weaker recruitment. Therefore, the enhanced rate of N-WASP turnover cannot induce filament growth in the same manner, leading to a shorter actin tail.

My data shows discrepancies between HeLa cells and the MEFs in the length of actin tails. Whereby the HeLa cells with Cdc42-N17 expression exhibited the same length of actin tail compared to controls whereas the N-WASP-H208D MEFs had shorter actin tails (Figure 4.10 and 4.12). I believe this is due to the type of inhibition assay performed. In the case of MEFs I have a clean knockout background, however, all experiments with HeLa involved expression of a dominant negative or depletion with siRNA. I would therefore propose that the knockout MEFs provide a cleaner background for analysis of the phenotype. It is also possible that these differences are cell type specific, and could suggest different thresholds for actin polymerisation.

6.2.3 How does vaccinia promote actin-based motility?

My work in chapters 4 and 5 identified a supporting signalling pathway that enhances actin-based motility of the virus. I found that Cdc42 is recruited to vaccinia virus, and acts predominantly to stabilise N-WASP beneath the viral particle (Figure 4.16). Cdc42 can also evoke weak recruitment of N-WASP, during both WR and YdF infection (Figure 4.8, 4.9, 4.18 and 4.19). Activation of Cdc42 alone, however, is not sufficient to induce robust actin-based motility. This is highlighted by the transient nature of actin propulsion induced by the YdF virus, as well as its short actin puncta (Figure 4.1 and 4.2). Altogether, this reinforces the importance of Nck-WIP-N-WASP, however, it is clear that other factors contribute to the induction and maintenance of an actin tail (Figure 6.5).

Dissection of the actin-signalling complex revealed that Nck interacts with WIP in complex with N-WASP, before it interacts with N-WASP directly (Donnelly et al., 2013). This suggests either a conformational change caused by the interaction of Nck with WIP allows an interaction between Nck and N-WASP, or more likely that once at the plasma membrane Nck can cooperate with other molecules to relieve the autoinhibition of N-WASP. Additionally, it appears that WIP-N-WASP although recruited as a complex, dissociate at the virus particle as they exhibit different turnover rates when the virus in undergoing actin-based motility (Weisswange et al., 2009). Their dissociation is likely due to active actin polymerisation, therefore it is important to consider how N-WASP becomes activated in complex with WIP, as activation must precede actin-based motility (Weisswange et al., 2009). Consistent with this, experiments using *Xenopus* egg extracts defined a pathway for actin nucleation

constituting $PI(4,5)P_2$, Cdc42, N-WASP and Arp2/3, however, these molecules were not sufficient in a physiological context where N-WASP is found in complex with WIP (Ho et al., 2004; Ma et al., 1998a; Rohatgi et al., 2000). Thus, how does vaccinia virus activate N-WASP?

The phenotype observed with N-WASP-H208D was stronger than that of N-WASP-ΔNck, suggesting that Cdc42 plays a more important role in activating N-WASP beneath the viral particle, although Nck does contribute (Figure 4.12 and 4.14) (Donnelly et al., 2013). Infection of N-WASP-ΔNck-H208D stable cell lines with the Y132F virus, which cannot recruit Grb2, did not abrogate actin polymerisation, however, the structures formed resembled puncta rather than an elongated tail (Figure 4.15). Altogether, this suggests that Nck, Grb2 and Cdc42 contribute to N-WASP activation, however, in their absence other factors are still able to promote N-WASP-dependent actin polymerisation.

Another factor that may contribute is $PI(4,5)P_2$, which is able to activate N-WASP in the presence of WIP (Papayannopoulos et al., 2005). The localisation and potential function of $PI(4,5)P_2$ at the vaccinia interface, however, has never been investigated. $PI(4,5)P_2$ can synergise with both Nck and Cdc42 to promote N-WASP activation, and in fact it has been suggested that $PI(4,5)P_2$ could promote the activation of Cdc42 upstream of N-WASP activation (Ho et al., 2001; Rohatgi et al., 2000; Rohatgi et al., 1999; Rohatgi et al., 2001). Consistent with the latter idea, $PI(4,5)P_2$ could explain the presence of ITSN1 at vaccinia virus. Indeed, clathrin recruitment and endocytosis in general occurs at $PI(4,5)P_2$-rich membranes (Cocucci et al., 2012), suggesting that the lipid if present could have a dual function in coordinating clathrin recruitment and simulating N-WASP-dependent actin polymerisation. Making its future study along with the general lipid composition at the interface integral to understanding the temporal events that occur at the plasma membrane during viral egress.

It appears that Cdc42 functions in a similar manner to Grb2, in that it is not required for, but enhances actin-based motility of the virus. The presence of N-WASP is also necessary for recruitment of both proteins, further highlighting the dominant and upstream role of Nck in initially recruiting the WIP-N-WASP complex (Figure 4.19) (Scaplehorn et al., 2002). It is possible that WIP is not sufficient to recruit N-WASP, as N-WASP-ΔPolyPro is not recruited to the virus despite an intact WIP interaction (WH1)

domain (Donnelly et al., 2013). Deletion of the entire polyproline-rich region may have a dramatic effect of N-WASP outside of the domains function, however, it could also implicate an unknown SH3-domain containing protein in N-WASP recruitment and activation. Obvious candidates would be the F-BAR family of proteins, including Toca-1, FBP17 and CIP4. The BAR domain constitutes a banana-shaped alpha helical dimer that functions to sense highly curved membranes, for example, during endocytosis or indeed perhaps proceeding viral fusion (Gallop et al., 2006; Masuda et al., 2006; Peter et al., 2004; Weissenhorn, 2005). They bind to phosphatidylserine (PS), with binding enhanced by $PI(4,5)P_2$, and are implicated in coupling the endocytic machinery with the actin cytoskeleton (Dawson et al., 2006). The F-BAR proteins contain an SH3 domain and a RhoGTPase regulatory or binding domain, and thus act as scaffolds binding Cdc42 and promoting the recruitment and activation of N-WASP (Ho et al., 2004; Itoh et al., 2005; Tsujita et al., 2006).

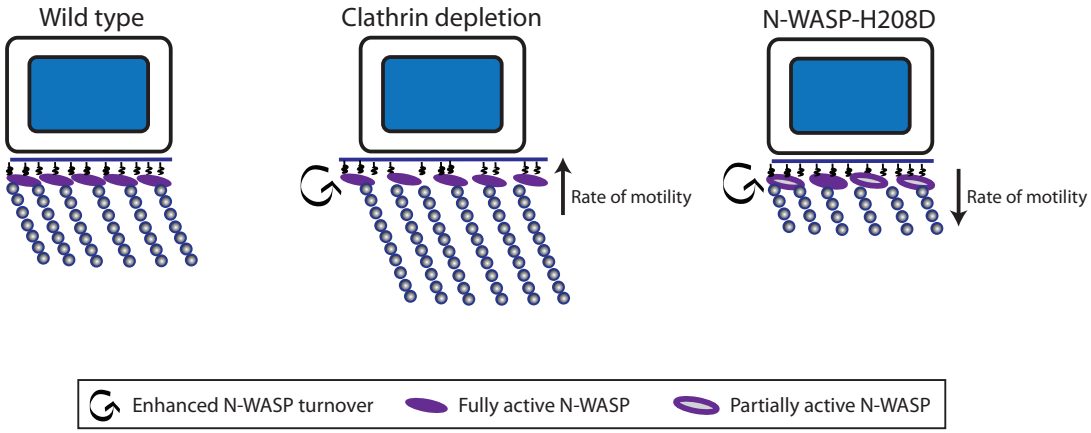

Figure 6.4 Regulation of N-WASP and the signalling output

Model depicting the different phenotypes of actin-based motility induced in the indicated backgrounds, which both lead to enhanced N-WASP turnover. Clathrin depletion induces a long actin tail with increased actin-based motility. While N-WASP-H208D exhibits shorter actin tails and decreased actin-based motility, most likely due to decreased N-WASP activation.

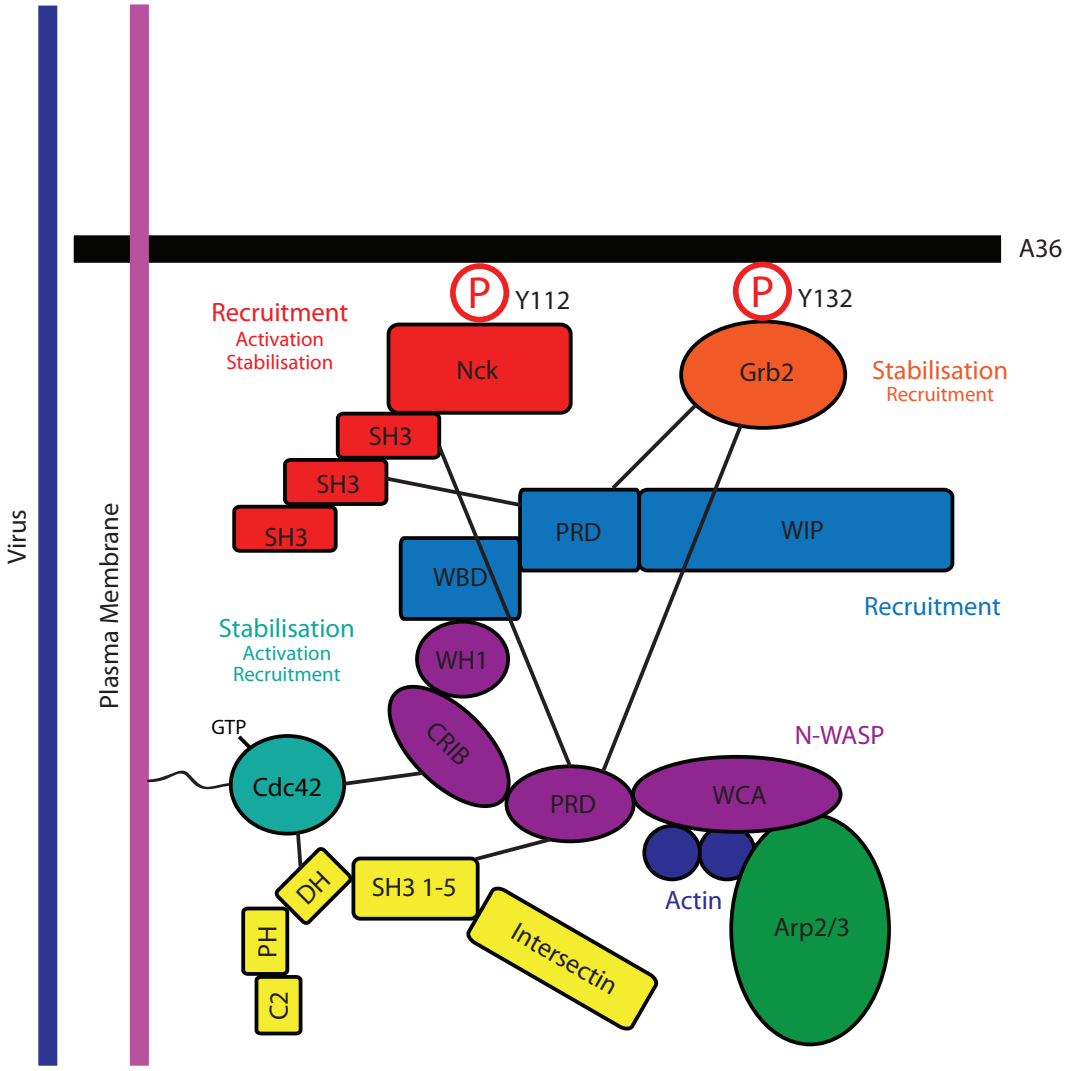

Figure 6.5 Updated model of the vaccinia actin-signalling network

Schematic of the vaccinia-actin signalling network, showing interactions that form between the different components. Also noted is the prescribed function of the component in N-WASP regulation, which are shown in different colours. At least one other unidentified component is required for full activation of N-WASP, which may interact with its polyproline-rich region.

6.3 Conservation of N-WASP signalling networks

ITSN1 has previously been shown to act as a GEF for Cdc42, with expression of DH-domain containing constructs sufficient to stimulate actin rearrangements consistent with Cdc42 activation (Hussain et al., 2001). N-WASP binds to ITSN1L and upregulates its GEF activity, enhancing binding between the DH-domain of ITSN1 and GDP-bound Cdc42. This promotes conversion from GDP to GTP-bound Cdc42, which interacts with N-WASP to promote Arp2/3-dependent actin polymerisation (Hussain et al., 2001). This model predicts a requirement for N-WASP upstream of Cdc42, which is consistent with my live-cell imaging data (Figure 4.20). It is also consistent with observations from FcγR-mediated phagocytosis, as like with vaccinia infection, Cdc42 failed to robustly localise to the phagocytic cup in the absence of N-WASP (Figure 4.19) (Dart et al., 2012). In both systems it was also shown that Nck is responsible for N-WASP recruitment, therefore, the pathways appear to function in a conserved manner. It is also intriguing that a parallel pathway of Rac activation leads to Arp2/3 activation during FcγR-mediated phagocytosis, as there is evidence of a N-WASP-independent pathway functioning during vaccinia infection (Figure 4.4). However, it is clear that this pathway is not dominant during the normal WR infection, as actin tail formation requires N-WASP (Snapper et al., 2001). It would therefore be interesting to determine whether Rac does play a supporting role during vaccinia infection, and if so why it is not as marked as the Nck/Cdc42-N-WASP pathway described in my thesis.

My work has found a role for ITSN1 in both vaccinia infection and FcγR-mediated phagocytosis, showing a potentially broad role for this RhoGEF in N-WASP-dependent processes. Consistent with this idea, my preliminary data shows that ITSN1 localises to and positively regulates invadopodia formation (Figure 6.6). As invadopodia facilitate the invasion of cancer cells, further investigation into the role of ITSN1 in cancer progression would be important. Particularly, as previous studies have largely focused on the neuronal system, where ITSN1 is known to be highly expressed (Gasman et al., 2004; Hussain et al., 2001; Hussain et al., 1999; Malacombe et al., 2006). My work has not identified whether the GEF activity of ITSN1 is required for invadopodia formation, and therefore the signalling pathway linking to ITSN1 would require investigation. Nonetheless, this data along with my earlier findings has unearthed an important role for ITSN1 in N-WASP-dependent signalling networks in general.

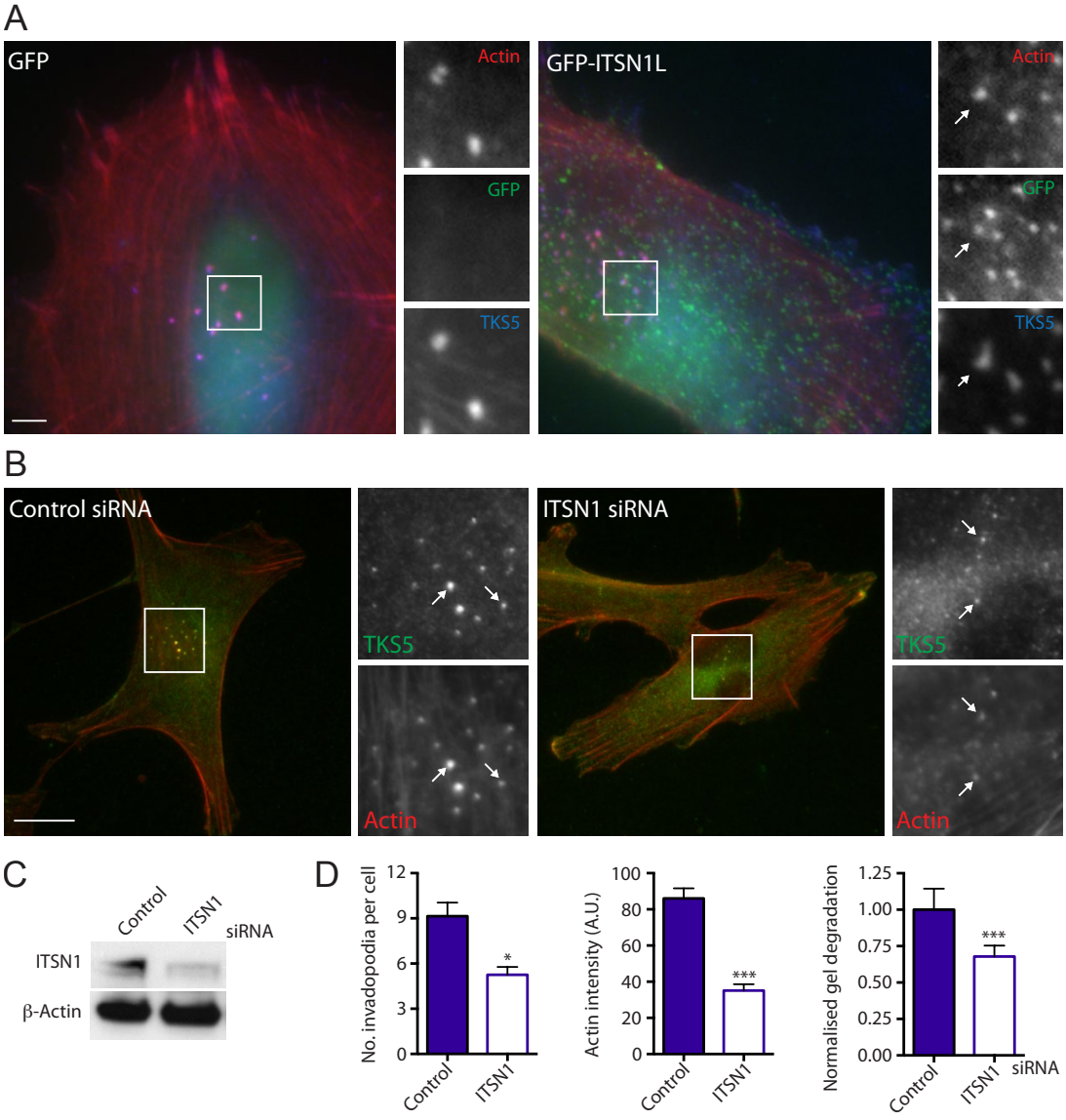

Figure 6.6 ITSN1 regulates invadopodia formation

A Immunofluorescence images of DX3, human melanoma cells, on clear gelatin. Cells are expressing the indicated GFP-tagged constructs and are stained for Tks5 and actin. White arrows highlight recruitment to invadopodia. Scale bar = 5 μm. **B** Immunofluorescence images of DX3 treated with the indicated siRNA, stained for Tks5 and actin. The inserts highlight invadopodia formation in each case (white arrows). Scale bar = 10 μm. **C** Western blot showing the efficiency of ITSN1 depletion, β-actin is used as a loading control. **D** Quantification of the number of and the intensity of actin staining at invadopodia in siRNA treated cells. Error bars represent SEM from 30 cells in total over 3 independent experiments. Also shown is the quantification of normalised number of degradative events produced in fluorescent gelatin. Error bars represent SEM from 21 areas of view from a 96 well plate from 3 independent experiments. A p value of <0.05 and <0.001 is indicated by * and ***, respectively.

6.4 Perspective

My work has furthered our understanding of the complex nature of vaccinia actin-based motility, and components that constitute part of the signalling network. In line with the current literature, N-WASP regulation at vaccinia virus involves the intersection of multiple signalling pathways that function in a highly cooperative manner. Furthermore, the dynamic stability of the signalling complex clearly constitutes a key factor in the regulation of actin-based motility. This observation combined with the conservation in signalling networks, suggests there is undoubtedly more to gain from the continued study of vaccinia and indeed, pathogens in general. Another important theme of my work is the interplay between clathrin and the actin cytoskeleton. In terms of vaccinia infection, clathrin is seemingly used in a multitude of ways. Even though clathrin is not maintained at the actin tail, it clearly promotes its formation, with the endocytic proteins facilitating a transition into actin-based motility. This is not only at the level of organisation, but also in the recruitment of proteins such as ITSN1. What remains to be determined, however, is what truly coordinates the different temporal stages that promote vaccinia virus egress on a whole.

Reference List

Abella, J.V., Vaillancourt, R., Frigault, M.M., Ponzo, M.G., Zuo, D., Sangwan, V., Larose, L., and Park, M. (2010). The Gab1 scaffold regulates RTK-dependent dorsal ruffle formation through the adaptor Nck. Journal of cell science *123*, 1306-1319.

Abercrombie, M., Heaysman, J.E., and Pegrum, S.M. (1970a). The locomotion of fibroblasts in culture. 3. Movements of particles on the dorsal surface of the leading lamella. Experimental cell research *62*, 389-398.

Abercrombie, M., Heaysman, J.E., and Pegrum, S.M. (1970b). The locomotion of fibroblasts in culture. I. Movements of the leading edge. Experimental cell research *59*, 393-398.

Abercrombie, M., Heaysman, J.E., and Pegrum, S.M. (1970c). The locomotion of fibroblasts in culture. II. "RRuffling". Experimental cell research *60*, 437-444.

Abercrombie, M., Heaysman, J.E., and Pegrum, S.M. (1971). The locomotion of fibroblasts in culture. IV. Electron microscopy of the leading lamella. Experimental cell research *67*, 359-367.

Abram, C.L., Seals, D.F., Pass, I., Salinsky, D., Maurer, L., Roth, T.M., and Courtneidge, S.A. (2003). The adaptor protein fish associates with members of the ADAMs family and localizes to podosomes of Src-transformed cells. The Journal of biological chemistry *278*, 16844-16851.

Aderem, A., and Underhill, D.M. (1999). Mechanisms of phagocytosis in macrophages. Annual review of immunology *17*, 593-623.

Aghamohammadzadeh, S., and Ayscough, K.R. (2009). Differential requirements for actin during yeast and mammalian endocytosis. Nat Cell Biol *11*, 1039-1042.

Ahuja, R., Pinyol, R., Reichenbach, N., Custer, L., Klingensmith, J., Kessels, M.M., and Qualmann, B. (2007). Cordon-bleu is an actin nucleation factor and controls neuronal morphology. Cell *131*, 337-350.

Allen, L.A., and Aderem, A. (1996). Molecular definition of distinct cytoskeletal structures involved in complement- and Fc receptor-mediated phagocytosis in macrophages. The Journal of experimental medicine *184*, 627-637.

Andrianantoandro, E., and Pollard, T.D. (2006). Mechanism of actin filament turnover by severing and nucleation at different concentrations of ADF/cofilin. Molecular cell *24*, 13-23.

Anitei, M., and Hoflack, B. (2012). Bridging membrane and cytoskeleton dynamics in the secretory and endocytic pathways. Nat Cell Biol *14*, 11-19.

Anton, I.M., Jones, G.E., Wandosell, F., Geha, R., and Ramesh, N. (2007). WASP-interacting protein (WIP): working in polymerisation and much more. Trends in cell biology *17*, 555-562.

Antonescu, C.N., Aguet, F., Danuser, G., and Schmid, S.L. (2011). Phosphatidylinositol-(4,5)-bisphosphate regulates clathrin-coated pit initiation, stabilization, and size. Mol Biol Cell *22*, 2588-2600.

Artym, V.V., Zhang, Y., Seillier-Moiseiwitsch, F., Yamada, K.M., and Mueller, S.C. (2006). Dynamic interactions of cortactin and membrane type 1 matrix metalloproteinase at invadopodia: defining the stages of invadopodia formation and function. Cancer research *66*, 3034-3043.

Assarsson, E., Greenbaum, J.A., Sundstrom, M., Schaffer, L., Hammond, J.A., Pasquetto, V., Oseroff, C., Hendrickson, R.C., Lefkowitz, E.J., Tscharke, D.C.*, et al.* (2008). Kinetic analysis of a complete poxvirus transcriptome reveals an immediate-early class of genes. Proceedings of the National Academy of Sciences of the United States of America *105*, 2140-2145.

Ayscough, K.R. (2000). Endocytosis and the development of cell polarity in yeast require a dynamic F-actin cytoskeleton. Curr Biol *10*, 1587-1590.

Ayscough, K.R., Stryker, J., Pokala, N., Sanders, M., Crews, P., and Drubin, D.G. (1997). High rates of actin filament turnover in budding yeast and roles for actin in establishment and maintenance of cell polarity revealed using the actin inhibitor latrunculin-A. The Journal of cell biology *137*, 399-416.

Batchelder, E.M., and Yarar, D. (2010). Differential requirements for clathrin-dependent endocytosis at sites of cell-substrate adhesion. Mol Biol Cell *21*, 3070-3079.

Beltzner, C.C., and Pollard, T.D. (2004). Identification of functionally important residues of Arp2/3 complex by analysis of homology models from diverse species. Journal of molecular biology *336*, 551-565.

Benesch, S., Polo, S., Lai, F.P., Anderson, K.I., Stradal, T.E., Wehland, J., and Rottner, K. (2005). N-WASP deficiency impairs EGF internalization and actin assembly at clathrin-coated pits. Journal of cell science *118*, 3103-3115.

Benmerah, A., Begue, B., Dautry-Varsat, A., and Cerf-Bensussan, N. (1996). The ear of alpha-adaptin interacts with the COOH-terminal domain of the Eps 15 protein. The Journal of biological chemistry *271*, 12111-12116.

Benmerah, A., Gagnon, J., Begue, B., Megarbane, B., Dautry-Varsat, A., and Cerf-Bensussan, N. (1995). The tyrosine kinase substrate eps15 is constitutively associated with the plasma membrane adaptor AP-2. The Journal of cell biology *131*, 1831-1838.

Bernardini, M.L., Mounier, J., d'Hauteville, H., Coquis-Rondon, M., and Sansonetti, P.J. (1989). Identification of icsA, a plasmid locus of Shigella flexneri that governs bacterial intra- and intercellular spread through interaction with F-actin. Proceedings of the National Academy of Sciences of the United States of America *86*, 3867-3871.

Bernheim-Groswasser, A., Wiesner, S., Golsteyn, R.M., Carlier, M.F., and Sykes, C. (2002). The dynamics of actin-based motility depend on surface parameters. Nature *417*, 308-311.

Blanchoin, L., and Pollard, T.D. (1998). Interaction of actin monomers with Acanthamoeba actophorin (ADF/cofilin) and profilin. The Journal of biological chemistry *273*, 25106-25111.

Blanchoin, L., and Pollard, T.D. (1999). Mechanism of interaction of Acanthamoeba actophorin (ADF/Cofilin) with actin filaments. The Journal of biological chemistry *274*, 15538-15546.

Blanchoin, L., and Pollard, T.D. (2002). Hydrolysis of ATP by polymerized actin depends on the bound divalent cation but not profilin. Biochemistry *41*, 597-602.

Blasco, R., and Moss, B. (1992). Role of cell-associated enveloped vaccinia virus in cell-to-cell spread. Journal of virology *66*, 4170-4179.

Boettner, D.R., Friesen, H., Andrews, B., and Lemmon, S.K. (2011). Clathrin light chain directs endocytosis by influencing the binding of the yeast Hip1R homologue, Sla2, to F-actin. Mol Biol Cell *22*, 3699-3714.

Bonazzi, M., Vasudevan, L., Mallet, A., Sachse, M., Sartori, A., Prevost, M.C., Roberts, A., Taner, S.B., Wilbur, J.D., Brodsky, F.M.*, et al.* (2011). Clathrin phosphorylation is required for actin recruitment at sites of bacterial adhesion and internalization. The Journal of cell biology *195*, 525-536.

Bonazzi, M., Veiga, E., Pizarro-Cerda, J., and Cossart, P. (2008). Successive post-translational modifications of E-cadherin are required for InlA-mediated internalization of Listeria monocytogenes. Cell Microbiol *10*, 2208-2222.

Bonder, E.M., Fishkind, D.J., and Mooseker, M.S. (1983). Direct measurement of critical concentrations and assembly rate constants at the two ends of an actin filament. Cell *34*, 491-501.

Bonifacino, J.S., and Traub, L.M. (2003). Signals for sorting of transmembrane proteins to endosomes and lysosomes. Annu Rev Biochem *72*, 395-447.

Boucrot, E., Saffarian, S., Zhang, R., and Kirchhausen, T. (2010). Roles of AP-2 in clathrin-mediated endocytosis. PloS one *5*, e10597.

Boukellal, H., Campas, O., Joanny, J.F., Prost, J., and Sykes, C. (2004). Soft Listeria: actin-based propulsion of liquid drops. Physical review E, Statistical, nonlinear, and soft matter physics *69*, 061906.

Boulant, S., Kural, C., Zeeh, J.C., Ubelmann, F., and Kirchhausen, T. (2011). Actin dynamics counteract membrane tension during clathrin-mediated endocytosis. Nat Cell Biol *13*, 1124-1131.

Boulter, E.A., and Appleyard, G. (1973). Differences between extracellular and intracellular forms of poxvirus and their implications. Progress in medical virology Fortschritte der medizinischen Virusforschung Progres en virologie medicale *16*, 86-108.

Brady, R.J., Damer, C.K., Heuser, J.E., and O'Halloran, T.J. (2010). Regulation of Hip1r by epsin controls the temporal and spatial coupling of actin filaments to clathrin-coated pits. Journal of cell science *123*, 3652-3661.

Bravo-Cordero, J.J., Magalhaes, M.A., Eddy, R.J., Hodgson, L., and Condeelis, J. (2013). Functions of cofilin in cell locomotion and invasion. Nat Rev Mol Cell Biol *14*, 405-417.

Brenner, S.L., and Korn, E.D. (1979). Substoichiometric concentrations of cytochalasin D inhibit actin polymerization. Additional evidence for an F-actin treadmill. The Journal of biological chemistry *254*, 9982-9985.

Brett, T.J., Legendre-Guillemin, V., McPherson, P.S., and Fremont, D.H. (2006). Structural definition of the F-actin-binding THATCH domain from HIP1R. Nature structural & molecular biology *13*, 121-130.

Brieher, W.M., Kueh, H.Y., Ballif, B.A., and Mitchison, T.J. (2006). Rapid actin monomer-insensitive depolymerization of Listeria actin comet tails by cofilin, coronin, and Aip1. The Journal of cell biology *175*, 315-324.

Brodsky, F.M. (1988). Living with clathrin: its role in intracellular membrane traffic. Science *242*, 1396-1402.

Brodsky, F.M. (2012). Diversity of clathrin function: new tricks for an old protein. Annu Rev Cell Dev Biol *28*, 309-336.

Brodsky, F.M., Chen, C.Y., Knuehl, C., Towler, M.C., and Wakeham, D.E. (2001). Biological basket weaving: formation and function of clathrin-coated vesicles. Annu Rev Cell Dev Biol *17*, 517-568.

Brown, S.S., and Spudich, J.A. (1979). Cytochalasin inhibits the rate of elongation of actin filament fragments. The Journal of cell biology *83*, 657-662.

Broyles, S.S. (2003). Vaccinia virus transcription. The Journal of general virology *84*, 2293-2303.

Bu, W., Lim, K.B., Yu, Y.H., Chou, A.M., Sudhaharan, T., and Ahmed, S. (2010). Cdc42 interaction with N-WASP and Toca-1 regulates membrane tubulation, vesicle formation and vesicle motility: implications for endocytosis. PloS one *5*, e12153.

Buccione, R., Caldieri, G., and Ayala, I. (2009). Invadopodia: specialized tumor cell structures for the focal degradation of the extracellular matrix. Cancer metastasis reviews *28*, 137-149.

Cai, L., Makhov, A.M., Schafer, D.A., and Bear, J.E. (2008). Coronin 1B antagonizes cortactin and remodels Arp2/3-containing actin branches in lamellipodia. Cell *134*, 828-842.

Cai, L., Marshall, T.W., Uetrecht, A.C., Schafer, D.A., and Bear, J.E. (2007). Coronin 1B coordinates Arp2/3 complex and cofilin activities at the leading edge. Cell *128*, 915-929.

Cameron, L.A., Footer, M.J., van Oudenaarden, A., and Theriot, J.A. (1999). Motility of ActA protein-coated microspheres driven by actin polymerization. Proceedings of the National Academy of Sciences of the United States of America *96*, 4908-4913.

Campellone, K.G., Cheng, H.C., Robbins, D., Siripala, A.D., McGhie, E.J., Hayward, R.D., Welch, M.D., Rosen, M.K., Koronakis, V., and Leong, J.M. (2008a). Repetitive N-WASP-binding elements of the enterohemorrhagic Escherichia coli effector EspF(U) synergistically activate actin assembly. PLoS Pathog *4*, e1000191.

Campellone, K.G., Webb, N.J., Znameroski, E.A., and Welch, M.D. (2008b). WHAMM is an Arp2/3 complex activator that binds microtubules and functions in ER to Golgi transport. Cell *134*, 148-161.

Campellone, K.G., and Welch, M.D. (2010). A nucleator arms race: cellular control of actin assembly. Nat Rev Mol Cell Biol *11*, 237-251.

Cao, H., Orth, J.D., Chen, J., Weller, S.G., Heuser, J.E., and McNiven, M.A. (2003). Cortactin is a component of clathrin-coated pits and participates in receptor-mediated endocytosis. Molecular and cellular biology *23*, 2162-2170.

Carlier, M.F. (1988). Role of nucleotide hydrolysis in the polymerization of actin and tubulin. Cell biophysics *12*, 105-117.

Carlier, M.F., Laurent, V., Santolini, J., Melki, R., Didry, D., Xia, G.X., Hong, Y., Chua, N.H., and Pantaloni, D. (1997). Actin depolymerizing factor (ADF/cofilin) enhances the rate of filament turnover: implication in actin-based motility. The Journal of cell biology *136*, 1307-1322.

Carlier, M.F., Nioche, P., Broutin-L'Hermite, I., Boujemaa, R., Le Clainche, C., Egile, C., Garbay, C., Ducruix, A., Sansonetti, P., and Pantaloni, D. (2000). GRB2 links signaling to actin assembly by enhancing interaction of neural Wiskott-Aldrich syndrome protein (N-WASp) with actin-related protein (ARP2/3) complex. The Journal of biological chemistry *275*, 21946-21952.

Carlier, M.F., and Pantaloni, D. (1986). Direct evidence for ADP-Pi-F-actin as the major intermediate in ATP-actin polymerization. Rate of dissociation of Pi from actin filaments. Biochemistry *25*, 7789-7792.

Carlier, M.F., and Pantaloni, D. (1997). Control of actin dynamics in cell motility. Journal of molecular biology *269*, 459-467.

Carlier, M.F., Pernier, J., and Avvaru, B.S. (2013). Control of actin filament dynamics at barbed ends by WH2 domains: From capping to permissive and processive assembly. Cytoskeleton.

Carlsson, L., Nystrom, L.E., Lindberg, U., Kannan, K.K., Cid-Dresdner, H., and Lovgren, S. (1976). Crystallization of a non-muscle actin. Journal of molecular biology *105*, 353-366.

Carlsson, L., Nystrom, L.E., Sundkvist, I., Markey, F., and Lindberg, U. (1977). Actin polymerizability is influenced by profilin, a low molecular weight protein in non-muscle cells. Journal of molecular biology *115*, 465-483.

Carlton, J.G., and Cullen, P.J. (2005). Coincidence detection in phosphoinositide signaling. Trends in cell biology *15*, 540-547.

Caron, E., and Hall, A. (1998). Identification of two distinct mechanisms of phagocytosis controlled by different Rho GTPases. Science *282*, 1717-1721.

Carter, G.C., Rodger, G., Murphy, B.J., Law, M., Krauss, O., Hollinshead, M., and Smith, G.L. (2003). Vaccinia virus cores are transported on microtubules. The Journal of general virology *84*, 2443-2458.

Castellano, F., Montcourrier, P., and Chavrier, P. (2000). Membrane recruitment of Rac1 triggers phagocytosis. Journal of cell science *113 (Pt 17)*, 2955-2961.

Chakrabarti, S., Sisler, J.R., and Moss, B. (1997). Compact, synthetic, vaccinia virus early/late promoter for protein expression. BioTechniques *23*, 1094-1097.

Chan, W.M., and Ward, B.M. (2012). The A33-dependent incorporation of B5 into extracellular enveloped vaccinia virions is mediated through an interaction between their lumenal domains. Journal of virology *86*, 8210-8220.

Chen, C.Y., and Brodsky, F.M. (2005). Huntingtin-interacting protein 1 (Hip1) and Hip1-related protein (Hip1R) bind the conserved sequence of clathrin light chains and thereby influence clathrin assembly in vitro and actin distribution in vivo. The Journal of biological chemistry *280*, 6109-6117.

Chen, H., Fre, S., Slepnev, V.I., Capua, M.R., Takei, K., Butler, M.H., Di Fiore, P.P., and De Camilli, P. (1998). Epsin is an EH-domain-binding protein implicated in clathrin-mediated endocytosis. Nature *394*, 793-797.

Chen, W.T. (1989). Proteolytic activity of specialized surface protrusions formed at rosette contact sites of transformed cells. The Journal of experimental zoology *251*, 167-185.

Chereau, D., Boczkowska, M., Skwarek-Maruszewska, A., Fujiwara, I., Hayes, D.B., Rebowski, G., Lappalainen, P., Pollard, T.D., and Dominguez, R. (2008). Leiomodin is an actin filament nucleator in muscle cells. Science *320*, 239-243.

Chereau, D., Kerff, F., Graceffa, P., Grabarek, Z., Langsetmo, K., and Dominguez, R. (2005). Actin-bound structures of Wiskott-Aldrich syndrome protein (WASP)-homology domain 2 and the implications for filament assembly. Proceedings of the National Academy of Sciences of the United States of America *102*, 16644-16649.

Chetrit, D., Ziv, N., and Ehrlich, M. (2009). Dab2 regulates clathrin assembly and cell spreading. The Biochemical journal *418*, 701-715.

Chhabra, E.S., and Higgs, H.N. (2007). The many faces of actin: matching assembly factors with cellular structures. Nat Cell Biol *9*, 1110-1121.

Chimini, G., and Chavrier, P. (2000). Function of Rho family proteins in actin dynamics during phagocytosis and engulfment. Nat Cell Biol *2*, E191-196.

Clark, E.S., and Weaver, A.M. (2008). A new role for cortactin in invadopodia: regulation of protease secretion. European journal of cell biology *87*, 581-590.

Clark, E.S., Whigham, A.S., Yarbrough, W.G., and Weaver, A.M. (2007). Cortactin is an essential regulator of matrix metalloproteinase secretion and extracellular matrix degradation in invadopodia. Cancer research *67*, 4227-4235.

Co, C., Wong, D.T., Gierke, S., Chang, V., and Taunton, J. (2007). Mechanism of actin network attachment to moving membranes: barbed end capture by N-WASP WH2 domains. Cell *128*, 901-913.

Cocucci, E., Aguet, F., Boulant, S., and Kirchhausen, T. (2012). The first five seconds in the life of a clathrin-coated pit. Cell *150*, 495-507.

Collins, A., Warrington, A., Taylor, K.A., and Svitkina, T. (2011). Structural organization of the actin cytoskeleton at sites of clathrin-mediated endocytosis. Curr Biol *21*, 1167-1175.

Collins, B.M., McCoy, A.J., Kent, H.M., Evans, P.R., and Owen, D.J. (2002). Molecular architecture and functional model of the endocytic AP2 complex. Cell *109*, 523-535.

Conley, C.A., Fritz-Six, K.L., Almenar-Queralt, A., and Fowler, V.M. (2001). Leiomodins: larger members of the tropomodulin (Tmod) gene family. Genomics *73*, 127-139.

Cooper, J.A., and Sept, D. (2008). New insights into mechanism and regulation of actin capping protein. International review of cell and molecular biology *267*, 183-206.

Cory, G.O., Cramer, R., Blanchoin, L., and Ridley, A.J. (2003). Phosphorylation of the WASP-VCA domain increases its affinity for the Arp2/3 complex and enhances actin polymerization by WASP. Molecular cell *11*, 1229-1239.

Cory, G.O., Garg, R., Cramer, R., and Ridley, A.J. (2002). Phosphorylation of tyrosine 291 enhances the ability of WASp to stimulate actin polymerization and filopodium formation. Wiskott-Aldrich Syndrome protein. The Journal of biological chemistry *277*, 45115-45121.

Cossart, P., and Sansonetti, P.J. (2004). Bacterial invasion: the paradigms of enteroinvasive pathogens. Science *304*, 242-248.

Cossart, P., and Veiga, E. (2008). Non-classical use of clathrin during bacterial infections. J Microsc *231*, 524-528.

Courtemanche, N., and Pollard, T.D. (2012). Determinants of Formin Homology 1 (FH1) domain function in actin filament elongation by formins. The Journal of biological chemistry *287*, 7812-7820.

Cox, D., Chang, P., Zhang, Q., Reddy, P.G., Bokoch, G.M., and Greenberg, S. (1997). Requirements for both Rac1 and Cdc42 in membrane ruffling and phagocytosis in leukocytes. The Journal of experimental medicine *186*, 1487-1494.

Cudmore, S., Cossart, P., Griffiths, G., and Way, M. (1995). Actin-based motility of vaccinia virus. Nature *378*, 636-638.

Cupers, P., ter Haar, E., Boll, W., and Kirchhausen, T. (1997). Parallel dimers and anti-parallel tetramers formed by epidermal growth factor receptor pathway substrate clone 15. The Journal of biological chemistry *272*, 33430-33434.

Cureton, D.K., Massol, R.H., Saffarian, S., Kirchhausen, T.L., and Whelan, S.P. (2009). Vesicular stomatitis virus enters cells through vesicles incompletely coated with clathrin that depend upon actin for internalization. PLoS Pathog *5*, e1000394.

Cureton, D.K., Massol, R.H., Whelan, S.P., and Kirchhausen, T. (2010). The length of vesicular stomatitis virus particles dictates a need for actin assembly during clathrin-dependent endocytosis. PLoS Pathog *6*, e1001127.

Da Costa, S.R., Sou, E., Xie, J., Yarber, F.A., Okamoto, C.T., Pidgeon, M., Kessels, M.M., Mircheff, A.K., Schechter, J.E., Qualmann, B*., et al.* (2003). Impairing actin filament or syndapin functions promotes accumulation of clathrin-coated vesicles at the apical plasma membrane of acinar epithelial cells. Mol Biol Cell *14*, 4397-4413.

Dart, A.E., Donnelly, S.K., Holden, D.W., Way, M., and Caron, E. (2012). Nck and Cdc42 co-operate to recruit N-WASP to promote FcgammaR-mediated phagocytosis. Journal of cell science *125*, 2825-2830.

Dawson, J.C., Legg, J.A., and Machesky, L.M. (2006). Bar domain proteins: a role in tubulation, scission and actin assembly in clathrin-mediated endocytosis. Trends in cell biology *16*, 493-498.

Dayel, M.J., Holleran, E.A., and Mullins, R.D. (2001). Arp2/3 complex requires hydrolyzable ATP for nucleation of new actin filaments. Proceedings of the National Academy of Sciences of the United States of America *98*, 14871-14876.

Delatour, V., Helfer, E., Didry, D., Le, K.H., Gaucher, J.F., Carlier, M.F., and Romet-Lemonne, G. (2008). Arp2/3 controls the motile behavior of N-WASP-functionalized GUVs and modulates N-WASP surface distribution by mediating transient links with actin filaments. Biophys J *94*, 4890-4905.

Dell'Angelica, E.C., Klumperman, J., Stoorvogel, W., and Bonifacino, J.S. (1998). Association of the AP-3 adaptor complex with clathrin. Science *280*, 431-434.

Derivery, E., Sousa, C., Gautier, J.J., Lombard, B., Loew, D., and Gautreau, A. (2009). The Arp2/3 activator WASH controls the fission of endosomes through a large multiprotein complex. Developmental cell *17*, 712-723.

Derry, J.M., Ochs, H.D., and Francke, U. (1994). Isolation of a novel gene mutated in Wiskott-Aldrich syndrome. Cell *78*, 635-644.

Desai, B., Ma, T., and Chellaiah, M.A. (2008). Invadopodia and matrix degradation, a new property of prostate cancer cells during migration and invasion. The Journal of biological chemistry *283*, 13856-13866.

Diekmann, D., Brill, S., Garrett, M.D., Totty, N., Hsuan, J., Monfries, C., Hall, C., Lim, L., and Hall, A. (1991). Bcr encodes a GTPase-activating protein for p21rac. Nature *351*, 400-402.

Ditlev, J.A., Michalski, P.J., Huber, G., Rivera, G.M., Mohler, W.A., Loew, L.M., and Mayer, B.J. (2012). Stoichiometry of Nck-dependent actin polymerization in living cells. The Journal of cell biology *197*, 643-658.

Doceul, V., Hollinshead, M., van der Linden, L., and Smith, G.L. (2010). Repulsion of superinfecting virions: a mechanism for rapid virus spread. Science *327*, 873-876.

Dodding, M.P., Mitter, R., Humphries, A.C., and Way, M. (2011). A kinesin-1 binding motif in vaccinia virus that is widespread throughout the human genome. The EMBO journal *30*, 4523-4538.

Dodding, M.P., Newsome, T.P., Collinson, L.M., Edwards, C., and Way, M. (2009). An E2-F12 complex is required for intracellular enveloped virus morphogenesis during vaccinia infection. Cell Microbiol *11*, 808-824.

Domi, A., Weisberg, A.S., and Moss, B. (2008). Vaccinia virus E2L null mutants exhibit a major reduction in extracellular virion formation and virus spread. Journal of virology *82*, 4215-4226.

Dominguez, R., and Holmes, K.C. (2011). Actin structure and function. Annual review of biophysics *40*, 169-186.

Donnelly, S.K., Weisswange, I., Zettl, M., and Way, M. (2013). WIP Provides an Essential Link between Nck and N-WASP during Arp2/3-Dependent Actin Polymerization. Curr Biol *23*, 999-1006.

Doray, B., Lee, I., Knisely, J., Bu, G., and Kornfeld, S. (2007). The gamma/sigma1 and alpha/sigma2 hemicomplexes of clathrin adaptors AP-1 and AP-2 harbor the dileucine recognition site. Mol Biol Cell *18*, 1887-1896.

Dovas, A., Gevrey, J.C., Grossi, A., Park, H., Abou-Kheir, W., and Cox, D. (2009). Regulation of podosome dynamics by WASp phosphorylation: implication in matrix degradation and chemotaxis in macrophages. Journal of cell science *122*, 3873-3882.

Ducka, A.M., Joel, P., Popowicz, G.M., Trybus, K.M., Schleicher, M., Noegel, A.A., Huber, R., Holak, T.A., and Sitar, T. (2010). Structures of actin-bound Wiskott-Aldrich syndrome protein homology 2 (WH2) domains of Spire and the implication for filament nucleation. Proceedings of the National Academy of Sciences of the United States of America *107*, 11757-11762.

Duleh, S.N., and Welch, M.D. (2010). WASH and the Arp2/3 complex regulate endosome shape and trafficking. Cytoskeleton *67*, 193-206.

Duncan, S.A., and Smith, G.L. (1992). Identification and characterization of an extracellular envelope glycoprotein affecting vaccinia virus egress. Journal of virology *66*, 1610-1621.

Earley, A.K., Chan, W.M., and Ward, B.M. (2008). The vaccinia virus B5 protein requires A34 for efficient intracellular trafficking from the endoplasmic reticulum to the site of wrapping and incorporation into progeny virions. Journal of virology *82*, 2161-2169.

Eden, S., Rohatgi, R., Podtelejnikov, A.V., Mann, M., and Kirschner, M.W. (2002). Mechanism of regulation of WAVE1-induced actin nucleation by Rac1 and Nck. Nature *418*, 790-793.

Egile, C., Loisel, T.P., Laurent, V., Li, R., Pantaloni, D., Sansonetti, P.J., and Carlier, M.F. (1999). Activation of the CDC42 effector N-WASP by the Shigella flexneri IcsA protein promotes actin nucleation by Arp2/3 complex and bacterial actin-based motility. The Journal of cell biology *146*, 1319-1332.

Egile, C., Rouiller, I., Xu, X.P., Volkmann, N., Li, R., and Hanein, D. (2005). Mechanism of filament nucleation and branch stability revealed by the structure of the Arp2/3 complex at actin branch junctions. PLoS Biol *3*, e383.

Engelstad, M., Howard, S.T., and Smith, G.L. (1992). A constitutively expressed vaccinia gene encodes a 42-kDa glycoprotein related to complement control factors that forms part of the extracellular virus envelope. Virology *188*, 801-810.

Engelstad, M., and Smith, G.L. (1993). The vaccinia virus 42-kDa envelope protein is required for the envelopment and egress of extracellular virus and for virus virulence. Virology *194*, 627-637.

Engqvist-Goldstein, A.E., Kessels, M.M., Chopra, V.S., Hayden, M.R., and Drubin, D.G. (1999). An actin-binding protein of the Sla2/Huntingtin interacting protein 1 family is a novel component of clathrin-coated pits and vesicles. The Journal of cell biology *147*, 1503-1518.

Engqvist-Goldstein, A.E., Warren, R.A., Kessels, M.M., Keen, J.H., Heuser, J., and Drubin, D.G. (2001). The actin-binding protein Hip1R associates with clathrin during early stages of endocytosis and promotes clathrin assembly in vitro. The Journal of cell biology *154*, 1209-1223.

Erickson, H.P. (2007). Evolution of the cytoskeleton. BioEssays : news and reviews in molecular, cellular and developmental biology *29*, 668-677.

Ferguson, S.M., Raimondi, A., Paradise, S., Shen, H., Mesaki, K., Ferguson, A., Destaing, O., Ko, G., Takasaki, J., Cremona, O.*, et al.* (2009). Coordinated actions of actin and BAR proteins upstream of dynamin at endocytic clathrin-coated pits. Developmental cell *17*, 811-822.

Fingerhut, A., von Figura, K., and Honing, S. (2001). Binding of AP2 to sorting signals is modulated by AP2 phosphorylation. The Journal of biological chemistry *276*, 5476-5482.

Firat-Karalar, E.N., Hsiue, P.P., and Welch, M.D. (2011). The actin nucleation factor JMY is a negative regulator of neuritogenesis. Mol Biol Cell *22*, 4563-4574.

Firat-Karalar, E.N., and Welch, M.D. (2011). New mechanisms and functions of actin nucleation. Curr Opin Cell Biol *23*, 4-13.

Ford, M.G., Mills, I.G., Peter, B.J., Vallis, Y., Praefcke, G.J., Evans, P.R., and McMahon, H.T. (2002). Curvature of clathrin-coated pits driven by epsin. Nature *419*, 361-366.

Ford, M.G., Pearse, B.M., Higgins, M.K., Vallis, Y., Owen, D.J., Gibson, A., Hopkins, C.R., Evans, P.R., and McMahon, H.T. (2001). Simultaneous binding of PtdIns(4,5)P2 and clathrin by AP180 in the nucleation of clathrin lattices on membranes. Science *291*, 1051-1055.

Frischknecht, F., Cudmore, S., Moreau, V., Reckmann, I., Rottger, S., and Way, M. (1999a). Tyrosine phosphorylation is required for actin-based motility of vaccinia but not Listeria or Shigella. Curr Biol *9*, 89-92.

Frischknecht, F., Moreau, V., Rottger, S., Gonfloni, S., Reckmann, I., Superti-Furga, G., and Way, M. (1999b). Actin-based motility of vaccinia virus mimics receptor tyrosine kinase signalling. Nature *401*, 926-929.

Frischknecht, F., and Way, M. (2001). Surfing pathogens and the lessons learned for actin polymerization. Trends in cell biology *11*, 30-38.

Fujiwara, I., Takahashi, S., Tadakuma, H., Funatsu, T., and Ishiwata, S. (2002). Microscopic analysis of polymerization dynamics with individual actin filaments. Nat Cell Biol *4*, 666-673.

Fukumatsu, M., Ogawa, M., Arakawa, S., Suzuki, M., Nakayama, K., Shimizu, S., Kim, M., Mimuro, H., and Sasakawa, C. (2012). Shigella targets epithelial tricellular junctions and uses a noncanonical clathrin-dependent endocytic pathway to spread between cells. Cell host & microbe *11*, 325-336.

Galkin, V.E., Orlova, A., Kudryashov, D.S., Solodukhin, A., Reisler, E., Schroder, G.F., and Egelman, E.H. (2011). Remodeling of actin filaments by ADF/cofilin proteins. Proceedings of the National Academy of Sciences of the United States of America *108*, 20568-20572.

Gallagher, H., Oleinikov, A.V., Fenske, C., and Newman, D.J. (2004). The adaptor disabled-2 binds to the third psi xNPxY sequence on the cytoplasmic tail of megalin. Biochimie *86*, 179-182.

Gallop, J.L., Jao, C.C., Kent, H.M., Butler, P.J., Evans, P.R., Langen, R., and McMahon, H.T. (2006). Mechanism of endophilin N-BAR domain-mediated membrane curvature. The EMBO journal *25*, 2898-2910.

Gallusser, A., and Kirchhausen, T. (1993). The beta 1 and beta 2 subunits of the AP complexes are the clathrin coat assembly components. The EMBO journal *12*, 5237-5244.

Gandhi, M., Achard, V., Blanchoin, L., and Goode, B.L. (2009). Coronin switches roles in actin disassembly depending on the nucleotide state of actin. Molecular cell *34*, 364-374.

Gasman, S., Chasserot-Golaz, S., Malacombe, M., Way, M., and Bader, M.F. (2004). Regulated exocytosis in neuroendocrine cells: a role for subplasmalemmal Cdc42/N-WASP-induced actin filaments. Mol Biol Cell *15*, 520-531.

Gautreau, A., Ho, H.Y., Li, J., Steen, H., Gygi, S.P., and Kirschner, M.W. (2004). Purification and architecture of the ubiquitous Wave complex. Proceedings of the National Academy of Sciences of the United States of America *101*, 4379-4383.

Geada, M.M., Galindo, I., Lorenzo, M.M., Perdiguero, B., and Blasco, R. (2001). Movements of vaccinia virus intracellular enveloped virions with GFP tagged to the F13L envelope protein. The Journal of general virology *82*, 2747-2760.

Gilbert, H.R., and Frieden, C. (1983). Preparation, purification and properties of a crosslinked trimer of G-actin. Biochemical and biophysical research communications *111*, 404-408.

Gimona, M., Buccione, R., Courtneidge, S.A., and Linder, S. (2008). Assembly and biological role of podosomes and invadopodia. Curr Opin Cell Biol *20*, 235-241.

Goebel, S.J., Johnson, G.P., Perkus, M.E., Davis, S.W., Winslow, J.P., and Paoletti, E. (1990). The complete DNA sequence of vaccinia virus. Virology *179*, 247-266, 517-263.

Goldberg, M.B., and Theriot, J.A. (1995). Shigella flexneri surface protein IcsA is sufficient to direct actin-based motility. Proceedings of the National Academy of Sciences of the United States of America *92*, 6572-6576.

Goley, E.D., Rodenbusch, S.E., Martin, A.C., and Welch, M.D. (2004). Critical conformational changes in the Arp2/3 complex are induced by nucleotide and nucleation promoting factor. Molecular cell *16*, 269-279.

Goley, E.D., and Welch, M.D. (2006). The ARP2/3 complex: an actin nucleator comes of age. Nat Rev Mol Cell Biol *7*, 713-726.

Gomez, C.E., Najera, J.L., Krupa, M., Perdiguero, B., and Esteban, M. (2011). MVA and NYVAC as vaccines against emergent infectious diseases and cancer. Current gene therapy *11*, 189-217.

Gomez, T.S., and Billadeau, D.D. (2009). A FAM21-containing WASH complex regulates retromer-dependent sorting. Developmental cell *17*, 699-711.

Goodman, O.B., Jr., Krupnick, J.G., Santini, F., Gurevich, V.V., Penn, R.B., Gagnon, A.W., Keen, J.H., and Benovic, J.L. (1996). Beta-arrestin acts as a clathrin adaptor in endocytosis of the beta2-adrenergic receptor. Nature *383*, 447-450.

Gottlieb, T.A., Ivanov, I.E., Adesnik, M., and Sabatini, D.D. (1993). Actin microfilaments play a critical role in endocytosis at the apical but not the basolateral surface of polarized epithelial cells. The Journal of cell biology *120*, 695-710.

Gouin, E., Egile, C., Dehoux, P., Villiers, V., Adams, J., Gertler, F., Li, R., and Cossart, P. (2004). The RickA protein of Rickettsia conorii activates the Arp2/3 complex. Nature *427*, 457-461.

Greenberg, S., Chang, P., and Silverstein, S.C. (1993). Tyrosine phosphorylation is required for Fc receptor-mediated phagocytosis in mouse macrophages. The Journal of experimental medicine *177*, 529-534.

Greenberg, S., Chang, P., and Silverstein, S.C. (1994). Tyrosine phosphorylation of the gamma subunit of Fc gamma receptors, p72syk, and paxillin during Fc receptor-mediated phagocytosis in macrophages. The Journal of biological chemistry *269*, 3897-3902.

Greene, B., Liu, S.H., Wilde, A., and Brodsky, F.M. (2000). Complete reconstitution of clathrin basket formation with recombinant protein fragments: adaptor control of clathrin self-assembly. Traffic *1*, 69-75.

Grosenbach, D.W., Ulaeto, D.O., and Hruby, D.E. (1997). Palmitylation of the vaccinia virus 37-kDa major envelope antigen. Identification of a conserved acceptor motif and biological relevance. The Journal of biological chemistry *272*, 1956-1964.

Groves, E., Dart, A.E., Covarelli, V., and Caron, E. (2008). Molecular mechanisms of phagocytic uptake in mammalian cells. Cellular and molecular life sciences : CMLS *65*, 1957-1976.

Gruenberg, J. (2009). Viruses and endosome membrane dynamics. Curr Opin Cell Biol *21*, 582-588.

Gruenheid, S., DeVinney, R., Bladt, F., Goosney, D., Gelkop, S., Gish, G.D., Pawson, T., and Finlay, B.B. (2001). Enteropathogenic E. coli Tir binds Nck to initiate actin pedestal formation in host cells. Nat Cell Biol *3*, 856-859.

Guttman, J.A., Lin, A.E., Veiga, E., Cossart, P., and Finlay, B.B. (2010). Role for CD2AP and other endocytosis-associated proteins in enteropathogenic Escherichia coli pedestal formation. Infection and immunity *78*, 3316-3322.

Haglund, C.M., Choe, J.E., Skau, C.T., Kovar, D.R., and Welch, M.D. (2010). Rickettsia Sca2 is a bacterial formin-like mediator of actin-based motility. Nat Cell Biol *12*, 1057-1063.

Haglund, C.M., and Welch, M.D. (2011). Pathogens and polymers: microbe-host interactions illuminate the cytoskeleton. The Journal of cell biology *195*, 7-17.

Hall, A. (2012). Rho family GTPases. Biochemical Society transactions *40*, 1378-1382.

Hanson, J., and Lowy, J. (1964). The Structure of Actin Filaments and the Origin of the Axial Periodicity in the I-Substance of Vertebrate Striated Muscle. Proceedings of the Royal Society of London Series B, Containing papers of a Biological character Royal Society *160*, 449-460.

Hart, M.J., Eva, A., Evans, T., Aaronson, S.A., and Cerione, R.A. (1991). Catalysis of guanine nucleotide exchange on the CDC42Hs protein by the dbl oncogene product. Nature *354*, 311-314.

Haucke, V. (2005). Phosphoinositide regulation of clathrin-mediated endocytosis. Biochemical Society transactions *33*, 1285-1289.

Heinzen, R.A., Hayes, S.F., Peacock, M.G., and Hackstadt, T. (1993). Directional actin polymerization associated with spotted fever group Rickettsia infection of Vero cells. Infection and immunity *61*, 1926-1935.

Henne, W.M., Boucrot, E., Meinecke, M., Evergren, E., Vallis, Y., Mittal, R., and McMahon, H.T. (2010). FCHo proteins are nucleators of clathrin-mediated endocytosis. Science *328*, 1281-1284.

Heuser, J. (2005). Deep-etch EM reveals that the early poxvirus envelope is a single membrane bilayer stabilized by a geodetic "honeycomb" surface coat. The Journal of cell biology *169*, 269-283.

Higgs, H.N., and Pollard, T.D. (2000). Activation by Cdc42 and PIP(2) of Wiskott-Aldrich syndrome protein (WASp) stimulates actin nucleation by Arp2/3 complex. The Journal of cell biology *150*, 1311-1320.

Hiller, G., and Weber, K. (1985). Golgi-derived membranes that contain an acylated viral polypeptide are used for vaccinia virus envelopment. Journal of virology *55*, 651-659.

Hinrichsen, L., Harborth, J., Andrees, L., Weber, K., and Ungewickell, E.J. (2003). Effect of clathrin heavy chain- and alpha-adaptin-specific small inhibitory RNAs on endocytic accessory proteins and receptor trafficking in HeLa cells. The Journal of biological chemistry *278*, 45160-45170.

Hinshaw, J.E. (2000). Dynamin and its role in membrane fission. Annu Rev Cell Dev Biol *16*, 483-519.

Ho, H.Y., Rohatgi, R., Lebensohn, A.M., and Kirschner, M.W. (2006). In vitro reconstitution of cdc42-mediated actin assembly using purified components. Methods in enzymology *406*, 174-190.

Ho, H.Y., Rohatgi, R., Lebensohn, A.M., Le, M., Li, J., Gygi, S.P., and Kirschner, M.W. (2004). Toca-1 mediates Cdc42-dependent actin nucleation by activating the N-WASP-WIP complex. Cell *118*, 203-216.

Ho, H.Y., Rohatgi, R., Ma, L., and Kirschner, M.W. (2001). CR16 forms a complex with N-WASP in brain and is a novel member of a conserved proline-rich actin-binding protein family. Proceedings of the National Academy of Sciences of the United States of America *98*, 11306-11311.

Hollinshead, M., Rodger, G., Van Eijl, H., Law, M., Hollinshead, R., Vaux, D.J., and Smith, G.L. (2001). Vaccinia virus utilizes microtubules for movement to the cell surface. The Journal of cell biology *154*, 389-402.

Hollinshead, M., Vanderplasschen, A., Smith, G.L., and Vaux, D.J. (1999). Vaccinia virus intracellular mature virions contain only one lipid membrane. Journal of virology *73*, 1503-1517.

Hoppe, A.D., and Swanson, J.A. (2004). Cdc42, Rac1, and Rac2 display distinct patterns of activation during phagocytosis. Mol Biol Cell *15*, 3509-3519.

Horsington, J., Lynn, H., Turnbull, L., Cheng, D., Braet, F., Diefenbach, R.J., Whitchurch, C.B., Karupiah, G., and Newsome, T.P. (2013). A36-dependent Actin Filament Nucleation Promotes Release of Vaccinia Virus. PLoS Pathog *9*, e1003239.

Humphries, A.C., Dodding, M.P., Barry, D.J., Collinson, L.M., Durkin, C.H., and Way, M. (2012). Clathrin potentiates vaccinia-induced actin polymerization to facilitate viral spread. Cell host & microbe *12*, 346-359.

Humphries, A.C., and Way, M. (2013). The non-canonical roles of clathrin and actin in pathogen internalization, egress and spread. Nature reviews Microbiology *11*, 551-560.

Humphries, C.L., Balcer, H.I., D'Agostino, J.L., Winsor, B., Drubin, D.G., Barnes, G., Andrews, B.J., and Goode, B.L. (2002). Direct regulation of Arp2/3 complex activity and function by the actin binding protein coronin. The Journal of cell biology *159*, 993-1004.

Hunter, M.P., Russo, A., and O'Bryan, J.P. (2013). Emerging Roles for Intersectin (ITSN) in Regulating Signaling and Disease Pathways. International journal of molecular sciences *14*, 7829-7852.

Husain, M., and Moss, B. (2002). Similarities in the induction of post-Golgi vesicles by the vaccinia virus F13L protein and phospholipase D. Journal of virology *76*, 7777-7789.

Husain, M., and Moss, B. (2003). Intracellular trafficking of a palmitoylated membrane-associated protein component of enveloped vaccinia virus. Journal of virology *77*, 9008-9019.

Husain, M., and Moss, B. (2005). Role of receptor-mediated endocytosis in the formation of vaccinia virus extracellular enveloped particles. Journal of virology *79*, 4080-4089.

Hussain, N.K., Jenna, S., Glogauer, M., Quinn, C.C., Wasiak, S., Guipponi, M., Antonarakis, S.E., Kay, B.K., Stossel, T.P., Lamarche-Vane, N*., et al.* (2001). Endocytic protein intersectin-l regulates actin assembly via Cdc42 and N-WASP. Nat Cell Biol *3*, 927-932.

Hussain, N.K., Yamabhai, M., Ramjaun, A.R., Guy, A.M., Baranes, D., O'Bryan, J.P., Der, C.J., Kay, B.K., and McPherson, P.S. (1999). Splice variants of intersectin are components of the endocytic machinery in neurons and nonneuronal cells. The Journal of biological chemistry *274*, 15671-15677.

Husson, C., Renault, L., Didry, D., Pantaloni, D., and Carlier, M.F. (2011). Cordon-Bleu uses WH2 domains as multifunctional dynamizers of actin filament assembly. Molecular cell *43*, 464-477.

Hyun, T.S., Rao, D.S., Saint-Dic, D., Michael, L.E., Kumar, P.D., Bradley, S.V., Mizukami, I.F., Oravecz-Wilson, K.I., and Ross, T.S. (2004). HIP1 and HIP1r stabilize receptor tyrosine kinases and bind 3-phosphoinositides via epsin N-terminal homology domains. The Journal of biological chemistry *279*, 14294-14306.

Ichihashi, Y., and Dales, S. (1971). Biogenesis of poxviruses: interrelationship between hemagglutinin production and polykaryocytosis. Virology *46*, 533-543.

Innocenti, M., Gerboth, S., Rottner, K., Lai, F.P., Hertzog, M., Stradal, T.E., Frittoli, E., Didry, D., Polo, S., Disanza, A*., et al.* (2005). Abi1 regulates the activity of N-WASP and WAVE in distinct actin-based processes. Nat Cell Biol *7*, 969-976.

Innocenti, M., Zucconi, A., Disanza, A., Frittoli, E., Areces, L.B., Steffen, A., Stradal, T.E., Di Fiore, P.P., Carlier, M.F., and Scita, G. (2004). Abi1 is essential for the formation and activation of a WAVE2 signalling complex. Nat Cell Biol *6*, 319-327.

Isaacs, S.N., Wolffe, E.J., Payne, L.G., and Moss, B. (1992). Characterization of a vaccinia virus-encoded 42-kilodalton class I membrane glycoprotein component of the extracellular virus envelope. Journal of virology *66*, 7217-7224.

Isenberg, G., Aebi, U., and Pollard, T.D. (1980). An actin-binding protein from Acanthamoeba regulates actin filament polymerization and interactions. Nature *288*, 455-459.

Ismail, A.M., Padrick, S.B., Chen, B., Umetani, J., and Rosen, M.K. (2009). The WAVE regulatory complex is inhibited. Nature structural & molecular biology *16*, 561-563.

Itoh, T., Erdmann, K.S., Roux, A., Habermann, B., Werner, H., and De Camilli, P. (2005). Dynamin and the actin cytoskeleton cooperatively regulate plasma membrane invagination by BAR and F-BAR proteins. Developmental cell *9*, 791-804.

Itoh, T., Koshiba, S., Kigawa, T., Kikuchi, A., Yokoyama, S., and Takenawa, T. (2001). Role of the ENTH domain in phosphatidylinositol-4,5-bisphosphate binding and endocytosis. Science *291*, 1047-1051.

Jackson, L.P., Kelly, B.T., McCoy, A.J., Gaffry, T., James, L.C., Collins, B.M., Honing, S., Evans, P.R., and Owen, D.J. (2010). A large-scale conformational change couples membrane recruitment to cargo binding in the AP2 clathrin adaptor complex. Cell *141*, 1220-1229.

Janmey, P.A., Hvidt, S., Oster, G.F., Lamb, J., Stossel, T.P., and Hartwig, J.H. (1990). Effect of ATP on actin filament stiffness. Nature *347*, 95-99.

Jaumouille, V., and Grinstein, S. (2011). Receptor mobility, the cytoskeleton, and particle binding during phagocytosis. Curr Opin Cell Biol *23*, 22-29.

Jeng, R.L., Goley, E.D., D'Alessio, J.A., Chaga, O.Y., Svitkina, T.M., Borisy, G.G., Heinzen, R.A., and Welch, M.D. (2004). A Rickettsia WASP-like protein activates the Arp2/3 complex and mediates actin-based motility. Cell Microbiol *6*, 761-769.

Johnston, S.C., and Ward, B.M. (2009). Vaccinia virus protein F12 associates with intracellular enveloped virions through an interaction with A36. Journal of virology *83*, 1708-1717.

Kaksonen, M., Toret, C.P., and Drubin, D.G. (2006). Harnessing actin dynamics for clathrin-mediated endocytosis. Nat Rev Mol Cell Biol *7*, 404-414.

Kandachar, V., and Roegiers, F. (2012). Endocytosis and control of Notch signaling. Curr Opin Cell Biol *24*, 534-540.

Kelleher, J.F., Atkinson, S.J., and Pollard, T.D. (1995). Sequences, structural models, and cellular localization of the actin-related proteins Arp2 and Arp3 from Acanthamoeba. The Journal of cell biology *131*, 385-397.

Kelly, B.T., McCoy, A.J., Spate, K., Miller, S.E., Evans, P.R., Honing, S., and Owen, D.J. (2008). A structural explanation for the binding of endocytic dileucine motifs by the AP2 complex. Nature *456*, 976-979.

Kessels, M.M., Dong, J., Leibig, W., Westermann, P., and Qualmann, B. (2006). Complexes of syndapin II with dynamin II promote vesicle formation at the trans-Golgi network. Journal of cell science *119*, 1504-1516.

Kessels, M.M., and Qualmann, B. (2002). Syndapins integrate N-WASP in receptor-mediated endocytosis. The EMBO journal *21*, 6083-6094.

Kessels, M.M., and Qualmann, B. (2004). The syndapin protein family: linking membrane trafficking with the cytoskeleton. Journal of cell science *117*, 3077-3086.

Keyel, P.A., Mishra, S.K., Roth, R., Heuser, J.E., Watkins, S.C., and Traub, L.M. (2006). A single common portal for clathrin-mediated endocytosis of distinct cargo governed by cargo-selective adaptors. Mol Biol Cell *17*, 4300-4317.

Kim, A.S., Kakalis, L.T., Abdul-Manan, N., Liu, G.A., and Rosen, M.K. (2000). Autoinhibition and activation mechanisms of the Wiskott-Aldrich syndrome protein. Nature *404*, 151-158.

Kinley, A.W., Weed, S.A., Weaver, A.M., Karginov, A.V., Bissonette, E., Cooper, J.A., and Parsons, J.T. (2003). Cortactin interacts with WIP in regulating Arp2/3 activation and membrane protrusion. Curr Biol *13*, 384-393.

Kirchhausen, T. (1999). Adaptors for clathrin-mediated traffic. Annu Rev Cell Dev Biol *15*, 705-732.

Kirchhausen, T., Harrison, S.C., Chow, E.P., Mattaliano, R.J., Ramachandran, K.L., Smart, J., and Brosius, J. (1987). Clathrin heavy chain: molecular cloning and complete primary structure. Proceedings of the National Academy of Sciences of the United States of America *84*, 8805-8809.

Kirn, D.H., and Thorne, S.H. (2009). Targeted and armed oncolytic poxviruses: a novel multi-mechanistic therapeutic class for cancer. Nature reviews Cancer *9*, 64-71.

Kleba, B., Clark, T.R., Lutter, E.I., Ellison, D.W., and Hackstadt, T. (2010). Disruption of the Rickettsia rickettsii Sca2 autotransporter inhibits actin-based motility. Infection and immunity *78*, 2240-2247.

Kocks, C., Gouin, E., Tabouret, M., Berche, P., Ohayon, H., and Cossart, P. (1992). L. monocytogenes-induced actin assembly requires the actA gene product, a surface protein. Cell *68*, 521-531.

Korn, E.D., Carlier, M.F., and Pantaloni, D. (1987). Actin polymerization and ATP hydrolysis. Science *238*, 638-644.

Kosaka, T., and Ikeda, K. (1983). Reversible blockage of membrane retrieval and endocytosis in the garland cell of the temperature-sensitive mutant of Drosophila melanogaster, shibirets1. The Journal of cell biology *97*, 499-507.

Krupnick, J.G., Goodman, O.B., Jr., Keen, J.H., and Benovic, J.L. (1997). Arrestin/clathrin interaction. Localization of the clathrin binding domain of nonvisual arrestins to the carboxy terminus. The Journal of biological chemistry *272*, 15011-15016.

Kueh, H.Y., Charras, G.T., Mitchison, T.J., and Brieher, W.M. (2008). Actin disassembly by cofilin, coronin, and Aip1 occurs in bursts and is inhibited by barbed-end cappers. The Journal of cell biology *182*, 341-353.

Kwiatkowska, K., and Sobota, A. (1999). Signaling pathways in phagocytosis. BioEssays : news and reviews in molecular, cellular and developmental biology *21*, 422-431.

Lai, F.P., Szczodrak, M., Block, J., Faix, J., Breitsprecher, D., Mannherz, H.G., Stradal, T.E., Dunn, G.A., Small, J.V., and Rottner, K. (2008). Arp2/3 complex interactions and actin network turnover in lamellipodia. The EMBO journal *27*, 982-992.

Lakadamyali, M., Rust, M.J., and Zhuang, X. (2006). Ligands for clathrin-mediated endocytosis are differentially sorted into distinct populations of early endosomes. Cell *124*, 997-1009.

Lamaze, C., Fujimoto, L.M., Yin, H.L., and Schmid, S.L. (1997). The actin cytoskeleton is required for receptor-mediated endocytosis in mammalian cells. The Journal of biological chemistry *272*, 20332-20335.

Langhorst, M.F., Schaffer, J., and Goetze, B. (2009). Structure brings clarity: structured illumination microscopy in cell biology. Biotechnology journal *4*, 858-865.

Le Clainche, C., Didry, D., Carlier, M.F., and Pantaloni, D. (2001). Activation of Arp2/3 complex by Wiskott-Aldrich Syndrome protein is linked to enhanced binding of ATP to Arp2. The Journal of biological chemistry *276*, 46689-46692.

Le Clainche, C., Pauly, B.S., Zhang, C.X., Engqvist-Goldstein, A.E., Cunningham, K., and Drubin, D.G. (2007). A Hip1R-cortactin complex negatively regulates actin assembly associated with endocytosis. The EMBO journal *26*, 1199-1210.

LeClaire, L.L., 3rd, Baumgartner, M., Iwasa, J.H., Mullins, R.D., and Barber, D.L. (2008). Phosphorylation of the Arp2/3 complex is necessary to nucleate actin filaments. The Journal of cell biology *182*, 647-654.

Legendre-Guillemin, V., Metzler, M., Lemaire, J.F., Philie, J., Gan, L., Hayden, M.R., and McPherson, P.S. (2005). Huntingtin interacting protein 1 (HIP1) regulates clathrin assembly through direct binding to the regulatory region of the clathrin light chain. The Journal of biological chemistry *280*, 6101-6108.

Lewis, A.K., and Bridgman, P.C. (1992). Nerve growth cone lamellipodia contain two populations of actin filaments that differ in organization and polarity. The Journal of cell biology *119*, 1219-1243.

Li, F., and Higgs, H.N. (2003). The mouse Formin mDia1 is a potent actin nucleation factor regulated by autoinhibition. Curr Biol *13*, 1335-1340.

Lin, A.E., Benmerah, A., and Guttman, J.A. (2011). Eps15 and Epsin1 are crucial for enteropathogenic Escherichia coli pedestal formation despite the absence of adaptor protein 2. The Journal of infectious diseases *204*, 695-703.

Lin, D.C., Tobin, K.D., Grumet, M., and Lin, S. (1980). Cytochalasins inhibit nuclei-induced actin polymerization by blocking filament elongation. The Journal of cell biology *84*, 455-460.

Linder, S. (2007). The matrix corroded: podosomes and invadopodia in extracellular matrix degradation. Trends in cell biology *17*, 107-117.

Liu, A.P., Loerke, D., Schmid, S.L., and Danuser, G. (2009). Global and local regulation of clathrin-coated pit dynamics detected on patterned substrates. Biophys J *97*, 1038-1047.

Liu, S.H., Wong, M.L., Craik, C.S., and Brodsky, F.M. (1995). Regulation of clathrin assembly and trimerization defined using recombinant triskelion hubs. Cell *83*, 257-267.

Loerke, D., Mettlen, M., Yarar, D., Jaqaman, K., Jaqaman, H., Danuser, G., and Schmid, S.L. (2009). Cargo and dynamin regulate clathrin-coated pit maturation. PLoS Biol *7*, e57.

Loisel, T.P., Boujemaa, R., Pantaloni, D., and Carlier, M.F. (1999). Reconstitution of actin-based motility of Listeria and Shigella using pure proteins. Nature *401*, 613-616.

Lorenzi, R., Brickell, P.M., Katz, D.R., Kinnon, C., and Thrasher, A.J. (2000). Wiskott-Aldrich syndrome protein is necessary for efficient IgG-mediated phagocytosis. Blood *95*, 2943-2946.

Lu, J., and Pollard, T.D. (2001). Profilin binding to poly-L-proline and actin monomers along with ability to catalyze actin nucleotide exchange is required for viability of fission yeast. Mol Biol Cell *12*, 1161-1175.

Ma, L., Cantley, L.C., Janmey, P.A., and Kirschner, M.W. (1998a). Corequirement of specific phosphoinositides and small GTP-binding protein Cdc42 in inducing actin assembly in Xenopus egg extracts. The Journal of cell biology *140*, 1125-1136.

Ma, L., Rohatgi, R., and Kirschner, M.W. (1998b). The Arp2/3 complex mediates actin polymerization induced by the small GTP-binding protein Cdc42. Proceedings of the National Academy of Sciences of the United States of America *95*, 15362-15367.

Machesky, L.M., Atkinson, S.J., Ampe, C., Vandekerckhove, J., and Pollard, T.D. (1994). Purification of a cortical complex containing two unconventional actins from Acanthamoeba by affinity chromatography on profilin-agarose. The Journal of cell biology *127*, 107-115.

Malacombe, M., Ceridono, M., Calco, V., Chasserot-Golaz, S., McPherson, P.S., Bader, M.F., and Gasman, S. (2006). Intersectin-1L nucleotide exchange factor regulates secretory granule exocytosis by activating Cdc42. The EMBO journal *25*, 3494-3503.

Marchand, J.B., Kaiser, D.A., Pollard, T.D., and Higgs, H.N. (2001). Interaction of WASP/Scar proteins with actin and vertebrate Arp2/3 complex. Nat Cell Biol *3*, 76-82.

Marsh, M., and Helenius, A. (2006). Virus entry: open sesame. Cell *124*, 729-740.

Martin, A.C., Welch, M.D., and Drubin, D.G. (2006). Arp2/3 ATP hydrolysis-catalysed branch dissociation is critical for endocytic force generation. Nat Cell Biol *8*, 826-833.

Martin, A.C., Xu, X.P., Rouiller, I., Kaksonen, M., Sun, Y., Belmont, L., Volkmann, N., Hanein, D., Welch, M., and Drubin, D.G. (2005). Effects of Arp2 and Arp3 nucleotide-binding pocket mutations on Arp2/3 complex function. The Journal of cell biology *168*, 315-328.

Martinez-Quiles, N., Ho, H.Y., Kirschner, M.W., Ramesh, N., and Geha, R.S. (2004). Erk/Src phosphorylation of cortactin acts as a switch on-switch off mechanism that controls its ability to activate N-WASP. Molecular and cellular biology *24*, 5269-5280.

Martinez-Quiles, N., Rohatgi, R., Anton, I.M., Medina, M., Saville, S.P., Miki, H., Yamaguchi, H., Takenawa, T., Hartwig, J.H., Geha, R.S.*, et al.* (2001). WIP regulates N-WASP-mediated actin polymerization and filopodium formation. Nat Cell Biol *3*, 484-491.

Massol, P., Montcourrier, P., Guillemot, J.C., and Chavrier, P. (1998). Fc receptor-mediated phagocytosis requires CDC42 and Rac1. The EMBO journal *17*, 6219-6229.

Massol, R.H., Boll, W., Griffin, A.M., and Kirchhausen, T. (2006). A burst of auxilin recruitment determines the onset of clathrin-coated vesicle uncoating. Proceedings of the National Academy of Sciences of the United States of America *103*, 10265-10270.

Masuda, M., Takeda, S., Sone, M., Ohki, T., Mori, H., Kamioka, Y., and Mochizuki, N. (2006). Endophilin BAR domain drives membrane curvature by two newly identified structure-based mechanisms. The EMBO journal *25*, 2889-2897.

Matsui, Y., Kikuchi, A., Araki, S., Hata, Y., Kondo, J., Teranishi, Y., and Takai, Y. (1990). Molecular cloning and characterization of a novel type of regulatory protein (GDI) for smg p25A, a ras p21-like GTP-binding protein. Molecular and cellular biology *10*, 4116-4122.

Maurer, M.E., and Cooper, J.A. (2006). The adaptor protein Dab2 sorts LDL receptors into coated pits independently of AP-2 and ARH. Journal of cell science *119*, 4235-4246.

May, R.C., Caron, E., Hall, A., and Machesky, L.M. (2000). Involvement of the Arp2/3 complex in phagocytosis mediated by FcgammaR or CR3. Nat Cell Biol *2*, 246-248.

McCann, R.O., and Craig, S.W. (1997). The I/LWEQ module: a conserved sequence that signifies F-actin binding in functionally diverse proteins from yeast to mammals. Proceedings of the National Academy of Sciences of the United States of America *94*, 5679-5684.

McGough, A., Pope, B., Chiu, W., and Weeds, A. (1997). Cofilin changes the twist of F-actin: implications for actin filament dynamics and cellular function. The Journal of cell biology *138*, 771-781.

McMahon, H.T., and Boucrot, E. (2011). Molecular mechanism and physiological functions of clathrin-mediated endocytosis. Nat Rev Mol Cell Biol *12*, 517-533.

McNiven, M.A., Kim, L., Krueger, E.W., Orth, J.D., Cao, H., and Wong, T.W. (2000). Regulated interactions between dynamin and the actin-binding protein cortactin modulate cell shape. The Journal of cell biology *151*, 187-198.

McNiven, M.A., and Thompson, H.M. (2006). Vesicle formation at the plasma membrane and trans-Golgi network: the same but different. Science *313*, 1591-1594.

Meller, N., Merlot, S., and Guda, C. (2005). CZH proteins: a new family of Rho-GEFs. Journal of cell science *118*, 4937-4946.

Mercer, J., Schelhaas, M., and Helenius, A. (2010). Virus entry by endocytosis. Annu Rev Biochem *79*, 803-833.

Merrifield, C.J. (2004). Seeing is believing: imaging actin dynamics at single sites of endocytosis. Trends in cell biology *14*, 352-358.

Merrifield, C.J., Feldman, M.E., Wan, L., and Almers, W. (2002). Imaging actin and dynamin recruitment during invagination of single clathrin-coated pits. Nat Cell Biol *4*, 691-698.

Merrifield, C.J., Moss, S.E., Ballestrem, C., Imhof, B.A., Giese, G., Wunderlich, I., and Almers, W. (1999). Endocytic vesicles move at the tips of actin tails in cultured mast cells. Nat Cell Biol *1*, 72-74.

Merrifield, C.J., Perrais, D., and Zenisek, D. (2005). Coupling between clathrin-coated-pit invagination, cortactin recruitment, and membrane scission observed in live cells. Cell *121*, 593-606.

Mettlen, M., Stoeber, M., Loerke, D., Antonescu, C.N., Danuser, G., and Schmid, S.L. (2009). Endocytic accessory proteins are functionally distinguished by their differential effects on the maturation of clathrin-coated pits. Mol Biol Cell *20*, 3251-3260.

Miki, H., Miura, K., and Takenawa, T. (1996). N-WASP, a novel actin-depolymerizing protein, regulates the cortical cytoskeletal rearrangement in a PIP2-dependent manner downstream of tyrosine kinases. The EMBO journal *15*, 5326-5335.

Miki, H., Sasaki, T., Takai, Y., and Takenawa, T. (1998). Induction of filopodium formation by a WASP-related actin-depolymerizing protein N-WASP. Nature *391*, 93-96.

Millius, A., Watanabe, N., and Weiner, O.D. (2012). Diffusion, capture and recycling of SCAR/WAVE and Arp2/3 complexes observed in cells by single-molecule imaging. Journal of cell science *125*, 1165-1176.

Minnigan, H., and Moyer, R.W. (1985). Intracellular location of rabbit poxvirus nucleic acid within infected cells as determined by in situ hybridization. Journal of virology *55*, 634-643.

Mishra, S.K., Keyel, P.A., Hawryluk, M.J., Agostinelli, N.R., Watkins, S.C., and Traub, L.M. (2002a). Disabled-2 exhibits the properties of a cargo-selective endocytic clathrin adaptor. The EMBO journal *21*, 4915-4926.

Mishra, S.K., Watkins, S.C., and Traub, L.M. (2002b). The autosomal recessive hypercholesterolemia (ARH) protein interfaces directly with the clathrin-coat machinery. Proceedings of the National Academy of Sciences of the United States of America *99*, 16099-16104.

Mogilner, A., and Oster, G. (1996). Cell motility driven by actin polymerization. Biophys J *71*, 3030-3045.

Mooren, O.L., Galletta, B.J., and Cooper, J.A. (2012). Roles for actin assembly in endocytosis. Annu Rev Biochem *81*, 661-686.

Moreau, V., Frischknecht, F., Reckmann, I., Vincentelli, R., Rabut, G., Stewart, D., and Way, M. (2000). A complex of N-WASP and WIP integrates signalling cascades that lead to actin polymerization. Nat Cell Biol *2*, 441-448.

Moreno-Ruiz, E., Galan-Diez, M., Zhu, W., Fernandez-Ruiz, E., d'Enfert, C., Filler, S.G., Cossart, P., and Veiga, E. (2009). Candida albicans internalization by host cells is mediated by a clathrin-dependent mechanism. Cell Microbiol *11*, 1179-1189.

Morgan, G.W., Hollinshead, M., Ferguson, B.J., Murphy, B.J., Carpentier, D.C., and Smith, G.L. (2010). Vaccinia protein F12 has structural similarity to kinesin light chain and contains a motor binding motif required for virion export. PLoS Pathog *6*, e1000785.

Moss, B. (1990). Regulation of vaccinia virus transcription. Annu Rev Biochem *59*, 661-688.

Moss, B., and Rosenblum, E.N. (1973). Letter: Protein cleavage and poxvirus morphogenesis: tryptic peptide analysis of core precursors accumulated by blocking assembly with rifampicin. Journal of molecular biology *81*, 267-269.

Moss, B., and Ward, B.M. (2001). High-speed mass transit for poxviruses on microtubules. Nat Cell Biol *3*, E245-246.

Motley, A., Bright, N.A., Seaman, M.N., and Robinson, M.S. (2003). Clathrin-mediated endocytosis in AP-2-depleted cells. The Journal of cell biology *162*, 909-918.

Mounier, J., Ryter, A., Coquis-Rondon, M., and Sansonetti, P.J. (1990). Intracellular and cell-to-cell spread of Listeria monocytogenes involves interaction with F-actin in the enterocytelike cell line Caco-2. Infection and immunity *58*, 1048-1058.

Mousa, G.Y., Trevithick, J.R., Bechberger, J., and Blair, D.G. (1978). Cytochalasin D induces the capping of both leukaemia viral proteins and actin in infected cells. Nature *274*, 808-809.

Mueller, S.C., Yeh, Y., and Chen, W.T. (1992). Tyrosine phosphorylation of membrane proteins mediates cellular invasion by transformed cells. The Journal of cell biology *119*, 1309-1325.

Mullins, R.D., Heuser, J.A., and Pollard, T.D. (1998). The interaction of Arp2/3 complex with actin: nucleation, high affinity pointed end capping, and formation of branching networks of filaments. Proceedings of the National Academy of Sciences of the United States of America *95*, 6181-6186.

Murphy, D.A., and Courtneidge, S.A. (2011). The 'ins' and 'outs' of podosomes and invadopodia: characteristics, formation and function. Nat Rev Mol Cell Biol *12*, 413-426.

Narayanan, A., LeClaire, L.L., 3rd, Barber, D.L., and Jacobson, M.P. (2011). Phosphorylation of the Arp2 subunit relieves auto-inhibitory interactions for Arp2/3 complex activation. PLoS computational biology *7*, e1002226.

Newpher, T.M., Idrissi, F.Z., Geli, M.I., and Lemmon, S.K. (2006). Novel function of clathrin light chain in promoting endocytic vesicle formation. Mol Biol Cell *17*, 4343-4352.

Newpher, T.M., Smith, R.P., Lemmon, V., and Lemmon, S.K. (2005). In vivo dynamics of clathrin and its adaptor-dependent recruitment to the actin-based endocytic machinery in yeast. Developmental cell *9*, 87-98.

Newsome, T.P., Scaplehorn, N., and Way, M. (2004). SRC mediates a switch from microtubule- to actin-based motility of vaccinia virus. Science *306*, 124-129.

Newsome, T.P., Weisswange, I., Frischknecht, F., and Way, M. (2006). Abl collaborates with Src family kinases to stimulate actin-based motility of vaccinia virus. Cell Microbiol *8*, 233-241.

Nishida, E., and Sakai, H. (1983). Kinetic analysis of actin polymerization. Journal of biochemistry *93*, 1011-1020.

Nolen, B.J., Littlefield, R.S., and Pollard, T.D. (2004). Crystal structures of actin-related protein 2/3 complex with bound ATP or ADP. Proceedings of the National Academy of Sciences of the United States of America *101*, 15627-15632.

Ohno, H., Stewart, J., Fournier, M.C., Bosshart, H., Rhee, I., Miyatake, S., Saito, T., Gallusser, A., Kirchhausen, T., and Bonifacino, J.S. (1995). Interaction of tyrosine-based sorting signals with clathrin-associated proteins. Science *269*, 1872-1875.

Oikawa, T., Itoh, T., and Takenawa, T. (2008). Sequential signals toward podosome formation in NIH-src cells. The Journal of cell biology *182*, 157-169.

Okreglak, V., and Drubin, D.G. (2007). Cofilin recruitment and function during actin-mediated endocytosis dictated by actin nucleotide state. The Journal of cell biology *178*, 1251-1264.

Orlova, A., and Egelman, E.H. (1992). Structural basis for the destabilization of F-actin by phosphate release following ATP hydrolysis. Journal of molecular biology *227*, 1043-1053.

Oser, M., Yamaguchi, H., Mader, C.C., Bravo-Cordero, J.J., Arias, M., Chen, X., Desmarais, V., van Rheenen, J., Koleske, A.J., and Condeelis, J. (2009). Cortactin regulates cofilin and N-WASp activities to control the stages of invadopodium assembly and maturation. The Journal of cell biology *186*, 571-587.

Otomo, T., Tomchick, D.R., Otomo, C., Panchal, S.C., Machius, M., and Rosen, M.K. (2005). Structural basis of actin filament nucleation and processive capping by a formin homology 2 domain. Nature *433*, 488-494.

Otsuki, M., Itoh, T., and Takenawa, T. (2003). Neural Wiskott-Aldrich syndrome protein is recruited to rafts and associates with endophilin A in response to epidermal growth factor. The Journal of biological chemistry *278*, 6461-6469.

Overstreet, E., Chen, X., Wendland, B., and Fischer, J.A. (2003). Either part of a Drosophila epsin protein, divided after the ENTH domain, functions in endocytosis of delta in the developing eye. Curr Biol *13*, 854-860.

Owen, D.J., Collins, B.M., and Evans, P.R. (2004). Adaptors for clathrin coats: structure and function. Annu Rev Cell Dev Biol *20*, 153-191.

Owen, D.J., and Evans, P.R. (1998). A structural explanation for the recognition of tyrosine-based endocytotic signals. Science *282*, 1327-1332.

Owen, D.J., Vallis, Y., Noble, M.E., Hunter, J.B., Dafforn, T.R., Evans, P.R., and McMahon, H.T. (1999). A structural explanation for the binding of multiple ligands by the alpha-adaptin appendage domain. Cell *97*, 805-815.

Padrick, S.B., Cheng, H.C., Ismail, A.M., Panchal, S.C., Doolittle, L.K., Kim, S., Skehan, B.M., Umetani, J., Brautigam, C.A., Leong, J.M*., et al.* (2008). Hierarchical regulation of WASP/WAVE proteins. Molecular cell *32*, 426-438.

Padrick, S.B., Doolittle, L.K., Brautigam, C.A., King, D.S., and Rosen, M.K. (2011). Arp2/3 complex is bound and activated by two WASP proteins. Proceedings of the National Academy of Sciences of the United States of America *108*, E472-479.

Panchal, S.C., Kaiser, D.A., Torres, E., Pollard, T.D., and Rosen, M.K. (2003). A conserved amphipathic helix in WASP/Scar proteins is essential for activation of Arp2/3 complex. Nature structural biology *10*, 591-598.

Panner, B.J., and Honig, C.R. (1967). Filament ultrastructure and organization in vertebrate smooth muscle. Contraction hypothesis based on localization of actin and myosin. The Journal of cell biology *35*, 303-321.

Pantaloni, D., Boujemaa, R., Didry, D., Gounon, P., and Carlier, M.F. (2000). The Arp2/3 complex branches filament barbed ends: functional antagonism with capping proteins. Nat Cell Biol *2*, 385-391.

Pantaloni, D., Le Clainche, C., and Carlier, M.F. (2001). Mechanism of actin-based motility. Science *292*, 1502-1506.

Papayannopoulos, V., Co, C., Prehoda, K.E., Snapper, S., Taunton, J., and Lim, W.A. (2005). A polybasic motif allows N-WASP to act as a sensor of PIP(2) density. Molecular cell *17*, 181-191.

Park, H., and Cox, D. (2009). Cdc42 regulates Fc gamma receptor-mediated phagocytosis through the activation and phosphorylation of Wiskott-Aldrich syndrome protein (WASP) and neural-WASP. Mol Biol Cell *20*, 4500-4508.

Parkinson, J.E., and Smith, G.L. (1994). Vaccinia virus gene A36R encodes a M(r) 43-50 K protein on the surface of extracellular enveloped virus. Virology *204*, 376-390.

Patel, J.C., Hall, A., and Caron, E. (2002). Vav regulates activation of Rac but not Cdc42 during FcgammaR-mediated phagocytosis. Mol Biol Cell *13*, 1215-1226.

Patterson, G.H., and Lippincott-Schwartz, J. (2002). A photoactivatable GFP for selective photolabeling of proteins and cells. Science *297*, 1873-1877.

Paul, A.S., and Pollard, T.D. (2008). The role of the FH1 domain and profilin in formin-mediated actin-filament elongation and nucleation. Curr Biol *18*, 9-19.

Pawson, T. (2004). Specificity in signal transduction: from phosphotyrosine-SH2 domain interactions to complex cellular systems. Cell *116*, 191-203.

Payne, L.G. (1980). Significance of extracellular enveloped virus in the in vitro and in vivo dissemination of vaccinia. The Journal of general virology *50*, 89-100.

Pearse, B.M. (1976). Clathrin: a unique protein associated with intracellular transfer of membrane by coated vesicles. Proceedings of the National Academy of Sciences of the United States of America *73*, 1255-1259.

Pearse, B.M., and Bretscher, M.S. (1981). Membrane recycling by coated vesicles. Annu Rev Biochem *50*, 85-101.

Pearse, B.M., and Robinson, M.S. (1984). Purification and properties of 100-kd proteins from coated vesicles and their reconstitution with clathrin. The EMBO journal *3*, 1951-1957.

Pelkmans, L., and Helenius, A. (2003). Insider information: what viruses tell us about endocytosis. Curr Opin Cell Biol *15*, 414-422.

Pellegrin, S., and Mellor, H. (2007). Actin stress fibres. Journal of cell science *120*, 3491-3499.

Perdiguero, B., and Blasco, R. (2006). Interaction between vaccinia virus extracellular virus envelope A33 and B5 glycoproteins. Journal of virology *80*, 8763-8777.

Perdiguero, B., Lorenzo, M.M., and Blasco, R. (2008). Vaccinia virus A34 glycoprotein determines the protein composition of the extracellular virus envelope. Journal of virology *82*, 2150-2160.

Peter, B.J., Kent, H.M., Mills, I.G., Vallis, Y., Butler, P.J., Evans, P.R., and McMahon, H.T. (2004). BAR domains as sensors of membrane curvature: the amphiphysin BAR structure. Science *303*, 495-499.

Pichot, C.S., Arvanitis, C., Hartig, S.M., Jensen, S.A., Bechill, J., Marzouk, S., Yu, J., Frost, J.A., and Corey, S.J. (2010). Cdc42-interacting protein 4 promotes breast cancer cell invasion and formation of invadopodia through activation of N-WASp. Cancer research *70*, 8347-8356.

Pinyol, R., Haeckel, A., Ritter, A., Qualmann, B., and Kessels, M.M. (2007). Regulation of N-WASP and the Arp2/3 complex by Abp1 controls neuronal morphology. PloS one *2*, e400.

Pizarro-Cerda, J., Bonazzi, M., and Cossart, P. (2010). Clathrin-mediated endocytosis: what works for small, also works for big. BioEssays : news and reviews in molecular, cellular and developmental biology *32*, 496-504.

Poincloux, R., Lizarraga, F., and Chavrier, P. (2009). Matrix invasion by tumour cells: a focus on MT1-MMP trafficking to invadopodia. Journal of cell science *122*, 3015-3024.

Pollard, T.D. (1983). Measurement of rate constants for actin filament elongation in solution. Analytical biochemistry *134*, 406-412.

Pollard, T.D., and Borisy, G.G. (2003). Cellular motility driven by assembly and disassembly of actin filaments. Cell *112*, 453-465.

Pollard, T.D., and Cooper, J.A. (1984). Quantitative analysis of the effect of Acanthamoeba profilin on actin filament nucleation and elongation. Biochemistry *23*, 6631-6641.

Pollard, T.D., and Cooper, J.A. (2009). Actin, a central player in cell shape and movement. Science *326*, 1208-1212.

Ponting, C.P., and Kerr, I.D. (1996). A novel family of phospholipase D homologues that includes phospholipid synthases and putative endonucleases: identification of duplicated repeats and potential active site residues. Protein science : a publication of the Protein Society *5*, 914-922.

Porta, J.C., and Borgstahl, G.E. (2012). Structural basis for profilin-mediated actin nucleotide exchange. Journal of molecular biology *418*, 103-116.

Poupon, V., Girard, M., Legendre-Guillemin, V., Thomas, S., Bourbonniere, L., Philie, J., Bright, N.A., and McPherson, P.S. (2008). Clathrin light chains function in mannose phosphate receptor trafficking via regulation of actin assembly. Proceedings of the National Academy of Sciences of the United States of America *105*, 168-173.

Prehoda, K.E., Scott, J.A., Mullins, R.D., and Lim, W.A. (2000). Integration of multiple signals through cooperative regulation of the N-WASP-Arp2/3 complex. Science *290*, 801-806.

Pruyne, D., Evangelista, M., Yang, C., Bi, E., Zigmond, S., Bretscher, A., and Boone, C. (2002). Role of formins in actin assembly: nucleation and barbed-end association. Science *297*, 612-615.

Qualmann, B., and Kessels, M.M. (2009). New players in actin polymerization--WH2-domain-containing actin nucleators. Trends in cell biology *19*, 276-285.

Quinlan, M.E., Heuser, J.E., Kerkhoff, E., and Mullins, R.D. (2005). Drosophila Spire is an actin nucleation factor. Nature *433*, 382-388.

Rafelski, S.M., and Theriot, J.A. (2004). Crawling toward a unified model of cell mobility: spatial and temporal regulation of actin dynamics. Annu Rev Biochem *73*, 209-239.

Ramjaun, A.R., and McPherson, P.S. (1998). Multiple amphiphysin II splice variants display differential clathrin binding: identification of two distinct clathrin-binding sites. Journal of neurochemistry *70*, 2369-2376.

Reeves, P.M., Bommarius, B., Lebeis, S., McNulty, S., Christensen, J., Swimm, A., Chahroudi, A., Chavan, R., Feinberg, M.B., Veach, D.*, et al.* (2005). Disabling poxvirus pathogenesis by inhibition of Abl-family tyrosine kinases. Nat Med *11*, 731-739.

Repass, S.L., Brady, R.J., and O'Halloran, T.J. (2007). Dictyostelium Hip1r contributes to spore shape and requires epsin for phosphorylation and localization. Journal of cell science *120*, 3977-3988.

Ricotta, D., Conner, S.D., Schmid, S.L., von Figura, K., and Honing, S. (2002). Phosphorylation of the AP2 mu subunit by AAK1 mediates high affinity binding to membrane protein sorting signals. The Journal of cell biology *156*, 791-795.

Ridley, A.J. (2011). Life at the leading edge. Cell *145*, 1012-1022.

Riedl, J., Crevenna, A.H., Kessenbrock, K., Yu, J.H., Neukirchen, D., Bista, M., Bradke, F., Jenne, D., Holak, T.A., Werb, Z.*, et al.* (2008). Lifeact: a versatile marker to visualize F-actin. Nature methods *5*, 605-607.

Rietdorf, J., Ploubidou, A., Reckmann, I., Holmstrom, A., Frischknecht, F., Zettl, M., Zimmermann, T., and Way, M. (2001). Kinesin-dependent movement on microtubules precedes actin-based motility of vaccinia virus. Nat Cell Biol *3*, 992-1000.

Rivera, G.M., Briceno, C.A., Takeshima, F., Snapper, S.B., and Mayer, B.J. (2004). Inducible clustering of membrane-targeted SH3 domains of the adaptor protein Nck triggers localized actin polymerization. Curr Biol *14*, 11-22.

Roberts, K.L., and Smith, G.L. (2008). Vaccinia virus morphogenesis and dissemination. Trends in microbiology *16*, 472-479.

Robinson, R.C., Turbedsky, K., Kaiser, D.A., Marchand, J.B., Higgs, H.N., Choe, S., and Pollard, T.D. (2001). Crystal structure of Arp2/3 complex. Science *294*, 1679-1684.

Rodal, A.A., Sokolova, O., Robins, D.B., Daugherty, K.M., Hippenmeyer, S., Riezman, H., Grigorieff, N., and Goode, B.L. (2005). Conformational changes in the Arp2/3 complex leading to actin nucleation. Nature structural & molecular biology *12*, 26-31.

Rodriguez, J.R., Risco, C., Carrascosa, J.L., Esteban, M., and Rodriguez, D. (1998). Vaccinia virus 15-kilodalton (A14L) protein is essential for assembly and attachment of viral crescents to virosomes. Journal of virology *72*, 1287-1296.

Rohatgi, R., Ho, H.Y., and Kirschner, M.W. (2000). Mechanism of N-WASP activation by CDC42 and phosphatidylinositol 4, 5-bisphosphate. The Journal of cell biology *150*, 1299-1310.

Rohatgi, R., Ma, L., Miki, H., Lopez, M., Kirchhausen, T., Takenawa, T., and Kirschner, M.W. (1999). The interaction between N-WASP and the Arp2/3 complex links Cdc42-dependent signals to actin assembly. Cell *97*, 221-231.

Rohatgi, R., Nollau, P., Ho, H.Y., Kirschner, M.W., and Mayer, B.J. (2001). Nck and phosphatidylinositol 4,5-bisphosphate synergistically activate actin polymerization through the N-WASP-Arp2/3 pathway. The Journal of biological chemistry *276*, 26448-26452.

Rohde, G., Wenzel, D., and Haucke, V. (2002). A phosphatidylinositol (4,5)-bisphosphate binding site within mu2-adaptin regulates clathrin-mediated endocytosis. The Journal of cell biology *158*, 209-214.

Romero, S., Le Clainche, C., Didry, D., Egile, C., Pantaloni, D., and Carlier, M.F. (2004). Formin is a processive motor that requires profilin to accelerate actin assembly and associated ATP hydrolysis. Cell *119*, 419-429.

Roper, R.L., Payne, L.G., and Moss, B. (1996). Extracellular vaccinia virus envelope glycoprotein encoded by the A33R gene. Journal of virology *70*, 3753-3762.

Rosel, J., and Moss, B. (1985). Transcriptional and translational mapping and nucleotide sequence analysis of a vaccinia virus gene encoding the precursor of the major core polypeptide 4b. Journal of virology *56*, 830-838.

Roth, T.F., and Porter, K.R. (1964). Yolk Protein Uptake in the Oocyte of the Mosquito Aedes Aegypti. L. The Journal of cell biology *20*, 313-332.

Rottger, S., Frischknecht, F., Reckmann, I., Smith, G.L., and Way, M. (1999). Interactions between vaccinia virus IEV membrane proteins and their roles in IEV assembly and actin tail formation. Journal of virology *73*, 2863-2875.

Rottner, K., Behrendt, B., Small, J.V., and Wehland, J. (1999). VASP dynamics during lamellipodia protrusion. Nat Cell Biol *1*, 321-322.

Rouiller, I., Xu, X.P., Amann, K.J., Egile, C., Nickell, S., Nicastro, D., Li, R., Pollard, T.D., Volkmann, N., and Hanein, D. (2008). The structural basis of actin filament branching by the Arp2/3 complex. The Journal of cell biology *180*, 887-895.

Saffarian, S., Cocucci, E., and Kirchhausen, T. (2009). Distinct dynamics of endocytic clathrin-coated pits and coated plaques. PLoS Biol *7*, e1000191.

Sagot, I., Rodal, A.A., Moseley, J., Goode, B.L., and Pellman, D. (2002). An actin nucleation mechanism mediated by Bni1 and profilin. Nat Cell Biol *4*, 626-631.

Salcini, A.E., Chen, H., Iannolo, G., De Camilli, P., and Di Fiore, P.P. (1999). Epidermal growth factor pathway substrate 15, Eps15. The international journal of biochemistry & cell biology *31*, 805-809.

Sanderson, C.M., Hollinshead, M., and Smith, G.L. (2000). The vaccinia virus A27L protein is needed for the microtubule-dependent transport of intracellular mature virus particles. The Journal of general virology *81*, 47-58.

Scaplehorn, N., Holmstrom, A., Moreau, V., Frischknecht, F., Reckmann, I., and Way, M. (2002). Grb2 and Nck act cooperatively to promote actin-based motility of vaccinia virus. Curr Biol *12*, 740-745.

Scheele, U., Kalthoff, C., and Ungewickell, E. (2001). Multiple interactions of auxilin 1 with clathrin and the AP-2 adaptor complex. The Journal of biological chemistry *276*, 36131-36138.

Schelhaas, M. (2010). Come in and take your coat off - how host cells provide endocytosis for virus entry. Cell Microbiol *12*, 1378-1388.

Schlossman, D.M., Schmid, S.L., Braell, W.A., and Rothman, J.E. (1984). An enzyme that removes clathrin coats: purification of an uncoating ATPase. The Journal of cell biology *99*, 723-733.

Schmelz, M., Sodeik, B., Ericsson, M., Wolffe, E.J., Shida, H., Hiller, G., and Griffiths, G. (1994). Assembly of vaccinia virus: the second wrapping cisterna is derived from the trans Golgi network. Journal of virology *68*, 130-147.

Schmid, E.M., and McMahon, H.T. (2007). Integrating molecular and network biology to decode endocytosis. Nature *448*, 883-888.

Schoumacher, M., Goldman, R.D., Louvard, D., and Vignjevic, D.M. (2010). Actin, microtubules, and vimentin intermediate filaments cooperate for elongation of invadopodia. The Journal of cell biology *189*, 541-556.

Selden, L.A., Kinosian, H.J., Estes, J.E., and Gershman, L.C. (1999). Impact of profilin on actin-bound nucleotide exchange and actin polymerization dynamics. Biochemistry *38*, 2769-2778.

Serio, A.W., Jeng, R.L., Haglund, C.M., Reed, S.C., and Welch, M.D. (2010). Defining a core set of actin cytoskeletal proteins critical for actin-based motility of Rickettsia. Cell host & microbe *7*, 388-398.

Shih, W., Gallusser, A., and Kirchhausen, T. (1995). A clathrin-binding site in the hinge of the beta 2 chain of mammalian AP-2 complexes. The Journal of biological chemistry *270*, 31083-31090.

Shin, N., Lee, S., Ahn, N., Kim, S.A., Ahn, S.G., YongPark, Z., and Chang, S. (2007). Sorting nexin 9 interacts with dynamin 1 and N-WASP and coordinates synaptic vesicle endocytosis. The Journal of biological chemistry *282*, 28939-28950.

Signoret, N., Hewlett L., Wavre S., Pelchen-Metthews A., Oppermann M., and March M. (2005). Agonist-induced endocytosis of CC chemokine receptor 5 is clathrin dependent. Mol Biol Cell *16*, 902-917

Slepnev, V.I., and De Camilli, P. (2000). Accessory factors in clathrin-dependent synaptic vesicle endocytosis. Nature reviews Neuroscience *1*, 161-172.

Small, J.V., Stradal, T., Vignal, E., and Rottner, K. (2002). The lamellipodium: where motility begins. Trends in cell biology *12*, 112-120.

Smith, G.A., Portnoy, D.A., and Theriot, J.A. (1995). Asymmetric distribution of the Listeria monocytogenes ActA protein is required and sufficient to direct actin-based motility. Molecular microbiology *17*, 945-951.

Smith, G.L., and Law, M. (2004). The exit of vaccinia virus from infected cells. Virus research *106*, 189-197.

Smith, G.L., Vanderplasschen, A., and Law, M. (2002). The formation and function of extracellular enveloped vaccinia virus. The Journal of general virology *83*, 2915-2931.

Smith-Pearson, P.S., Greuber, E.K., Yogalingam, G., and Pendergast, A.M. (2010). Abl kinases are required for invadopodia formation and chemokine-induced invasion. The Journal of biological chemistry *285*, 40201-40211.

Snapper, S.B., Takeshima, F., Anton, I., Liu, C.H., Thomas, S.M., Nguyen, D., Dudley, D., Fraser, H., Purich, D., Lopez-Ilasaca, M.*, et al.* (2001). N-WASP deficiency reveals distinct pathways for cell surface projections and microbial actin-based motility. Nat Cell Biol *3*, 897-904.

Steffen, A., Rottner, K., Ehinger, J., Innocenti, M., Scita, G., Wehland, J., and Stradal, T.E. (2004). Sra-1 and Nap1 link Rac to actin assembly driving lamellipodia formation. The EMBO journal *23*, 749-759.

Stokes, G.V. (1976). High-voltage electron microscope study of the release of vaccinia virus from whole cells. Journal of virology *18*, 636-643.

Stradal, T.E., and Scita, G. (2006). Protein complexes regulating Arp2/3-mediated actin assembly. Curr Opin Cell Biol *18*, 4-10.

Stylli, S.S., Stacey, T.T., Verhagen, A.M., Xu, S.S., Pass, I., Courtneidge, S.A., and Lock, P. (2009). Nck adaptor proteins link Tks5 to invadopodia actin regulation and ECM degradation. Journal of cell science *122*, 2727-2740.

Sundborger, A., Soderblom, C., Vorontsova, O., Evergren, E., Hinshaw, J.E., and Shupliakov, O. (2011). An endophilin-dynamin complex promotes budding of clathrin-coated vesicles during synaptic vesicle recycling. Journal of cell science *124*, 133-143.

Svitkina, T.M., and Borisy, G.G. (1999). Arp2/3 complex and actin depolymerizing factor/cofilin in dendritic organization and treadmilling of actin filament array in lamellipodia. The Journal of cell biology *145*, 1009-1026.

Symons, M., Derry, J.M., Karlak, B., Jiang, S., Lemahieu, V., McCormick, F., Francke, U., and Abo, A. (1996). Wiskott-Aldrich syndrome protein, a novel effector for the GTPase CDC42Hs, is implicated in actin polymerization. Cell *84*, 723-734.

Symons, M.H., and Mitchison, T.J. (1991). Control of actin polymerization in live and permeabilized fibroblasts. The Journal of cell biology *114*, 503-513.

Takano, K., Toyooka, K., and Suetsugu, S. (2008). EFC/F-BAR proteins and the N-WASP-WIP complex induce membrane curvature-dependent actin polymerization. The EMBO journal *27*, 2817-2828.

Tarone, G., Cirillo, D., Giancotti, F.G., Comoglio, P.M., and Marchisio, P.C. (1985). Rous sarcoma virus-transformed fibroblasts adhere primarily at discrete protrusions of the ventral membrane called podosomes. Experimental cell research *159*, 141-157.

Taunton, J., Rowning, B.A., Coughlin, M.L., Wu, M., Moon, R.T., Mitchison, T.J., and Larabell, C.A. (2000). Actin-dependent propulsion of endosomes and lysosomes by recruitment of N-WASP. The Journal of cell biology *148*, 519-530.

Taylor, M.J., Perrais, D., and Merrifield, C.J. (2011). A high precision survey of the molecular dynamics of mammalian clathrin-mediated endocytosis. PLoS Biol *9*, e1000604.

Tehrani, S., Tomasevic, N., Weed, S., Sakowicz, R., and Cooper, J.A. (2007). Src phosphorylation of cortactin enhances actin assembly. Proceedings of the National Academy of Sciences of the United States of America *104*, 11933-11938.

ter Haar, E., Musacchio, A., Harrison, S.C., and Kirchhausen, T. (1998). Atomic structure of clathrin: a beta propeller terminal domain joins an alpha zigzag linker. Cell *95*, 563-573.

Theriot, J.A., and Mitchison, T.J. (1991). Actin microfilament dynamics in locomoting cells. Nature *352*, 126-131.

Ti, S.C., and Pollard, T.D. (2011). Purification of actin from fission yeast Schizosaccharomyces pombe and characterization of functional differences from muscle actin. The Journal of biological chemistry *286*, 5784-5792.

Tilney, L.G., Bonder, E.M., Coluccio, L.M., and Mooseker, M.S. (1983). Actin from Thyone sperm assembles on only one end of an actin filament: a behavior regulated by profilin. The Journal of cell biology *97*, 112-124.

Tilney, L.G., and Portnoy, D.A. (1989). Actin filaments and the growth, movement, and spread of the intracellular bacterial parasite, Listeria monocytogenes. The Journal of cell biology *109*, 1597-1608.

Tooze, J., Hollinshead, M., Reis, B., Radsak, K., and Kern, H. (1993). Progeny vaccinia and human cytomegalovirus particles utilize early endosomal cisternae for their envelopes. European journal of cell biology *60*, 163-178.

Torres, E., and Rosen, M.K. (2003). Contingent phosphorylation/dephosphorylation provides a mechanism of molecular memory in WASP. Molecular cell *11*, 1215-1227.

Torres, E., and Rosen, M.K. (2006). Protein-tyrosine kinase and GTPase signals cooperate to phosphorylate and activate Wiskott-Aldrich syndrome protein (WASP)/neuronal WASP. The Journal of biological chemistry *281*, 3513-3520.

Traub, L.M. (2005). Common principles in clathrin-mediated sorting at the Golgi and the plasma membrane. Biochim Biophys Acta *1744*, 415-437.

Traub, L.M. (2009). Clathrin couture: fashioning distinctive membrane coats at the cell surface. PLoS Biol *7*, e1000192.

Traub, L.M., Downs, M.A., Westrich, J.L., and Fremont, D.H. (1999). Crystal structure of the alpha appendage of AP-2 reveals a recruitment platform for clathrin-coat assembly. Proceedings of the National Academy of Sciences of the United States of America *96*, 8907-8912.

Tsujita, K., Suetsugu, S., Sasaki, N., Furutani, M., Oikawa, T., and Takenawa, T. (2006). Coordination between the actin cytoskeleton and membrane deformation by a novel membrane tubulation domain of PCH proteins is involved in endocytosis. The Journal of cell biology *172*, 269-279.

Uhlik, M.T., Temple, B., Bencharit, S., Kimple, A.J., Siderovski, D.P., and Johnson, G.L. (2005). Structural and evolutionary division of phosphotyrosine binding (PTB) domains. Journal of molecular biology *345*, 1-20.

Ungewickell, E., Ungewickell, H., Holstein, S.E., Lindner, R., Prasad, K., Barouch, W., Martin, B., Greene, L.E., and Eisenberg, E. (1995). Role of auxilin in uncoating clathrin-coated vesicles. Nature *378*, 632-635.

Uruno, T., Liu, J., Zhang, P., Fan, Y., Egile, C., Li, R., Mueller, S.C., and Zhan, X. (2001). Activation of Arp2/3 complex-mediated actin polymerization by cortactin. Nat Cell Biol *3*, 259-266.

van Eijl, H., Hollinshead, M., Rodger, G., Zhang, W.H., and Smith, G.L. (2002). The vaccinia virus F12L protein is associated with intracellular enveloped virus particles and is required for their egress to the cell surface. The Journal of general virology *83*, 195-207.

van Eijl, H., Hollinshead, M., and Smith, G.L. (2000). The vaccinia virus A36R protein is a type Ib membrane protein present on intracellular but not extracellular enveloped virus particles. Virology *271*, 26-36.

Veiga, E., Guttman, J.A., Bonazzi, M., Boucrot, E., Toledo-Arana, A., Lin, A.E., Enninga, J., Pizarro-Cerda, J., Finlay, B.B., Kirchhausen, T.*, et al.* (2007). Invasive and adherent bacterial pathogens co-Opt host clathrin for infection. Cell host & microbe *2*, 340-351.

von Kleist, L., Stahlschmidt, W., Bulut, H., Gromova, K., Puchkov, D., Robertson, M.J., MacGregor, K.A., Tomilin, N., Pechstein, A., Chau, N.*, et al.* (2011). Role of the clathrin terminal domain in regulating coated pit dynamics revealed by small molecule inhibition. Cell *146*, 471-484.

Wagenaar, T.R., and Moss, B. (2007). Association of vaccinia virus fusion regulatory proteins with the multicomponent entry/fusion complex. Journal of virology *81*, 6286-6293.

Wang, L.H., Rothberg, K.G., and Anderson, R.G. (1993). Mis-assembly of clathrin lattices on endosomes reveals a regulatory switch for coated pit formation. The Journal of cell biology *123*, 1107-1117.

Wang, Y.L. (1985). Exchange of actin subunits at the leading edge of living fibroblasts: possible role of treadmilling. The Journal of cell biology *101*, 597-602.

Ward, B.M. (2005). Visualization and characterization of the intracellular movement of vaccinia virus intracellular mature virions. Journal of virology *79*, 4755-4763.

Ward, B.M., and Moss, B. (2000). Golgi network targeting and plasma membrane internalization signals in vaccinia virus B5R envelope protein. Journal of virology *74*, 3771-3780.

Ward, B.M., and Moss, B. (2004). Vaccinia virus A36R membrane protein provides a direct link between intracellular enveloped virions and the microtubule motor kinesin. Journal of virology *78*, 2486-2493.

Watanabe, N., and Mitchison, T.J. (2002). Single-molecule speckle analysis of actin filament turnover in lamellipodia. Science *295*, 1083-1086.

Waterman-Storer, C.M., Desai, A., Bulinski, J.C., and Salmon, E.D. (1998). Fluorescent speckle microscopy, a method to visualize the dynamics of protein assemblies in living cells. Curr Biol *8*, 1227-1230.

Wear, M.A., Yamashita, A., Kim, K., Maeda, Y., and Cooper, J.A. (2003). How capping protein binds the barbed end of the actin filament. Curr Biol *13*, 1531-1537.

Weaver, A.M., Heuser, J.E., Karginov, A.V., Lee, W.L., Parsons, J.T., and Cooper, J.A. (2002). Interaction of cortactin and N-WASp with Arp2/3 complex. Curr Biol *12*, 1270-1278.

Weaver, A.M., Karginov, A.V., Kinley, A.W., Weed, S.A., Li, Y., Parsons, J.T., and Cooper, J.A. (2001). Cortactin promotes and stabilizes Arp2/3-induced actin filament network formation. Curr Biol *11*, 370-374.

Wegner, A. (1976). Head to tail polymerization of actin. Journal of molecular biology *108*, 139-150.

Wegner, A., and Isenberg, G. (1983). 12-fold difference between the critical monomer concentrations of the two ends of actin filaments in physiological salt conditions. Proceedings of the National Academy of Sciences of the United States of America *80*, 4922-4925.

Weissenhorn, W. (2005). Crystal structure of the endophilin-A1 BAR domain. Journal of molecular biology *351*, 653-661.

Weisswange, I., Newsome, T.P., Schleich, S., and Way, M. (2009). The rate of N-WASP exchange limits the extent of ARP2/3-complex-dependent actin-based motility. Nature *458*, 87-91.

Welch, M.D., DePace, A.H., Verma, S., Iwamatsu, A., and Mitchison, T.J. (1997a). The human Arp2/3 complex is composed of evolutionarily conserved subunits and is localized to cellular regions of dynamic actin filament assembly. The Journal of cell biology *138*, 375-384.

Welch, M.D., Iwamatsu, A., and Mitchison, T.J. (1997b). Actin polymerization is induced by Arp2/3 protein complex at the surface of Listeria monocytogenes. Nature *385*, 265-269.

Welch, M.D., Rosenblatt, J., Skoble, J., Portnoy, D.A., and Mitchison, T.J. (1998). Interaction of human Arp2/3 complex and the Listeria monocytogenes ActA protein in actin filament nucleation. Science *281*, 105-108.

Welman, A., Serrels, A., Brunton, V.G., Ditzel, M., and Frame, M.C. (2010). Two-color photoactivatable probe for selective tracking of proteins and cells. The Journal of biological chemistry *285*, 11607-11616.

Wiesner, S., Helfer, E., Didry, D., Ducouret, G., Lafuma, F., Carlier, M.F., and Pantaloni, D. (2003). A biomimetic motility assay provides insight into the mechanism of actin-based motility. The Journal of cell biology *160*, 387-398.

Wigge, P., Kohler, K., Vallis, Y., Doyle, C.A., Owen, D., Hunt, S.P., and McMahon, H.T. (1997). Amphiphysin heterodimers: potential role in clathrin-mediated endocytosis. Mol Biol Cell *8*, 2003-2015.

Wilbur, J.D., Chen, C.Y., Manalo, V., Hwang, P.K., Fletterick, R.J., and Brodsky, F.M. (2008). Actin binding by Hip1 (huntingtin-interacting protein 1) and Hip1R (Hip1-related protein) is regulated by clathrin light chain. The Journal of biological chemistry *283*, 32870-32879.

Wilbur, J.D., Hwang, P.K., Ybe, J.A., Lane, M., Sellers, B.D., Jacobson, M.P., Fletterick, R.J., and Brodsky, F.M. (2010). Conformation switching of clathrin light chain regulates clathrin lattice assembly. Developmental cell *18*, 841-848.

Wilde, A., and Brodsky, F.M. (1996). In vivo phosphorylation of adaptors regulates their interaction with clathrin. The Journal of cell biology *135*, 635-645.

Wolffe, E.J., Isaacs, S.N., and Moss, B. (1993). Deletion of the vaccinia virus B5R gene encoding a 42-kilodalton membrane glycoprotein inhibits extracellular virus envelope formation and dissemination. Journal of virology *67*, 4732-4741.

Wolffe, E.J., Weisberg, A.S., and Moss, B. (1998). Role for the vaccinia virus A36R outer envelope protein in the formation of virus-tipped actin-containing microvilli and cell-to-cell virus spread. Virology *244*, 20-26.

Wong, W.T., Schumacher, C., Salcini, A.E., Romano, A., Castagnino, P., Pelicci, P.G., and Di Fiore, P.P. (1995). A protein-binding domain, EH, identified in the receptor tyrosine kinase substrate Eps15 and conserved in evolution. Proceedings of the National Academy of Sciences of the United States of America *92*, 9530-9534.

Woodrum, D.T., Rich, S.A., and Pollard, T.D. (1975). Evidence for biased bidirectional polymerization of actin filaments using heavy meromyosin prepared by an improved method. The Journal of cell biology *67*, 231-237.

Xu, X.P., Rouiller, I., Slaughter, B.D., Egile, C., Kim, E., Unruh, J.R., Fan, X., Pollard, T.D., Li, R., Hanein, D*., et al.* (2012). Three-dimensional reconstructions of Arp2/3 complex with bound nucleation promoting factors. The EMBO journal *31*, 236-247.

Yamabhai, M., Hoffman, N.G., Hardison, N.L., McPherson, P.S., Castagnoli, L., Cesareni, G., and Kay, B.K. (1998). Intersectin, a novel adaptor protein with two Eps15 homology and five Src homology 3 domains. The Journal of biological chemistry *273*, 31401-31407.

Yamaguchi, H., and Condeelis, J. (2007). Regulation of the actin cytoskeleton in cancer cell migration and invasion. Biochim Biophys Acta *1773*, 642-652.

Yamauchi, A., Kim, C., Li, S., Marchal, C.C., Towe, J., Atkinson, S.J., and Dinauer, M.C. (2004). Rac2-deficient murine macrophages have selective defects in superoxide production and phagocytosis of opsonized particles. Journal of immunology *173*, 5971-5979.

Zalevsky, J., Lempert, L., Kranitz, H., and Mullins, R.D. (2001). Different WASP family proteins stimulate different Arp2/3 complex-dependent actin-nucleating activities. Curr Biol *11*, 1903-1913.

Zencheck, W.D., Xiao, H., Nolen, B.J., Angeletti, R.H., Pollard, T.D., and Almo, S.C. (2009). Nucleotide- and activator-dependent structural and dynamic changes of arp2/3 complex monitored by hydrogen/deuterium exchange and mass spectrometry. Journal of molecular biology *390*, 414-427.

Zettl, M., and Way, M. (2002). The WH1 and EVH1 domains of WASP and Ena/VASP family members bind distinct sequence motifs. Curr Biol *12*, 1617-1622.

Zhang, W.H., Wilcock, D., and Smith, G.L. (2000). Vaccinia virus F12L protein is required for actin tail formation, normal plaque size, and virulence. Journal of virology *74*, 11654-11662.

Zhang, Y., and Moss, B. (1992). Immature viral envelope formation is interrupted at the same stage by lac operator-mediated repression of the vaccinia virus D13L gene and by the drug rifampicin. Virology *187*, 643-653.

Zuchero, J.B., Coutts, A.S., Quinlan, M.E., Thangue, N.B., and Mullins, R.D. (2009). p53-cofactor JMY is a multifunctional actin nucleation factor. Nat Cell Biol *11*, 451-459.